

Alma Mater Studiorum – Università di Bologna

DOTTORATO DI RICERCA IN

Chimica Industriale

Ciclo XXII

Settore/i scientifico-disciplinare/i di afferenza: CHIM/04

***Liquid crystal polymers: macromolecular design for
enhanced performances***

Presentata da: Fabio Paris

Coordinatore Dottorato

F. Cavani

Relatore

Dott. L. Giorgini

Co-relatore:

Prof. L. Angiolini

Esame finale anno 2010

*You see things and ask: why?
But I dream things that there aren't
and maybe will not exist at all
and I say: why not?*

Wolfgang Güllich

Index

Overview	1
Introduction	3
Atom Transfer Radical Polymerization – ATRP.....	3
Mechanism	5
ATRP kinetics	8
Component of the reaction mixture	13
Conditions for an ATRP	16
Surface Initiated ATRP.	19
Liquid Crystals	23
Liquid crystals as fourth state of matter	24
Liquid crystal phases	29
Physical properties of liquid crystals.....	36
References	44
Photoexpansion.....	47
Introduction and Scope	47
Synthesis and Spectroscopic Characterization	50
Thermal Properties, Polarized Optical Microscopy and XRD Characterization.....	57
Photoexpansion and photomechanical effects.....	62
Effects of molecular weight	65
Comparative study between linear and star shaped polymers	67
Conclusions	70
Experimental.....	71
Physico-chemical measurements	71
Materials	73
Synthesis of polymeric derivatives by ATRP.....	73
References	75
Chirality in Azopolymers	77
Introduction	77
Synthesis of monomer and polymers.....	82

Synthesis of 4- ω -methacryloyloxy-hexyloxy-4'-ethoxyazobenzene (M6A) and its polymeric derivatives	87
Synthesis of monomers and polymeric derivatives bearing the chromophore 4'-cyano-4-oxy-azobenzene.....	87
Characterization and photoinduction of chirality.....	93
Polymeric derivatives of (S)-ML6A	93
UV-Vis Spectra and chiroptical properties in solution.	98
UV-Vis spectra and chiroptical properties in thin film.....	100
Photoinduced switching of supramolecular chirality.....	104
Polymeric derivatives of M6A: photoinduction of chirality in achiral azopolymer and photo transition.....	109
UV-Vis properties	110
Chiroptical properties and photoinduced switching of supramolecular chirality	112
4-oxy-4'-cyano-azobenzene containing polymers	115
UV-Vis analysis in solution:	115
Thermal and liquid crystalline characterization.....	116
Chiroptical properties in solution.....	121
Photomodulation of chiroptical properties in thin films	122
Conclusion	126
Experimental Section	127
Physico-chemical measurements:	127
Polymer film preparation, characterization and.....	128
Polymerization of monomer (S)-ML6A	131
Synthesis of monomers and polymeric derivatives bearing the chromophore 4'-cyano-4-oxy-azobenzene.....	133
References	145
Cholesteric polymers.....	149
Introduction.....	149
Monomers synthesis.....	154
Synthesis of the polymeric derivatives	156
Thermal analysis and optical characterization	159
UV-Vis analysis and photochromic properties	164
Chiroptical properties.....	167
Conclusion	170
Experimental part:.....	171

Synthesis of acrylic polymers.....	171
Synthesis of the methacrylic polymeric derivatives	176
References	179
Functionalization of surfaces with polymeric chains	181
Introduction	181
Grafting onto	184
Grafting from.....	184
Functionalization with azoaromatic polymers: photocontrol and chirality.....	186
Introduction	186
Surface Initiated ATRP polymerizations (SI ATRP):	190
Photochromic and photomechanic properties: comparison between spin coated film and brush.	200
Chiroptical properties of brushes of chiral monomers	202
Command surfaces	206
Adaptative surfaces.....	210
Initiator synthesis and SAM formation	212
RATRP of nBA	214
Growth of the mixed brush.....	217
Adaptative surfaces by “grafting onto”	218
Surface modification.....	219
Synthesis of alkyne terminated polymers.....	220
“Grafting onto” and hydrolysis of PtBA chains	222
Surface reorganization.....	224
Conclusions	229
Experimental part	230
Polymerization reaction:.....	232
References	235

Overview

During this work, done mainly in the laboratories of the department of Industrial Chemistry and Materials of the University of Bologna but also in the laboratories of the Carnegie Mellon University in collaboration with prof. K. Matyjaszewski and at the university of Zaragoza in collaboration with prof. J. Barberá, was focused mainly on the synthesis and characterization of new functional polymeric materials.

In the past years our group gained a deep knowledge about the photomodulation of azobenzene containing polymers. The aim of this thesis is to push forward the performances of these materials by the synthesis of well defined materials, in which, by a precise control over the macromolecular structures, better or even new functionality can be delivered to the synthesized material.

For this purpose, besides the rich photochemistry of azoaromatic polymers that brings to the application, the control offered from the recent techniques of controlled radical polymerization, ATRP over all, gives an enormous range of opportunity for the developing of a new generation of functional materials whose properties are determinate not only by the chemical nature of the functional center (e.g. azoaromatic chromophore) but are tuned and even amplified by a synergy with the whole macromolecular structure. Old materials in new structures.

In this contest the work of this thesis was focused mainly on the synthesis and characterization of well defined azoaromatic polymers in order to establish, for the first time, precise structure-properties correlation. In fact a series of well defined different azopolymers, chiral and achiral, with different molecular weight and highly monodisperse were synthesized and their properties were studied, in terms of photoexpansion and photomodulation of chirality. We were then able to study the influence of the macromolecular structure in terms of molecular weight and ramification on the studied properties.

The huge amount of possibility offered by the tailoring of the macromolecular structure were exploited for the synthesis of new cholesteric photochromic polymers that can be used as a smart label for the certification of the thermal history of any thermosensitive product.

Finally the ATRP synthesis allowed us to synthesize a total new class of material, named molecular brushes: a flat surface covered with an ultra thin layer of polymeric chain covalently bond onto the surface from one end. This new class of materials is of extreme interest as they offer the possibility to tune and manage the interaction of the surface with the environment. In this contest we synthesized both azoaromatic surfaces, growing directly the polymer from the surface, and mixed brushes: surfaces covered with incompatible macromolecules. Both type of surfaces acts as “smart” surfaces: the first it is able to move the orientation of a LC cell by simply photomodulation and, thanks to the robustness of the covalent bond, can be used as a command surface overcoming all the limitation due to the dewetting of the active layer. The second type of surface, functionalized by a grafting-to method, can self assemble the topmost layer responding to changed environmental conditions, exposing different functionality according to different environment.

*Chapter 1****Introduction******Atom Transfer Radical Polymerization – ATRP***

Radical polymerization is industrially the most widespread method to produce polymeric materials such as plastics, rubbers and fibers ^[1]. The advantages of radical polymerizations over ionic or coordination polymerizations are numerous: a large variety of vinyl monomers have been polymerized or copolymerized and the reaction conditions require only the absence of oxygen. Water, as in suspension or emulsion polymerization, or other impurities are well tolerated and the reactions occur at a convenient temperature range, typically from 0 to 100°C. The major drawbacks of conventional radical polymerizations are related to the lack of control over the polymer structure. Due to the slow initiation, fast propagation and subsequent transfer or termination, polymers with high molecular weights and high polydispersities are generally produced. These features are reflected in the physical and mechanical properties of the produced polymers and to alter and improve these properties, random copolymerizations have been traditionally used.

The development of ionic polymerization methods allowed for the preparation of well-defined polymers with controlled chain end functionalities and the synthesis of well-defined block and graft copolymers ^[2]. However, these polymerizations have to be carried out with nearly complete exclusion of moisture and often at very low temperatures. Moreover, only a limited number of monomers can be used, and the presence of functionalities in the monomers can cause undesirable side reactions.

A relatively new method to synthesize well-defined polymers and copolymers is controlled radical polymerization ^[3-5]. In this field, several systems have been applied to control molecular weights and end functionalities: iniferters ^[6], nitroxides ^[7-9], Co-based systems^[10, 11], degenerative transfer with alkyl iodides ^[12-14], most recently the RAFT-process^[15], and Ru- ^[16] and Ni-mediated ^[17] polymerizations. One of the most successful methods, however, is atom transfer radical polymerization (ATRP), based on a copper

halide/nitrogen based ligand catalyst^[18, 19]. This controlled radical polymerization allows for the polymerization of a wide range of monomers such as styrenes^[20, 21], acrylates^[22] and methacrylates^[23] including a variety of functional monomers (vide infra). Since ATRP is a controlled/‘living’ radical polymerization, well-defined polymers with molecular weights determined by the ratio of consumed monomer to introduced initiator are obtained, $DP_n = \Delta[M]/[I]_0$, the polydispersities are generally low ($M_w/M_n < 1.3$). Because of its mechanism, ATRP allows for the preparation of more precisely controlled polymers and many new materials have been synthesized^[24]. New materials are made by varying the topology of the polymer (linear, branched, hyperbranched, stars, etc.) and/or the composition of the polymeric chains (statistical/gradient copolymers, block copolymers, grafts, etc.). Moreover, with this process, the end groups of the polymers are well-defined as they derive from the initiator used. As a variety of initiators can be used, including initiators containing functional groups, end functionalities can easily be incorporated^[25].

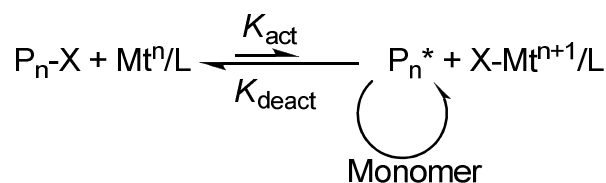
Mechanism

ATRP reactions require the addition, or in situ formation, of four essential components for an ATRP reaction:

- a molecule, which we have called a (macro)initiator, with at least one transferable atom or group, frequently a halogen, R-X, where X = Cl or Br;
- a transition metal (compound),
- a ligand that forms a complex with the transition metal (compound) to modify solubility and catalyst activity,
- one or more radically (co)polymerizable monomers.

One or more of these functions can be combined in a single molecule, e.g. an initiator and monomer, which directly forms a (hyper)branched structure when (co)polymerized.

The general mechanism of ATRP is shown below.



Scheme 1: General mechanism of an ATRP polymerization

Mechanistically, ATRP is based on an inner sphere electron transfer process^[26], which involves a reversible homolytic (pseudo)halogen transfer between a dormant species, an added initiator or the dormant propagating chain end, (P_n-X) and a transition metal complex in the lower oxidation state (Mt^m/L_n) resulting in the formation of propagating radicals (R*)^[27] and the metal complex in the higher oxidation state with a coordinated halide ligand (e.g. X-Mt^{m+1}/L_n).

The active radicals form at a rate constant of activation (k_{act}), subsequently propagate with a rate constant (k_{p}) and reversibly deactivate (k_{deact}), but also terminate (k_{t}). As the reaction progresses, radical termination is diminished as a result of the persistent radical effect, (PRE)^[28], and the equilibrium is strongly shifted towards the dormant species ($k_{\text{act}} \ll k_{\text{deact}}$).

Addition of the persistent radical, $(X-Mt^{m+1}/L_n)$, to the initial reaction medium increases the efficiency of initiation by avoiding the need to form the persistent radical by early stage termination reactions. This results in better polymerization control and higher initiation efficiency.

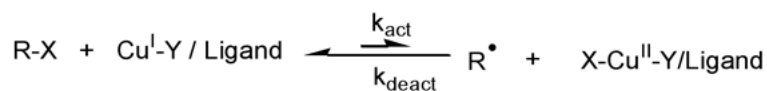
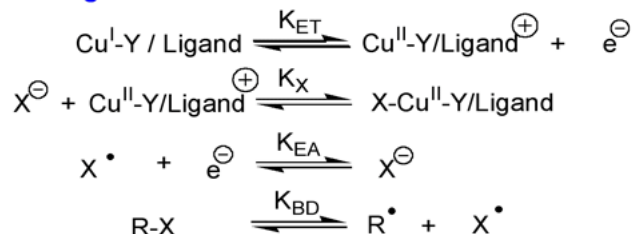
The equilibrium can be approached from both sides:

- a standard or "normal" ATRP starting with RX/Mt_n (an ATRP initiator and a catalyst in a lower oxidation state) ^[18] and,
- a "reverse" ATRP which starts with radicals generated from a standard free radical initiator and the added $X-Mt^{n+1}$ species. Successful polymerizations have been carried out starting with conventional free radical initiators, such as AIBN ^[29] and BPO ^[30] and higher oxidation state transition metal complexes. The higher oxidation state catalyst complex for an ATRP can also be activated by adding Mt^0 , or many other reducing agents, which then reduces the higher oxidation state transition metal complex, $X-Mt^{m+1}/L_n$ to form the $X-Mt^m/L_n$ activator in situ ^[31].

In order to have a well controlled polymerization the rate of activation and deactivation should be faster (at least for one magnitude order) than the propagation rate, otherwise the addition kinetics would follow a pathway similar to a conventional free radical polymerization, with loss of control.

If the above conditions are met and the radical concentration is kept low to minimize the rate of termination reactions (bimolecular reactions) at each cycle just a few monomers are added to the growing chain and the polymerization can run in a controlled fashion.

The total equilibrium described above can be idealized as the sum of other four elementary reactions:

Atom Transfer (Overall Equilibrium)**Contributing Reactions**

$$K_{\text{ATRP}} = \frac{k_{\text{act}}}{k_{\text{deact}}} = K_{\text{ET}}K_{\text{EA}}K_{\text{BD}}K_{\text{X}} \quad \text{or} \quad \frac{K_{\text{ATRP}}}{K_{\text{ET}}K_{\text{EA}}K_{\text{X}}} = K_{\text{BD}}$$

Scheme 2: ATRP equilibrium and elementary reactions

1. Oxidation of the catalytic process, ruled by a electronic transfer constant (K_{ET})
2. Reduction of an halogen atom to an anion, ruled by an electronic affinity constant (K_{EA})
3. Homolitic dissociation of the C-X bond of the (macro)initiator or growing chain (K_{BD})
4. Association of the halogen to the catalytic complex (K_{X})

The ATRP constant therefore can be express as the combination of these equilibriums:

$$K_{\text{ATRP}} = \frac{k_d}{k_a} = K_{\text{ET}}K_{\text{EA}}K_{\text{BD}}K_{\text{X}}$$

In fact it was found a linear correlation between $\log(K_{\text{ATRP}})$ and the redox potential of different catalytic systems with the same halogenophilicity (same K_{D}) with the same K_{BD} and K_{EA} (same initiator and monomer).

It is widely accepted that a controlled polymerization process should display the following features^[5]:

1. First-order Kinetics Behavior
2. Pre-determinable Degree of Polymerization
3. Narrow Molecular Weight Distribution
4. Long-lived Polymer Chains

ATRP kinetics

In agreement with the mechanism described above, neglecting the contribution of the chain termination, and considering a rapid equilibrium the reaction kinetic can be described as:

$$R_p = k_p [M][P^\bullet] = k_p K_{eq} [M][I]_0 \cdot \frac{[Cu^I]}{[Cu^{II}]}$$

The reaction rate is first order kinetic respect to the monomer and the number of growing chains, which depends only on the initiator concentration and on the ratio between activator and deactivator (Cu^I and Cu^{II}).

The polymerization rate (R_p) with respect to the monomer concentration ($[M]$) is a linear function of time. This is due to the lack of termination, so that the concentration of the active propagating species ($[P^*]$) is constant.

$$R_p = \frac{-d[M]}{dt} = k_p [P^*][M]$$

$$\ln \frac{[M]_0}{[M]} k_p [P^*] t = k_p^{app} [P^*] t$$

The consequence of the above equations and the effect of changes in P^* are illustrated in Figure 1

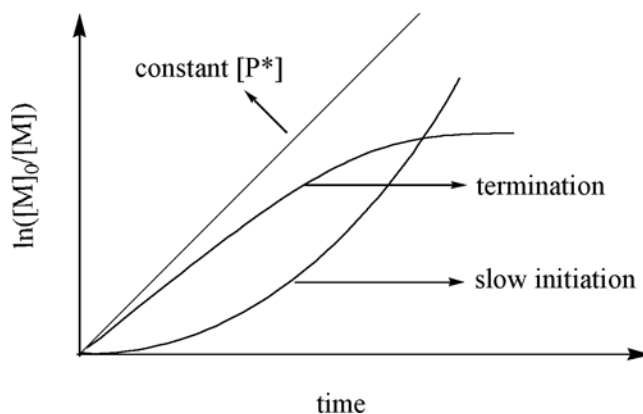


Figure 1 Illustration of the dependence of $\ln([M]_0/[M])$ on time

This semilogarithmic plot is very sensitive to any change of the concentration of the active propagating species. A constant $[P^*]$ is revealed by a straight line. An upward curvature indicates an increase in $[P^*]$, which occurs in case of slow initiation. On the other hand, a downward curvature suggests a decrease in $[P^*]$, which may result from termination reactions increasing the concentration of the persistent radical, or some other side reactions such as the catalytic system being poisoned or redox processes on the radical.

It should also be noted that the semilogarithmic plot is not sensitive to chain transfer processes or slow exchange between different active species, since they do not affect the number of the active propagating species.

Predeterminable degree of polymerization (X_n),

The number average molecular weight (\bar{M}_n) is a linear function of monomer conversion.

$$X_n = \frac{M_n}{M_0} = \frac{\Delta[M]}{[I]_0} = \frac{[M]_0}{[I]_0} (\text{conversion})$$

This result comes from a constant number of chains throughout the polymerization, which requires the following two conditions:

1. that initiation should be sufficiently fast so that nearly all chains start to grow simultaneously;
2. no chain transfer occurs that increases the total number of chains

Figure 2 shows that the ideal growth of molecular weights with conversion, as well as the effects of slow initiation and chain transfer on the molecular weight evolution.

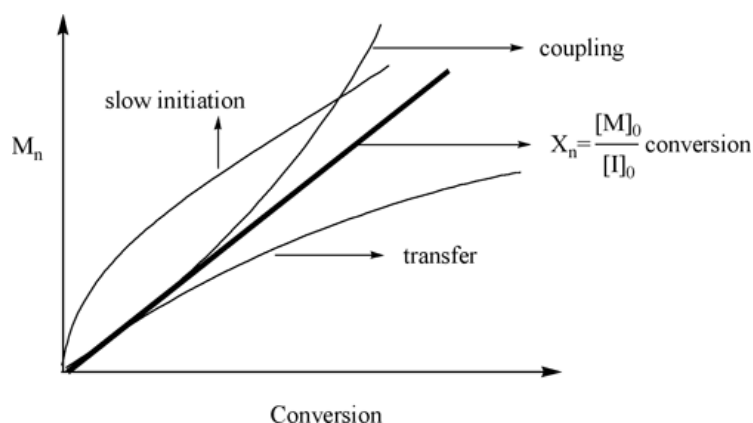


Figure 2: The dependency of molecular weight on conversion

It is important to recognize that the evolution of molecular weight is not very sensitive to chain termination, since the number of chains remains unchanged. The effect of termination is only observable on the plot when coupling reactions for polymers with very high molecular weights start to play a significant role.

Narrow molecular weight distribution

Although this feature is very desirable, it is not necessarily the result of a controlled polymerization, which only requires the absence of chain transfer and termination, but ignores the effect of rate of initiation, exchange and depropagation. Substantial studies ^[32-34] indicate that in order to obtain a polymer with a narrow molecular weight distribution, each of the following five requirements should be fulfilled.

1. ***The rate of initiation is competitive with the rate of propagation.*** This condition allows the simultaneous growth of all the polymer chain.
2. ***The exchange between species of different reactivity is faster than propagation.*** This condition ensures that all the active chain termini are equally susceptible to reaction with monomer for a uniform growth.
3. ***There must be negligible chain transfer or termination.***
4. ***The rate of depropagation is substantially lower than propagation.*** This guarantees that the polymerization is irreversible.
5. ***The system is homogenous and mixing is sufficiently fast.*** Therefore all active centers are introduced at the onset of the polymerization.

This should yield a Poisson distribution, as quantified in equation.

$$\frac{X_w}{X_n} = \frac{M_w}{M_n} = 1 + \frac{X_n}{(X_n + 1)^2} \cong 1 + \frac{1}{X_n}$$

According to equation Eq 1.6, polydispersity (\bar{M}_w/\bar{M}_n) decreases with increasing molecular weight.

Systems with slow exchange do not follow this perfect distribution but PDI's are defined by the following equation^[35].

$$\text{PDI} = \frac{M_w}{M_n} = 1 + \left(\frac{k_p [RX]_0}{k_{deact} [Cu^{II} L_n X]} \right) \left(\frac{2}{conv} - 1 \right)$$

A polymerization that satisfies all five prerequisites listed above is expected to form a final polymer with a polydispersity less than 1.1 for X_n greater than 10.

Long-lived polymer chains.

This is a consequence of negligible chain transfer and termination. Hence, all the chains retain their active centers after the full consumption of the monomer. Propagation resumes upon introduction of additional monomer. This unique feature enables the preparation of block copolymers by sequential monomer addition.

The significance of controlled polymerization as a synthetic tool is widely recognized and polymers having uniform predictable chain length are readily available. Controlled polymerization provides the best opportunity to control the bulk properties of a target material through control of the multitude of possible variations in composition, functionality and topology now attainable at a molecular level.

Through appropriate selection of the functional (macro)initiator, copolymers formed in a "living"/controlled polymerization process can have any desired topology. Further, as noted at the foot of the figure showing what CRP can do, we highlight that mechanistic

transformations permit the use of macroinitiators or macromonomers prepared by other polymerization procedures in any CRP process which allows incorporation of a spectrum of functionalities and polymer segments prepared by any other controlled polymerization process into segments of copolymers prepared by CRP.

Indeed a plethora of previously unattainable polymeric materials have been prepared. Numerous examples of gradient^[36], block^[37] and graft^[38] copolymers have been reported, as well as polymers with complex architectures, including comb shaped polymer brushes^[39], stars^[40], and hyperbranched^[41] copolymers.

Component of the reaction mixture

Initiator

The role of the initiator is to start the polymerization reaction and to determinate the number of growing chain. In a well controlled ATRP reaction, as mentioned above, the medium degree of polymerization is related to the ratio between monomer and initiator and the conversion.

The initiator is a molecule containing a group that can undergoes to homolytic cleavage of the C-X bond and can be reversibly added to the catalytic systems. Usually this group is an halogen atom (Cl or, mainly, Br). In this way at the end of the reaction one end of the polymer is the initiator itself, and on the other end there will still be a reactive halogen atom.

In this way, with an opportune design of the initiator molecule, is pretty easy to synthesize macromolecules bearing a functional end group (e.a.: a fluorescent marker) using a functional initiator.

On the other hand the presence of a reactive halogen end group (in this case mainly bromine end group) can be exploited for the synthesis of block copolymer (see after) or for further post functionalization via substitution reaction. As an example the bromine atom can be substituted by an azide group and therefore the macromolecule can be functionalized via 1,3 dipolar Huisgen cycloaddition (click reaction). This approach demonstrate to be successful for the synthesis of a wide range of hybrid or functional material.

Another important feature of the initiator molecules is to establish the ATRP equilibrium in a very short time, shorter than the time needed for the addition of monomers. This feature is of crucial importance for obtaining a monodisperse polymeric material.

Several functional group can be used as initiator, α -halogen esters are the most used initiator group, also for the possibility of an easy functionalization of the initiator molecule with a suitable moiety.

For the synthesis of highly complex architectures (e.a. star polymers, hyperbranched or bottle-brush polymer) suitable initiator should be used. In Figure 3 are depicted a multifunctional initiator for the synthesis of star polymers, reactive polymers for brush bottle macromolecules and monomers bearing an initiating group for the synthesis of hyperbranched polymers. Moreover the choice of a engineered initiator can be a simple and smart choice to introduce at one end of the polymeric chain a tailored functionality as a florescent marker (e.g. rhodamine B, Figure 3)

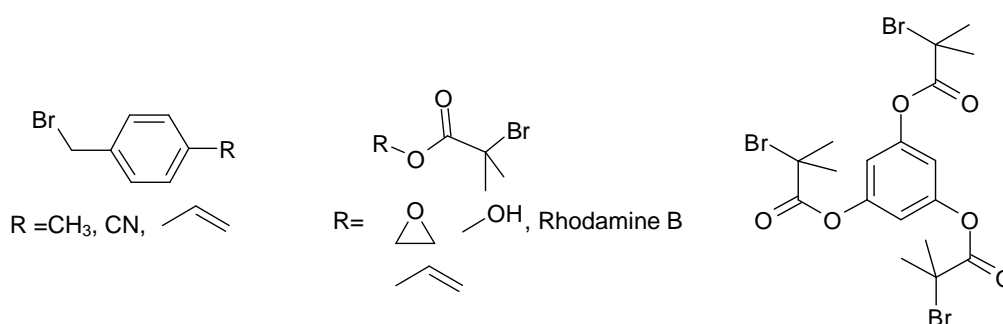


Figure 3: various initiator for an ATRP polymerization

Catalyst

The instaurance of the ATRP equilibrium, between the capped and the radical form of the growing chains is determined by the catalyst. In order to have a controlled polymerization, as mentioned above, a low concentration of radical should be present (to minimize the termination) and the rate of activation and deactivation should be as fast as possible (to enable all the chains to grow simultaneously).

In order to use a metal as the catalyst center some requirement should be met:

- the metal should have two stable oxidation state with only one electron of difference
- the metal center should have an high halogenophilicity (high K_D) and the coordination number should increase of one in the high oxidation state
- should be highly selective for the desired process avoiding side reaction
- should form a stable complex with the used ligand

Therefore are used catalyst based on transition metals, in which the ligand plays an important role to tailor the activity and selectivity of the catalyst.

A wide number of metals can be used, mainly from 6 to 11 group, but the most used is copper, for its low cost and versatility. The copper has two different stable oxidation state Cu^{I} and Cu^{II} separated by only one electron and possess all the characteristics mentioned above.

Anyway other metals are studied, in particular ruthenium and iron, which are of great interest for the polymerization of acidic monomers, as acrylic acid, which can poison the copper catalyst and up to now cannot be polymerized via ATRP.

As said above the catalytic system is composed by the transition metal and the ligand. Of course different metals are associated with different ligand; we are going to examine the ligands used for copper.

The main role of the ligand in an ATRP reaction is to increase the solubility of the metal and to tailor its redox potential in order to model its activity. It was shown that activity increase using aliphatic amines instead of aromatic, and that the use of multidentated ligand and a C-2 bridge between nitrogen atoms increase activity.

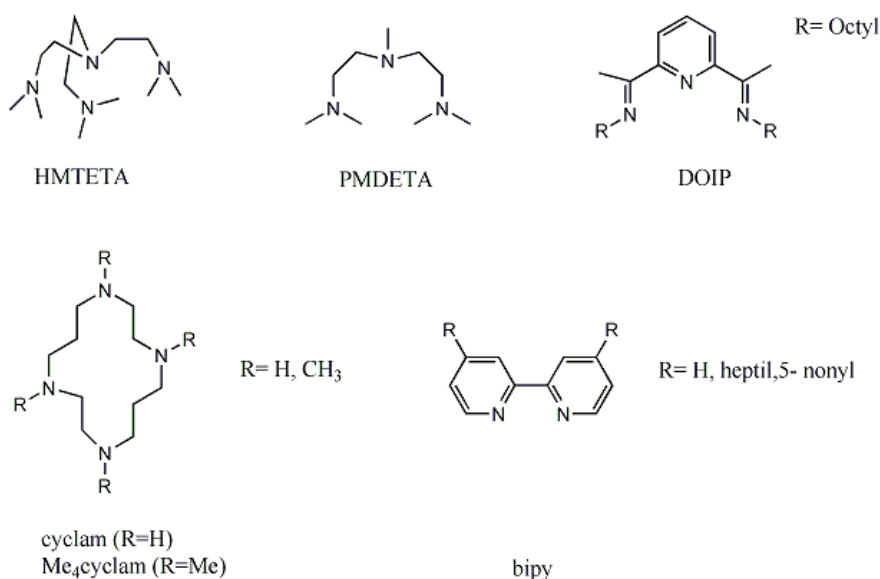


Figure 4: Typical ligand for ATRP Cu based catalyst

Conditions for an ATRP

ATRP reactions are highly versatile, are quite robust towards impurity and therefore can be carried out in several ways, both in solution, bulk or in heterogeneous system as emulsion, microemulsion or suspension. Several solvents can be used, apolar as toluene or benzene or polar as DMF or THF, or even protic solvent as water or ethanol.

Normal ATRP

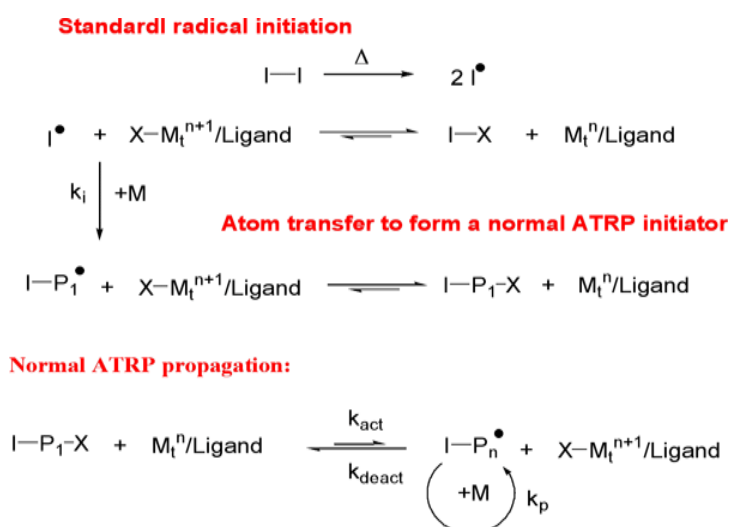
Usually to carry out an ATRP the only precaution that should be taken is to deoxygenate the system prior to add the Cu(I) which is highly sensitive to air and rapidly oxidized to Cu(II). No further precaution should be taken.

In this way the equilibrium is reached as described before and the reaction goes through the pathway mentioned above.

Reverse ATRP

In this procedure a complex of the metal in the higher oxidation state is added to the solution of monomer and initiator. The catalyst is generated *in situ* by decomposition of a conventional thermal initiator such as AIBN. The advantage is that the components are insensitive to air and can be handled easier, making this process more attractive for industrial process.

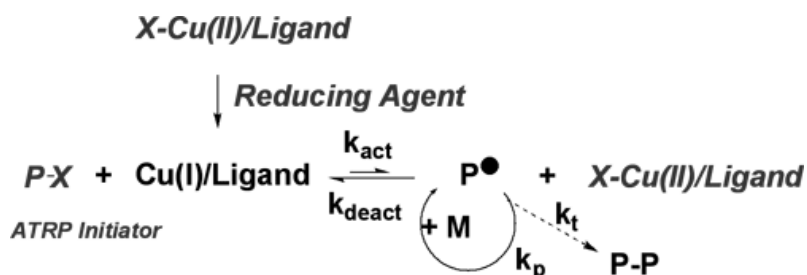
The disadvantage is that the terminations are not anymore uniform, being generated by the thermal initiator and the early growing chains.



Scheme 3 RARTP mechanism

Activator Generated by Electron Transfer, AGET ATRP

This procedure is similar to reverse ATRP, in fact in the systems only monomer, ATRP initiator, and the catalyst in the high oxidation state are present. The activator is generated in situ by the action of a reducing agent (e.g.: ascorbic acid or *tin*(II) 2-ethylhexanoate) which is able to reduce the metal catalyst but cannot generate radicals and therefore cannot start polymerization. This procedure has the advantage, in comparison with Reverse ATRP, to produce polymers with well defined end group.



Scheme 4: AGET ATRP mechanism

ARGET ATRP

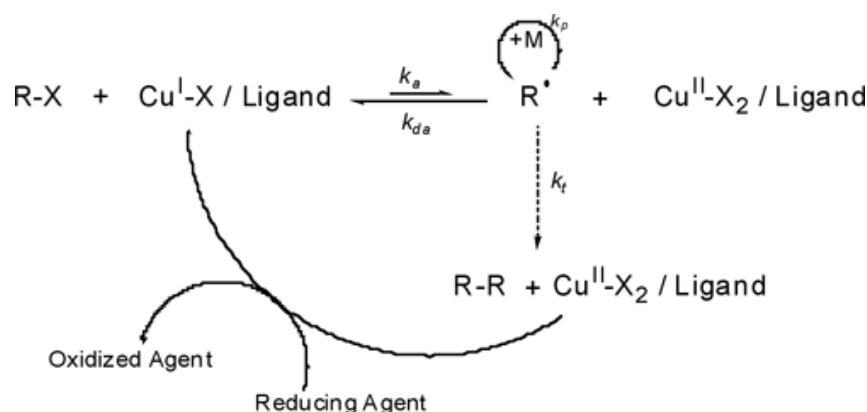
Catalysts have been developed that show a broad range of activity. It is possible, therefore, to select an active catalyst and run the reaction with lower levels of catalyst^[42, 43]. Indeed with an extension of the concept of AGET ATRP^[44] to include continuous regeneration of the transition metal complex throughout the reaction, ARGET ATRP^[43-46], it is possible to reduce the level of catalyst below that of natural termination reactions and ATRP can be conducted with ppm levels of catalyst. ARGET ATRP arose when we considered the implications of the convenient procedure for initiating an ATRP system described in AGET ATRP, where the activators are generated by electron transfer (AGET) ATRP. It should be possible to use the reducing agents to constantly regenerate the ATRP activator, the Cu(I) species, from the Cu(II) species, formed during termination process, without directly or indirectly producing initiating species that generate new chains. A detailed examination of the ATRP rate law shows that the polymerization rate depends only on the ratio of the concentration of Cu(I) to X-Cu(II), and does not depend on the absolute concentration of the copper complexes, therefore in principle, one could reduce the absolute amount of copper complex to ppm levels without affecting the polymerization rate.

$$R_p = k_p [M][P^*] = k_p [M] K_{eq} [I]_0 \frac{[Cu^I]}{[X-Cu^{II}]}$$

However, a residual amount of deactivating species (i.e. X-Cu(II)) is required for a well-controlled polymerization since both, molecular weight distribution and initial molecular weight, depend on the ratio of the propagation and deactivation rate constants and the concentration of deactivator.

$$PDI = \frac{M_w}{M_n} = 1 + \left(\frac{k_p [RX]_0}{k_{deact} [Cu^{II} L_n X]} \right) \left(\frac{2}{conv} - 1 \right)$$

This means that in order to obtain polystyrene with $M_w/M_n \sim 1.2$, when targeting a $DP \sim 200$ and 90% conversion at ~ 100 °C, the actual amount of X-Cu(II) species required to conduct a controlled reaction is ~ 2 ppm, meaning that it could be reduced over 1,000 times from the level typically used in the initial ATRP of styrene. Unfortunately, if the amount of Cu(I) is reduced 1,000 fold, unavoidable radical-radical termination reactions irreversibly consume all of the activators present in the reaction media and the reactions stops; i.e. if the amount of Cu(I) initially added to the system was below 10 mole% of the initiator (i.e., all Cu(I) would be consumed if 10% of chains terminate). However, this situation could be overcome if there was constant regeneration of the Cu(I) activator species by environmentally acceptable reducing agents to compensate for any loss of Cu(I) by termination.



Scheme 5: ARGET ATRP mechanism

Generally, it is desirable to add an excess of the ligands compared to the transition metal complex, in order to compensate for competitive complexation by monomer/solvent/reducing agent all present in excess compared to the transition metal^[44, 47, 48]. For example, styrene was polymerized by the addition of 5 ppm of CuCl₂/Me₆TREN and 500 ppm of Sn(EH)₂ to the reaction resulting in a polystyrene with Mn=12,500 (Mn,th = 12,600) and Mw/Mn = 1.28.

An added advantage of using low levels of catalyst is that catalyst induced side reactions are reduced and it is possible to prepare high molecular weight copolymers^[48] and conduct the reaction in the presence of limited amounts of oxygen^[49]. However ARGET is not the answer to all problems since the impact of the by products of the reduction reaction have to be considered.

Surface Initiated ATRP.

The functionalization of organic and inorganic surfaces with polymeric chains is a topic of extreme scientific interest for the numerous applications in the field of material science, biomedicine and for the fabrication of electronic devices.

This kind of functionalization can be made in two ways: starting the polymerization from functional groups anchored on the surface (grafting from) or by a functionalization of the surface with telechelic polymeric chains (grafting to).

With both approach is possible to obtain a coverage of the surface with polymeric chains, but with the former is possible to have higher grafting densities and smoother surfaces. If the lateral separation between adjacent chains is smaller than the gyration radius the chains are forced to adopt an extended conformation (brush) and not the usual random coil. This organization led to new properties of the polymeric layer such as extra low friction, higher glass transition and different supramolecular organization.

Grafting onto

The functionalization of surface is made by anchoring a telechelic polymer to the surface. ATRP is very functional for this approach because the functionality can be easily incorporate in the initiator (e.g.: a propargyl containing initiator) or can be introduced in the

polymeric chain by post functionalization (e.g.: substitution of the terminal bromine atom with an azide group). The polymeric chain is then reacted with functional group on the surface. In fact this scheme is very reproducible and has the great advantage of a extreme control over the polymers composition.

As an example we can report the grafting of polystyrene (PS) chains onto silica nanoparticles. In the first case an alkyne terminated PS synthesized by ATRP is grafted via click chemistry onto silica nanoparticles previously modified with an azide containing silane [50].

In a second example silica nanoparticles were modified with a layer of a silane bearing a benzophenone residue. PS chains were then attached by fotoreaction. In this case, anyway, it was not possible to obtain a well defined monolayer of PS^[51].

Anyway with this approach is quite difficult to obtain a dense layer of polymer chains. In fact there is a high entropic barrier to overcome for the polymeric chains to adopt an extended conformation loosing the random coil. Moreover, if the grafting is made in solution, also the solvation energy plays an important role, because before the grafting (that is thermodynamically favorite) the chain should be desolvated and adsorbed on the surface. As a consequence grafting densities higher than 0.15 chains nm⁻² are quite impossible to obtain with this method.

Grafting from

The grafting from method is very useful for obtaining a very dense polymeric layer. With this approach the surface is functionalized with an ATRP initiating group using a suitable chemistry to graft it onto the surface (e.g.: silane for the functionalization of silicon or metal oxides, thiol for gold) and then the polymerization is started on the surface. In this way no entropic barrier have to be overcome and thus the synthesis of layer with a grafting densities up to 1 chain nm⁻² is possible.

Modification of flat surfaces.

The first step is the formation of a monolayer of initiator. This can be done using a proper initiator with an anchoring site as ethoxy or chloro silane for silica or thiol or disulfide for gold.

The amount of initiator anchored on the surface is, anyway, extremely small (calculated to be 10⁻⁷ mol/L), in comparison with the amount of initiator usually used in a

conventional polymerization. As a consequence no control over the polymerization in a surface initiated ATRP (SI-ATRP) can be achieved: due to the persistent radical effect in fact the ATRP equilibrium cannot be reached and so the polymerization will not be a controlled process but will be a conventional free radical polymerization with a redox initiator.

In order to have a good control over the polymerization we should permit the formation of the persistent radical. This can be made in two ways:

- by addition of free initiator: some termination will occur in the bulk of the reaction leading to the formation of the necessary Cu(II) and then a control over the polymerization will be possible.
- by the addition of the Cu(II) ligand complex (persistent radical). In this way the ATRP equilibrium will be present from the beginning of the reaction.

These two different methods have both some advantages and drawbacks. In the first case the formation of polymer in solution is helpful for the characterization of the chains grown on the surface, as is usually accepted that the polymer grown in solution and on the surface are identical. In the latter case the advantage is that no polymer will be formed in solution, making not necessary the purification of the surfaces from the adsorbed polymer. Moreover in the case of expensive functional monomer none will be lost and the unreacted monomer can be reused after purification from the catalyst.

Modification of nanoparticles

By the grafting from method also nanoparticles have been functionalized. The reaction procedure is quite similar to the functionalization of flat surfaces, but some slight difference can be found.

First of all for this kind of polymerization the choice between the addition of free initiator and deactivator should be taken first considering the purification of the modified particles. In fact if the size of the nanoparticles is too small the purification from the free polymer can be quite difficult and then the addition of deactivator will be preferred. On the other side it was observed that for particles too big^[52] the use of deactivator is not efficient as the ratio initiator/monomer is too low. In this case the addition of free initiator should be preferred, as the purification of big particles is quite easy.

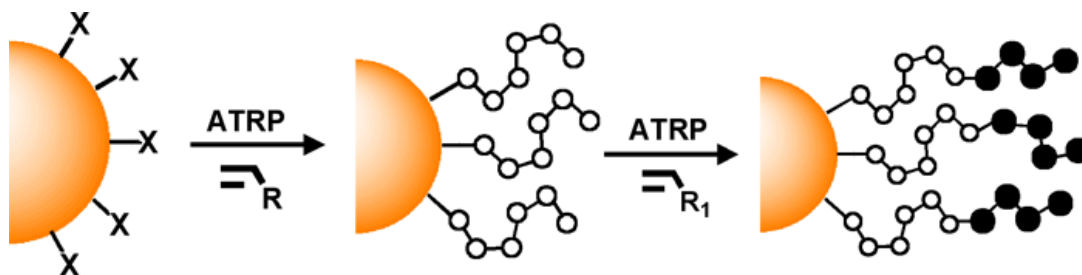


Figure 5: Modification of nanoparticles by SI-ATRP

Is also possible to use the polymer modified nanoparticles as macroinitiator for a second polymerization, synthesizing a block copolymer bound to the surface of the nanoparticles. In this way colloids consisting of an inorganic core and a shell made of polymethyl methacrylate, polystyrene or polybutylacrylate were synthesized^[53].

Liquid Crystals

The discovery of liquid crystals is thought to have occurred nearly 150 years ago although its significance was not fully understood until over a hundred years later. Around the middle of the last century Virchow, Mettenheimer and Valentin found that the nerve fiber they were studying formed a fluid substance when left in water, which exhibited a strange behavior when viewed using polarized light. They did not realize this was a different phase but they are attributed with the first observation of liquid crystals.

Later, in 1877, Otto Lehmann used a polarizing microscope with a heated stage to investigate the phase transitions of various substances. He found that one substance would change from a clear liquid to a cloudy liquid before crystallizing but he thought that this was simply an imperfect phase transition from liquid to crystalline. In 1888 Reinitzer^[54] observed that a material known as cholesteryl benzoate had two distinct melting points. In his experiments, Reinitzer increased the temperature of a solid sample and watched the crystal change into a hazy liquid. As he increased the temperature further, the material changed again into a clear, transparent liquid. Because of this early work, Reinitzer is often credited with discovering a new phase of matter. He has consequently been given the credit for the discovery of the liquid crystalline phase. Up till 1890 all the liquid crystalline substances that had been investigated, had been naturally occurring and it was then that the first synthetic liquid crystal, p- azoxyanisole, was produced by Gatterman and Ritschke. Subsequently more liquid crystals were synthesized and it is now possible to produce liquid crystals with specific predetermined material properties.

In the beginning of this century George Freidel conducted many experiments on liquid crystals and he explained the orienting effect of electric fields and the presence of defects in liquid crystals. In 1922 he proposed a classification of liquid crystals based upon the different molecular orderings of each substance. It was between 1922 and the World War II that Oseen and Zocher developed a mathematical basis for the study of liquid crystals^[55, 56].

After the start of the war many scientists believed that the important features of liquid crystals had been already discovered and it was not until the 1950's that work by Brown in America, Chistiakoff in the Soviet Union and Gray and Frank in England led to a revival of interest in liquid crystals. Maier and Saupe^[57] formulated a microscopic theory of liquid crystals; Frank^[58] and later Leslie^[59] and Ericksen^[60] developed continuum theories for

static and dynamic systems and in 1968 scientists from RCA first demonstrated a liquid crystal display. The interest in the study of liquid crystals has grown ever since, partly due to the great variety of phenomena exhibited by liquid crystals and partly because of the enormous commercial interest and importance of liquid crystal displays. As research on this field continues and as new applications are developed, the role of liquid crystals in modern technology will continue to grow.

Liquid crystals as fourth state of matter

The three common states of the matter: solid, liquid and gas, are different because the molecules in each state have a different degree of order. In the solid state there exists a rigid arrangement of molecules, which stay in fixed positions and orientations with a small amount of variation due to molecular vibrations. To maintain this arrangement, large attractive forces are required to hold the molecules in piece and therefore a solid is difficult to deform.

In the liquid phase the molecules have no fixed positions or orientations and are free to move in a random fashion; consequently, the liquid state has less order than the solid state. The random motions of the molecules mean that the intermolecular attractive forces are not strong as in solids but are only strong enough to keep the liquid molecules fairly close together. A liquid can therefore be easily deformed.

In the gas state the random motion of the molecules overcomes the intermolecular forces, and the molecules spread out to fill any container that holds them. The order in a liquid, which derives from the closeness of the molecules, is lost in a gas. The probability of molecules in a certain region being in a rigid arrangement, and having the same orientation can be used to define a positional and orientational order. These parameters have the greatest value in the solid state and the least one in the gaseous state.

A liquid crystalline phase occurs in some substances in a temperature region between the solid and liquid states. In this state the substance possesses properties of both liquids and solids. A liquid crystal is a fluid like a liquid but it is anisotropic, in its optical and electromagnetic characteristics, like a solid. When the liquid crystal is formed from the isotropic state, some amount of positional or orientational order is gained. It is this order that accounts for the anisotropies of the substance. The distinguishing characteristic of the liquid crystalline state is the tendency of the molecules (mesogens) to point along a common axis, called the director. This is in contrast to molecules in the liquid phase, which have no intrinsic order. In

the solid state, molecules are highly ordered and have little translational freedom. The characteristic orientational order of the liquid crystal state is between the traditional solid and liquid phases and this is the origin of the term mesogenic state, used synonymously with liquid crystal state. Note the average alignment of the molecules for each phase (Figure 5):

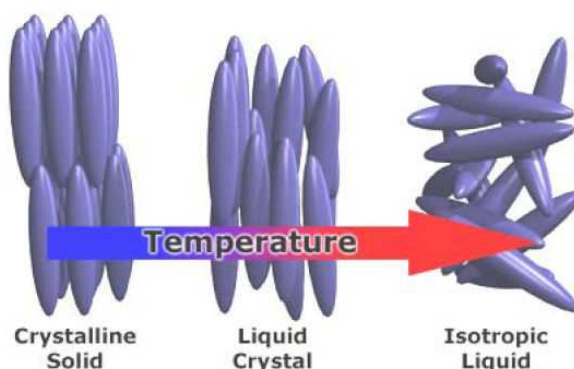


Figure 6 Average alignment of the molecules: a) solid phase, b) liquid crystal phase, c) liquid phase.

It is sometimes difficult to determine whether a material is in a crystal or liquid crystal state. Crystalline materials demonstrate long range periodic order in three dimensions^[61]. By definition, an isotropic liquid has no orientational order.

Substances that are not as ordered as a solid, yet have some degree of alignment, are thus properly called liquid crystals. Liquid crystals can be classified into two main categories:

- thermotropic liquid crystals;
- lyotropic liquid crystals.

While these two types of liquid crystals are distinguished by the mechanisms that drive their self-organization, they are similar in many ways. Thermotropic transitions occur in most liquid crystals, and they are defined by the fact that the transitions to the liquid crystalline state are thermally induced. That is, one can arrive at the liquid crystalline state by raising the temperature of a solid *and/or* lowering the temperature of a liquid. Thermotropic liquid crystals can be classified into two types: enantiotropic liquid crystals, which can be changed into the liquid crystal state from either lowering the temperature of a liquid or raising of the temperature of a solid, and monotropic liquid crystals, which can only be changed into the liquid crystal state from either an increase in the temperature of a solid or a decrease in the

temperature of a liquid, but not both. In general, thermotropic mesophases occur because of anisotropic dispersion forces between the molecules and because of packing interactions [62, 63].

There are mainly two types of mesogenic molecules which can originate thermotropic liquid crystals: discotics and rod-shaped molecules.

Discotics are flat disc-like molecules consisting of a core of adjacent aromatic rings. This allows for two-dimensional columnar ordering. Rod-shaped molecules have an elongated, anisotropic geometry, which allows for preferential alignment along one spatial direction.

As showed in Figure 7, rod-like molecules (a) organize themselves into layers, whereas disc-like molecules (b) form columns that can be arranged parallel to each other in a two-dimensional lattice.

A bend introduced in the rigid core leads to 'banana-shaped' molecules (c). The rotation of these molecules around their long axis is restricted and they adopt a directed order within the layers. Depending on the bending direction in adjacent layers, either antiferroelectric or ferroelectric smectic phases may result.

Molecules with a conical shape (d) can lead to a polar order within columns.

The polar direction of neighbouring columns may be parallel or anti-parallel.

Sawamura [64] have made a 'shuttlecock-shaped' molecule (e) based on the C60 molecule, whose distinctive shape leads to directed organization in columns [65].

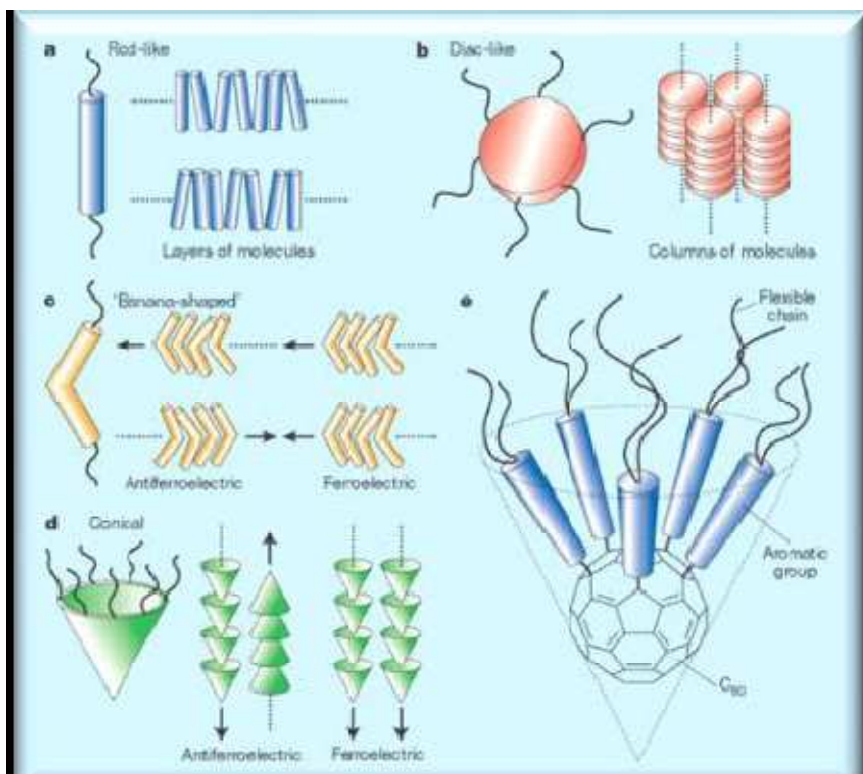


Figure 7 Shape-depending organization of Liquid crystal molecules

In contrast to thermotropic mesophases, lyotropic liquid crystal transitions occur both by the influence of solvents, and by change in temperature (Figure 8).

Lyotropic mesophases occur as a result of solvent-induced aggregation of the constituent mesogens into anisotropic micellar structures. Lyotropic mesogens are typically amphiphilic, meaning that they are composed of both lyophilic (solvent-attracting) and lyophobic (solvent-repelling) parts. This causes them to form micellar structures in the presence of a solvent, since the lyophobic ends will collect together, out of the solvent environment. As the concentration of the solution is increased and the solution is cooled, the micelles increase in size and eventually coalesce. This process separates the newly formed liquid crystalline state from the solvent. A very large number of chemical compounds are known to exhibit one or several liquid crystalline phases. Despite significant differences in chemical composition, these molecules have some common features such as anisotropy of molecular shape and physical properties^[66].

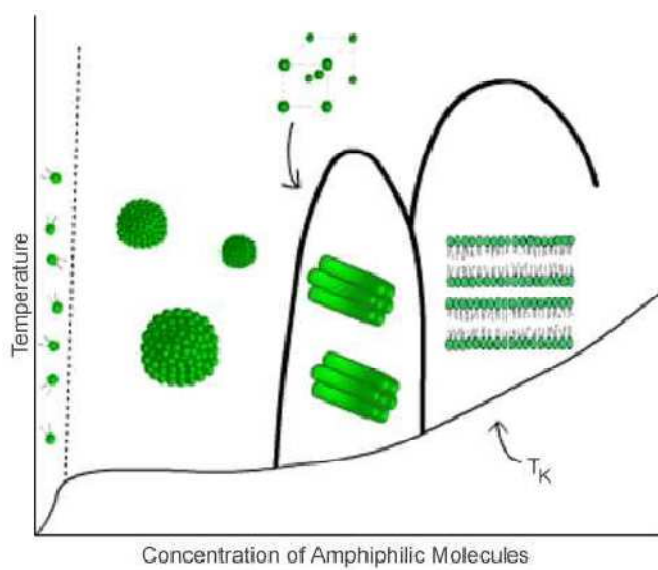


Figure 8: Lyotropic mesophases depending on the Temperature and amphiphile concentration

Liquid crystal phases ^[67]

Most liquid crystal compounds exhibit polymorphism, or a condition where more than one phase is observed in the liquid crystalline state. The term mesophase is used to describe the "subphases" of liquid crystal materials.

Mesophases are formed by changing the amount of order in the sample, either by imposing order in only one or two dimensions, or by allowing the molecules to have a degree of translational motion ^[68].

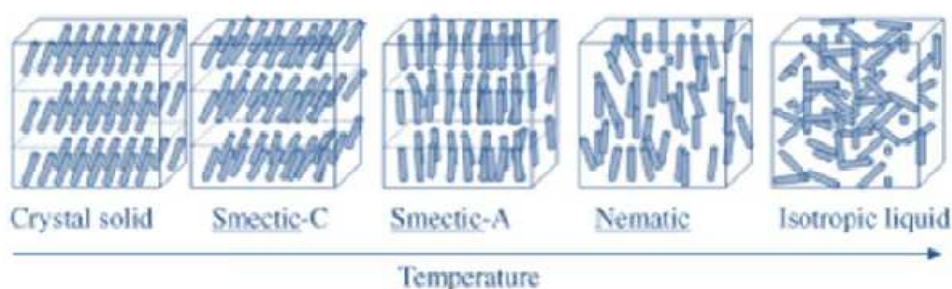


Figure 9: Schematic representation of the liquid crystal phases for rod-like molecules

Nematic liquid crystal phase

It is characterized by molecules that have no positional order but tend to point in the same direction (Figure 9). This reordering is thought to be due to the packing constraints of the molecules. This claim is supported by the fact that most liquid crystal molecules tend to be long thin molecules with a rigid central region.

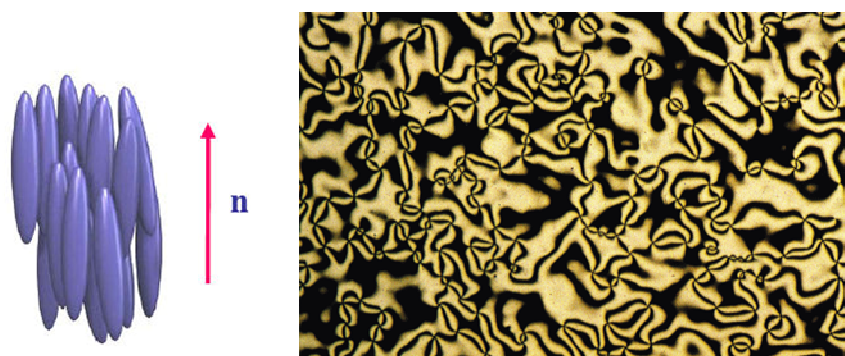


Figure 10: Schematic representation of the nematic mesophase(left) and typical texture corresponding, showed by Polarized Optical Microscopy(right)

Molecules in this phase possess three degree of translational freedom, and they can move in all the directions. The viscosity of the nematic liquid crystals is similar to that of the isotropic liquid.

Smectic liquid crystal phase

The smectic state is another distinct mesophase present in some liquid crystal substances. Molecules in this phase show a degree of translational state not present in the nematic. In the smectic state, the molecules maintain the general orientational order of nematics, but in addition tend to align themselves in layers or planes. Motion is restricted to within these planes, and separate planes are observed to flow past each other. Within each layer the liquid crystal is essentially a two dimensional nematic liquid crystal. The increased order means that the smectic state is more "solid-like" than the nematic. This positional ordering may be described in terms of the density of the mass centers of the molecules:

$$\rho(z) = \rho_0 \left[1 + \psi \cos \left(\frac{2\pi z}{d} \right) \right]$$

where z is the coordinate parallel to the layer normal; the average density of the fluid is ρ_0 , d is the distance between layers and ψ is the order parameter. When $|\psi|=0$ there is no layering and the material is nematic, but if $|\psi|>0$ then some amount of sinusoidal layering exists and the material is smectic. There are many types of smectic materials^[69]. In particular, in the smectic-A mesophase, the director is perpendicular to the smectic plane, and there is no particular positional order in the layer (Figure 11a).

In the smectic-C mesophase (Figure 11b), molecules are arranged as in the smectic-A mesophase, but the director is at a constant tilt angle measured normally to the smectic plane. In some smectic materials, called Sm-CA (Figure 10c) or Anti-Ferroelectric Liquid Crystal (AFLC), the direction of this tilt may alternate to form a so called "herringbone structure". Smectic materials have potential advantages over nematics when used in liquid crystal displays. They exhibit better viewing angle characteristics, contrast ratio and can operate at high speed.

Similarly, the smectic-B mesophase (Figure 10d) orients with the director perpendicular to the smectic plane, but the molecules are arranged into a network of hexagons within the layer.

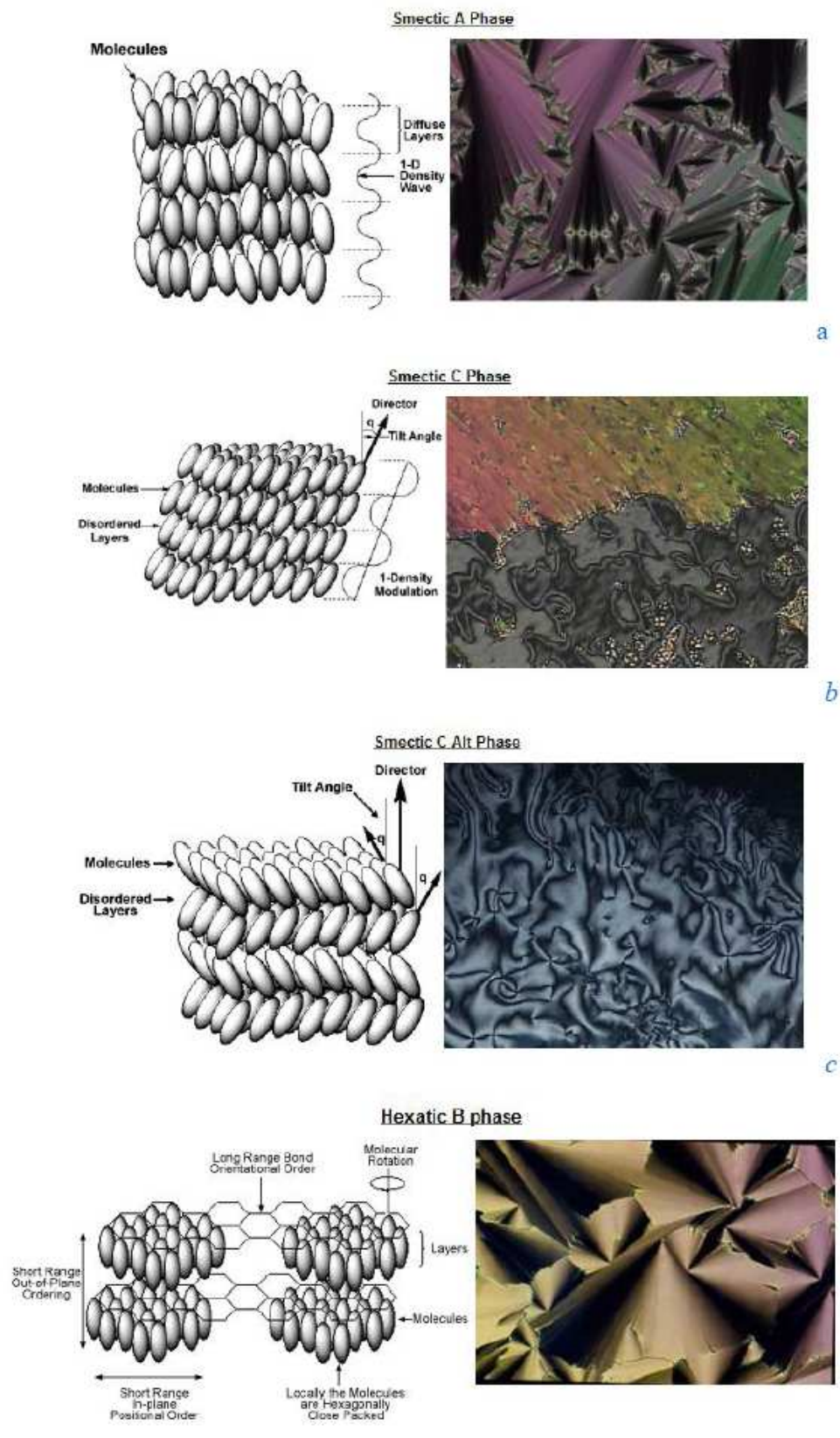


Figure 11: Smectic A (a), Smectic C(b), Smectic CA (c) and (Hexatic) Smectic B phases (d)

Chiral nematic liquid crystal phase

This phase is typically composed of nematic mesogenic molecules containing a chiral center which produces intermolecular forces that favor alignment between molecules at a slight angle to one another. This leads to the formation of a structure which can be visualized as a stack of very thin 2-D nematic-like layers with the director in each layer twisted with respect to those above and below.

This induces a helical director configuration in which the director rotates through the material (Figure 12). The molecules shown are merely representations of the many chiral nematic mesogens lying in the slabs of infinitesimal thickness with a distribution of orientation around the director. This is not to be confused with the planar arrangement found in smectic mesophases.

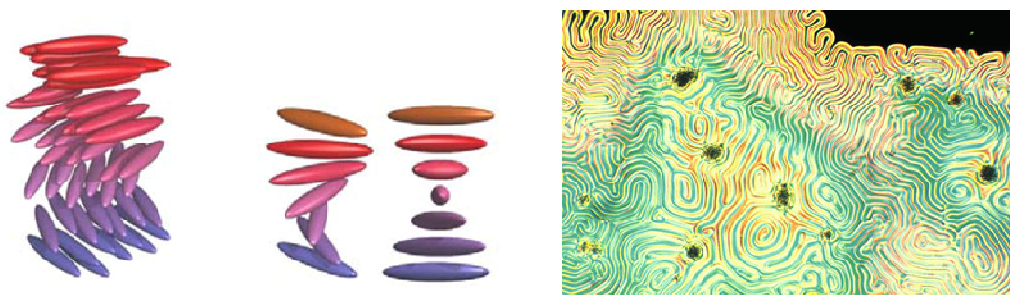


Figure 12: Schematic view of the helical director configuration and mesophase microphotograph between crossed polarized.

Mesophases having this type of structure are called cholesteric mesophases. An important characteristic of the cholesteric mesophase is the pitch, p , which is defined as the distance the director rotates one full turn in the helix (Figure 12). A by-product of the helical structure of the chiral nematic phase is its ability to selectively reflect light of wavelengths equal to the pitch length, so that a color will be reflected when the pitch is equal to the corresponding wavelength of light in the visible spectrum. Due to this phenomenon, cholesterics change color when the temperature changes. The effect is based on the temperature dependence of the gradual change in director orientation between successive layers, which modifies the pitch length resulting in an alteration of the wavelength of reflected light according to the temperature. The angle at which the director changes, can be made

larger, and thus tighten the pitch, by increasing the temperature of the molecules, hence giving them more thermal energy.

Similarly, decreasing the temperature of the molecules increases the pitch length of the chiral nematic liquid crystal. This makes it possible to build a liquid crystal thermometer that displays the temperature of its environment by the reflected color. Mixtures of various types of these liquid crystals are often used to create sensors with a wide variety of responses to temperature change.

Such sensors are used for thermometers often in the form of heat sensitive films. In the fabrication of films, since putting chiral nematic liquid crystals directly on a black background would lead to degradation and perhaps contamination, the crystals are micro-encapsulated into particles of very small dimensions. The particles are then treated with a binding material that will shrink upon curing so as to flatten the microcapsules and produce the best alignment for brighter colors. Adjusting the chemical composition can also control the wavelength of the reflected light, since cholesterics can either consist of exclusively chiral molecules or of nematic molecules with a chiral dopant dispersed throughout. In this case, the dopant concentration is used to adjust the chirality and thus the pitch.

Chiral smectics liquid crystal phase

In a similar way to chiral nematics there are chiral forms of smectic phases.

Figure 13 shows schematically a chiral smectic C material, denoted by smectic-C*. Consistent with the smectic-C, the director makes a tilt angle with respect to the smectic layer. The difference is that this angle rotates from layer to layer forming a helical structure. In other words, the director of the smectic-C* mesophase is not parallel or perpendicular to the layers, and it rotates from one layer to the next (Figure 14).

This helix may be suppressed by placing the liquid crystal in a cell where the material is sandwiched between two glass plates. Such systems are said to be surface stabilized. Once the helix is suppressed and the directors in each layer are forced to lie in the plane of the glass plates the chiral nature of the molecules creates a spontaneous polarization within each layer.

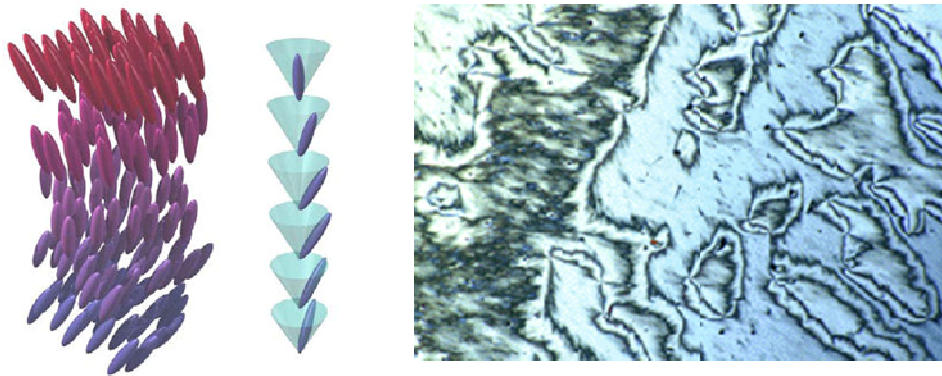


Figure 13: Director tilt in smectic-C* phase

In some smectic mesophases, the molecules are affected by the various layers above and below them. Therefore, a small amount of three-dimensional order is observed. The Smectic-G phase is an example demonstrating this type of arrangement (Figure 15)

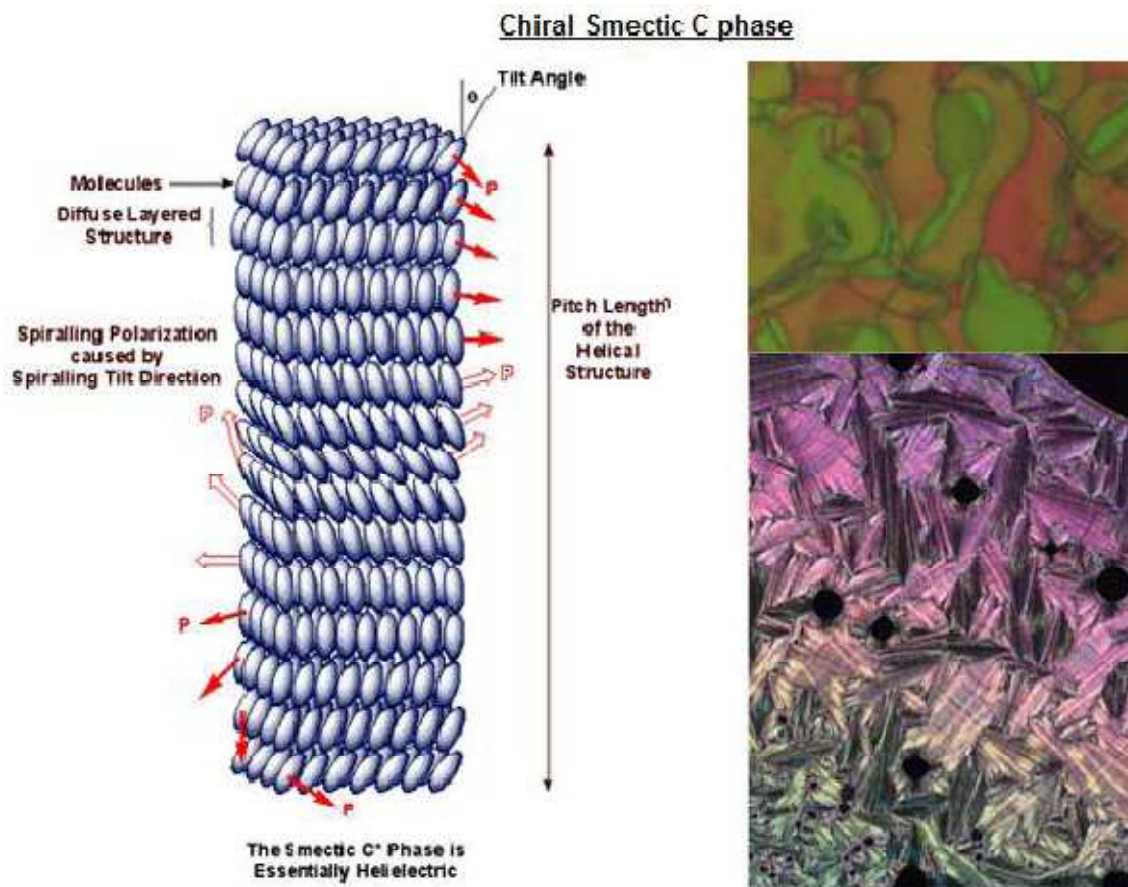


Figure 14: Smectic C* structure and texture

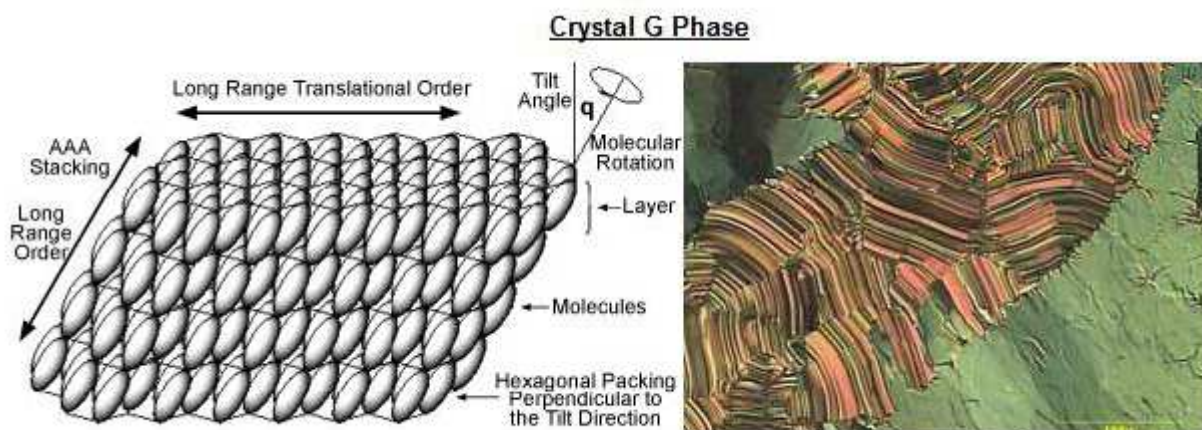


Figure 15: Crystal G phase structure and texture

Columnar liquid crystals phases

These phases are different from the previous types because they are shaped like disks instead of long rods. This mesophase is characterized by stacked columns of molecules (Figure 16). The columns are packed together to form a two-dimensional crystalline array. The arrangement of the molecules within the columns and the arrangement of the columns themselves leads to new mesophases.

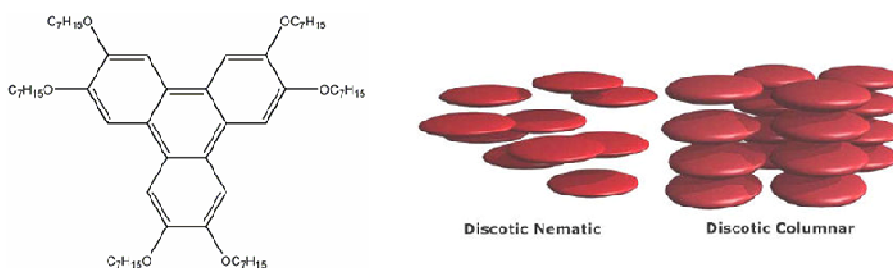


Figure 17: Columnar liquid crystal phase.

Physical properties of liquid crystals

The physical behavior of liquid crystals can be divided into scalar and non scalar properties. A typical scalar property is the orientational order parameter S .

Important non scalar properties are the dielectric, diamagnetic, optical, and elastic coefficients.

Orientational order parameter

To quantify just how much order is present in a liquid crystal material, an order parameter (S) is defined. Traditionally, the order parameter is given as follows:

$$S = \frac{1}{2} \langle 3\cos^2\theta - 1 \rangle$$

In this equation θ is the angle between the axis of an individual molecule and the director of the liquid crystal. The brackets denote an average over all of the molecules in the sample (Figure 17).

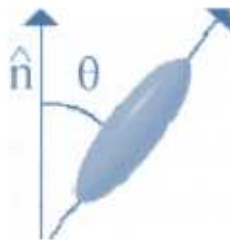


Figure 17: Tilt angle between the molecular axis and the director \hat{n} .

In an isotropic liquid, where all the orientations are possible, the average of the cosine terms is zero, and therefore the order parameter is equal to zero. For a perfect crystal, the order parameter evaluates to one. Typical values for the order parameter of a liquid crystal range between 0.3 and 0.9, with the exact value a function of temperature, as a result of kinetic molecular motion.

When the molecular symmetry is not perfectly cylindrical, as in a real nematic liquid crystal, the order parameter becomes a matrix whose generic element is ^[70]:

$$S_{ij}^{\alpha\beta} = \frac{1}{2} \langle 3\cos\vartheta_{ij} \cos\vartheta_{i\beta} - \delta_{ij}\delta_{\alpha\beta} \rangle$$

where ij and $\alpha\beta$ are respectively the coordinates of the fixed and molecular system; $\vartheta_{j\beta}$ is the angle between the j axis and the β axis; δ_{ij} and $\delta_{\alpha\beta}$ are Kroenecker's delta functions.

Dielectric anisotropy

The response of liquid crystal molecules to an electric field is the major characteristic utilized in industrial applications. The ability of the director to align along an external field is caused by the electric nature of the molecules.

Permanent electric dipoles result when one end of a molecule has a net positive charge while the other end has a net negative charge, giving an unbalanced distribution of charge. A liquid crystal molecule containing a permanent dipole might or might not be polar, depending on the symmetry of the dipoles within or attached to the main molecular body. When an external electric field is applied to the liquid crystal, the dipole molecules tend to orient themselves along the direction of the field. In the Figure 19, the black arrows represent the electric field vector and the red arrows show the electric force on the molecule.

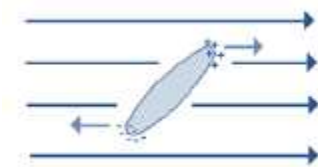


Figure 19: Effect of the applied electric field on the dipole molecules

Even if a molecule does not form a permanent dipole, it can still be influenced by an electric field. In some cases, the field produces slight rearrangement of electrons and protons in molecules such that an *induced electric dipole* results.

While not as strong as permanent dipoles, orientation with the external field still occurs. By applying an electric field along the long axis of the liquid crystal, the permittivity (i.e. parallel to the director) is observed. However, the application of an electric field perpendicular to this axis results in a permittivity . The anisotropy of the dielectric permittivity is given by

$$\Delta\varepsilon = \varepsilon_{||} - \varepsilon_{\perp}$$

the dielectric anisotropy can be positive or negative depending by the orientation (respectively parallel or perpendicular) of the molecular dipole respect to the molecular axis. The electric energy density for volume unit depends on the electrical displacement according to the following equation:

$$E_{electr} = -\frac{1}{4} \int \mathbf{D}d\mathbf{E} = -\left(\frac{\varepsilon_{\perp}}{8\pi}\right)E - \left(\frac{\Delta\varepsilon}{8\pi}\right)(nE)^2$$

when is positive there is a minimum in the energy if n and E are parallel, while when is negative the energy reaches a minimum if n is perpendicular to E . Values for of technically useful material range from between -6 to +50. The mean dielectric permittivity for a nematic liquid crystal can be described by^[71]:

$$\bar{\varepsilon} = \frac{\varepsilon_{||} - 2\varepsilon_{\perp}}{3}$$

Diamagnetic anisotropy

The effects of magnetic fields on liquid crystal molecules are analogous to electric fields. Because magnetic fields are generated by moving electric charges, permanent magnetic dipoles are produced by electrons moving about atoms.

When a magnetic field is applied, the molecules will tend to align along or opposite the field. The macroscopic magnetization M is given by:

$$\mathbf{M} = \chi_{\alpha\beta}\mathbf{H}_{\beta}$$

where ε and β are the axis of the molecular reference system; χ is the magnetic susceptibility. The diamagnetic properties of nematogenic liquid crystal can be described by two susceptibilities and The diamagnetic anisotropy is defined as

$$\Delta\chi = \chi_{||} - \chi_{\perp}$$

using the above equation, the magnetization can be written as follows:

$$\mathbf{M} = \chi_{\perp} \mathbf{H} + (\chi_{\parallel} - \chi_{\perp})(\mathbf{H} \cdot \mathbf{n})\mathbf{n}$$

and the corresponding density of magnetic energy far volume unit is then given by ^[72]:

$$E_{magn} = - \int_0^H \mathbf{M} d\mathbf{H} = -\frac{1}{2} \chi_{\perp} \mathbf{H}^2 = -\frac{1}{2} \Delta\chi (\mathbf{n} \cdot \mathbf{H})^2$$

Usually for this reason the minimum of the energy is reached when n has the same orientation of the field. The director orientation also depends on surface interactions: for a nematic liquid crystal tangentially oriented respect to the surface and subjected to a strong surface interaction, the director reorientation increases with the distance from the surface, until it become parallel to the field direction. It has been calculated that the angle between the director and the magnetic field is described by the following expression ^[73]:

$$\theta = \frac{1}{r} e^{-\left\{\frac{r}{\xi(H)}\right\}}$$

S is the length of magnetic coherence, and assuming $K=K_{11}=K_{22}=K_{33}$ it is expressed by the following equation:

$$\xi = \left(\frac{K}{\mu_0 \Delta\chi} \right)^{\frac{1}{2}} \frac{1}{H}$$

A magnetic field H is able to induce an elastic deformation over a length scale ; over a nematic liquid crystal with diamagnetic anisotropy and elastic constant K (μ_0 is the magnetic permeability constant). This equation provides an order of magnitude estimate for the field required to reorient the liquid crystal director. Intuitively ; can be defined as the thickness of the nematic liquid crystal layer where the orientation depends more on the surface interaction than on the field action.

The diamagnetic anisotropy is linked to the order parameter S by ^[70]:

$$S = \frac{\chi_{||} - \chi_{\perp}}{\chi_l - \chi_t}$$

where $\chi_{||}$ and χ_{\perp} are the susceptibilities of the nematic liquid crystal parallel and perpendicular to the magnetic field and χ_l and χ_t are the susceptibilities of the liquid crystal molecule parallel and perpendicular to the molecular longitudinal axis.

Optical anisotropy

Liquid crystals are found to be birefringent, due to their anisotropic nature: they exhibit double refraction (having two indices of refraction). Light polarized parallel to the director has a different index of refraction (that is to say it travels at a different velocity) than light polarized perpendicular to the director.

Thus, when light enters a birefringent material, such as a nematic liquid crystal sample, the process is modeled in terms of the light being broken up into the fast (called the ordinary ray) and slow (called the extraordinary ray) components (Figure 19).

Because the two components travel at different velocities, the waves get out of phase. When the light rays are recombined as they exit the birefringent material, the polarization state has changed because of this phase difference ^[74].

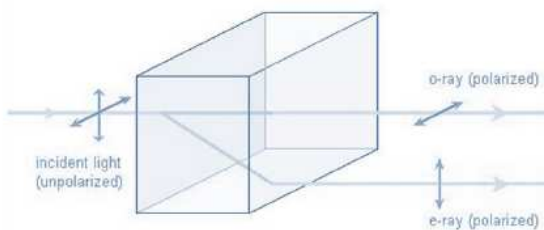


Figure 19: Light traveling through a birefringent medium.

The birefringence of a material is characterized by the difference, Δn , in the indices of refraction for the ordinary and extraordinary rays.

Quantitatively, since the index of refraction of a material is defined as the ratio of the speed of light in vacuum to that in the material, we have for this case:

$$n_e = \frac{c}{v_{\parallel}}$$

$$n_o = \frac{c}{v_{\perp}}$$

for the velocities of a wave traveling perpendicular to the director. The maximum value for the birefringence is given by:

$$\Delta n = n_e - n_o = n_{\parallel} - n_{\perp}$$

where n_{\parallel} and n_{\perp} are the refraction index of the light polarized having the electrical vector respectively parallel and perpendicular to the director. Δn varies from zero to the maximum value, depending on the travel direction. In the general case of a wave traveling in an arbitrary direction relative to the director in a liquid crystal sample, n_o is coincident with n_{\perp} and is given by ^[75]:

$$\Delta n = \frac{n_{\parallel} n_{\perp}}{\sqrt{n_{\parallel}^2 \cos^2 \theta + n_{\perp}^2 \sin^2 \theta}}$$

where θ is the angle between the incident ray and the director.

The condition $n_e > n_o$ describes a positive uniaxial material, so that nematic liquid crystals are in this category. For typical nematic liquid crystals, n_o is approximately 1.5 and the maximum difference, Δn , may range between 0.05 and 0.5. The Δn value depends on the wavelength of the light and the temperature.

Elastic constants

Liquid crystals respond to an external stimulus with an elastic reaction, varying only the molecules orientation. The elastic reaction for volume unit in apolar, achiral, nematic liquid crystal with cylindrical symmetry depends on three elastic constant K_{11} , K_{22} and K_{33} as follow ^[76]:

$$F = \frac{1}{2} [K_1(\nabla \mathbf{n})^2 + K_2(\mathbf{n} \nabla \times \mathbf{n})^2 + K_3(\mathbf{n} \nabla \mathbf{n})^2]$$

Each term in this equation is related to a particular deformation: splay (K_{11}), twist (K_{22}) and bend (K_{33}) (Figure 20).

The elastic constants are strongly temperature dependent.

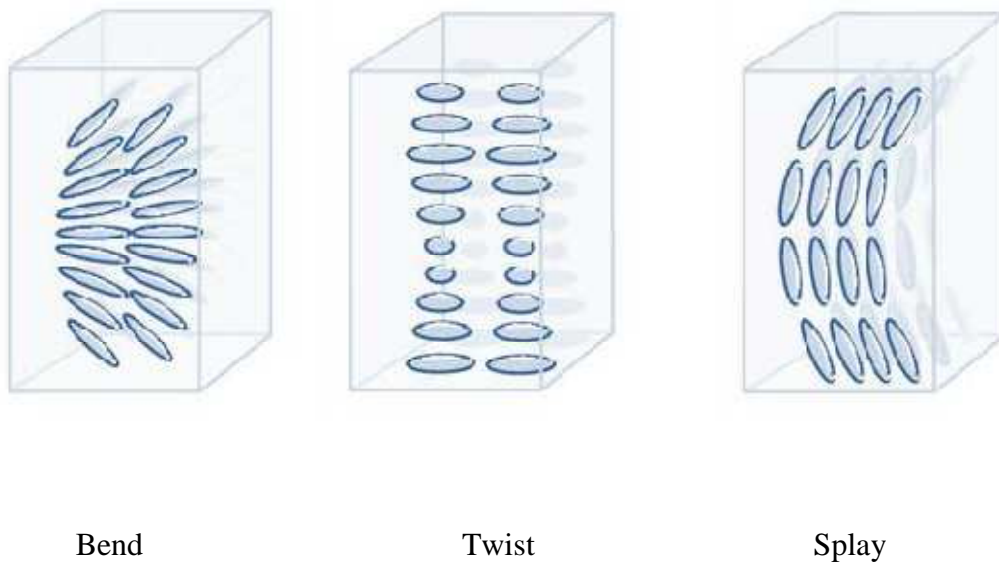


Figure 21: Elastic deformations of a liquid crystal

Anchoring energy

The director orientation in a nematic liquid crystal at the interface with a solid surface can be defined by two angles: the polar angle α , and the azimuthal angle φ . The orientation is homeotropic when $\theta=0$, while gives a planar or homogenous orientation.

The surface energy F_s it is composed by two terms: the isotropic superficial energy F_{is} , and the anchoring energy. The latter is expressed by the following equation ^[77]:

$$F_a^s = \frac{1}{2} W \sin^2 \delta\theta$$

Where W is the angular anchoring and F_a^s is the necessary energy to turn the director by an angle $\delta\theta$ from the equilibrium direction.

The alignment of liquid crystal molecules, was from the beginning a problem of main importance, in order to obtain macroscopically mono-oriented liquid crystal films to be employed in the display technology. Thus many devices, as command surfaces for the alignment of liquid crystals, are of main interest for the fabrication of optical devices.

References

- [1] G. Moad, D. Solomon, *The chemistry of free radical polymerization*, Pergamon, Oxford, **1995**.
- [2] J. P. Kennedy, S. Jacob, *Acc. Chem. Res.* **1998**, *31*, 835.
- [3] K. Matyjaszewski, *ACS Symp. Ser.* **1998**, *685*, 258.
- [4] K. Matyjaszewski, *Chem.--Eur. J.* **1999**, *5*, 3095.
- [5] K. Matyjaszewski, *Macromol. Symp.* **1998**, *132*, 85.
- [6] T. Otsu, M. Yoshida, T. Tazaki, *Makromol. Chem., Rapid Commun.* **1982**, *3*, 133.
- [7] A. Goto, T. Fukuda, *Macromolecules* **1999**, *32*, 618.
- [8] D. Benoit, V. Chaplinski, R. Braslau, C. J. Hawker, *J. Am. Chem. Soc.* **1999**, *121*, 3904.
- [9] D. Benoit, S. Grimaldi, S. Robin, J.-P. Finet, P. Tordo, Y. Gnanou, *J. Am. Chem. Soc.* **2000**, *122*, 5929.
- [10] B. B. Wayland, G. Poszmik, S. L. Mukerjee, M. Fryd, *J. Am. Chem. Soc.* **1994**, *116*, 7943.
- [11] L. D. Arvanitopoulos, M. P. Greuel, B. M. King, A. K. Shim, H. J. Harwood, *ACS Symp. Ser.* **1998**, *685*, 316.
- [12] K. Matyjaszewski, S. G. Gaynor, J. S. Wang, *Macromolecules* **1995**, *28*, 2093.
- [13] A. Goto, K. Ohno, T. Fukuda, *Macromolecules* **1998**, *31*, 2809.
- [14] M. Lansalot, C. Farcet, B. Charleux, J.-P. Vairon, R. Pirri, *Macromolecules* **1999**, *32*, 7354.
- [15] J. Chiefari, Y. K. Chong, F. Ercole, J. Krstina, J. Jeffery, T. P. T. Le, R. T. A. Mayadunne, G. F. Meijs, C. L. Moad, G. Moad, E. Rizzardo, S. H. Thang, *Macromolecules* **1998**, *31*, 5559.
- [16] M. Kato, M. Kamigaito, M. Sawamoto, T. Higashimura, *Macromolecules* **1995**, *28*, 1721.
- [17] C. Granel, P. Dubois, R. Jerome, P. Teyssie, *Macromolecules* **1996**, *29*, 8576.
- [18] J. S. Wang, K. Matyjaszewski, *J. Am. Chem. Soc.* **1995**, *117*, 5614.
- [19] T. E. Patten, J. Xia, T. Abernathy, K. Matyjaszewski, *Science* **1996**, *272*, 866.
- [20] K. Matyjaszewski, T. E. Patten, J. Xia, *J. Am. Chem. Soc.* **1997**, *119*, 674.
- [21] V. Percec, B. Barboiu, *Macromolecules* **1995**, *28*, 7970.
- [22] K. A. Davis, H.-j. Paik, K. Matyjaszewski, *Macromolecules* **1999**, *32*, 1767.
- [23] J. L. Wang, T. Grimaud, K. Matyjaszewski, *Macromolecules* **1997**, *30*, 6507.
- [24] T. E. Patten, K. Matyjaszewski, *Adv. Mater.* **1998**, *10*, 901.
- [25] K. Matyjaszewski, S. Coca, Y. Nakagawa, J. Xia, *Polym. Mater. Sci. Eng.* **1997**, *76*, 147.
- [26] K. Matyjaszewski, *Macromol. Symp.* **1998**, *134*, 105.
- [27] D. A. Singleton, D. T. Nowlan, N. Jahed, K. Matyjaszewski, *Macromolecules* **2003**, *36*, 8609.
- [28] H. Fischer, *J. Polym. Sci., Part A: Polym. Chem.* **1999**, *37*, 1885.
- [29] J. Xia, K. Matyjaszewski, *Macromolecules* **1997**, *30*, 7692.
- [30] J. Xia, K. Matyjaszewski, *Macromolecules* **1999**, *32*, 5199.
- [31] K. Matyjaszewski, S. Coca, S. G. Gaynor, M. Wei, B. E. Woodworth, *Macromolecules* **1997**, *30*, 7348.
- [32] M. R. Korn, M. R. Gagne, *Chem. Commun.* **2000**, 1711.
- [33] Q. Yu, F. Zeng, S. Zhu, *Macromolecules* **2001**, *34*, 1612.
- [34] K. Matyjaszewski, H.-j. Paik, P. Zhou, S. J. Diamanti, *Macromolecules* **2001**, *34*, 5125.
- [35] K. Matyjaszewski, *Macromol. Symp.* **1996**, *111*, 47.

- [36] K. Matyjaszewski, M. J. Ziegler, S. V. Arehart, D. Greszta, T. Pakula, *J. Phys. Org. Chem.* **2000**, *13*, 775.
- [37] K. A. Davis, K. Matyjaszewski, *Adv. Polym. Sci.* **2002**, *159*, 1.
- [38] S. G. Gaynor, K. Matyjaszewski, *ACS Symp. Series* **1998**, 685, 396.
- [39] K. L. Beers, S. G. Gaynor, K. Matyjaszewski, S. S. Sheiko, M. Moeller, *Macromolecules* **1998**, *31*, 9413.
- [40] K. Matyjaszewski, *Polym. Int.* **2003**, *52*, 1559.
- [41] K. Matyjaszewski, S. G. Gaynor, A. Kulfan, M. Podwika, *Macromolecules* **1997**, *30*, 5192.
- [42] K. Min, H. Gao, K. Matyjaszewski, *J. Am. Chem. Soc.* **2005**, *127*, 3825.
- [43] W. Jakubowski, K. Matyjaszewski, *Macromolecules* **2005**, *38*, 4139.
- [44] W. Jakubowski, K. Min, K. Matyjaszewski, *Macromolecules* **2006**, *39*, 39.
- [45] W. Jakubowski, K. Matyjaszewski, *Angew. Chem., Int. Ed.* **2006**, *45*, 4482.
- [46] K. Matyjaszewski, W. Jakubowski, K. Min, W. Tang, J. Huang, W. A. Braunecker, N. V. Tsarevsky, *Proc. Natl. Acad. Sci. U. S. A.* **2006**, *103*, 15309.
- [47] K. Matyjaszewski, W. Jakubowski, K. Min, W. Tang, J. Huang, W. A. Braunecker, N. V. Tsarevsky, *Proc. Natl. Acad. Sci. U.S.A.* **2006**, *103*, 15309.
- [48] J. Pietrasik, H. Dong, K. Matyjaszewski, *Macromolecules* **2006**, *39*, 6384.
- [49] K. Matyjaszewski, H. Dong, W. Jakubowski, J. Pietrasik, A. Kusumo, *Langmuir* **2007**, *23*, 4528.
- [50] R. Ranjan, W. J. Brittain, *Macromolecules* **2007**, *40*, 6217
- [51] G. K. Raghuraman, R. Dhamodharan, O. Prucker, J. Rühle, *Macromolecules* **2008**, *41*, 873.
- [52] T. Von Werne, T. E. Patten, *J. Am. Chem. Soc.* **1999**, *121*, 7409.
- [53] J. Pyun, S. Jia, T. Kowalewski, G. D. Patterson, K. Matyjaszewski, *Macromolecules* **2003**, *36*, 5094
- [54] F. Reinitzer, *Monatsh. Chem.* **1888**, *9*, 421
- [55] C. Oseen, *Trans. Faraday Soc.* **1933**, *29*, 883
- [56] H. Zocher, *Trans. Faraday Soc.* **1933**, *29*.
- [57] W. Maier, Z. N. A. Saupe: , A 13, 564-566 (1958), *Eine einfache molekulare Theorie des nematischen kristallinußigen Zustandes.*
- [58] F. C. Frank, *Discussions Faraday Soc.* **1958**, *25*, 19
- [59] F. M. L. Quart, *J. Mech. Appl. Math* **1966**, *19*, 357
- [60] J. L. Ericksen, *Arch. Ratl. Mech. Anal* **1960**, *4*, 231
- [61] I. C. Khoo, *Liquid Crystals*, 2nd ed., Wiley, New York, **2007**.
- [62] D. Demus, J. Goodby, *Handbook of Liquid Crystals, Vol. Vol.1 - Fundamentals*, Wiley-VCH, New York, **1998**.
- [63] S. Singh, *Liquid Crystals Fundamentals*, WSP **2002**.
- [64] M. Sawamura, *Nature* **2002**, *419*, 702
- [65] T. Kato, *Liquid Crystalline Functional Assemblies and Their Supramolecular Structures*, Springer **2008**.
- [66] A. M. Neto, *The Physics of Lyotropic Liquid Crystals - Phase Transitions and Structural Properties*, Pergamon Press, Oxford **2005**.
- [67] I. Dierking, *Textures of Liquid Crystals*, Wiley-VCH, New York, **2003**.
- [68] S. Chandrasekhar, *Liquid Crystals*, 2th ed., Cambridge **1992**.
- [69] H. Sackmann, D. Demus, *Mol. Cryst.* **1996**, *2*, 81
- [70] W. Maier, A. Saupe, *Z. Naturf.* **1958**, *13 A*, 564
- [71] W. Maier, G. Meier, *Z. Naturf.* **1961**, *16 A*, 262
- [72] E. A. Guggenheim, *Thermodynamics*, 5th ed., North-Holland Amsterdam, **1967**.
- [73] F. Brochard, P. G. d. Gennes, *J. Phys* **1970**, *21*, 691

- [74] T. Scharf, *Polarized Light In Liquid Crystals And Polymers*, Wiley New York, **2007**.
- [75] K. Kondo, M. Arakawa, A. Fukuda, E. Kuze, *Jpn. J. Appl. Phys* **1983**, 22, 394
- [76] A. Rapini, M. J. Papoular, *J. Phys.* **1969**, 4, 30.
- [77] P. G. D. Gennes, J. Prost, *The physics of liquid crystals*, 2th ed., Oxford University Press, Oxford, **1993**.

*Chapter 2**Photoexpansion**Introduction and Scope*

Recently, intensive activity has been directed towards the development of materials for recording, transfer and processing of data. In this context photochromic liquid crystalline polymeric (LCP) systems have become of great interest, because they combine the physico-chemical properties of macromolecular compounds, the mesomorphic properties of liquid crystals and the photosensitivity of chromophores anchored to the main chain as side groups [1].

Among these materials, polymers functionalized with azobenzenes appear to be one of the most suitable materials for holographic storage [2, 3], photoorienting layers of liquid crystalline displays [4] etc. This feature is associated with a number of advantages offered by azoaromatic compounds, such as high quantum yield of forward *trans*-to-*cis* and back *cis*-to-*trans* isomerization, relatively high stability and durability of polymer films, as well as the possibility of multiple photoirradiation cycles, etc.

An area of increasing interest includes the use of azobenzenes to generate photomechanical effects or even macroscopic motion. In particular, it appears possible that azoic materials could act as photo-actuators or artificial muscles [5, 6] in some carefully selected applications [7]. For example, single-wavelength ellipsometry measurements on amorphous azopolymers show a linear expansion of the material (about 4%) during irradiation [8]. The expansion involves both a reversible and an irreversible component, suggesting the presence of both elastic expansion and viscoelastic flow. Subsequent, reversible expansions and contractions were observed with repeated irradiation cycles, the relative expansion resulting 0.6–1.6%. Although the photomechanical effect is relatively small, it can be amplified to larger scale motion, as the bending of freestanding liquid-crystalline elastomers (LCEs) films demonstrates [5, 6].

Similarly, the photo-induced bending of a microcantilever coated with an azobenzene monolayer that expands upon irradiation ^[9] shows how azobenzene photoexpansion below the glass transition temperature (T_g) can be applied to device structures.

The photoinduced volume variation is a property exhibited by various azobenzene containing systems ^[10], such as gels, elastomers, cross-linked polymers or dendrites, which possess as common feature the network structure with different degree of coupling between the network elements or branches. Our study aimed to investigate the influence on the photomechanical effects of the network elements length and their coupling. We studied therefore linear polymers with different chain lengths and the related star polymers where a defined coupling element is introduced by the central core, instead of the statistical links present in gel, dendrites or cross-linked polymers.

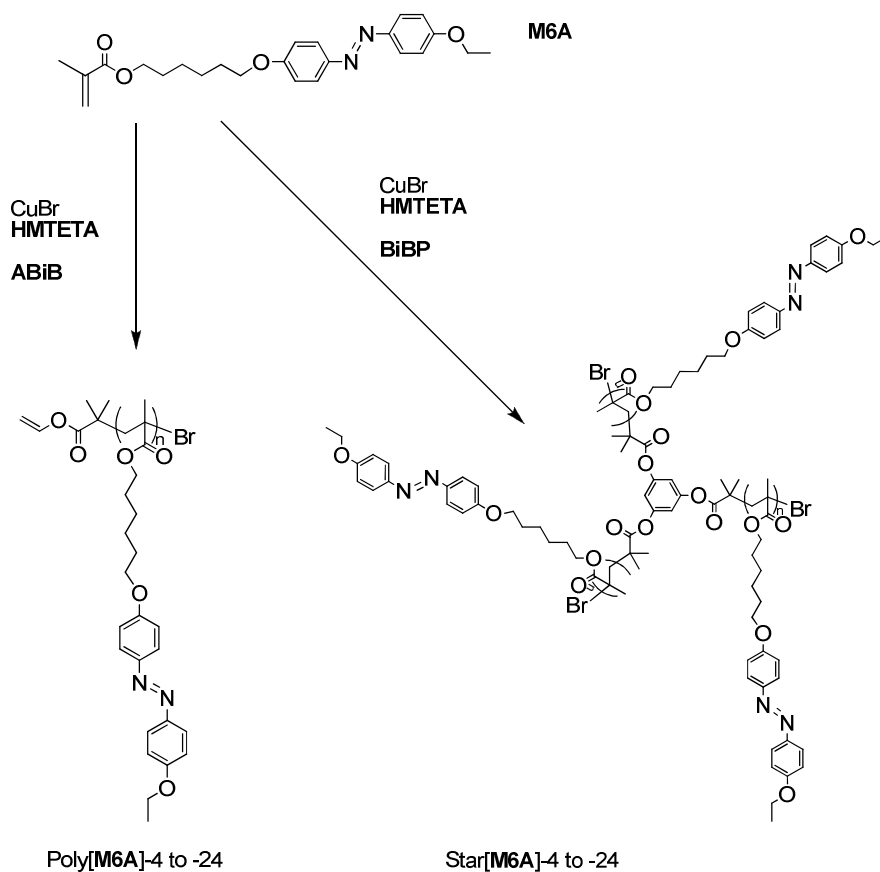
For these investigations it appears that polymeric samples with a well-defined structure are needed for a better understanding of the structure-properties correlation; hence, derivatives with a carefully selected molecular mass and low polydispersity are required. This goal can be achieved by using a controlled polymerisation procedure such as atom transfer radical polymerisation (ATRP) ^[11].

This procedure is in fact very versatile, being suitable to polymerize a wide range of monomers, insensitive to many functional groups and tolerant towards impurities present in solvent and reactants, including water. Several methacrylic esters have been successfully polymerized with this method, for example n-butyl methacrylate ^[12, 13], fluorinated methacrylic esters ^[14] and 1-phenoxy-carbonyl ethyl methacrylate ^[15], as well as amorphous ^[16, 17] and liquid crystalline (LC) ^[18, 19] polymers containing azoaromatic moieties in the side-chain.

Herein, we report a comparison between the different behaviour of linear and star shaped liquid crystalline polymers under optical pumping of the azo-benzene photoisomerisation, aimed at a better understanding of the role played by the macromolecular structure in the photomechanical effects of side-chain LC polymers.

In particular, we have considered the two series of homopolymers depicted in Scheme 1: four linear, poly(4-x-methacryloyloxy-hexyloxy-ethoxyazobenzene) [Poly(**M6A**)-2 through Poly(**M6A**)-24] ^[20, 21], and four related three-arms branched macromolecular derivatives with controlled average molecular weight, Star(4-x-methacryloyloxy-hexyloxy-ethoxyazobenzene) [Star(**M6A**)-2 through Star(**M6A**)-24] ^[22, 23], obtained by ATRP of monomer 4-x-methacryloyloxy-hexyloxy-ethoxyazobenzene (**M6A**) (Scheme 1) in the

presence of allyl 2-bromo-isobutyrate (**ABiB**), or 1,3,5-(2'-bromo-2'-methylpropionato)benzene (**BMPB**), as the mono- or trifunctional initiator, respectively, having variable average chain length with low polydispersity just by varying the process duration.



Scheme 1: Synthesis of linear and star-shaped polymeric derivatives

All the derivatives have been characterized by standard spectroscopic techniques and their liquid-crystalline behavior investigated by differential scanning calorimetry (DSC) and polarized optical microscopy (POM). The structure–property relationships of these systems have been compared with those of the previously reported [24] analogue Poly(**M6A**), obtained by AIBN free radical polymerization, having $\bar{M}_w = 74,000$ and $\bar{M}_w/\bar{M}_n = 1.9$.

Finally, the photomechanical effect has been investigated by ellipsometry by monitoring the photo-induced volume variation of thin films of the samples in order to evaluate the relevance of the polymer molecular weight for future applications of these materials.

Synthesis and Spectroscopic Characterization

Well-defined LC linear and star shaped homopolymers were obtained by polymerization of **M6A** in the presence of **ABiB** (as monofunctional initiator for linear polymers) or **BiBP** (as trifunctional for three-arm shaped star polymers) and Cu(I)Br with **HMTETA** as ligand. The occurrence of polymerization involving the methacrylic double bond was confirmed by FT-IR, showing the disappearance of the band at 1640 cm^{-1} related to the stretching vibration of the double bond in the monomer, and by $^1\text{H-NMR}$ spectra, in which the resonances at 5.60 and 6.10 ppm related to the vinylidenic protons of monomer **M6A** are absent. As an example, Figure 1 reports the $^1\text{H-NMR}$ spectrum of Poly(**M6A**)-2.

In all the $^1\text{H-NMR}$ spectra of synthesized polymers the signals related to the methylic protons of the initiator are partially overlapped on those of the repeating units. Whereas the resonances of the methylene and methyl groups bonded to the quaternary carbon atom bearing the terminal Br atom at 1.95 and 2.20 ppm, respectively, and the resonance of the CH, CH₂ and CH₂-O allyl protons of **ABiB** residue at 5.85, 5.30 and 4.60 ppm, respectively, are well visible (Figure 1).

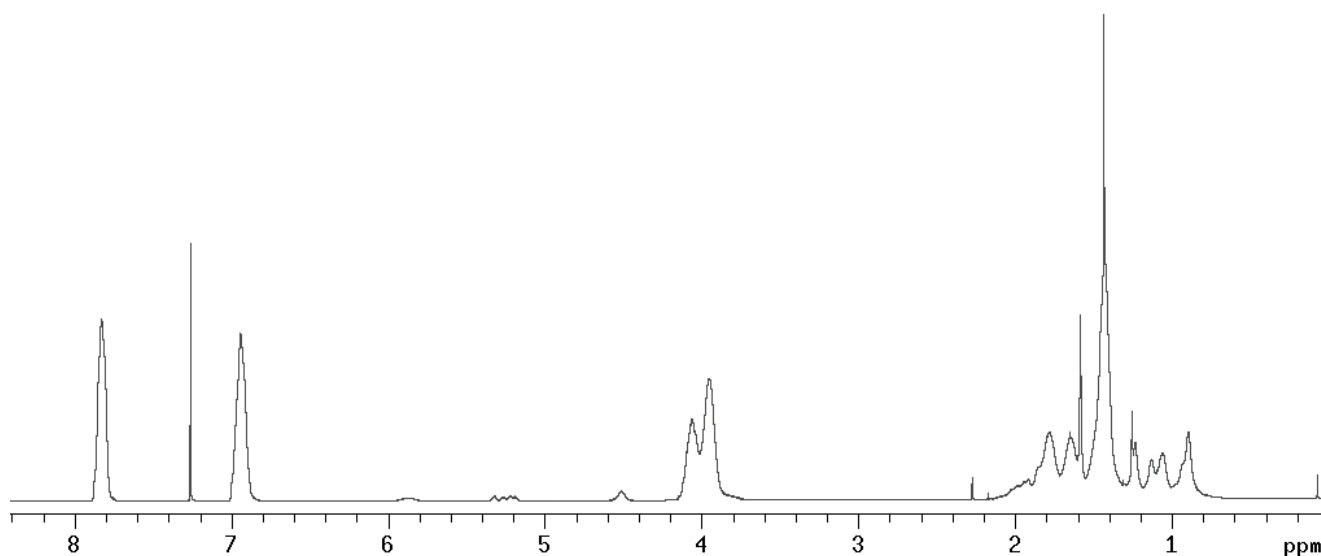


Figure 1: $^1\text{H-NMR}$ spectrum of Poly(**M6A**)-2 in CDCl_3 . Starred signal refers to solvent resonances.

On the other hand, the signals related to the aromatic and aliphatic protons of the central core in the star shaped polymers Star(**M6A**)-4 to Star(**M6A**)-24 are overlapped on those of the repeating units. The sample obtained at lower reaction times, Star(**M6A**)-2,

displays the resonances of the methylene and methyl groups bonded to the quaternary carbon atom bearing the terminal Br atom at 1.9 and 2.3 ppm, respectively. Their intensity decreases by increasing the reaction time and becomes progressively obscured by the more intense resonances related to the aliphatic protons of the main chain, thus preventing assessment of the number average molecular weight of each sample directly by integration of the NMR signals.

The living character of the polymerization is confirmed by ^{13}C -NMR spectra, which display signals related to the quaternary carbon atom bonded to Br at 58.0 ppm and to the methyl and methylene carbon atoms of the growing chain end-group at 27.5 and 38.9 ppm, respectively.

The average molecular weight can be calculated by ^1H -NMR spectroscopy for the linear derivatives by the ratio of the integral of the protons of the initiator residue and of the aromatic and $\text{CH}_2\text{-O}$ protons of the photochromic repeating unit. Molecular weights calculated in this manner are in good agreement with the ones determined by SEC (Table 1).

This operation is not possible for the star shaped polymers, as mentioned above, because of the overlapping of the aromatic signals of the core and of the azoaromatic moieties, therefore their molecular weight can be determined only by SEC analysis (Table 1).

Yields and number average molecular weight values of the obtained polymers (Table 1) show a strong dependence on the reaction duration: by varying this last parameter only, we have obtained several samples of various average chain length.

Figure 2 shows an approximately linear relationship between $\ln([\text{M}]_0/[\text{M}]_t)$ (where $[\text{M}]_0$ and $[\text{M}]_t$ are the initial and at t time monomer concentrations, respectively) and the reaction time, thus indicating a first-order kinetics of the polymerization rate with respect to the monomer concentration and a relatively constant concentration of the growing species throughout the process, apart a negative deviation at higher conversion as observed elsewhere for ATRP polymerisations ^[14].

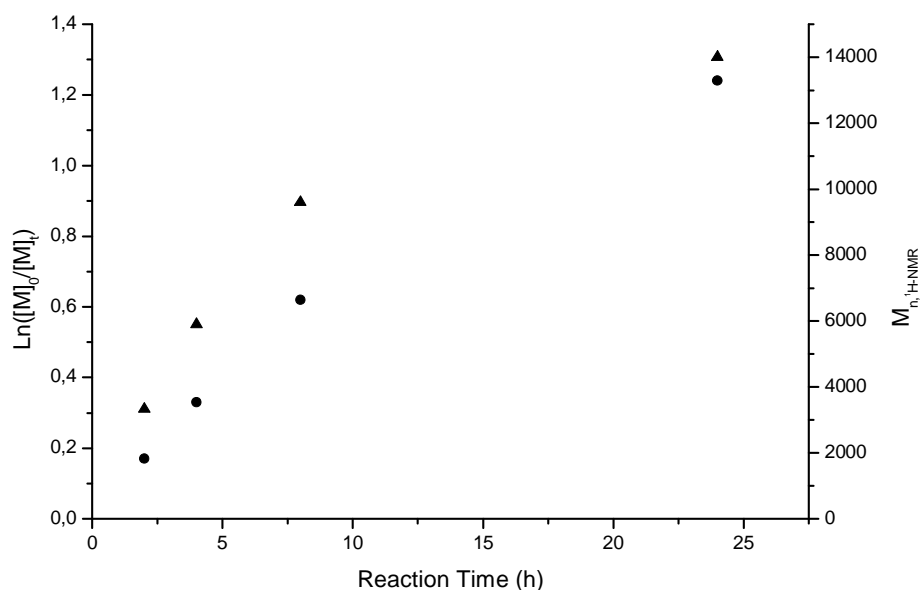


Figure 2: Time dependence of $\ln([M]_0/[M]_t)$ [•] and of the average molecular weight $\bar{M}_{n,^1H-NMR}$ [▲] in the ATRP of **M6A** in THF.

Table 1: synthetic data for the polymeric derivatives

Sample	Time (h)	$\bar{M}_{n,SEC}$	$\bar{M}_{n,^1H-NMR}$	$\bar{M}_{n,th}$	$\ln([M]_0/[M]_t)$
Poly(M6A)-2	2	4600	3300	4400 ^c	0.17
Poly(M6A)-4	4	6000	5900	5800 ^c	0.33
Poly(M6A)-8	8	9700	9600	10000 ^c	0.62
Poly(M6A)-24	24	14800	14000	15300 ^c	1.24
Star(M6A)-2	2	5900	-	5600 ^c	0.12
Star(M6A)-4	4	7800	-	8600 ^c	0.23
Star(M6A)-8	8	17400	-	19000 ^c	0.38
Star(M6A)-24	24	29400	-	43700 ^c	1.25

^a Determinated by SEC in THF at 25°C

^b Calculated by ¹H-NMR spectroscopy integrating the peak of methylenic allyl protons (at 5.30 ppm) and averaging on the values of the integrals of aromatic protons (at 7.90 and 6.80 ppm) and CH₂-O protons (around 4 ppm)

^c Calculated by equation: $[M]_t = [M]_0 - \frac{\bar{M}_n - PM_{Initiator}}{PM_{Monomer}} [I]$

There is also a relationship between the reaction time and the number average molecular weight. In fact just varying the time of polymerisation is possible to modulate the molecular weight of the polymer, obtaining always a monodispersed system with a typical ATRP lower polydispersity index, in the range 1.12-1.17 as shown in Figure 3 by the superimposition of the SEC traces at different conversions for the series of the star derivatives Star(M6A)-2 to Star(M6A)-24 (Figure 3 and Table 2).

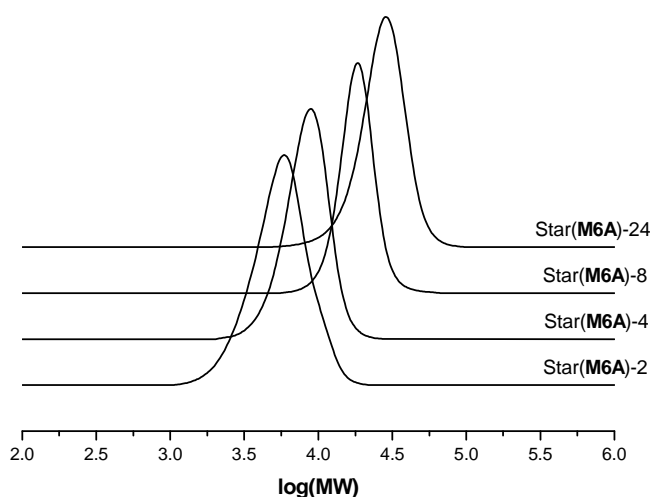


Figure 3: Normalized molecular weight distributions of star polymers as determined by SEC in THF at 25°C.

The plot of the number average molecular weight of the resulting star-shaped polymers as determined by SEC $\bar{M}_{n,SEC}$ against monomer conversion (calculated by unreacted monomer collection from polymerization mixture) is shown in Figure 4. The theoretical values of \bar{M}_n , ($\bar{M}_{n,th}$), that are valid only in the absence of chain termination and transfer reactions, may be calculated by the following equation ^[19]:

$$\bar{M}_{n,th} = \text{Conversion} * (M_{M6A} / M_{BIBP}) * M_{w,M6A} + M_{w,BMPB}$$

where M_{M6A} and M_{BMPB} are the initial amounts in moles of monomer and trifunctional initiator, respectively, and $M_{w,M6A}$ and $M_{w,BMPB}$ their respective molecular weights. As reported in Figure 4, calculated and SEC values are coincident only at low values of monomer conversion but, as the conversion increases, they diverge to an increasing extent. Such a behavior, previously reported for star-shaped chiral photochromic polymethacrylates ^[16], cannot be ascribed to termination reactions taking place under the real polymerization conditions, as proved by the low and almost constant values of \bar{M}_w/\bar{M}_n (in the range 1.08–1.21), reported in Table 2, but to the particular molecular structure of multiarms polymers. It

is well known, in fact, that star polymers have a smaller hydrodynamic volume with respect to that of linear polystyrenes having the same molecular weight. As a consequence SEC analysis gives underestimated molecular weight values for star-shaped polymers when measured with reference to the usually adopted linear polystyrene standards ^[25, 26].

Anyway, the approximately linear correlation between $\bar{M}_{n,SEC}$ and monomer conversion is indicative of the living character of the ATRP process and SEC analysis proves to be useful to confirm that a steady increment of the average molecular weight with conversion has taken place.

Table 2: Structural and Thermal Characteristics of the Polymeric Materials

Sample	Structural properties			Thermal transitions ^c		
	M_n ^a	PDI ^a	X_n ^b	T_g (°C)	$T_{S \rightarrow N}$ (°C)	T_i (°C)
Poly(M6A)-2	4600	1.13	11.2	57	66	116
Poly(M6A)-4	6000	1.12	14.6	63	76	129
Poly(M6A)-8	9700	1.13	23.6	69	79	129
Poly(M6A)-24	14800	1.17	36.0	76	92	148
Star(M6A)-2	5600 ^d	1.21	4.5	57	78	124
Star(M6A)-4	8600 ^d	1.12	7.0	57	80	127
Star(M6A)-8	19000 ^d	1.08	15.4	71	87	142
Star(M6A)-24	43700 ^d	1.14	35.5	85	94	150

^a Determined by SEC in THF at 25°C.

^b Average polymerisation degree (X_n) for linear macromolecules and for each branch of the star shaped derivatives calculated by M_n values.

^c Obtained from the second DSC heating cycle under nitrogen at 10°C min⁻¹ heating rate. g (glass), S (smectic A1), N (nematic), I (isotropic) phases.

^d Calculated by $\bar{M}_{n,th} = \text{Conversion} * (M_{M6A} / M_{BIBP}) * M_{w,M6A} + M_{w,BMPB}$, where M_{M6A} and M_{BMPB} are the initial amounts in moles of monomer and trifunctional initiator and $M_{w,M6A}$ and $M_{w,BMPB}$ are their molecular weights, respectively.

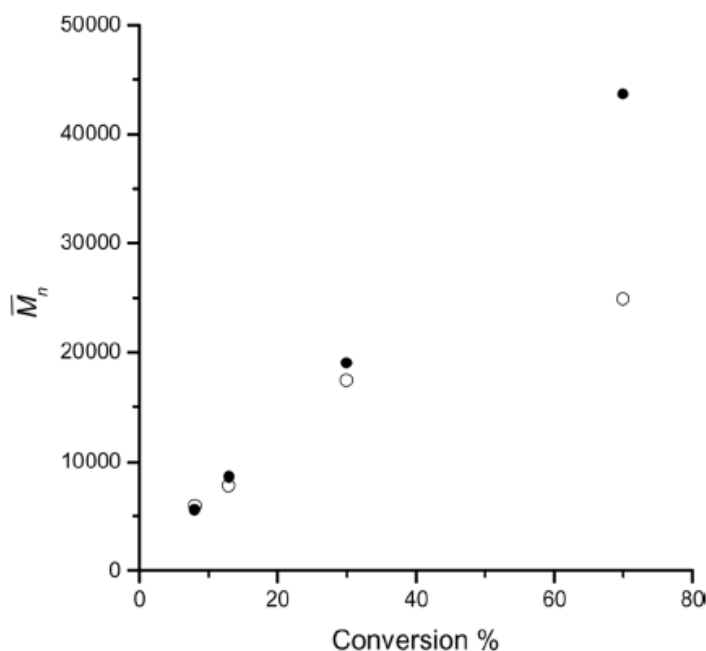


Figure 4: Evolution of the number average molecular weight determined by SEC in THF at 25°C (o) and calculated values (●) versus conversion in the ATRP of **M6A**.

In conclusion, all the instrumental characterization techniques confirm that living linear and star shaped polymers with varying molecular size have been successfully obtained. Each chain contains a bromine atom as end group that could be replaced through a variety of reactions leading either to end-functionalized polymers or used as the initiating site for the polymerization of a different monomer to obtain novel block copolymers.

The UV-Vis absorption spectra in CHCl_3 solution of all the investigated polymers, as well as the monomer **M6A**, exhibit, in the 250–650 nm spectral region, two bands related to the $n-\pi^*$ and $\pi-\pi^*$ electronic transitions of the azobenzene chromophore in *trans*-configuration with maxima centered at about 360 nm ($\epsilon \approx 28000 \text{ L mol}^{-1} \text{ cm}^{-1}$) and 440nm ($\epsilon \approx 1500 \text{ L mol}^{-1} \text{ cm}^{-1}$), respectively ^[27] and within the limits of experimental error they appear qualitatively and quantitatively independent of polymerization degree.

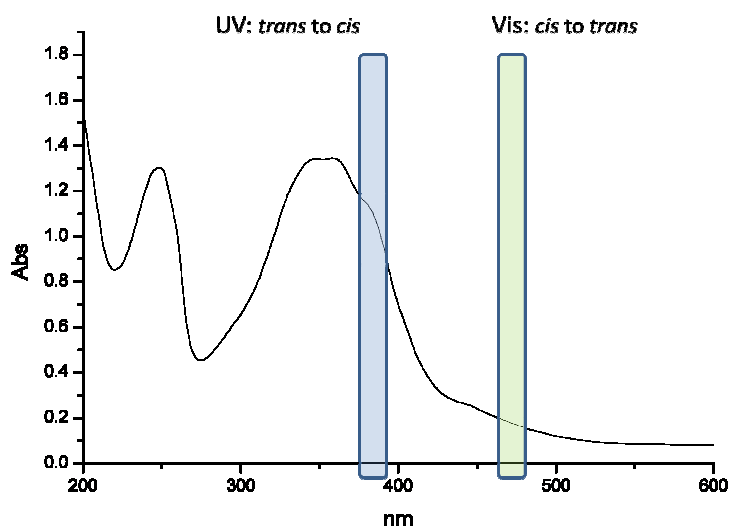


Figure 5: UV-Vis spectra of Poly(M6A)-8 and irradiation light

The polymer were therefore irradiated with UV light at 390 nm in order to performo *trans* to *cis* isomerization until the photostationary equilibrium is reached. The *cis* to *trans* isomerization is induced by illumination with blue light at 470 nm (Figure 5).

Thermal Properties, Polarized Optical Microscopy and XRD Characterization

With the aim to study their LC properties, all the polymeric derivatives have been characterized by differential scanning calorimetry (DSC) and polarized optical microscopy (POM). Phase transition temperatures determined by DSC are summarized in Table 1: all the macromolecules display on heating a glass transition temperature (T_g), a smectic liquid-crystal phase melting endotherm (T_{SM}) with a consequent nematic liquid-crystal phase melting endotherm and finally an isotropization temperature (T_i). In all cases, on cooling, the latter transitions show a modest degree of supercooling (4–7 °C), whereas this effect is much pronounced for smectic-nematic transition and a stable frozen nematic mesophase is obtained and maintained at room temperature. In Figure 6 we report, as an example, the first cooling and the second cycle heating curves for the sample Poly(**M6A**)-8.

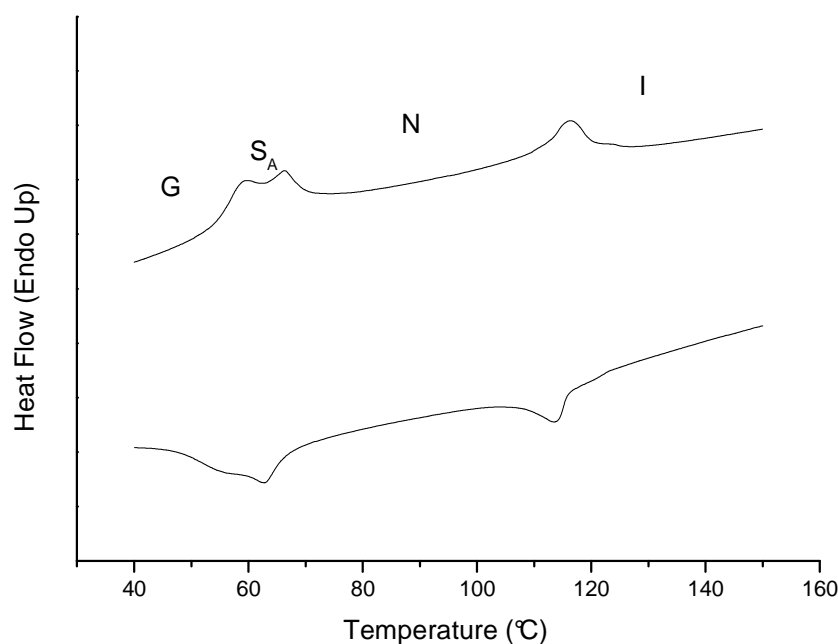


Figure 6: DSC cooling (first scan) and heating curves (second scan) for Poly(**M6A**)-8

The smectic (S_{A1}) and nematic (N) liquid-crystalline phases have been identified by comparison of their DSC traces with that one of Poly(**M6A**)-AIBN, obtained by AIBN-initiated free radical polymerization, extensively studied by DSC, POM, and X-ray diffraction [24]; the nematic phase has been observed also by POM (Figure 7) while, due to the closeness

of T_g and T_{SM} , the smectic phase can not be observed. Indeed, the LC texture and the thermal properties of Poly(**M6A**) homopolymers obtained by ATRP are in agreement with those of Poly(**M6A**)-AIBN with the expected differences in the transition temperatures values (Table 2).

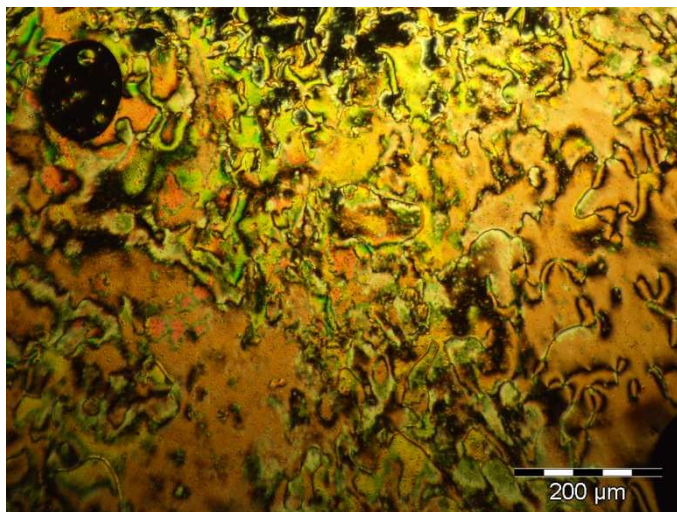


Figure 7. Polarizing optical micrographs of a typical schlieren texture of Poly(**M6A**)-8 in nematic phase after isotropisation and annealing at 100°C.

The transition temperatures appear strongly dependent on the polymerization degree, the glass (T_g), the smectic-nematic (T_{SM}) and the nematic–isotropic transition temperatures (T_i) of the series diminishing with the decrease of chain length (Figure 7 and Table 2).

In particular, the T_i and T_{SM} values of Poly(**M6A**)-2 to Poly(**M6A**)-24 increase from 116 to 148 °C and from 66 to 92°C (Table 2) approaching the maximum values of 152° and 97°C, respectively, found for Poly(**M6A**)-AIBN with $\bar{M}_w = 74;000$, obtained by AIBN-initiated free radical polymerization ^[24]. The polymeric samples characterized by lower average molecular weight show wider smectic phase (S_{A1}) ranges and, similarly to the other polymeric samples, a liquid crystalline nematic phase stable for approximately 50 degrees.

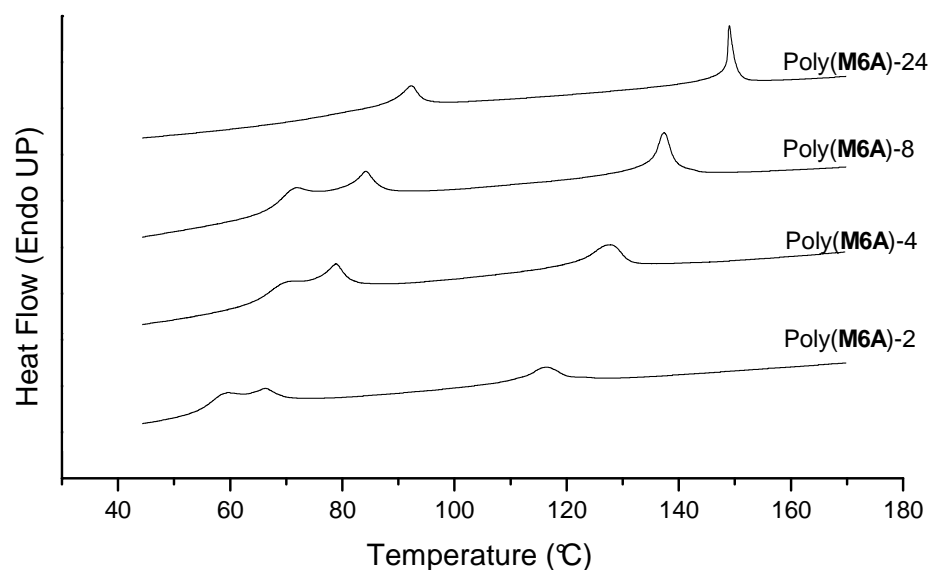


Figure 8: DSC heating curves (second scan) of the linear polymers investigated

Also the macromolecular structure plays an important role on the thermal characteristic: we observed how the presence of a branching in the central part of the polymers induce higher transition temperatures for derivatives with the same average molecular weight and similar polydispersities (Table 2). This behaviour can be explained by the higher stiffness of the central core and thus the reduced mobility of these branched system that will form more entanglements compared to the linear ones.

With the aim of verifying the type of mesophase and confirming that the LC structures are the same for the linear and the star polymers, the two derivatives have been analysed by X-ray diffraction (XRD) and compared with the similar Poly(M6A)-AIBN^[24]. The samples have been investigated in the glassy smectic phase in order to observe any difference in the layer spacing. To develop a smectic mesophase, the samples were submitted to a thermal treatment consisting of a heating cycle above the T_i , followed by cooling at 10 °C/min to a temperature between the $T_{S \rightarrow N}$ and the T_g and a final annealing for one hour. The XRD diffraction patterns of the annealed samples are characteristic of a smectic phase (Figure 8).

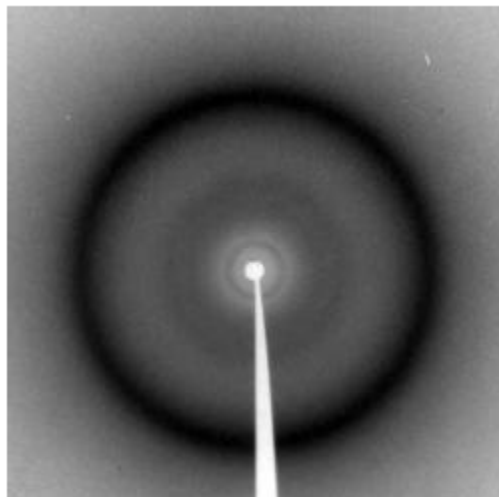


Figure 9: XRD diffraction pattern of Poly(**M6A**)-24 in the glassy smectic phase.

They contain two scattering maxima: the first, at low angles, is sharp and related to the layer spacing of the smectic phase; the second, at high angles, is broad and diffuse, and corresponds roughly to a distance of 4.4-4.5 Å, related to the liquid-like lateral interaction between the azoaromatic chromophores. In the absence of annealing at the smectic temperature the mesogens cannot organize themselves in the layer structure and the XRD diffraction pattern shows only the presence of a glassy nematic phase. The measured layer spacings in the smectic mesophase are gathered in Table 3

Table 3. Structural data by XRD

Sample	Phase	Measured layer spacing in Å	Predicted length in Å ^{a)}
Poly[M6A]-24	S _{A1}	28,5 ±0,5	30
Star[M6A]-24	S _{A1}	26,4 ±0,5	
Poly[M6A]-AIBN ^{b)}	S _{A1}	26,2 ±0,5	

a) Monomer length assessed by Dreiding stereomodels for a fully extended conformation;

b) ref. ^[24]

Comparing the measured layer spacings in the smectic mesophase, 28,5±0,5 and 26,4±0,5 Å for Poly(**M6A**)-24 and Star(**M6A**)-24, respectively, with the predicted monomer length of 30 Å, as assessed from Dreiding stereomodels for a fully extended conformation, it is evident that the experimental measurements are consistent with a single-layer smectic A (S_{A1}) mesophase, without significant differences in layer periodicity between Poly(**M6A**)-24

and Star(**M6A**)-24. Therefore the liquid crystal phase structure appears unaffected by the presence of branching in the macromolecules.

Photoexpansion and photomechanical effects

The photomechanical effects (i.e. the dependence of volume and density under illumination) have been studied by ellipsometry as a function of molecular weight on the synthesized compounds, with a particular attention to the parameters important for the potential applications such: total percentage volume variation, response time, stability and reproducibility. Ellipsometry, by a simultaneous and independent determination of film thickness and refractive index, allows an estimation of volume and density variation, moreover when applied to thin samples, it allows a uniform optical pumping with rather low optical power densities (10-1000 $\mu\text{W}/\text{cm}^2$).

A study of the photo-expansion and contraction mechanisms as a function of the polymeric chain length with a narrow polydispersity is an important issue, since in such phenomena (as well in the photoinduced molecular reorientation) a key role is played by the free volume distribution (Figure 10).

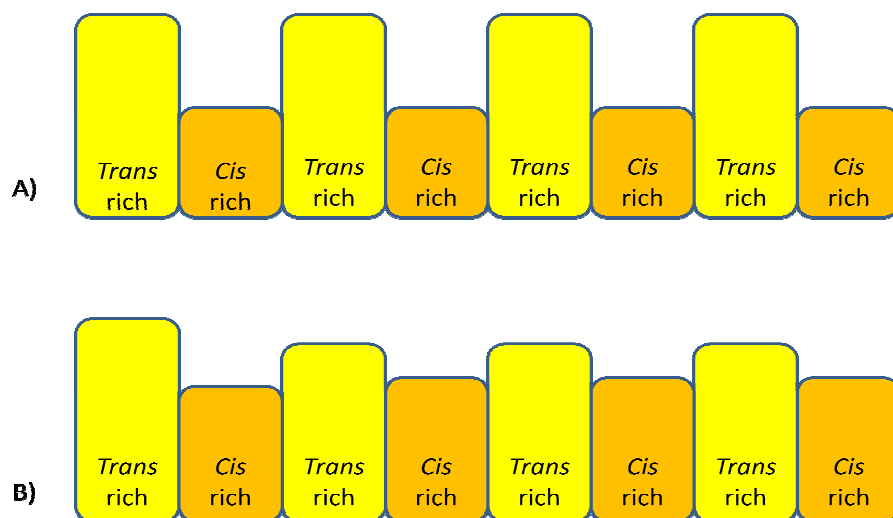
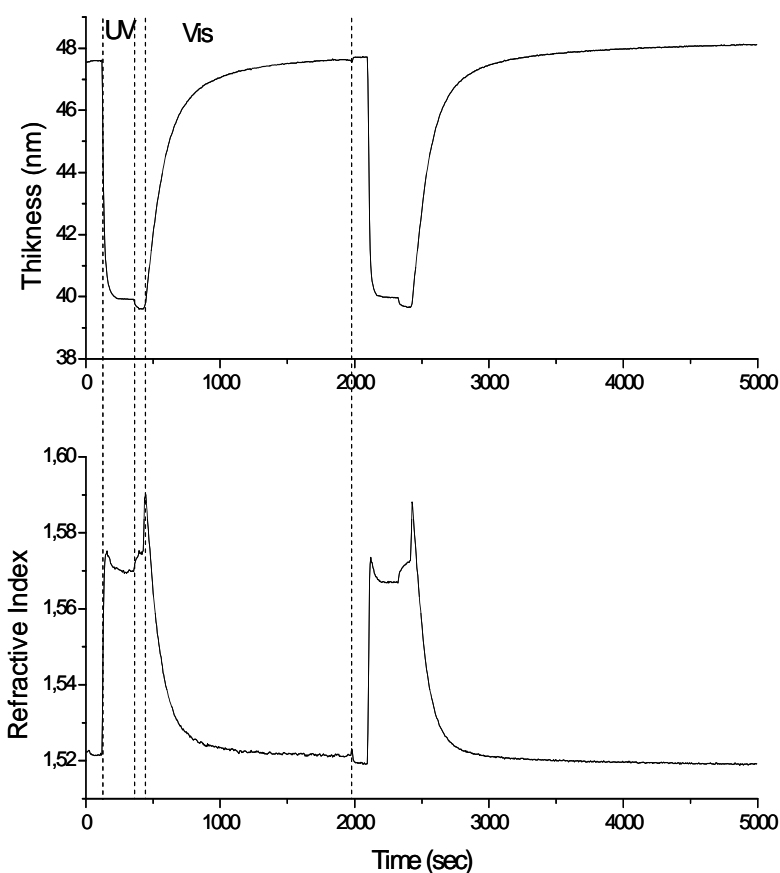


Figure 10: Idealization of several cycles of photoexpansion and photocontraction in monodisperse systems (A) and polydisperse ones (B)

Beyond the direct influence of excluded volume on the mechanical response of the material, it may have effects even the photoisomerization process: both optical and thermally induced isomerization rates are sensitive to the molecular environment, as has been characterized in various azobenzene systems by absorption spectroscopy both in solid state and solutions^[28]. In particular in polymers, especially below the glass transition temperature as a consequence of the interaction with the surrounding matrix, the isomerization processes deviate from the first order kinetic typical of solution in good solvents, and the rates vary one

order of magnitude. The study of the dependence of photoinduced processes in azo polymers on the molecular weight has been carried out with photoinduced birefringence^[29] which shows how an increasing material viscosity slows down the dynamics and stabilizes the effect. Less attention has been paid on the effect of polydispersity, such a parameter becomes fundamental in the phenomenology of photoinduced macroscopic volume variation, since a broadening in the distribution of the polymeric chain lengths strongly influences the microscopic excluded volume as evidenced by positron lifetime spectroscopy studies^[30].

Figure 11: Typical thickness (a) and refractive index (b) variations of Poly(M6A)-24 during two optical cycles of photoisomerization at 30°C with both UV (385 nm) and vis (470 nm) light power set at 200 $\mu\text{W}/\text{cm}^2$. Dashed



vertical lines indicate the UV and vis illumination switched alternatively on and off during the first cycle.

We studied therefore the photomechanical effect on these highly monodisperse polymers with different molecular weight; experimentally we observed several contraction and expansion cycles of the samples, induced respectively through an UV (385 nm) and Vis (470 nm) illumination. A typical measurement is shown in Figure 11: illumination in UV region compacts the film down to a thickness that we found to be independent on the starting values. The photoinduced *trans* to *cis* conversion clears the thermal history of sample and brings it to the highest density state. The fluidification^[31-33] effect due to the high concentration of *cis* isomers allows the system to relax toward the same equilibrium state

even at temperatures below the glass transition, clearing all memory effects. Such contraction has been found to be stable: no variation was found even after the trans recovery taking place in several hours with the thermal activated isomerization, as can be monitored by the measurement of the refractive index, which is different in the two isomers. When the UV induced contraction is followed by a visible illumination, the sample expands and the achieved volume remains as well stable with no dependence on temperature below T_g . The refractive index, increases at higher *cis*-isomer concentration or density; a simultaneous variation of those parameters in opposite direction determines a change of sign of the refractive index trend as shown in the lower panel of Figure 11.

Several optical cycles were performed and evidencing a complete reproducibility of both volume variation and response time, the stability was checked by detecting no variation on the measured parameters on the days time scale.

Effects of molecular weight^[21]

We focused our attention on the volume variation and response time of the sample as a function of molecular weight, obtaining the result summarized in Figure 11.

The volume variations of the material under study, as reported for a similar compound^[34], show a higher value compared to other reported in literature^[8], the difference is due in our opinion to the type of azobenzene dye employed. In the present study, we used azobenzene chromophore of the first class (azobenzene-type), according to the Rau classification scheme^[35], which are characterized spectroscopically by a low intensity *cis* band in the visible region well separated from a high intensity *trans* band in the UV and with a slow thermal *cis*-to-*trans* back-isomerization. The other two classes: the amino and pseudo-stilbene types are characterized on the contrary by overlapping bands, which allow only a resonant photoisomerization, and a shorter *cis* isomer lifetime. Both effects don't allow an efficient *trans* to *cis* isomerization while in azobenzene of the first class an almost complete conversion is possible. The possibility of moving the relative isomer population in a wider range allows obtaining a higher macroscopic volume variation.

We measured the variation on the different compounds at room temperature (25 °C) as shown in the first panel in Figure 12 while response time of photo-expansion is reported in the second panel. A longer polymeric chain was found to allow a higher volume variation through the photoinduced effect while on other hand it slows down the dynamics as observed in the measured relaxation times.

The dependence of photoinduced volume variation reflects the behavior of the microscopic free volume as a function of the polymeric chain length reported in literature^[30]. Materials with higher molecular weight seem therefore more suitable for applications requiring volume variation since they can store more free volume, while the slow dynamic response may be improved by acting both on temperature or optical pump power.

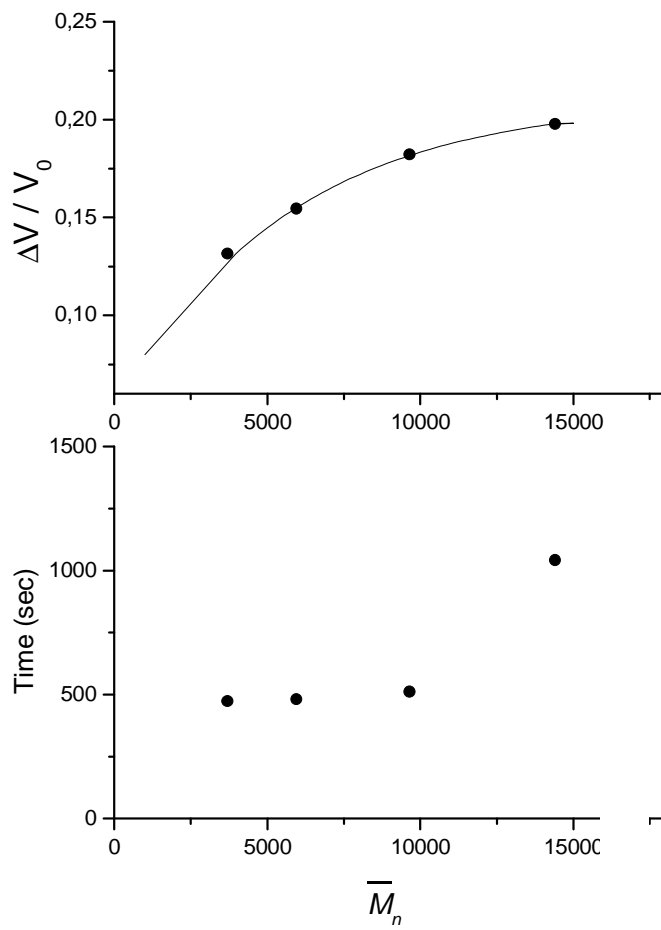


Figure 12: Photoinduced volume expansion (a) and relaxation times (b) versus the increment of sample average molecular weight after irradiation with $200 \mu\text{W}/\text{cm}^2$ UV light (385 nm) at room temperature.

Comparative study between linear and star shaped polymers ^[36]

The thickness and refractive index variations of samples during irradiation have been monitored in real time using an ellipsometer by measuring the ellipsometric angles Δ and Ψ with 5 second time resolution.

An example of photoexpansion at room temperature of samples previously compacted with UV illumination is reported in Figure 13; where the dynamics of thickness of a linear [Poly(M6A)-4] and a star polymer [Star(M6A)-4] are reported for comparison.

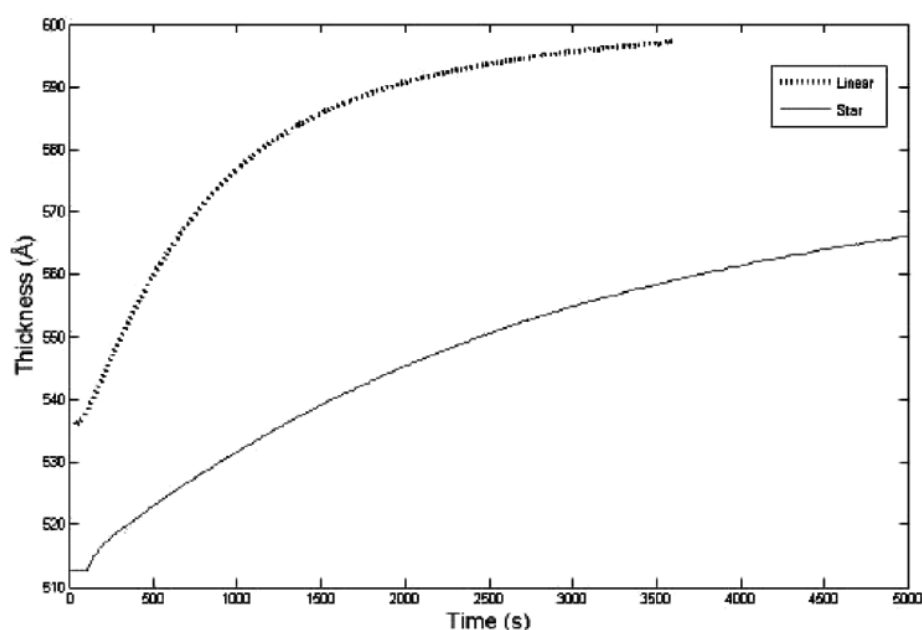


Figure 13: Examples of expansion dynamics Poly(M6A)-4 and Star(M6A)-4.

Generally the photoinduced dynamics in azo-PLC depends on the system viscosity, resulting on slower relaxation times with increasing molecular weight as reported in the case of photoinduced birefringence ^[29]. Here we observe, as a first remarkable difference between the two macromolecule types, that the branched polymer with a comparable T_g (even lower see Table 2) and molecular weight displays a higher relaxation time. Such result suggests that the star macromolecular geometry inhibits the photoinduced softening/fluidification effect ^[33] which allows the molecular reorientation in azo-PLC polymers even well below the T_g . The coupling introduced by the star geometry influences not only the dynamics but also the

overall effect, namely the final volume variation, as it can be deduced from Figure 13. The data obtained for the eight investigated polymers are gathered in Figure 14.

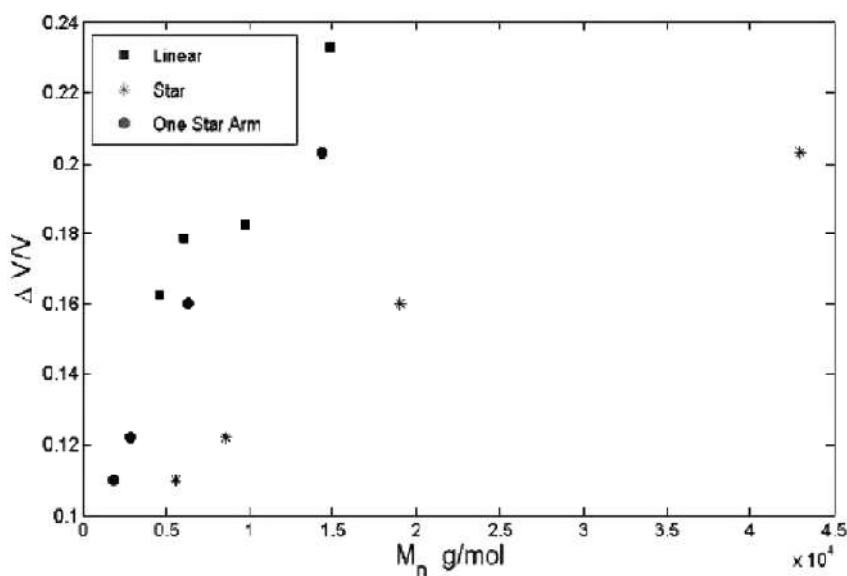


Figure 14: Percentage volume variation as a function of the molecular weight of the linear polymers (squares), Star Polymers (Stars) and of each branch ($N_f=3$) of the Star polymers (Circles).

The measurements were performed below the T_g of each compound at 55°C ; this higher temperature was chosen in order to gain a faster dynamics. The final film percentage expansion ($\Delta V/V$) of the compounds, plotted as a function of their molecular weight (Figure 12), clearly indicates a frustration introduced by the branched geometry in the photoexpansion. The percentage volume expansion increases with the molecular weight in both cases, either for linear and star polymers, due to the ability of longer chain to store more free volume. However the effect of central core coupling present in the star polymers, could suggest that for an efficient photoexpansion also independent chains are required. As a matter of fact, also plotting the expansion as a function of the single arm length of the star polymers, obtained by molecular weight (Table 1) divided by the number of arms (functional number $N_f = 3$), the trend of expansivity remains still lower than that of the related linear polymers (Figure 12). Such phenomenon can be ascribed to the reduction of possible chain conformations introduced by the constrain represented by the aromatic central core.

Moreover an other possible cause of this effect may lay in the initial structure of the star polymers which is generally characterised by an higher density at given molecular weight, as it can be measured by the refractive index values. In Figure 13 we report the photoinduced expansivity for films of different composition (star and linear geometry, with

different chain lengths) as a function of the refractive index, which in turn, at a given molar refractivity, is related to the sample density via the Lorentz–Lorenz equation. Data were taken at RT and at 55°C. The major finding observing Figure 13 is that there is an overall correlation between the density and the photoinduced expansivity: the samples with higher refractive index and hence higher density exhibit a smaller expansivity, which is a clear indication of the importance of the free volume in determining not only the time scale on which the expansion occurs, but also its overall extension. Interestingly enough, focusing on the linear polymers only, as the polymeric length is increased, a larger photoinduced expansion is found, while the refractive index stays roughly constant. This suggests that the amount of the photoinduced expansion can be reduced by the rearrangement that can occur with a high density of free polymer ends, as it happens for the shorter polymers. Comparing star and linear geometry, it seems that, at a given chain length, the presence of the three arms originating at the same central rigid core induces a larger refractive index, which is reasonable, being the star polymer a more dense material, while at the same time the star geometry reduces the expansion.

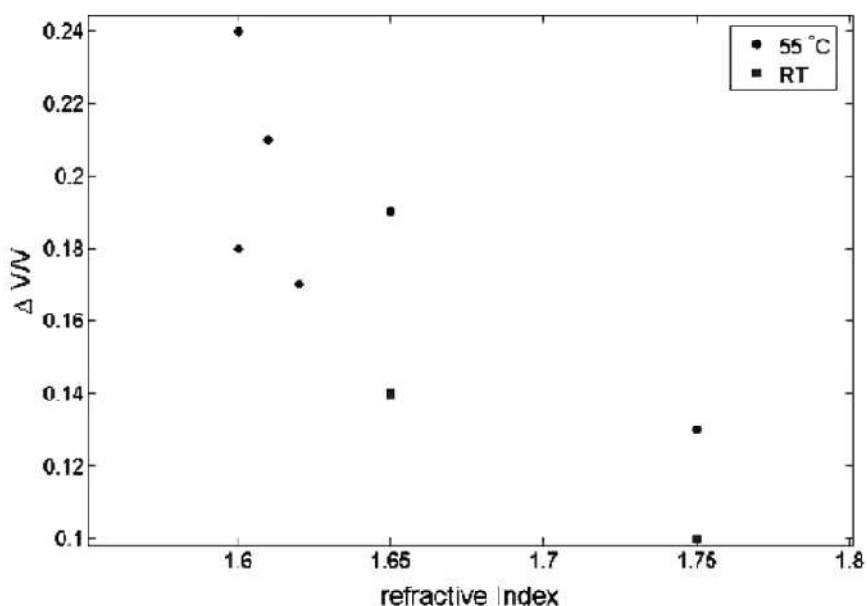


Figure 15: Correlation between expansion and refractive index (density), data acquired at 55°C (circles) and at room temperature (squares).

Conclusions

Atom Transfer Radical Polymerization has been successfully applied to the preparation of a series of linear liquid crystalline polymers with different average molecular weights and low polydispersity. The living character of the ATRP process is confirmed by the first-order kinetics, a linear molecular weight-conversion profile and narrow molecular weight distribution. Therefore the obtained photochromic LC polymers with well defined living end-groups could be employed to prepare novel block copolymers with interesting properties and potential applications in advanced technologies.

The liquid-crystalline behaviour of the macromolecular samples has been confirmed by DSC measurements and POM characterization pointing out the presence of smectic and nematic phases. The transition temperatures are in agreement with those of analogous linear derivatives obtained by AIBN initiated free radical polymerization and result strongly dependent on polymerization degree and polydispersity index.

Investigation of the photomechanical effects induced by light irradiation indicates that the ability of azobenzene polymeric materials of storing free volume is of fundamental relevance, since allows to achieve a higher photo-induced expansion with increased molecular mass. Such property, depending by polydispersity index, strictly suggests the need and convenience of employing highly monodisperse material for the study and applications of polymers containing azoaromatic moieties.

In particular, a comparative study of star polymers with the related linear ones. The synthesized highly monodispersed compounds with a fixed number of arms allowed us to investigate a well defined coupling element. Such a coupling is required and generally introduced statistically in other azo systems ^[7] in order to transfer the transduction from a molecular to a macroscopic level. We observed however that such desirable inter-chain interactions, in the case of star polymer correspond to a slowdown of dynamics and a reduction in photoexpansion. Our results indicate that trade off between an efficient macroscopic transduction and overall extension should be sought.

Experimental

Physico-chemical measurements

^1H - and ^{13}C -NMR spectra were obtained at room temperature, from 5–10% CDCl_3 solutions, using a Varian NMR Gemini 300 spectrometer. Chemical shifts are given in ppm from tetramethylsilane (TMS) as the internal reference. ^1H -NMR spectra were run at 300 MHz by using the following experimental conditions: 24,000 data points, 4.5-kHz spectral width, 2.6-s acquisition time, 128 transients. ^{13}C -NMR spectra were recorded at 75.5 MHz, under full proton decoupling, by using the following experimental conditions: 24,000 data points, 20-kHz spectral width, 0.6-s acquisition time, 64,000 transients. FT-IR spectra were obtained by a Perkin-Elmer 1750 spectrophotometer, equipped with an Epson Endeavour II data station, on samples prepared as KBr pellets. UV-Vis absorption spectra of the samples in solution were recorded at 25 °C in CHCl_3 on a Perkin-Elmer Lambda 19 spectrophotometer. The spectral region 650–250 nm was investigated by using cells path length of 1 and 0.1 cm. Concentrations of azobenzene chromophore of about $3.0 \times 10^{-4} \text{ mol L}^{-1}$ were used.

Number average molecular weights of the polymers (\overline{M}_n) and their polydispersity indexes ($\overline{M}_w/\overline{M}_n$) were determined in THF solution by SEC using HPLC Lab Flow 2000 apparatus, equipped with an injector Rheodyne 7725i, a Phenomenex Phenogel 5-micron MXL column and a UV-VIS detector Linear Instrument model UVIS-200, working at 254 nm. Calibration curve was obtained by using monodisperse polystyrene standards in the range 800–35,000. The phase transition temperatures values were determined by differential scanning calorimetry (DSC) on a TA Instrument DSC 2920 Modulated apparatus at a heating/cooling rate of 10 K/min under nitrogen atmosphere on samples weighing 5–9 mgr. Optical microscopy observations were performed on polymer films obtained by casting on glass slides with a Zeiss Axioscope2 polarizing microscope through crossed polarizers fitted with a Linkam THMS 600 hot stage.

The samples of the eight synthesised polymers for the ellipsometric study have been prepared on silicon substrates by spin coating technique.

The compounds have been dissolved in chloroform at 5 mg/ml concentration and cast on the substrates spinning at 2000 rpm, yielding film thicknesses in the range of 35–60 nm. The thickness has been adjusted in such range in order to study thin samples required for a

uniform optical pumping without self screening effects due to the high optical extinction coefficient of the azobenzene chromophore and at the same time sufficiently thick to neglect surface effects. As a matter of facts, such surface interactions, due to the change of hydrophilicity between *trans* to *cis* isomers, become dominant for ultrathin or single molecular layer^[37]. Both refractive index and thickness of samples, thermostated on a Peltier plate, were measured by high resolution null ellipsometry using a single wavelength ellipsometer (Multiskop, Optrel GmbH), set up in a pump probe configuration. The instrument is equipped with a He-Ne laser impinging on the sample with an angle of incidence of 70° operating at 632.8 nm, which probes the materials outside the azobenzene absorption region, while the optical pumping has been obtained by means of two Light Emitting Diodes LEDs, positioned above the sample. Two LEDs with emission peaks centered at 390nm and 470nm were necessary in order to induce respectively *trans* to *cis* and the reverse isomerizations of the azobenzene chromophore which in turn result in a contraction and expansion of film^[21, 38]. The samples of each compound, before the experiments, have been annealed some hours at 5°C above their glass transition temperature (T_g) (see Table 1), in order to remove solvent residues and to obtain a stabilization of the film. The annealing process was monitored by ellipsometry and continued until the achievement of a stable film thickness. The samples cooled to room temperature exhibit an isotropic phase as after their preparation by the spin coating technique as characterised by polarizing optical microscopy. Particular attention has been paid to avoid a smectic crystallization which inhibits the photomechanical effects and can be induced by the annealing process above T_g therefore before the ellipsometric measurement the isotropic structure of samples or the absence of birefringent islands has been checked through the polarising microscope.

Materials

The monomer 4- ω -methacryloyloxy-hexyloxy-4'-ethoxyazobenzene (**M6A**) was synthesized as previously reported [24]. THF was purified and dried according to the reported procedures [39] and stored under nitrogen. Allyl 2-bromoisobutyrate (**ABIB**), 1,1,4,7,10,10-hexamethyltriethylenetetramine (**HMTETA**), copper bromide and all the other reagents and solvents were purchased from Aldrich and used as received.

The trifunctional initiator 1,3,5-(2'-bromo-2'-methylpropionate)benzene (**BMPB**) was prepared as previously described [40, 41]

Synthesis of polymeric derivatives by ATRP

A typical ATRP experimental procedure carried out in glass vials for homopolymerization of **M6A** using **ABIB** as monofunctional initiator (or **BMPB** as trifunctional initiator), **HMTETA** as the ligand, Cu(I)Br as catalyst in dry THF [**M6A**/THF 1/20 g/ml] is described as follows: every mixture [**M6A**/**ABIB**/**HMTETA**/CuBr = 50/1/1/1 or **M6A**/**BMPB**/**HMTETA**/CuBr = 150/1/1/1 by mol] was introduced into several vials under nitrogen atmosphere, submitted to several freeze-thaw cycles, and heated at 60°C. To terminate the polymerization reaction, the vials were frozen in liquid nitrogen after known reaction times, ranging from 2 to 24 h. The obtained product was purified by precipitation in a large excess of cold methanol and the coagulated polymer [Poly(**M6A**)-2 through Poly(**M6A**)-24] filtered off, redissolved in CHCl₃, precipitated again with cold methanol and finally dried at 50°C under vacuum for one day to constant weight. Relevant data for the synthesized derivatives are reported in Table 1. All the products were characterized by FT-IR, ¹H- and ¹³C-NMR. As an example, the spectroscopic data for Poly(**M6A**)-24, obtained after 24 h of reaction, are here reported.

¹H-NMR (CDCl₃): 7.80 (m, 4H, 2- and 2'-H), 6.90 (m, 4H, 3- and 3'-H), 5.85 (m, 1H, CH₂=CH-CH₂-O) 5.30 (m, 2H, CH₂=CH-CH₂), 4.60 (m, 2H, CH₂=CH-CH₂), 4.10–3.80 (m, 6H, CH₂-O), 2.20 (s, 2H CH₂-C-Br terminal units), 1.95 (m, 3H, CH₃-C-Br), 1.90–0.80 (m, 8H, aliph spacer CH₂, 5H, main chain CH₃ and CH₂ and 6H, -C(CH₃)₂-COO-) ppm.

^{13}C -NMR (CDCl_3): 178.2 and 177.3 (CO repeating unit), 161.7 and 161.6 (arom 4-C and 4'-C), 147.6 (arom 1-C and 1'-C), 132.8 ($\text{CH}_2=\text{CH}-\text{CH}_2-$), 125.0 (arom 2-C and 2'-C), 118.8 ($\text{CH}_2=\text{CH}-\text{CH}_2-$), 115.3 (arom 3-C and 3'-C), 68.4 ($\text{CH}_2-\text{CH}_2-\text{O}-$), 66.0 ($\text{CH}_2=\text{CH}-\text{CH}_2-$), 65.3 ($\text{CH}_3-\text{CH}_2-\text{O}$), 64.1 ($\text{COO}-\text{CH}_2-$), 58.5 ($\text{C}(\text{CH}_3)-\text{Br}$), 55.0 (main chain $\text{C}-\text{CH}_2$), 45.8 and 45.5 (main chain CH_2-C), 42.2 ($\text{C}(\text{CH}_3)_2-\text{CH}_2$), 35.7 ($\text{CH}_2-\text{C}(\text{CH}_3)-\text{Br}$), 27.5 ($\text{C}(\text{CH}_3)-\text{Br}$), 29.8, 28.8, 26.6, 26.4 (aliph spacer CH_2), 23.0 ($\text{C}(\text{CH}_3)_2-\text{CH}_2$), 19.3 and 17.0 (main chain CH_3), 15.4 (CH_3-CH_2) ppm.

FT-IR (KBr): 3068 (ν_{CH} arom), 2977 and 2866 (ν_{CH} aliph), 1724 (ν_{CO} ester), 1598 ($\nu_{\text{C}=\text{C}}$ arom), 1392 (ν_{CH} CH_3), 1145, 1113 ($\nu_{\text{C}-\text{O}}$ ether), 839 (δ_{CH} 1,4-disubst. arom ring) cm^{-1} .

References

- [1] V. Shibaev, A. Bobrovsky, N. Boiko, *Prog. Polym. Sci.* **2003**, *28*, 729.
- [2] M. Eich, J. Wendorff, *J. Opt. Soc. Am. B: Opt. Phys.* **1990**, *7*, 1428.
- [3] K. Anderle, J. H. Wendorff, *Mol. Cryst. Liq. Cryst. Sci. Technol., Sect. A* **1994**, *243*, 51.
- [4] H. J. Eichler, S. Orlic, R. Schulz, J. Rubner, *Opt. Lett.* **2001**, *26*, 581.
- [5] Y. Yu, M. Nakano, T. Ikeda, *Nature (London, U. K.)* **2003**, *425*, 145.
- [6] T. Ikeda, M. Nakano, Y. Yu, O. Tsutsumi, A. Kanazawa, *Adv. Mater. (Weinheim, Ger.)* **2003**, *15*, 201.
- [7] T. Ikeda, J.-i. Mamiya, Y. Yu, *Angew. Chem., Int. Ed.* **2007**, *46*, 506.
- [8] O. M. Tanchak, C. J. Barrett, *Macromolecules* **2005**, *38*, 10566.
- [9] H.-F. Ji, Y. Feng, X. Xu, V. Purushotham, T. Thundat, G. M. Brown, *Chem. Commun. (Cambridge, U. K.)* **2004**, 2532.
- [10] M. Yamada, M. Kondo, J.-i. Mamiya, Y. Yu, M. Kinoshita, C. J. Barrett, T. Ikeda, *Angew. Chem., Int. Ed.* **2008**, *47*, 4986.
- [11] K. Matyjaszewski, J. Xia, *Chemical Reviews* **2001**, *101*, 2921.
- [12] V. Percec, H. J. Kim, B. Barboiu, *Macromolecules* **1997**, *30*, 8526.
- [13] K. Ibrahim, B. Lofgren, J. Seppala, *Eur. Polym. J.* **2003**, *39*, 939.
- [14] J. Xia, T. Johnson, S. G. Gaynor, K. Matyjaszewski, J. DeSimone, *Macromolecules* **1999**, *32*, 4802.
- [15] K. Demirelli, A. Kurt, M. Coskun, *Eur. Polym. J.* **2004**, *40*, 451.
- [16] L. Angiolini, T. Benelli, L. Giorgini, E. Salatelli, *Macromolecules* **2006**, *39*, 3731.
- [17] L. Angiolini, T. Benelli, L. Giorgini, E. Salatelli, *Polymer* **2005**, *46*, 2424.
- [18] X. He, H. Zhang, X. Wang, *Polym. J. (Tokyo, Jpn.)* **2002**, *34*, 523.
- [19] X.-Z. Wang, H.-L. Zhang, D.-C. Shi, J.-F. Chen, X.-Y. Wang, Q.-F. Zhou, *Eur. Polym. J.* **2005**, *41*, 933.
- [20] V. Coessens, T. Pintauer, K. Matyjaszewski, *Prog. Polym. Sci.* **2001**, *26*, 337.
- [21] L. Angiolini, T. Benelli, L. Giorgini, F. Paris, E. Salatelli, M. P. Fontana, P. Camorani, *Eur. Polym. J.* **2008**, *44*, 3231.
- [22] V. Percec, B. Barboiu, A. Neumann, J. C. Ronda, M. Zhao, *Macromolecules* **1996**, *29*, 3665.
- [23] L. Angiolini, T. Benelli, L. Giorgini, F. Paris, E. Salatelli, T. Zuccheri, *Int. J. Polym. Mater.* **2007**, *56*, 789.
- [24] D. Wolff, H. Cackovic, H. Krueger, J. Ruebner, J. Springer, *Liq. Cryst.* **1993**, *14*, 917.
- [25] K. Matyjaszewski, P. J. Miller, J. Pyun, G. Kickelbick, S. Diamanti, *Macromolecules* **1999**, *32*, 6526.
- [26] S. Angot, K. S. Murthy, D. Taton, Y. Gnanou, *Macromolecules* **1998**, *31*, 7218.
- [27] H. H. Jaffé, M. Orchin, *Theory and application of ultraviolet spectroscopy*, Wiley, New York, **1962**.
- [28] Z. Sekkat, W. Knoll, *Photoreactive organic thin films*, Academic Press, USA, **2002**.
- [29] L. L. Carvalho, T. F. C. Borges, M. R. Cardoso, C. R. Mendonca, D. T. Balogh, *Eur. Polym. J.* **2006**, *42*, 2589.
- [30] K. Süvegh, M. Klapper, A. Domján, S. Mullins, W. Wunderlich, A. Vértes, *Macromolecules* **1999**, *32*, 1147.
- [31] N. Mechau, D. Neher, V. Borger, H. Menzel, K. Urayama, *Appl. Phys. Lett.* **2002**, *81*, 4715.
- [32] N. Mechau, M. Saphiannikova, D. Neher, *Macromolecules* **2005**, *38*, 3894.

- [33] T. Sriksirin, A. Laschitsch, D. Neher, D. Johannsmann, *Appl. Phys. Lett.* **2000**, *77*, 963.
- [34] L. Cristofolini, S. Arisi, M. P. Fontana, *Phys. Rev. Lett.* **2000**, *85*, 4912.
- [35] H. Rau, *Photochemistry and photophysics*, CRC, USA, **1990**.
- [36] P. Camorani, L. Cristofolini, M. P. Fontana, L. Angiolini, L. Giorgini, F. Paris, *Mol. Cryst. Liq. Cryst.* **2009**, *500*, 1.
- [37] O. Karthaus, M. Shimomura, M. Hioki, R. Tahara, H. Nakamura, *J. Am. Chem. Soc.* **1996**, *118*, 9174.
- [38] C. D. Eisenbach, *Polymer* **1980**, *21*, 1175.
- [39] D. D. Perrin, W. L. F. Amarego, D. R. Perrin, *Purification of Laboratory Chemicals*, Pergamon Press, Oxford, **1996**.
- [40] A. Carlmark, R. Vestberg, E. M. Jonsson, *Polymer* **2002**, *43*, 4237.
- [41] D. M. Haddleton, C. Waterson, *Macromolecules* **1999**, *32*, 8732.

Chapter 3

Chirality in Azopolymers

Introduction

Azobenzene containing polymeric systems are well known for their photochromic properties related to the *trans*–*cis*–*trans* photoisomerization of the azo–chromophore, and have been proposed for reversible data storage, signal modulation and switching ^[1]. The induction of helical polymers has been the subject of intensive research not only because of its potential applications in chiroptical switching, reversible optical storage ^[2-6], chiral amplification ^[7] and chiral discrimination ^[8], but also its possible occurrence at the early stages of life ^[9]. Optically active polymers containing a chiral group and an azobenzene chromophore show a well-pronounced circular dichroism (CD) signal in the absorption region of azobenzene, demonstrating that the chiral center induces a predominant helical screw sense in the polymer both as film and in solution ^[10-12]. Recently, the fascinating possibility of inducing circular birefringence (optical activity) in nonchiral azobenzene-containing polymers by using circularly polarised light (CPL) has also been reported. The phenomenon was observed for the first time by Nikolova and co-workers in switches obtained by direct irradiation of films of liquid-crystalline (LC) cyanoazobenzene polyesters ^[13, 14]. Upon illumination with CPL at 488 nm, the films are provided with an unusually strong optical activity: right circularly polarised (*r*-CPL) radiation induces right-hand rotation of the probe beam polarisation, the reverse being observed with left circularly polarised (*l*-CPL) pump light. In a first report ^[13], the authors suggested that the observed effect may be initiated by a transfer of angular momentum from the CPL to the azobenzene chromophores and that the observed phenomena are related to the presence of LC ordering (smectic-A phase) in the polymer films prior to irradiation. Analogous results have been found for an amorphous cyanoazobenzene methylmethacrylate copolymer previously ordered by illumination with linearly polarised light (LP) ^[15]. In a further work, Nikolova et al. discovered a self-induced rotation of the azimuth of elliptically polarised light (EPL) on passing through films of photobirefringent azopolymers ^[16]. The EPL propagating through the sample was found to

induce an optical axis that gradually rotates along the propagation direction, thus inducing a chiral orientation of the azobenzene chromophores with the same sense of rotation as that of the input light electric vector. The whole film assumes a chiral structure similar to that found in cholesteric liquid crystals with large pitch. The control of chirality with CPL on films of a smectic-A liquid-crystalline nitroazobenzene polymethacrylate has also been achieved by Natansohn and coworkers^[17]. The authors found that, by irradiation with CPL at 514 nm, the initially achiral films became chiral and showed strong CD signals. The CD spectra of two different films, one irradiated with *r*-CPL and the other with *l*-CPL, exhibited opposite signs and were virtually mirror images of each other. In contrast, the amorphous films (not annealed) did not show any induced circular anisotropy, thus pointing out the essential role of the LC arrangement and suggesting that the original circular polarisation of the incoming light is made elliptical by the first layers of the smectic domains of the film. In this way, on the basis of the model proposed by Nikolova et al.^[16], the EPL radiation that propagates into the film produces a progressive rotation of the optical axis of each LC domain, resulting in a supramolecular helical arrangement of the smectic domains to form an organization similar to a twisted grain boundary (TGB) phase.

According to Kim^[18], chirality can be induced also in amorphous epoxy-based side-chain azopolymers by illumination with one handed EPL. In this context, Giorgini reported the first example of chiroptical switching only with *r*- or *l*-CPL of amorphous thin films of chiral polymethacrylates containing azoaromatic moieties in the side-chain, in the absence of preliminar alignment with LP light^[19-21]. Hore et al. reported the observation of a selective circular Bragg reflection in CD spectra of a nematic glassy thin film (100 nm thick) of a side-chain LC azopolymer irradiated with CPL, which was assigned to the structure produced by superposition of the forward-propagating wave and the back-reflected wave^[22]. More recently, Tejedor et al. discussed the influence of LC structures and detected a circular Bragg reflection in thin films (200 nm) of achiral glassy nematic azopolymers^[23, 24], but not in a homologous smectic one^[23] irradiated with CPL of opposite sign. Although several mechanisms of photoinduced chirality process in side chain azobenzene containing polymers have been proposed, the model based on a helical arrangement of aggregated chromophores in the side-chain^[22], appears more realistic.

To induce chirality in soft matters, two different structural levels must be mainly considered: at molecular and supramolecular level. The first one is provided by the chirality of molecules, which is of configurational and conformational origin. The second level of

chirality arises from the organization of molecules with formation of a chiral superstructure by means of long-range positional and orientational orders of molecules [25]. As above described, several research groups have contributed to the experimental findings on chirality induced by CPL (or EPL) stimuli in achiral polymer systems with azobenzene side chains, but studies of liquid-crystalline polymers containing a chiral group of one absolute configuration and an azobenzene chromophore in the side-chain suitable to demonstrate CPL-induced chirality have not been reported. Furthermore, from all these investigations it appears that polymeric samples with a well-defined structure are needed for a better understanding of the structure-properties correlation; hence, derivatives with a carefully selected molecular mass and low polydispersity are required.

This goal can easily be achieved by use of a controlled polymerisation procedure such as atom transfer radical polymerization (ATRP) [26] which gives the possibility also to obtain polymeric derivatives with structure of the star branched type.

Herein, we report a comparison between the different behaviour of several linear and star shaped liquid crystalline polymers under irradiation with CPL aimed at a better understanding of the role played by the macromolecular structure in the photoinduction of chiral supramolecular arrangement.

In particular three groups of LC polymers, chiral and achiral, have been synthesized and investigated:

- 1) a linear one, poly[(*S*)-4-[6-(2-methacryloyloxypropanoyloxy) hexyloxy]]-4'-ethoxyazobenzene] Poly[(*S*)-**ML6A**]-14, and four related three-arms branched macromolecular derivatives with controlled average molecular weight, star[(*S*)-4-[6-(2-methacryloyloxypropanoyloxy)hexyloxy]]-4'-ethoxyazobenzene] Star[(*S*)-**ML6A**]-2 through Star[(*S*)-**ML6A**]-24, obtained by ATRP of the novel chiral monomer (*S*)-4-[6-(2-methacryloyloxypropanoyloxy)hexyloxy]]-4'-ethoxyazobenzene [(*S*)-**ML6A**], containing the intrinsically chiral L-lactic acid residue suitable to affect the supramolecular organization of the liquid crystal phase. With the aim to investigate the structure-property relationships of these systems, they have been compared with the analogue polydisperse linear derivative Poly[(*S*)-**ML6A**]-AIBN (Scheme 1) obtained by AIBN free radical polymerization
- 2) two homopolymers, a linear one, poly(4- ω -methacryloyloxy-hexyloxy-4'-ethoxyazobenzene) {Poly[**M6A**]-24} [27] and a related three-arms branched

macromolecular derivative, star(4- ω -methacryloyloxy-hexyloxy-4'-ethoxyazobenzene) {Star[**M6A**]-24} ^[28], obtained by ATRP of monomer 4- ω -methacryloyloxy-hexyloxy-4'-ethoxyazobenzene (**M6A**) in the presence of allyl 2-bromoisobutyrate, or 1,3,5-(2'-bromo-2'-methylpropionato)benzene, as the mono- or trifunctional initiator, respectively. These polymeric materials display LC behaviour and give glassy nematic thin films.

- 3) linear and star shaped polymeric derivatives of several methacrylic monomers [(*S*)-**ML6A-C**, (*S,S*)-**MLL6A-C** (*S,S,S*)-**MLLL6A-C**, (*S*)-**ML2A-C**, (*S,S*)-**MLL2A-C**] bearing in the side chains the 4-cyano-4'oxy azobenzene chromophore, with different alkylic spacer between the polymerizable group and the azoaromatic chromophore containing one, two or three residues of L-lactic acid as chiral centers.

The structures of the investigated polymeric derivatives are reported in Figure 1.

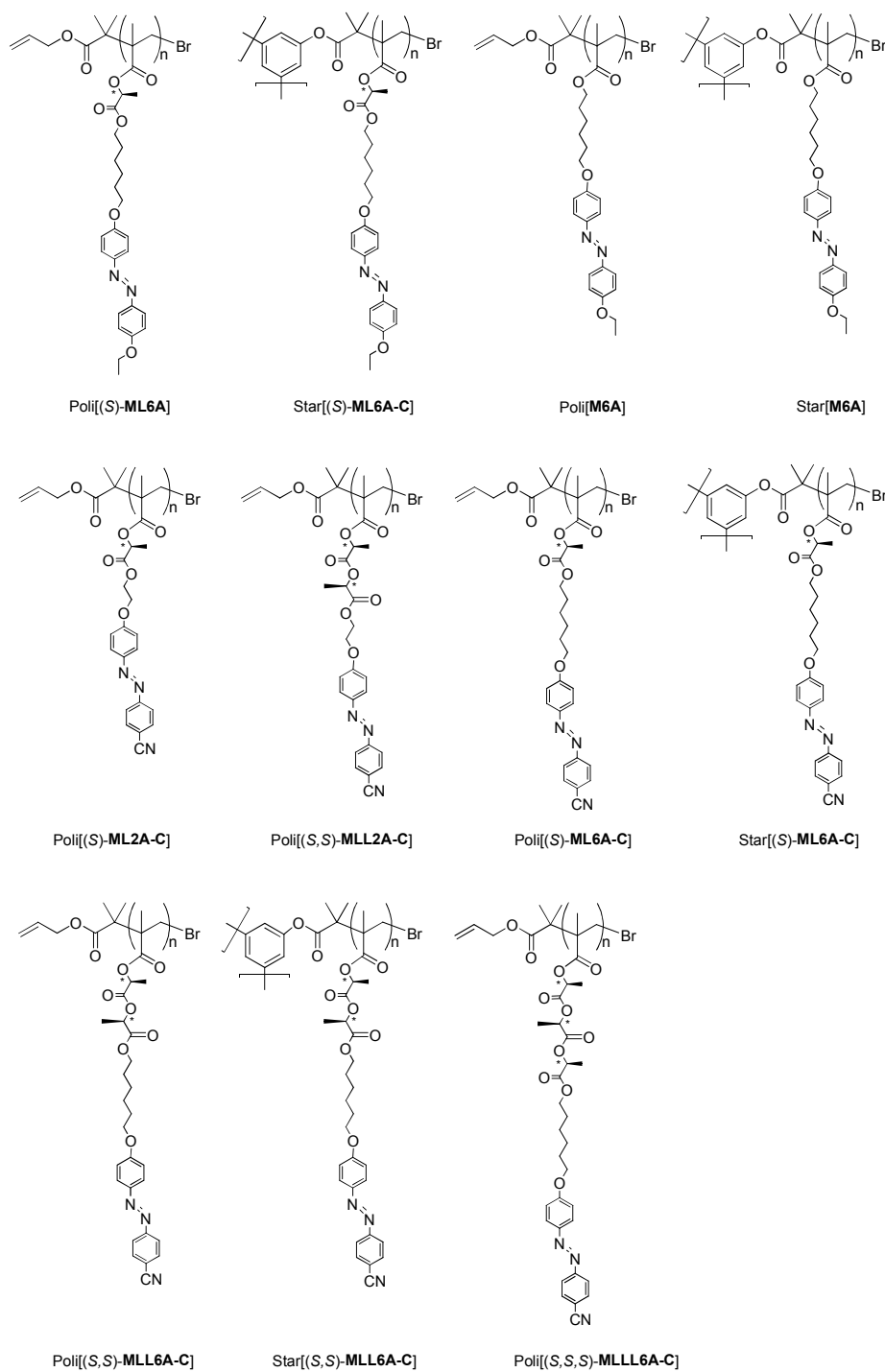
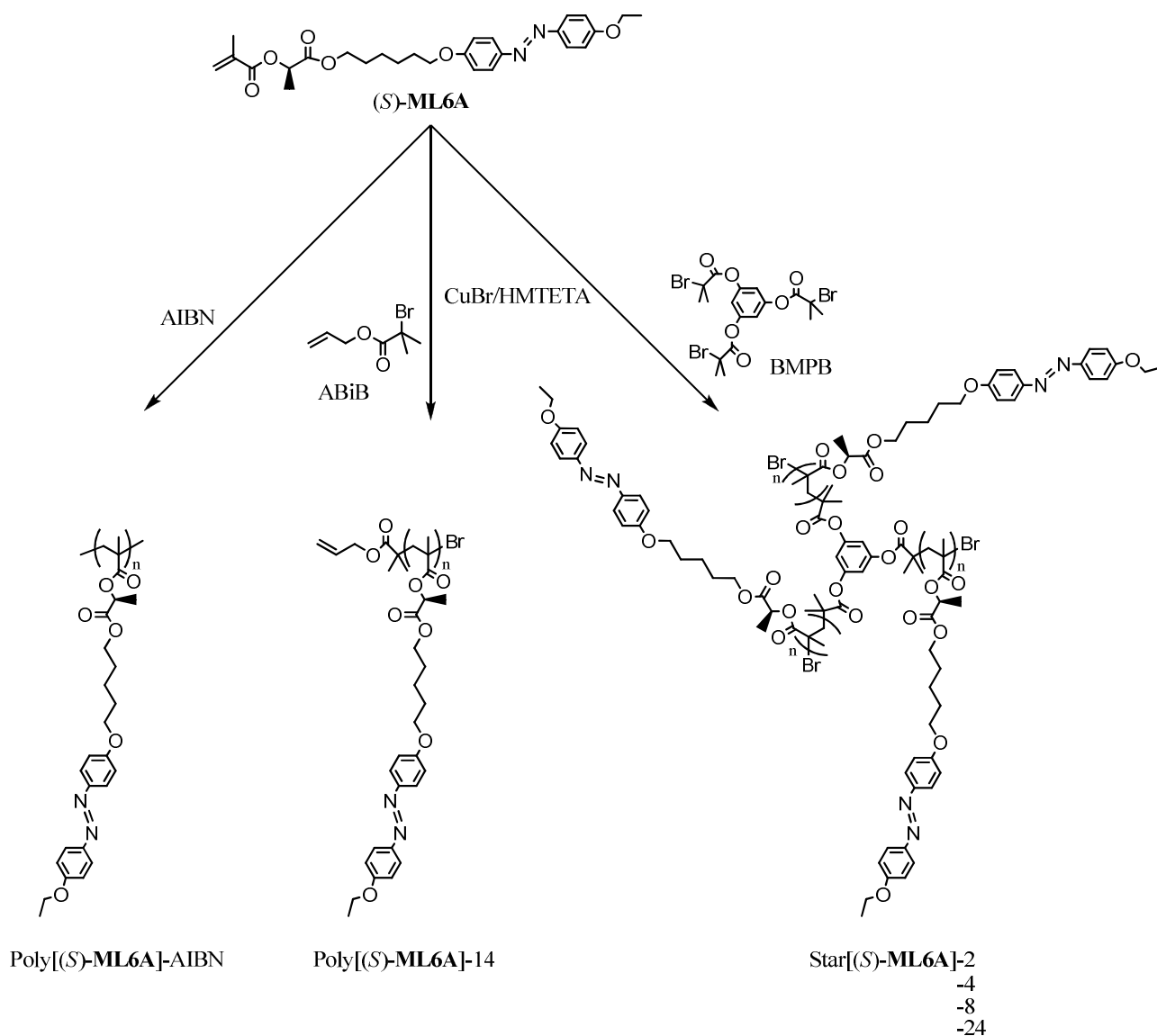


Figure 1: Structures of the investigated polymeric derivatives



Scheme 2: Synthetic procedures and chemical structures of the (S)-ML6A polymers

Poly[(S)-ML6A]-AIBN, prepared by AIBN free radical polymerization under long polymerization time, was obtained in a quite high yield (85 %), with average molecular weight appreciably high and molecular weight distribution typical of a free radical polymerization process (Table 1). The polymers synthesised by ATRP show low values of polydispersity index ($\overline{M}_w/\overline{M}_n$) in accordance to this polymerisation method (Table 1). In the $^1\text{H-NMR}$ spectra of the samples obtained by ATRP the signals related to the aliphatic and aromatic protons of the initiators are overlapped to those of the repeating units in the case of the star derivatives (see Experimental). For example, the star shaped sample obtained at shorter reaction times {Star[(S)-ML6A]-2} displays the resonances of the methylene and

methyl groups bonded to the quaternary carbon atom bearing the terminal Br atom at 1.9 and 2.3 ppm, respectively.

Table 1. Relevant synthetic data and characterization

Samples	Reaction time (h)	Yield ^[a] (%)	$\bar{M}_{n,th}$ ^[b]	$\bar{M}_{n,SEC}$ ^[c]	\bar{M}_w/\bar{M}_n	$[\alpha]_D^{25}$	$[\Phi]_D^{25}$ ^[d]
(S)-ML6A	-	-	-	-	-	-4.0	-17.1
Poly[(S)-ML6A]-AIBN	72	85	-	15400	1.54	-26.9	-115.3
Poly[(S)-ML6A]-14	14	37	26700	13900	1.19	-27.6	-118.3
Star[(S)-ML6A]-2	2	10	7800	8000	1.22	-26.8	-114.8
Star[(S)-ML6A]-4	4	14	10900	11400	1.20	-27.0	-115.7
Star[(S)-ML6A]-8	8	35	18700	19000	1.16	-27.8	-119.1
Star[(S)-ML6A]-24	24	48	35600	27600	1.15	-28.5	-122.1

[a] Calculated as (g of polymer / g of monomer) · 100. [b] $\bar{M}_{n,th}$ calculated by equation 1. [c] Determined by SEC in THF at 25°C. [d] Molar optical rotation, calculated as ($[\alpha]_D^{25} \cdot M/100$), where M represents the molecular weight of one repeating unit of Poly[(S)-ML6A] or of Star[(S)-ML6A].

The living character of the polymerization is confirmed by ¹³C-NMR spectra, which display signals related to the quaternary carbon atom bonded to Br at 58.0 ppm and to the methyl and methylene carbon atoms of the growing chain end-group at 27.5 and 38.9 ppm, respectively.

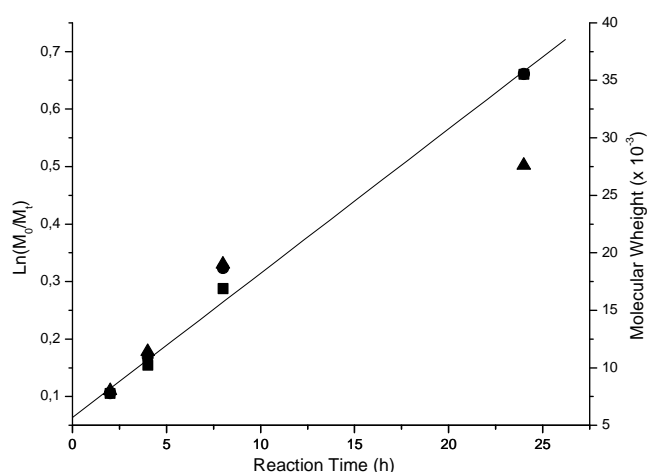


Figure 2. Evolution of $\ln([M]_0/[M]_t)$ (■) and of the number average molecular weight determined by SEC in THF at 25°C (▲) and calculated values (●) versus time in the ATRP of (S)-ML6A in THF for Star[(S)-ML6A] series.

An analysis of the yields and of the molecular weights of the star polymers obtained with different polymerisation times shows that the polymerisation rates followed an effective first-order kinetics. Figure 1 shows a linear relationship between $\ln([M]_0/[M]_t)$ (where $[M]_0$ and $[M]_t$ are the initial and at t time monomer concentrations, respectively) and the reaction time, indicating a clear first-order kinetics of the polymerization rate with respect to the monomer concentration, a relatively constant concentration of the growing species throughout the process, also at relatively high conversion, thus proving the living character of the process.

The plot of the number average molecular weight of the resulting star-shaped polymers as determined by SEC ($\bar{M}_{n,SEC}$) against monomer conversion (determined by collecting the unreacted monomer from the polymerization mixture) is also shown in Figure 1. The theoretical values of \bar{M}_n ($\bar{M}_{n,th}$), that are valid only in the absence of chain termination and transfer reactions, may be calculated by the following equation^[33]:

$$\bar{M}_{n,th} = \text{Conversion} \cdot (M_{(S)\text{-ML6A}} / M_{\text{BMPB}}) \cdot MW_{(S)\text{-ML6A}} + MW_{\text{BMPB}}$$

where $M_{(S)\text{-ML6A}}$ and M_{BMPB} are the initial amounts in moles of monomer and trifunctional initiator, respectively, and $MW_{(S)\text{-ML6A}}$ and MW_{BMPB} their respective molecular weights. As reported in Figure 1, calculated and experimental (by SEC) values are coincident only at low values of monomer conversion but, as the conversion increases, they diverge to an increasing extent. Such a behaviour, previously reported for star-shaped chiral photochromic polymethacrylates^[34], cannot be ascribed to termination reactions taking place under the real polymerisation conditions, as proved by the low and almost constant values of \bar{M}_w / \bar{M}_n (in the range 1.15-1.22), reported in Table 1, but to the particular molecular structure of multiarms polymers. It is well known, in fact, that star polymers have a smaller hydrodynamic volume with respect to that of linear polystyrenes having the same polymerization degree. As a consequence, SEC analysis gives underestimated molecular weight values for star-shaped polymers when measured with reference to the usually adopted linear polystyrene standards^[35, 36]. Anyway, the approximately linear correlation between $\bar{M}_{n,SEC}$ and time is indicative of the living character of the ATRP process and SEC analysis proves to be useful to confirm that a steady increment of the average molecular weight with conversion has taken place, as shown by the chromatograms reported in Figure 2. In conclusion, all the instrumental characterization techniques confirm that three-arms star polymers with C_3 symmetry and varying molecular size have been successfully obtained. Each chain contains a bromine atom

as end group which could be replaced through a variety of reactions leading either to end-functionalized polymers or used as the initiating site for the polymerization of a different monomer to obtain novel interesting star-shaped block copolymers as well as linear block copolymers starting, e.g., from Poly[(*S*)-**ML6A**]-14.

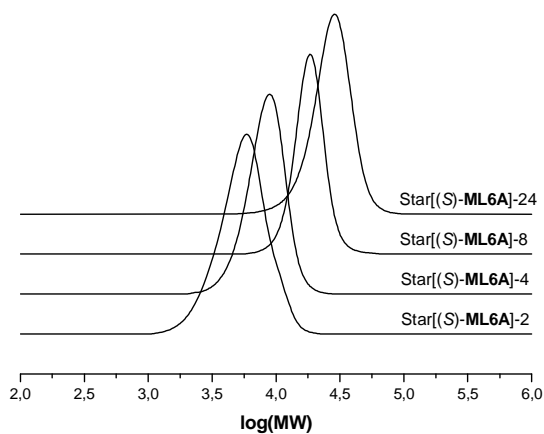


Figure 3. Normalized molecular weight distributions of Star[(*S*)-**ML6A**] polymers as determined by SEC in THF at 25°C.

Synthesis of 4- ω -methacryloyloxy-hexyloxy-4'-ethoxyazobenzene (M6A) and its polymeric derivatives

The synthesis of **M6A** and its polymeric derivatives is reported in Chapter 2

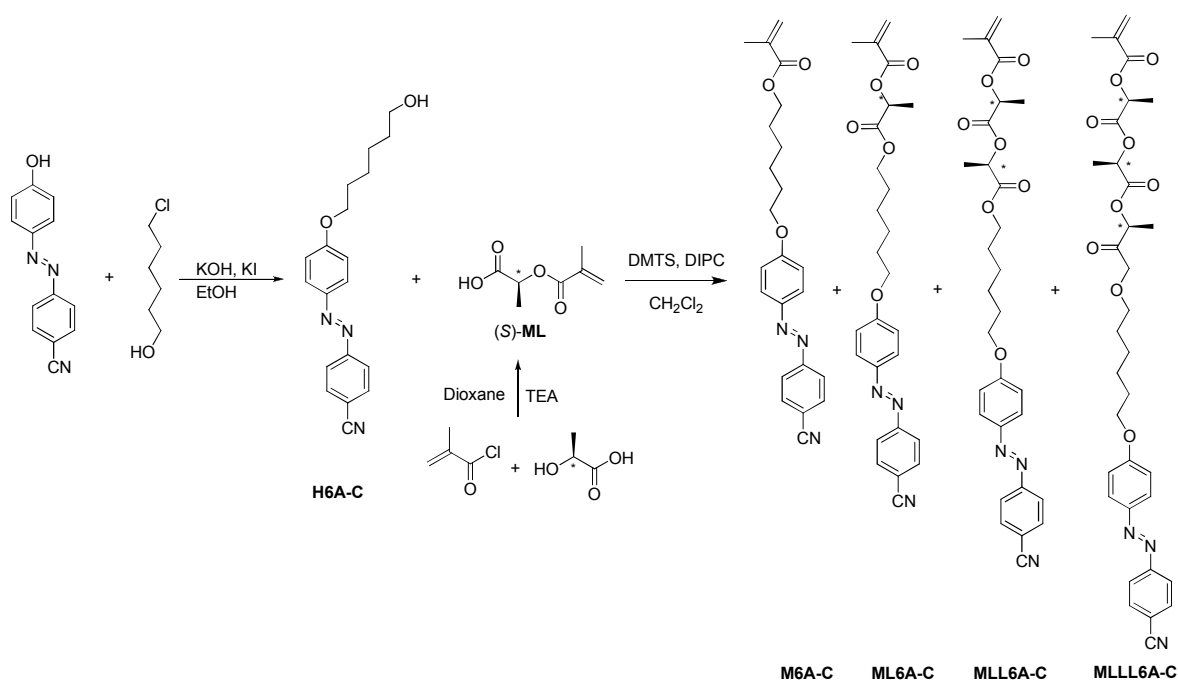
Synthesis of monomers and polymeric derivatives bearing the chromophore 4'-cyano-4-oxy-azobenzene

These monomers and their polymeric derivatives were synthesized following the same synthetic pathway as for (*S*)-**ML6A** starting with the azoic alcohol 4'-cyano-4-hydroxy azobenzene. The structural formula of the monomers and their polymeric derivatives are reported in Figure 3.

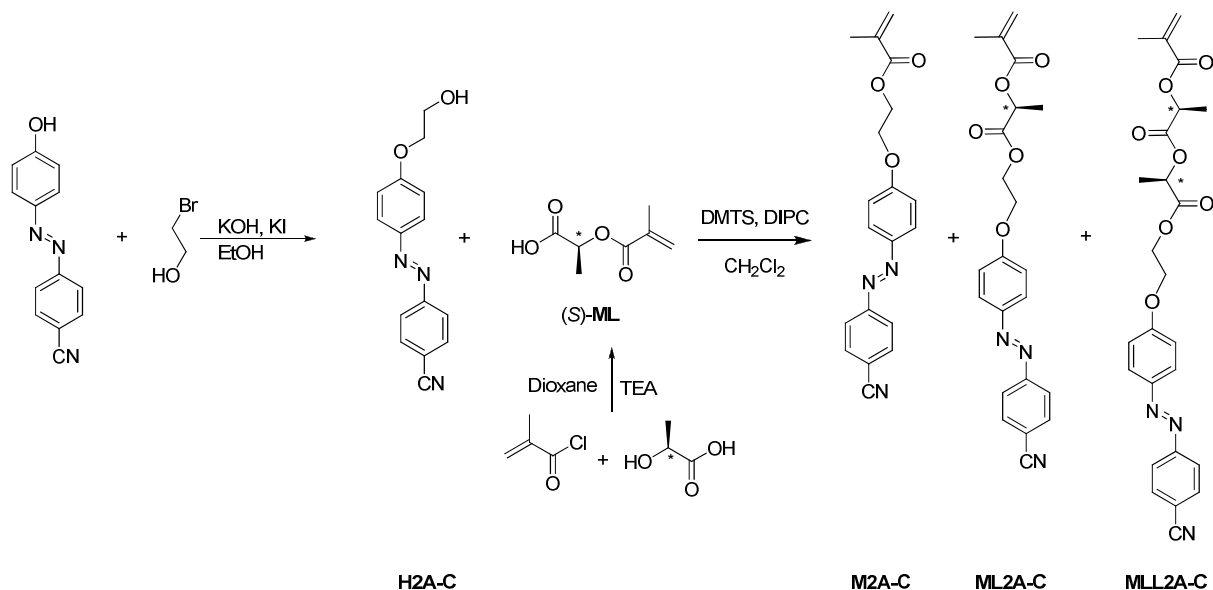
The azoic alcohols 4-(6-hydroxyhexyloxy)-4'-cyano-azobenzene (**H6A-C**) and 4-(2-hydroxyethoxy)-4'-cyano-azobenzene (**H2A-C**) were prepared by etherification under basic condition of with respectively 6-chlorohexanol and 2-bromoethanol with 4-hydroxy-4'-cyanoazobenzene.

During the esterification of these alcohol with (*S*)-**ML** some transesterification reactions can occur. In this way it has been possible to synthesize in one pot three different monomers bearing one, two or three acid lactic residues between the azoaromatic moieties and the methacrylic polymerizable group. These compounds were then separated by chromatography on silica gel, using dichloromethane as eluent with a yield from 34% to 20%.

In fact during this synthesis of the monomer 4-{6-[(*S*)-methacryloyloxypropanoyloxy]hexyloxy}-4'cyanoazobenzene [(*S*)-**ML6A-C**] also the two different optically active and the achiral monomer 4-(6-{(*S*)-2-[(*S*)-methacryloyloxypropanoyloxy]propanoyloxy}hexyloxy)-4'cyanoazobenzene [(*S,S*)-**MLL6A-C**], 4-(6-[(*S*)-2-{(*S*)-2-[(*S*)-2-methacryloyloxypropanoyloxy]propanoyloxy}-propanoyloxy]hexyloxy)-4'cyanoazobenzene [(*S,S,S*)-**MLLL6A-C**] and the achiral one 4- ω -methacryloyloxy-hexyloxy-4'-cyanoazobenzene **M6A-C**. were synthesized and then isolated (Scheme 3)

Scheme 3: Synthesis of *(S)*-ML6A-C and related monomeric derivatives

The new monomer 4-{2-[(*S*)-methacryloyloxypropanoyloxy]ethoxy}-4'-cyanoazobenzene (**ML2A-C**) also the monomer was synthesized in the same way using 2-bromoethanol. Also 4-(2-[(*S*)-2-[(*S*)-methacryloyloxypropanoyloxy]propanoyloxy]ethoxy)-4'-cyanoazobenzene (**MLL2A-C**) and the achiral monomer 4-(ω -methacryloyloxy-ethoxy)-4'-cyanoazobenzene (**M2A-C**) were synthesized and isolated. (Scheme 4).

Scheme 4: of *(S)*-ML2A-C and related monomeric derivatives

The FT-IR, ^1H - and ^{13}C -NMR characterizations are in agreement with the expected structures.

Figure 4: ^1H -NMR of ML6A-C (a), Poly(ML6A-C) (b) and Star(ML6A-C) (c). Starred signals are due to solvent resonance. The signal relative to the resonance of the terminal allylic $\text{CH}_2\text{-O}$ at 4.6 ppm in Poly(ML6A-C) are marked with #.

As an example in Figure 4 are reported the ^1H -NMR spectra of linear Poly[(*S*)-**ML6A-C**], of the three arm star polymer Star[(*S*)-**ML6A-C**] and the monomer (*S*)-**ML6A-C**. In the ^1H -NMR spectra of (*S*)-**ML6A-C** (Figure 4a) at 7.9 ppm the signal of the two aromatic protons in 2- and 2'- can be observed, while the 3'- and 3- protons resonate at 7.8 and 7.0

ppm respectively. At 6.2 and 5.6 are present the signals of the diastereotopic protons of the methacrylic methylene. The quarted of the CH of the acid lactic residue can be observed at 5.1 ppm and the two CH₂-O groups show two triplet at 4.3 and 4.1 ppm. At 2.0 ppm is present the singlet of the methacrylic CH₃ and the aliphatic protons of the CH₂ of the alkyl chain resonate between 1.8 and 1.4 ppm. The singlet of the methyl of the lactic acid residue resonates at 1.65 ppm.

Figure 5: ¹³C-NMR of ML6A-C (high panel). In the lower section are reported magnifications of the signal of CH (69 ppm, left panel) and CH₃ (17 ppm, right panel) of the residues of L-lactic acid for ML6A-C (a), MLL6A-C (b), MLLL6A-C (c).

In Figure 5 is reported the ¹³C-NMR spectrum of (*S*)-**ML6A-C**: at 171.3 ppm is observed the signal of the carbonyl of the L-lactic residue, well separated from the methacrylic carbonyl at 163 ppm. Between 155 and 113 ppm are the aromatic carbons, the -CN and the two vinylic carbons, at 135.7 and 126.8 respectively. At 69.2 and 17.7 ppm are respectively the signals of the CH and CH₃ of the lactic residue. At 68.6 and 65.6 ppm are the two methylenic carbons in α to the ether and ester oxygen respectively. Between 30 and 20

ppm are present the signal of the other CH₂ of the aliphatic chain and finally at 18.9 ppm is the signal of the methacrylic methyl.

The monomers with different numbers of L-lactic units were easily characterized by ¹³C-NMR spectroscopy. In Figure 5 magnification of the spectral zones of the ¹³C-NMR spectra of (*S*)-**ML6A-C**, (*S,S*)-**MLL6A-C** and (*S,S,S*)-**MLLL6A-C** between 70-60 and 20-10 ppm are shown.

In the spectra of (*S*)-**ML6A-C** only one signal at 69.2 ppm due to the CH of the acid lactic residue is visible while in the spectra of (*S,S*)-**MLL6A-C** and (*S,S,S*)-**MLLL6A-C** two and three signal can be observed respectively. The signal of the CH₃ of the lactic acid residue has the same behavior: from (*S*)-**ML6A-C** to (*S,S,S*)-**MLLL6A-C** the number of signal at 17 ppm passes from one to three.

These monomers have been homopolymerized using **ABiB** as monofunctional initiator and **BMPB** as a trifunctional one using the same procedure reported for (*S*)-**ML6A**.

The relevant data about the structural characterization of these polymeric derivatives are reported in Table 2.

Table 2: Structural characterization of the polymeric derivatives

Sample	$\overline{M}_{n,GPC}$ ^{a)}	$\overline{M}_{n,^1H-NMR}$ ^{b)}	$\overline{M}_w/\overline{M}_n$ ^{a)}	$\overline{X}_{n,GPC}$ ^{c)}
Poly[ML2A-C]	9700	10700	1,21	23,8
Poly[MLL2A-C]	20700	-----	1,18	43,1
Poly[ML6A-C]	18100	15600	1,18	39,0
Star[ML6A-C]	31400	-----	1,15	22,6
Poly[MLL6A-C]	17000	16400	1,19	31,8
Star[MLL6A-C]	27000	-----	1,14	13,1
Poly[MLLL6A-C]	22300	23000	1,22	35,9

a) Determinated by GPC in THF at 25°C with a column Phenogel MXM

b) Determinated by ¹H-NMR spectroscopy by integration of the terninal units signals

c) Average polymerisation degree (\overline{X}_n) for linear macromolecules and for each branch of the star shaped derivatives calculated by Mn values.

Due to the presence of several chiral centers on one single absolute conformation in the synthesized systems, polarimetric measurements were done, in order to verify the optical activity and the influence of the molecular structure on the chirality of the synthesized derivatives Table 3.

From these datas it can be easily observed how the number of the L-lactic residues has an high influence on their optical activity: from one to two L-lactic units the value of the molar rotation ($[\Phi]_D^{25}$) is seven time greater in the case of monomers with a short alkylic spacer and twenty times in the case of a six carbon atoms chain. When the number of L-lactic unit pass to three the value of $[\alpha]_D^{25}$ increase of only a 25% Table 3.

Table 3: specific and molar rotation of the synthesized derivatives

Campione	$[\alpha]_D^{25}$	$[\Phi]_D^{25 \text{ a)}$
(S)-ML2A-C	-7,10	-28,9
(S,S)-MLL2A-C	-44,3	-211,0
(S)-ML6A-C	-2,32	-10,7
(S,S)-MLL6A-C	-37,3	-200,0
(S,S,S)-MLLL6A-C	-43,5	-264,0
Poly[(S)-ML2A-C]	-29,0	-118,0
Poly[(S,S)-MLL2A-C]	-52,8	-253,2
Poly[(S)-ML6A-C]	-23,4	-108,3
Star[(S)-ML6A-C]	-24,5	-113,4
Poly[(S,S)-MLL6A-C]	-43,3	-232,1
Star[(S,S)-MLL6A-C]	-47,0	-252,0
Poly[(S,S,S)-MLLL6A-C]	-61,2	-371,5

Molar rotation, calculated as $([\alpha]_D^{25} \cdot M/100)$, where M is the molecular weight of the repeting units in the polymeric derivatives

A comparison between the monomeric and polymeric systems with the same number of chiral residues shows that the systems with a short aliphatic spacer displays higher rotations. This behave can be attributed to the higher stiffness of the lateral chain that impart higher conformational rigidity.

All the polymeric derivatives displays an higher rotation than their correspondent monomeric derivatives due to the presence of ordered macromolecular conformation that increase the conformational chirality. Finally no significant differences between linear and star polymers are observed. The optical purity of the synthesized derivatives was not measured because previous studies ^[37-39] on similar compounds had demonstrate that the enantiomeric excess of the synthesized monomers was greater than 90%. Because of our compounds are synthesized from enantiomeric pure L-lactic acid with analogous reactions, we can reasonably deduce that these monomers and polymers have the same optical purity.

Characterization and photoinduction of chirality

Polymeric derivatives of (S)-ML6A

POM, DSC and XRD characterization.

With the aim to study their LC properties, all the polymeric derivatives have been characterized by differential scanning calorimetry (DSC), polarized optical microscopy (POM) and X-ray diffraction (XRD). Phase-transition temperatures determined by DSC are summarized in Table 4: all the samples display on heating a glass-transition temperature (T_g) and a liquid-crystal-phase with a consequent isotropization temperature (T_i). The high enthalpy of isotropization, about $9,6 \text{ J g}^{-1}$, is related to the presence of a typical smectic phase.

In all cases, on cooling, the latter transitions show a modest degree of supercooling (4-5°C) and a stable frozen liquid-crystal mesophase is achieved and maintained at room temperature.

Table 4: Thermal transitions^[a] and mesomorphism determined by DSC, POM and XRD of the polymeric derivatives of (S)-ML6A

Samples	Thermal transition °C				
Poly[(S)-ML6A]-AIBN	G	53	SmA _{1/2}	129	I
Poly[(S)-ML6A]-14	G	56	SmA _{1/2}	129	I
Star[(S)-ML6A]-2	G	48	SmA _{1/2}	114	I
Star[(S)-ML6A]-4	G	49	SmA _{1/2}	117	I
Star[(S)-ML6A]-8	G	59	SmA _{1/2}	132	I
Star[(S)-ML6A]-24	G	61	SmA _{1/2}	133	I

[a] Obtained from the second heating DSC thermal cycle in nitrogen atmosphere (10°C/min).

XRD studies were carried out at variable temperature on some representative compounds such as Poly[(S)-ML6A]-14, Star[(S)-ML6A]-2 and Star[(S)-ML6A]-24. Firstly, X-ray patterns were recorded at room temperature on the above samples annealed for two hours 40°C above the T_g , in order to develop the mesophase. Patterns were also taken at variable temperatures on virgin and unannealed samples. Finally, these compounds were mechanically aligned with the aim to obtain oriented patterns. The diffractograms of Poly[(S)-

ML6A]-14 under these several physical conditions are reported in Figure 7. In all cases the diffractograms are qualitatively very similar: all of them display a sharp Bragg reflection in the low-angle region and a diffuse, broad maximum in the high-angle region. This kind of pattern is characteristic of a liquid crystal phase with a layered structure and confirms that the mesophase order exists at room temperature and is stable at high temperatures. The high-angle diffuse halo corresponds roughly to a mean distance of 4.4 Å and is associated to the liquid-like lateral interactions of the azoaromatic mesogenic groups. The measured spacing, deduced by applying Bragg's law to the low-angle reflection, is very close to 16 Å in all cases, regardless the compound examined, the conditions of temperature and the thermal treatment. The predicted length of the mesogenic moiety calculated from Dreiding stereomodels, assuming a fully-extended conformation of the hydrocarbon chains, is 31 Å (33 Å including the methacrylate group). Therefore, it appears that the observed low-angle maximum corresponds to the second order (d_{002}) reflection and the actual layer spacing is close to 32 Å, which is comparable to the value expected for a SmA arrangement of the mesogenic monomers. The fact that the first order (d_{001}) reflection is not visible must arise from the presence of a period $d/2$ in the projection of the electron density profile along the normal to the layers. This phenomenon has been described for other side-chain LC polymers and is accounted for by the confinement of the polymeric backbones in a thin sublayer layer perpendicular to the director, so that the polymeric backbones produce an electron density maximum comparable to that of the mesogenic cores^[40]. These features are consistent with a fully-interdigitated smectic A (SmA_{1/2}) mesophase (Figure 8). The absence of significant differences in layer periodicity by changing the macromolecular shape or the average molecular weight indicates that the same structural model is valid for all the samples, both with a linear polymeric backbone and a star-like arrangement.

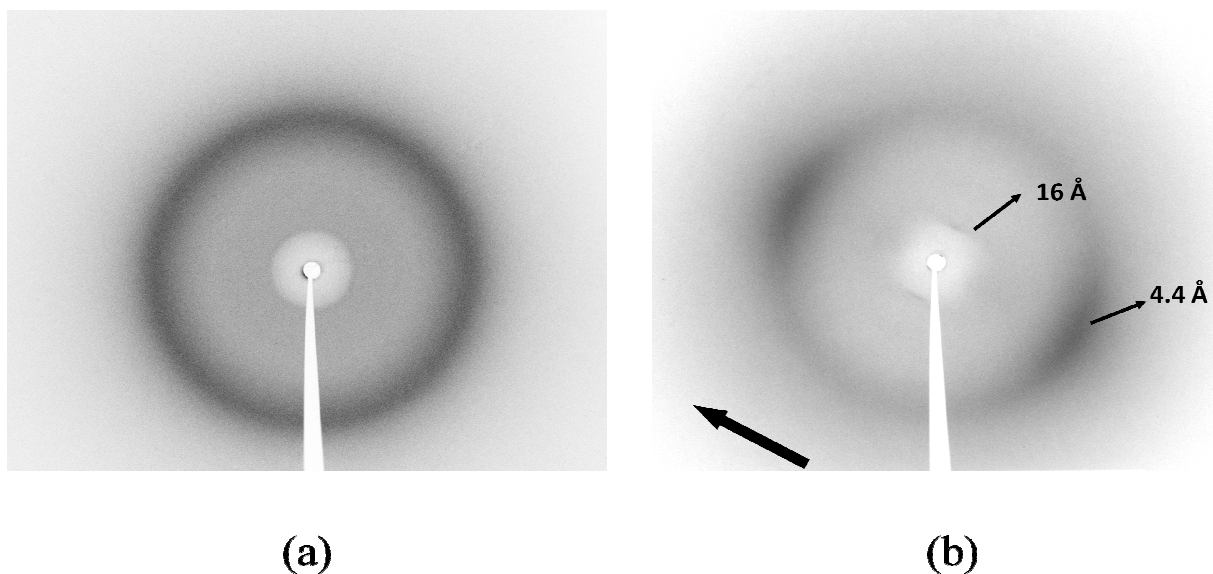


Figure 6: X-ray diffraction pattern of the SmA mesophase of Poly[(S)-ML6A]-14 recorded at room temperature after heating at 135°C (a) and oriented X-ray diffraction pattern of the SmA mesophase of Poly[(S)-ML6A]-14 recorded at room temperature (b). The sample was mechanically aligned in the direction of thick arrow.

Table 5 Spacing, determined by applying Bragg's law to the small-angle reflection observed in the patterns, in the smectic A mesophase of Poly[(S)-ML6A]-14, Star[(S)-ML6A]-2 and Star[(S)-ML6A]-24 measured by XRD at variable temperatures.

Sample	Conditions	Measured d_{002} spacing (Å) ^[a]	Layer spacing (Å) ^[a]
Poly[(S)-ML6A]-14	25°C, Virgin	15.5	31.0
	25°C, Annealed	16.5	33.0
	25°C, Aligned	16.3	32.6
	75°C	15.8	31.6
Star[(S)-ML6A]-2	25°C, Annealed	16.5	33.0
Star[(S)-ML6A]-24	25°C, Virgin	15.8	31.6
	25°C, Annealed	16.5	33.0
	25°C, Aligned	16.1	32.2
	75°C	15.7	31.4

[a] The spacing was measured with an estimated accuracy of $\pm 0.5\text{Å}$

Finally, mechanically-aligned samples of Poly[(S)-ML6A]-14 and Star[(S)-ML6A]-24 were obtained by shearing the samples on the capillary wall with a metal rod at a temperature at which the mesophase is fluid. Oriented patterns were obtained when the samples submitted

to this treatment were irradiated at room temperature (Table 5). In the resulting patterns the low-angle reflection appears as a pair of sharp spots aligned along the direction perpendicular to the shearing, whereas the high-angle halo becomes a pair of diffuse crescents centred in the shearing direction.

These features indicate that the smectic planes are oriented along the stretching direction with the mesogenic units oriented perpendicular to that direction. This behaviour is common for side-chain LC polymers. An accurate analysis of the nature of this mesophase was achieved by the observation of their typical optical texture by POM in analogy with previous studies on similar azo-polymers^[41]. All the samples, during the heating-cooling process, show textures that indicate the presence of macrodomains with a SmA phase, as shown for example for poly[(*S*)-**ML6A**]-14 in Figure 8. In particular, the thin film slowly cooled from the isotropic melt at 128°C shows small drops of birefringent mesophases separating from the melt that develop after shearing and annealing at 110°C for 48 hours into cylindrical LC domains on an homeotropic background (Figure 8a and b). A polymeric film after isotropization and annealing at 120°C develops a typical cylindrical conicofocal texture like as a SmA phase (Figure 8 c, d, e).

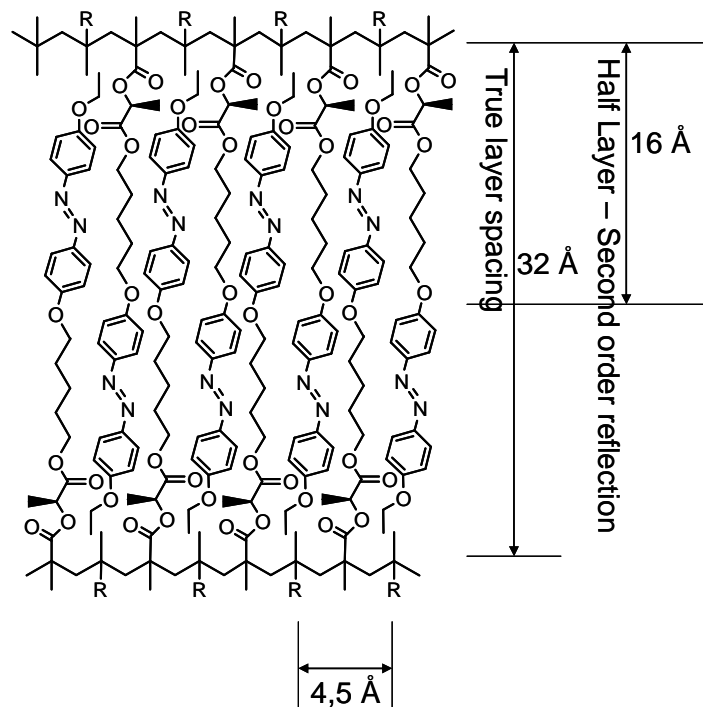


Figure 7. Smectic layer spacings of a fully interdigitated side-chain chromophoric configuration determined by XRD (R = chromophoric moieties located in the side chain outside the layer).

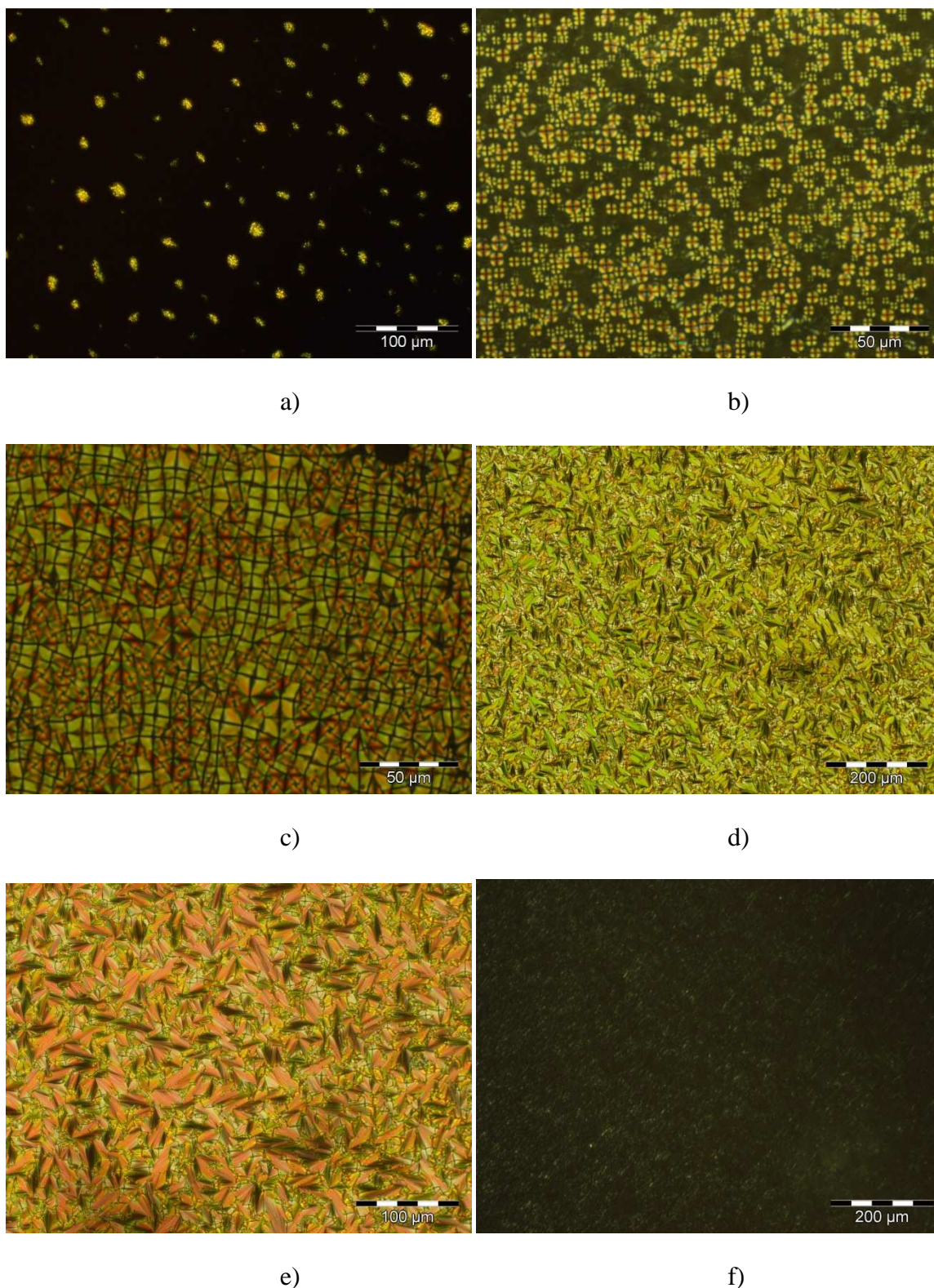


Figure 8: POM microphotographs of Poly[(S)-ML6A]-14 (sample prepared between two glasses) (a) at 128 °C upon cooling from the isotropic liquid, (b) thin film annealed for 48h at 110°C after isotropization and shear and (c) thin film annealed for 24h at 120°C after isotropization (d, e) thin film annealed for 24h at 90°C after isotropization, (e) thin film after pressure: homeotropic alignment is induced.

UV-Vis Spectra and chiroptical properties in solution.

The UV-Vis absorption spectra (Figure 10 and Table 6) in CHCl_3 solution of all the investigated linear and star polymers, as well as the monomer (*S*)-**ML6A**, exhibit, in the 250–550 nm spectral region, two bands related to the $n \rightarrow \pi^*$ and $\pi \rightarrow \pi^*$ electronic transitions of the *trans*-azobenzene chromophore with maxima centered at about 440 nm ($\epsilon \cong 1500 \text{ L}\cdot\text{mol}^{-1}\cdot\text{cm}^{-1}$) and 360 nm ($\epsilon \cong 28000 \text{ L}\cdot\text{mol}^{-1}\cdot\text{cm}^{-1}$), respectively ^[42], appearing, within the limits of experimental error, qualitatively and quantitatively independent from molecular structure and polymerization degree.

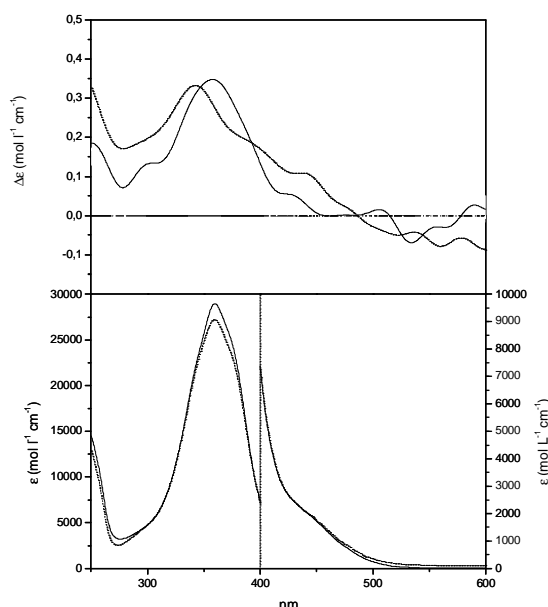


Figure 9. CD (up) and UV-vis (bottom) spectra of (*S*)-**ML6A** (—) and Poly[(*S*)-**ML6A**]-14 (---) in CHCl_3 .

The UV spectra do not exhibit any variation on passing from the monomer to the polymer, indicating the substantial absence of electrostatic dipole-dipole interactions between neighbouring aromatic moieties, the symmetry of the absorption band at 360 nm providing evidence that the azoaromatic chromophores are essentially isolated in solution. The monomer and all high molecular weight samples in the *trans* configuration are optically active in chloroform solution at the sodium D-line (Table 6). Indeed, the macromolecules investigated display molar optical rotatory powers $[\alpha]_{\text{D}}^{25}$ for repeating unit constantly around -28 , seven times larger than that of (*S*)-**ML6A** ($[\alpha]_{\text{D}}^{25} = -4.0$), thus suggesting that the macromolecules are characterized by a appreciable conformational chirality

The CD spectrum of (*S*)-**ML6A** in chloroform solution (Figure 9) displays one weak positive dichroic absorption with maximum at 360 nm ($\Delta\epsilon \approx +0,35 \text{ L mol}^{-1} \text{ cm}^{-1}$), strictly

related to the UV-Vis absorption maximum connected with the $\pi \rightarrow \pi^*$ electronic transition. Similarly, the CD spectra of the polymeric samples in solution exhibit in the spectral region related to the $\pi \rightarrow \pi^*$ electronic transition only one positive dichroic band centred at about 350-360 nm ($\Delta\epsilon \approx +0,2 \text{ L mol}^{-1} \text{ cm}^{-1}$), in close correspondence with the UV absorption (Figure 10), and related to isolated chromophores, in a similar manner as the monomeric compound, with no influence by the average molecular weight value and macromolecular shape, in agreement with the specific optical rotatory powers (Table 1).

These behaviours are different from what reported in the literature for chiral rigid methacrylic amorphous polymers that exhibit an increase of optical activity on increasing the molecular weight^[43] or passing from linear to star-shaped structures^[34]. The contribution to the overall optical activity in solution by the conformational dissymmetry of liquid crystal polymeric derivatives, characterized by longer and flexible aliphatic spacer between the main chain and the azoaromatic chromophore, appears therefore of limited extent, as suggested also by the specific optical rotatory power at the sodium D line.

UV-Vis spectra and chiroptical properties in thin film.

The UV-Vis spectra and chiroptical properties of the synthesized polymers have been investigated also in the solid state, as thin films prepared by casting from dichloromethane solution over clean slides of fused silica. By inspection with POM, the virgin films at room temperature appear optically isotropic: neither any birefringence nor scattering being observed.

The main UV-Vis data of relevant polymeric samples are collected in Table 6 and the absorption spectra of Poly[(*S*)-**ML6A**]-14 in the solid state are reported as an example in Figure 10a: in addition to the typical $\pi \rightarrow \pi^*$ and $n \rightarrow \pi^*$ electronic transitions of the azoaromatic chromophore centered at around 357 and 440 nm, respectively, an additional band at around 248 nm, associated with the $\pi \rightarrow \pi^*$ transition of the single aromatic ring, is present.

The absorption band of the $\pi \rightarrow \pi^*$ transition in the virgin films appears broader with respect to the spectra in solution, with two additional shoulders at 340 and 380 nm, related respectively to the formation of H- (blue shift) and J-like (red shift) aggregates^[44] imposed by the structural constraints of the macromolecules in the solid state. The relatively high absorbance of the transition at 340 nm indicates high concentration of H aggregates in the amorphous solid state.

In order to develop the mesophase, a thermal treatment consisting of a heating above the clearing point temperature (T_i) for 5 minutes followed by annealing for 15 minutes at a temperature reduced by a factor of about 0.7 (T_{anneal}/T_i) has been carried out.

The annealed film of Poly[(*S*)-**ML6A**]-14 displays broader, less intense absorption bands (Figure 11a and Table 6) and produces LC domains as observed by POM. The main absorption band is characterized by a small bathochromic shift of the $\pi \rightarrow \pi^*$ azoaromatic absorption maximum to 362 nm. In addition, the shoulders related to the H- and J-aggregates located around 340 and 380 nm, increase relatively in importance.

This can be related to development of aggregates and thus to more ordered dipolar intra- and inter-chain interactions that the chromophores experience in the $\text{SmA}_{1/2}$ phase (Figure 8) compared to the solution and the amorphous solid state.

Table 6: UV-Vis data of the investigated compounds in CHCl₃ solution and as thin films after different treatments.

Samples		$\lambda^{\phi \rightarrow \phi^* [a]}$	$\lambda^{\pi \rightarrow \pi^* [a]}$	$\lambda^{\text{H-agg. [a,b]}}$	$\lambda^{\text{J-agg. [a,b]}}$	$\lambda^{\text{n} \rightarrow \pi^* [a,b]}$
(S)- ML6A	solution	- ^[c]	360	-	-	440
Poly[(S)- ML6A]-14	solution	- ^[c]	360	-	-	440
Star[(S)- ML6A]-24	solution	- ^[c]	360	-	-	440
Poly[(S)- ML6A]-14	virgin film	248	357	340	380	440
Poly[(S)- ML6A]-14	annealed film	248	362	340	385	440
Poly[(S)- ML6A]-14	irradiated film	248	360	345	385	440
Star[(S)- ML6A]-24	virgin film	248	360	340	378	440
Star[(S)- ML6A]-24	annealed film	248	360	340	380	440
Star[(S)- ML6A]-24	irradiated film	248	360	344	385	440

[a] Wavelength of maximum absorbance in nm. [b] Shoulder. [c] Not observed due to solvent cut-off.

In particular, the decrease in absorbance of the $\pi \rightarrow \pi^*$ transition can be attributed to the aggregation of the azobenzene fragments possessing elevated anisotropy^[45, 46], while the $\pi \rightarrow \pi^*$ band at 248 nm of the single aromatic ring, not influenced by orientation, remains substantially unaffected. Finally, the increase of absorbance at wavelengths over 400 nm can be mainly associated with the light scattering due to the formation of the birefringent domains of liquid-crystal phase after annealing.

By comparing several CD spectra recorded at different film positions and rotated around the light beam direction it was also confirmed that the contribution of linear dichroism and linear birefringence to the CD spectra of the polymeric films is negligible.

The CD spectrum of a fresh film of Poly[(S)-**ML6A**]-14 (a) exhibits two relatively intense dichroic signals of opposite sign and similar intensity, connected to the $\pi \rightarrow \pi^*$ electronic transitions of the azoaromatic chromophores, with a crossover point around 335 nm, close to the UV maximum absorption. This behaviour is typical of exciton splitting determined by cooperative dipole-dipole interactions between neighbouring side chain azobenzene chromophores arranged in a mutual chiral geometry of one prevailing handedness^[2, 43, 47, 48]. Significantly, the CD spectrum of the same sample in dilute solution (Figure 9) displays only one weak positive dichroic signal at 360 nm, indicative of the absence in solution of chiral chromophore aggregates.

The thermal annealing strongly affects the chiroptical properties of the film (a). Upon prolonged heating a strong enhancement of CD signals takes place, and the ellipticity values become much more intense than those observed before annealing.

The crossover point of the couplets in the solid state appears blue-shifted with respect to the UV maximum absorbance (ellipticity = 0 at around 335 nm against UV λ_{max} at 360 nm). As the negative band appears of higher intensity, and close to the electronic transition wavelength associated to chiral H-aggregates (340 nm), the CD spectrum can be interpreted as originated from the overlapping of a exciton splitted CD band given by the H-aggregates with a negative CD band having its maximum at 385 nm, corresponding to the maximum absorbance of J-aggregated chromophores, differently sensitive to the chiral geometry of the material [23]

The UV-Vis and CD spectra of star polymers of comparable thickness appear essentially similar to those of Poly[(*S*)-**ML6A**]-14, as shown for example in Figure 10b for Star[(*S*)-**ML6A**]-24. The star shaped polymers as native films, as well as in the LC state, exhibit CD couplets with crossover points centered at 340 and 332 nm, respectively, of the same sign and shape as the related linear derivatives, but always less intense at equal film thickness.

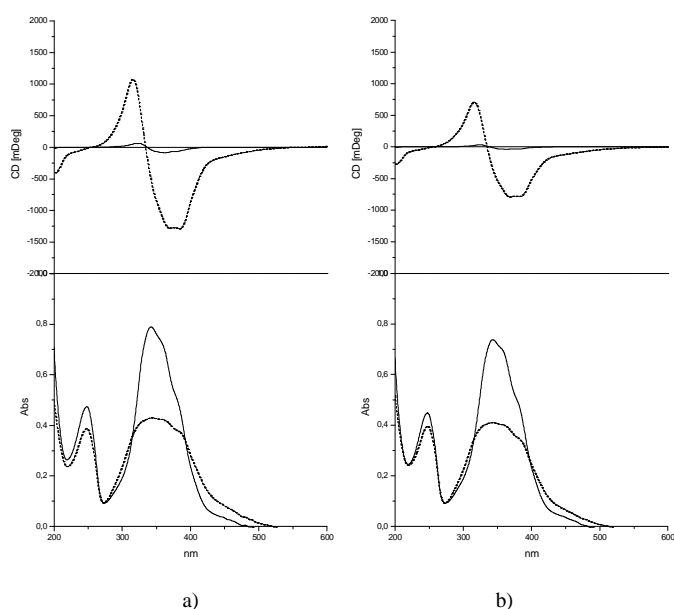


Figure 10. CD (up) and UV-Vis (bottom) spectra of a thin film of Poly[(*S*)-**ML6A**]-14 (a) and Star[(*S*)-**ML6A**]-24 (b) in the virgin state (—) and after isotropisation and annealing at 90°C for 15 minutes (---).

From the CD spectra it can be clearly seen how branching affects the chirality of the system: the films of Star[(*S*)-**ML6A**]-24 always exhibit a lower optical rotation power than those of Poly[(*S*)-**ML6A**]-14, thus suggesting that chirality is related to a certain way to the

main chain conformational order and/or to supramolecular liquid crystalline organization. A less ordered LC phase in the star-shaped derivatives could be supposed as originated by the stiffness of the rigid central unit that creates defects in the LC supramolecular conformation. In any case, the above findings suggest that similar conformational arrangements with a prevailing chirality are assumed both in the amorphous and particularly in the LC phase, regardless the molecular structure.

It is generally accepted that chirality is induced in these materials as a consequence of chiral interchromophoric interactions, however short-range chromophoric aggregates in liquid crystal arrangements could not be the only responsible of the remarkable amplification of chirality that is observed. Examples of amorphous azopolymeric systems, in which the chirality is related to the presence of chromophores aggregated in a mutual chiral arrangement are reported in the literature, but these systems display lower optical rotation values^[34, 43, 48].

In the present case, the presence of exciton couplets and surprisingly high ellipticity (up to 9000 mdeg/ μm at 361 nm, Figure 10a) are quite noticeable for a normal smectic A phase with uniaxial symmetry and hence lacking of any kind of supramolecular chirality. Consequently, the high chiroptical properties observed could suggest the presence of a chiral liquid crystal phase similar to a planar twist-grain-boundary (TGB) phase or Sm-A* phases, reported only when chiral mesogens with high helical twisting power are present,^[49, 50] but POM observation of thick films, as mentioned above, clearly suggests the presence of a normal smectic A phase. In the SmA phase, where the chromophoric molecules are arranged perpendicular to the layer planes, the mesogenic moieties cannot adopt a supramolecular helix structure perpendicular to the layers. It can only occur parallel to the layers and only for systems with a strong twisting power. Therefore, a helical superstructure is only possible if screw dislocations punctuate the layers, giving rise to the so-called twisted grain boundary A phase (TGBA)^[51, 52]. In the present case the formation of this particular mesophase appears highly improbable. Moreover, thin films of chiral smectic A liquid crystals possessing high chirality due to the Surface Electroclinic Effect (SEC) that induce in the film a chiral smectic C phase are reported in literature: the polar interaction between the glass wall and the LC material induces a polarization resulting in a chiral reorientation of the LC director near the surface.^[53, 54] Further information regarding the molecular arrangement in these thin film (100-200 nm) by XRD and polarized optical microscopy (texture analysis) could not be obtained so far, as thicker film samples are required and the behavior could be different when compared to the thin films here investigated.

Photoinduced switching of supramolecular chirality.

Annealed thin films of Poly[(*S*)-**ML6A**]-14 and Star[(*S*)-**ML6A**]-24 of thickness about 140 nm in the glassy liquid crystal state were irradiated with *r*-CPL and *l*-CPL, respectively, with an Ar⁺ laser (power = 20 mW/cm²) at 488 nm for 30 min. The UV-Vis spectra of irradiated polymers result similar to those of annealed corresponding films (Table 6 and Figure 11). These results suggest that the dipolar azoaromatic aggregations (H- and J-aggregates) in the liquid crystalline phase remain substantially unaffected by CPL irradiation.

Upon irradiation of Poly[(*S*)-**ML6A**]-14 with *r*-CPL, the CD spectrum displays a net inversion of sign as well as a relevant amplification of chirality, particularly evident for the dichroic bands associated with the $\pi \rightarrow \pi^*$ azoaromatic electronic transition (see e.g. Figure 11).

According to the chiral exciton coupling rules,^[55] this behaviour suggests that *r*-CPL induces a right-handed screw sense of coupled neighbouring azobenzene chromophores. The CD spectra of this polymer after a cycle of illumination with *r*-CPL and *l*-CPL are presented in Figure 12. In all cases, no linear dichroism was observed before and after irradiation by comparing several CD spectra recorded at different angles around the incident light beam.

Similar results, but with lower ellipticity values, were also obtained from Star[(*S*)-**ML6A**]-24 (Figure 12). One negative Cotton effect, with the same crossover wavelength (333 nm) as the non-irradiated film (334 nm) which changes alternatively sign in the 250-600 nm spectral region was obtained with both the investigated polymers. The observed effects are reversible: when the handedness of the pump beam was switched from right to left and the irradiation performed on the same illuminated region for 30 min, similar and opposite CD spectra of Poly[(*S*)-**ML6A**]-14 and Star[(*S*)-**ML6A**]-24 were obtained (Figure 12).

The resulting spectra actually appear as mirror images of each other both for linear and star-shaped samples. Again, the CD spectra of the linear polymer display higher ellipticity values than the CD spectra of the star one.

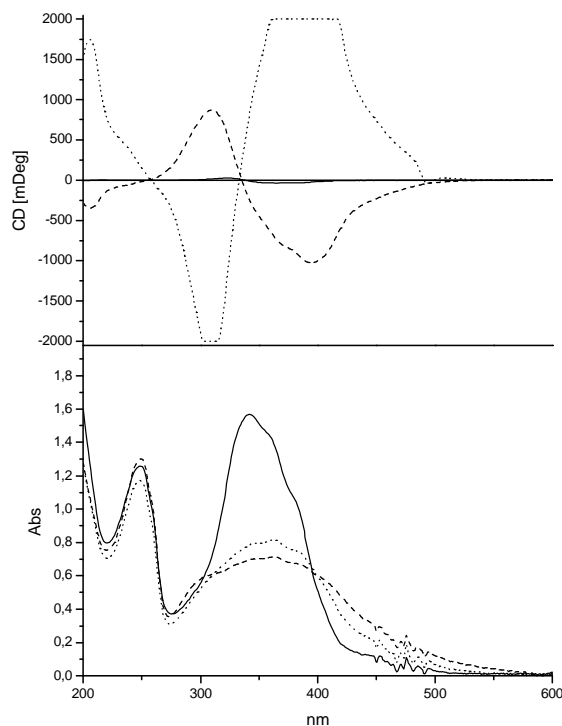


Figure 11: CD (up) and UV-Vis (bottom) spectra of a thin film of Poly[(*S*)-**ML6A**]-14 in the virgin state (—), in smectic phase (---) and after irradiation with *r*-CPL at 488 nm for 30 minutes (····).

The irradiation with *l*-CPL of another annealed film of poly[(*S*)-**ML6A**]-14 afforded also an induced optical activity of similar magnitude to that observed after the irradiation with *r*-CPL, but of opposite sign.

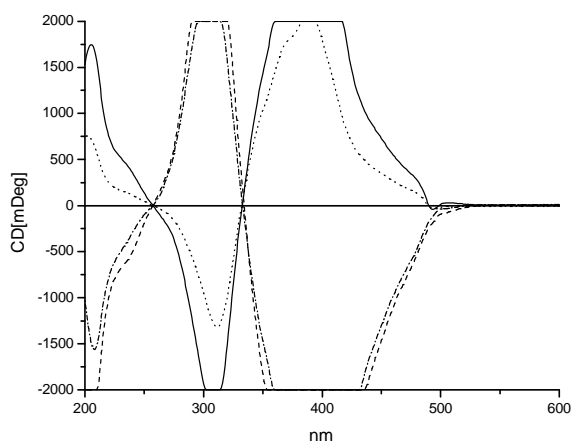


Figure 12: CD spectra of films of Poly[(*S*)-**ML6A**]-14 irradiated with *r*-CPL (—) or *l*-CPL (---) and Star[(*S*)-**ML6A**]-24 irradiated with *r*-CPL (····) or *l*-CPL (- . -) for 30 minutes after isotropization and annealing at 90°C for 15 minutes.

As a first conclusion, the photoinduced experiments suggest that *r*-CPL induces right-handed supramolecular chirality of the materials which can be erased and reinscribed with *l*-CPL, as reported elsewhere for other smectic, achiral azopolymers.^[17, 24] However, the

induced circular anisotropy has to be erased in the latter case by heating the irradiated samples to the isotropization temperature.

The observed phenomena appear to be related to the induction of chirality by irradiation with CPL of achiral azobenzene-containing polymers reported by Nikolova,^[13, 15] Natansohn,^[17] Sourisseau^[56], and Tejedor^[23, 24], even though the measured absolute ellipticity of our samples, normalised to film thickness, is of considerably higher magnitude. Indeed, in our case, an intrinsic chirality of the samples related to optical activity of the L-lactic acid residue interposed between the azo chromophores and the polymer backbone is present, and the chiral geometry of the mesogenic aggregates in the annealed films gives rise to thermodynamically stable and unusual chiral LC phases with a predominant helical conformation, as previously reported when chiral mesogens are present.^[49, 50] These observations reveal that the photoinduced chirality in liquid-crystal polymers is more efficiently achieved when dissymmetric groups and chiral LC phases are present.

The mechanism of reversible chiroptical inversion induced by CPL radiation is not well understood. In any case, for the investigated polymers, it appears related to a preliminary chiral supramolecular ordering of the azobenzene moieties, as demonstrated in our experiments. In fact, no reproducible circular anisotropies can be photoinduced in the native films (not annealed), pointing out the essential role of the liquid crystalline arrangement. This also indicates that orientational preorganization is required to obtain a controlled photomodulation of chirality.^[15]

Moreover, the photoinduced change of chiroptical properties does not perturb the texture of the investigated polymeric films as shown by POM analysis of the irradiated area, before and after application of CPL (see Supporting Information).

Natansohn reported the photoinduction of a similar chiral supramolecular structure by illumination of a achiral azopolymer with CPL.^[17] The results were attributed to ability of the chiral CPL propagating through the film to produce a progressive rotation of the optical axis of each LC domain, resulting finally in a supramolecular helical arrangement of the smectic domains to form an organization similar to a TGB phase.

In the case of the investigated polymers, it is reasonable to hypothesize that the LC phase in the annealed films assumes a helical supramolecular structure with a prevailing twist sense due to the thermodynamically favoured chiral interaction between neighbouring L-lactic-azoaromatic moieties, thus conferring a prevailing chirality to the material. Thus, the CPL should be able to alter this interaction between the chromophores and consequently the

chiral supramolecular structure, so as to reverse the macroscopic chirality of the material without modifying the observable LC texture (Figure 13). This phenomenon would therefore resemble the enantioselective CPL photochemical formation of optically active compounds from prochiral starting materials^[57, 58] and the CPL photoresolution of photochemically interconvertible enantiomers.^[59, 60]

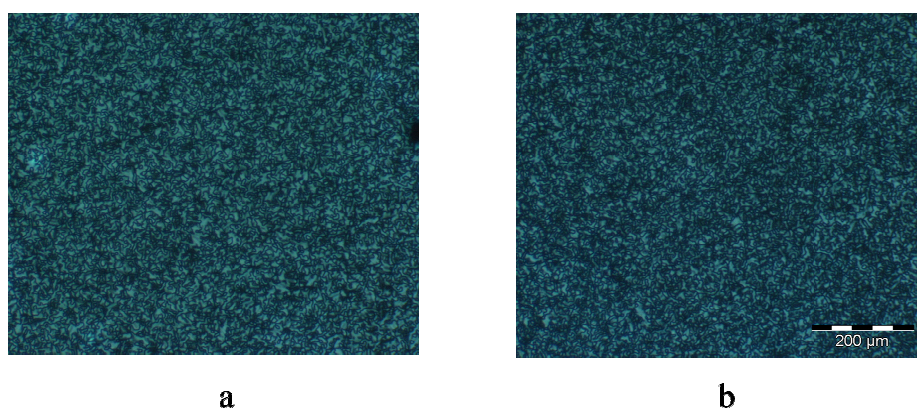


Figure 13 Optical microscopy images of a smectic thin film of Poly[(*S*)-ML6A]-14 before (a) and after irradiation with *l*-CPL for 30 minutes (b).

In fact, it is known that chiral CP electromagnetic radiation is able to induce enantioselective conversion^[61] and tends to align the azobenzene side groups along directions close to the light propagation.^[14, 62] It is possible that transfer of angular momentum from the CPL to the medium, as occurs when a CP photon is absorbed, induces a precession of the chromophores with a sense of rotation congruent with the sense of the CPL. This would mean that *l*-CPL induces a left-handed organisation of the azobenzene molecules, whereas *r*-CPL induces a right-handed one. In this way, the sign of the CD signals associated with the conformational aggregation of neighbouring chromophores can be inverted, as we have recently observed on the dimeric model derivative 2,4-dimethylglutaric acid bis (*S*)-3-[1-(4'-nitro-4-azobenzene)pyrrolidine ester, corresponding to the smallest section of the polymeric chain where side-chain interchromophore interactions are relevant.^[48] Its CD spectrum shows an exciton couplet of strong amplitude which suggests that the chiral interactions between a couple of chromophores in solution are already important and that the optical activity of these materials should be substantially related to relatively short chain sections with chromophoric aggregates having conformational dissymmetry of one prevailing screw sense.

These observations are also supported by recent studies of photoinduced chirality onto a Bx liquid crystalline phase of bent-shaped twin dimeric compound, where two

alkoxyazobenzene groups are linked together by a polymethylene spacer, which spontaneously segregate in chiral domains of the two possible dimeric conformers (racemic form).^[63] Selective *r*- or *l*-CPL irradiation, as a method of photoresolution of enantiomers, interconverts the two native domains producing an enantiomeric excess of one of them and as a result a macroscopically measurable CD chirality related to the preferential screw sense of the irradiating CPL.

All the aforementioned CD effects persist for at least one month at room temperature and are well reproducible. Clearly, for technological applications, the switching time would also be important.

Polymeric derivatives of M6A: photoinduction of chirality in achiral azopolymer and photo transition

The formula of the investigated are reported in Figure 14. The detailed synthesis of these polymeric systems and their spectroscopic, thermal and liquid crystalline characterization are described in detail in Chapter 2.

The chiroptical properties of the films after irradiation with r-CPL and/or l-CPL were investigated in detail by CD spectroscopy and their dependence on the macromolecular structure discussed.

Figure 14. Structural formulas of the investigated polymeric samples

UV-Vis properties

The UV-Vis absorption spectra in CHCl_3 solution (Figure 15) of all the investigated polymers, as well as the monomer **M6A**, exhibit, in the 250–650 nm spectral region, two bands related to the $n \rightarrow \pi^*$ and $\pi \rightarrow \pi^*$ electronic transitions of the azobenzene chromophore in *trans*-configuration with maxima centered at about 360 nm ($\epsilon \approx 28000 \text{ L mol}^{-1} \text{ cm}^{-1}$) and 440 nm ($\epsilon \approx 1500 \text{ L mol}^{-1} \text{ cm}^{-1}$), respectively ^[42], qualitatively and quantitatively independent by branching within the limits of the experimental error. The symmetry of the absorption band at 360 nm provides evidence that the azoaromatic chromophores in solution are essentially isolated.

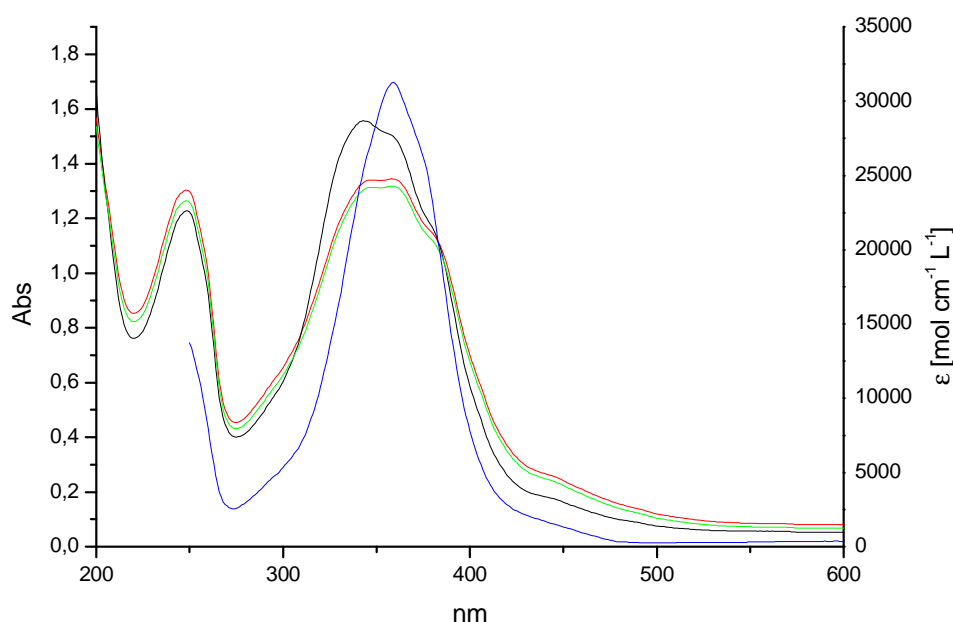


Figure 15: UV-Vis spectra of Poly[**M6A**]-24 in solution (—), and in the solid state as casted (—), annealed (—), and finally irradiated with l-CPL (—) thin films. The UV-Vis spectra of Star[**M6A**]-24 under the above conditions are superimposable.

The UV-Vis spectra of thin films of the synthesized polymers prepared by casting from dichloromethane solution over clean slides of fused silica have also been investigated in the 200–600 nm spectral range (Figure 15): they display the typical $\pi \rightarrow \pi^*$ and $n \rightarrow \pi^*$ electronic transitions of the azoaromatic isolated chromophore centered at around 360 nm and 440 nm, respectively, and an additional band centered at 248 nm associated with the $\pi \rightarrow \pi^*$ transition of the single aromatic ring.

The absorption band of the $\pi \rightarrow \pi^*$ azoaromatic transition becomes broader in the films, with two additional shoulders at 340 and 380 nm, related respectively to the formation of H-

aggregates (blue shift) and J-like (red shift) aggregates ^[42] imposed by the structural constraints of the macromolecules in the solid state.

By inspection with POM, the virgin films at room temperature appear optically isotropic, without any birefringence and scattering. In order to develop the mesophase, a thermal treatment has been made consisting of heating above the clearing point temperature (T_i) for 5 minutes followed by annealing for 15 minutes at lower temperature ($T_{\text{annealing}}/T_i$ of about 0.7). This treatment allows to obtain the presence of a glassy nematic liquid crystalline phase, as confirmed by POM.

The UV-Vis spectra of annealed films result similar to the spectra of the corresponding as prepared casted films (Figure 15), with a broadening of the long-wavelength side and a minor presence of H-aggregates (band at 340 nm). This can be related to more ordered dipolar intra- and inter-chain interactions that the chromophores experience in the nematic phase compared to those in solution and in the amorphous solid state. In particular, the decrease in the $\pi \rightarrow \pi^*$ band can be interpreted as being due to aggregation of the azobenzene fragment, which possesses elevated anisotropy ^[45, 46], while the $\pi \rightarrow \pi^*$ band at 248 nm of the single aromatic ring, not influenced by orientation, remains unchanged. The absorbance at longer wavelengths never reaches zero, this behaviour being associated with light scattering due to the formation of the birefringent domains of liquid-crystal phase upon annealing.

The UV-Vis spectrum of Poly[**M6A**]-24 in thin film after annealing and illumination with l-CPL with an Ar+ laser (power = 20 mW cm⁻²) at 488 nm for 30 min is presented in Figure 15. The irradiation does not change the shape of the spectrum of the annealed sample, similar UV spectra being obtained by irradiation with r-CPL as well as from Star[**M6A**]-24 samples. These results suggest that the dipolar azoaromatic aggregations (H- and J-aggregation) in the nematic liquid crystalline phase remain substantially unaffected by CPL irradiation.

Chiroptical properties and photoinduced switching of supramolecular chirality

Whereas the UV-Vis spectra of irradiated polymers result similar to the spectra of corresponding annealed films (Figure 15), the related CD spectra, silent before irradiation, now show the presence of high chirality. No linear dichroism was observed before and after irradiation by comparing several CD spectra recorded at different angles around the light beam.

The CD spectra of Poly[**M6A**]-24 in the glassy nematic phase irradiated with r-CPL with an Ar⁺ laser (power = 20 mW/cm²) at 488 nm for 30 min, exhibit an high, asymmetric, exciton couplet centred around 335 nm which does not strictly coincide with the maxima of the UV-Vis absorption bands (Figure 16). The positive band appears of higher intensity and displays a shoulder around 366 nm associated with the electronic transitions of the isolated azobenzene moieties. The crossover point of this couplet is close to the electronic transition associated to chiral H-aggregates (340 nm) and is interpreted as originating from the overlapping of the exciton splitting CD band (H-aggregates) with a positive CD band having its maximum at 380 nm, corresponding to the maximum absorbance of the J-aggregated chromophores ^[23].

Moreover, the CD spectrum of the irradiated films show a sharp negative band at 492 nm due to a Bragg selective reflection of a helical organization ^[22-24]. This behaviour is similar to the selective reflection of a chiral nematic mesophase with a helix pitch due to induced cholesteric mesophase ^[32, 33]. Recent calculations by Takezoe et al. ^[61] of the shape of a Bragg reflection of a helix pitch larger than the film thickness, reported that a reflection at 492 nm means an helix pitch of 312 nm, much larger than the film thickness of our samples, which is around 200 nm. Under this condition, only a broad reflection should be seen. However, Tejedor et al. ^[24] observed a photoinduced iridescent green reflection of a glassy nematic azopolymer filmed over a planar wedge cell.

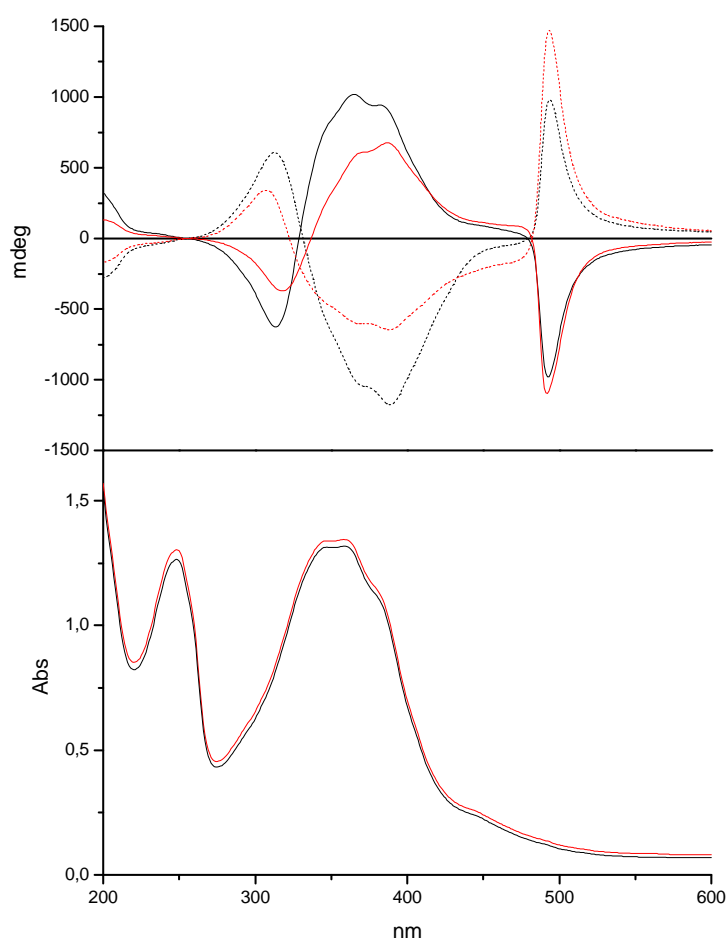


Figure 16: UV-Vis spectra (bottom) and CD (up) of irradiated films of Poly[M6A]-24 (—), and Star[M6A]-24 (—) irradiated with r-CPL (straight line) or l-CPL (dashed line).

In order to confirm this result and investigate the change in the macroscopic optical properties and optical textures of Poly[M6A]-24 irradiated with CPL, a 4 μm cell with an aligning layer for planar orientation was filled with the polymer. A portion of the cell was irradiated and the other part masked in order to avoid photoisomerization.

After irradiation the initial orientation of the mesogenic units is vanished and, aligning the polarizer along the alignment direction, a bright selective reflection, related to the sharp signal at 492 nm, can clearly be seen (Figure 17). This is a further confirmation of induced helical organization of the chromophore^[24].

Therefore, the presence of high ellipticity values and of selective Bragg reflections demonstrate the presence of a supramolecular chirality with a prevalent handedness similar to a chiral nematic phase.

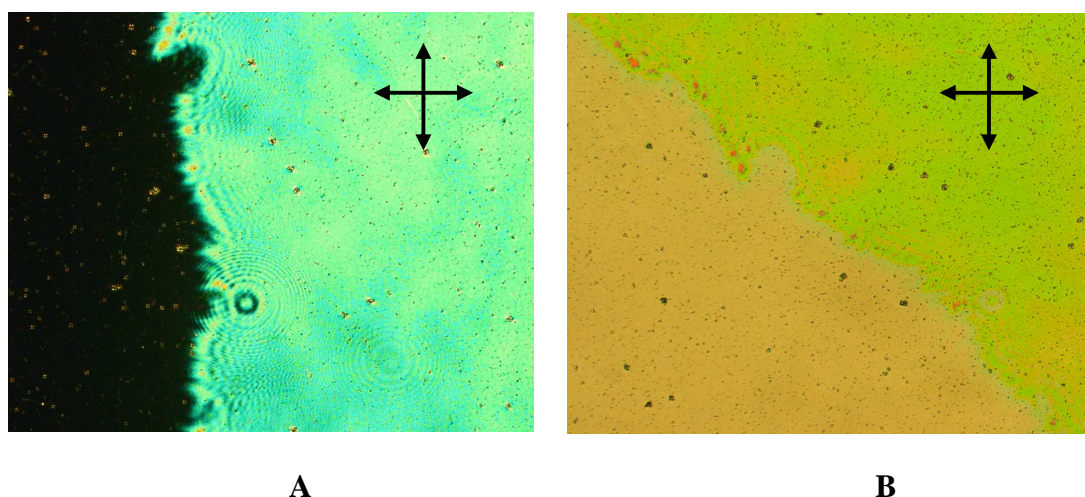


Figure 17: POM textures of a planar-cell filled with Poly[M6A]-24. The right part has been irradiated with r-CPL for 30 minutes. (A) Crossed polarizers parallel and perpendicular to the alignment director: the irradiated zone exhibits a colour while the non irradiated zone is dark. (B) Crossed polarizers rotated of 45° with respect to the mesogen director: two different colours are still visible.

According to the chiral exciton coupling rules^[22, 55], the CD spectrum of Poly[M6A]-24 suggests that l-CPL induces left-handed screw sense of the supramolecular azobenzenic structure. When the handedness of the pump beam was switched from left to right and the irradiation was maintained for 30 min, a similar but opposite CD spectrum was obtained (Figure 16). The resulting CD spectra are the mirror images of each other. Also, the sign of the selective reflection, in accordance with the optical behaviour of ideal helices, changes sign switching between a positive reflection after irradiation with l-CPL and a negative value for irradiation with r-CPL. This suggests that the interconversion of two enantiomeric supramolecular structures can be easily obtained by changing the CPL handedness.

The CD spectra of the irradiated nematic Star[M6A]-24 display similar behaviour, but lower ellipticity values than the CD spectra of irradiated Poly[M6A]-24 of same thickness (Figure 16). In fact, the integrated area values of the CD spectra indicate that the exciton couplet of the star polymer is about the $2/3$ of that one of the linear polymer.

The above observed difference appears to be due to the different structure of the polymeric samples and not to differences in the starting LC phase as demonstrated by XRD. It thus appears that the branching of the macromolecular chain acts as a defect in the liquid crystalline phases, leading to a less ordered chiral supramolecular structure with lower chirality. Anyway, the position of the exciton couplets and the position and intensities of the reflection at 492 nm are unaffected by the molecular structures of both the star and the linear polymer.

4-oxy-4'cyano-azobenzene containing polymers

UV-Vis analysis in solution:

Absorption spectra of the monomers and polymers bearing the 4-cyano-4'oxy-azobenzene chromophore (Figure 18) are all similar among them, and, within the experimental error, no significant differences can be found between monomeric and polymeric derivatives.

Anyway due to the different dipolar moment and conjugation of the chromophore the UV-Vis spectra is slightly different from the systems containing the 4-ethoxy-4'oxy azobenzene chromophore.

In fact the UV-Vis spectra of all the synthesized compounds display in the spectral region between 240-550 nm three different absorption band centred at 250, 365 and 440 nm due respectively to the $\pi \rightarrow \pi^*$ transition of the single aromatic rings ($\epsilon = 16000$), to the $\pi \rightarrow \pi^*$ ($\epsilon = 32700$, $\lambda = 365\text{nm}$) and $n \rightarrow \pi^*$ transition of the *trans*-azoaromatic chromophore .

According to Rau's classification of azoaromatic systems ^[64] the chromophore 4-oxy-4'cyano-azobenzene and the 4-ethoxy-4'-oxy azobenzene belong both to the azobenzene-type class, in fact they have similar UV-Vis spectra. We can observe only a small redshift of the $\pi \rightarrow \pi^*$ electronic transition of the azoaromatic chromophore (from 360 to 365 nm in the 4-cyano-4'-oxy azobenzene) and a substantial increase of molar absorbance for all transitions of the azoaromatic chromophore (the value of ϵ for $\pi \rightarrow \pi^*$ transition increases from 27000 to 32700 $\text{L mol}^{-1} \text{cm}^{-1}$ and the $n \rightarrow \pi^*$ from 1500 to 2000 $\text{L mol}^{-1} \text{cm}^{-1}$).

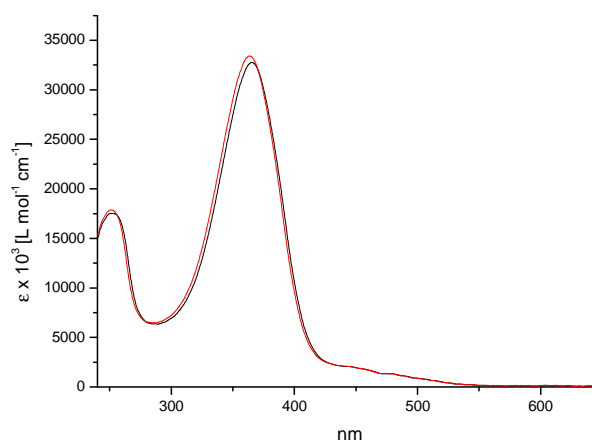


Figure 18: UV-Vis spectra of (S)-ML6A-C (—) and Poly[(S)-ML6A-C] (—).

Thermal and liquid crystalline characterization

All the polymeric derivatives were investigated through DSC, POM and XRD spectroscopy in order to establish their LC properties.

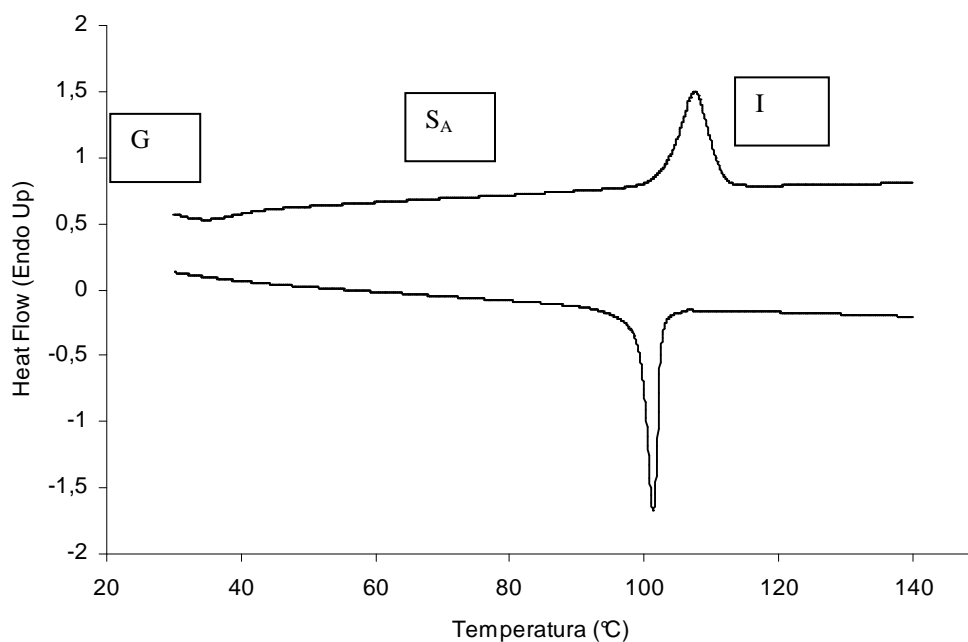


Figure 19: Thermogram of Poly[(*S*)-**ML6A-C**] under nitrogen atmosphere, at a heating and cooling rate of 10°C/min. G = glassy state, S_A = Smectic A phase, I = isotropic phase.

In Figure 19 is shown as an example the first cooling and the second heating of Poly[(*S*)-**ML6A-C**]: a glass transition at 39°C, a smectic A phase (identified by POM and XRD analysis) and an isotropization temperature at 108°C are present.

In Table 7 are reported the transition temperature and the enthalpies (ΔH^i) of the liquid crystalline – isotropic transitions.

All the polymeric systems display on heating a glass transition and a isotropization temperature, except for Poly[(*S,S*)-**MLL2A-C**] which seems to be totally amorphous (Figure 20).

Table 7: Thermal transition ^{a)} of the polymeric derivatives

Sample	T _g (°C)	Phase	T _i (°C)	ΔH ⁱ (J g ⁻¹)
Poly[M2A-C] ^{b)}	105	N	158	-
Poly[M6A-C] ^{b)}	56	SmA	163	-
Poly[(S)-ML2A-C]	69		87	0,8
Poly[(S,S)-MLL2A-C]	82		-	-
Poly[(S)-ML6A-C]	39	SmA	108	5,2
Star[(S)-ML6A-C]	40	SmA	118	4,9
Poly[(S,S)-MLL6A-C]	40		71	3,0
Star[(S,S)-MLL6A-C]	44		82	2,7
Poly[(S,S,S)-MLLL6A-C]	51		76	2,8

a) Obtained from the second heating DSC thermal cycle in nitrogen atmosphere (10°C/min)

b) Ref: [23]

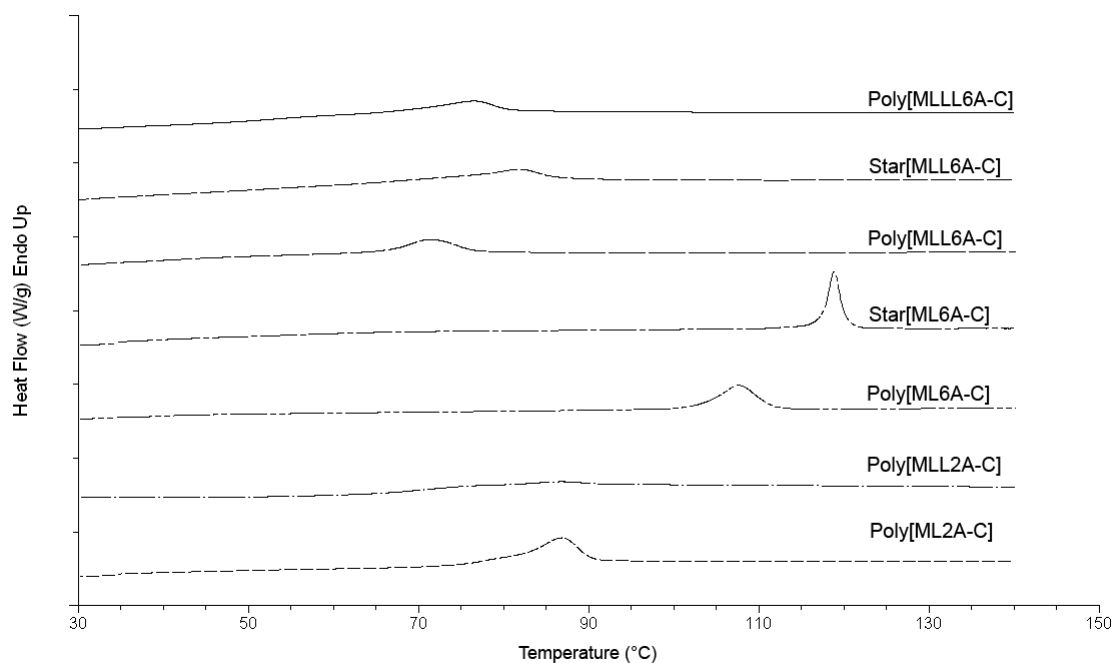


Figure 20: DSC traces of the second heating of the polymeric derivatives

The nature of the mesophase of Poly and Star[**ML6A-C**] was determined by POM analysis (Figure 21) and XRD measurement and was identified as a normal smectic A (SmA) phase with no interdigitation.

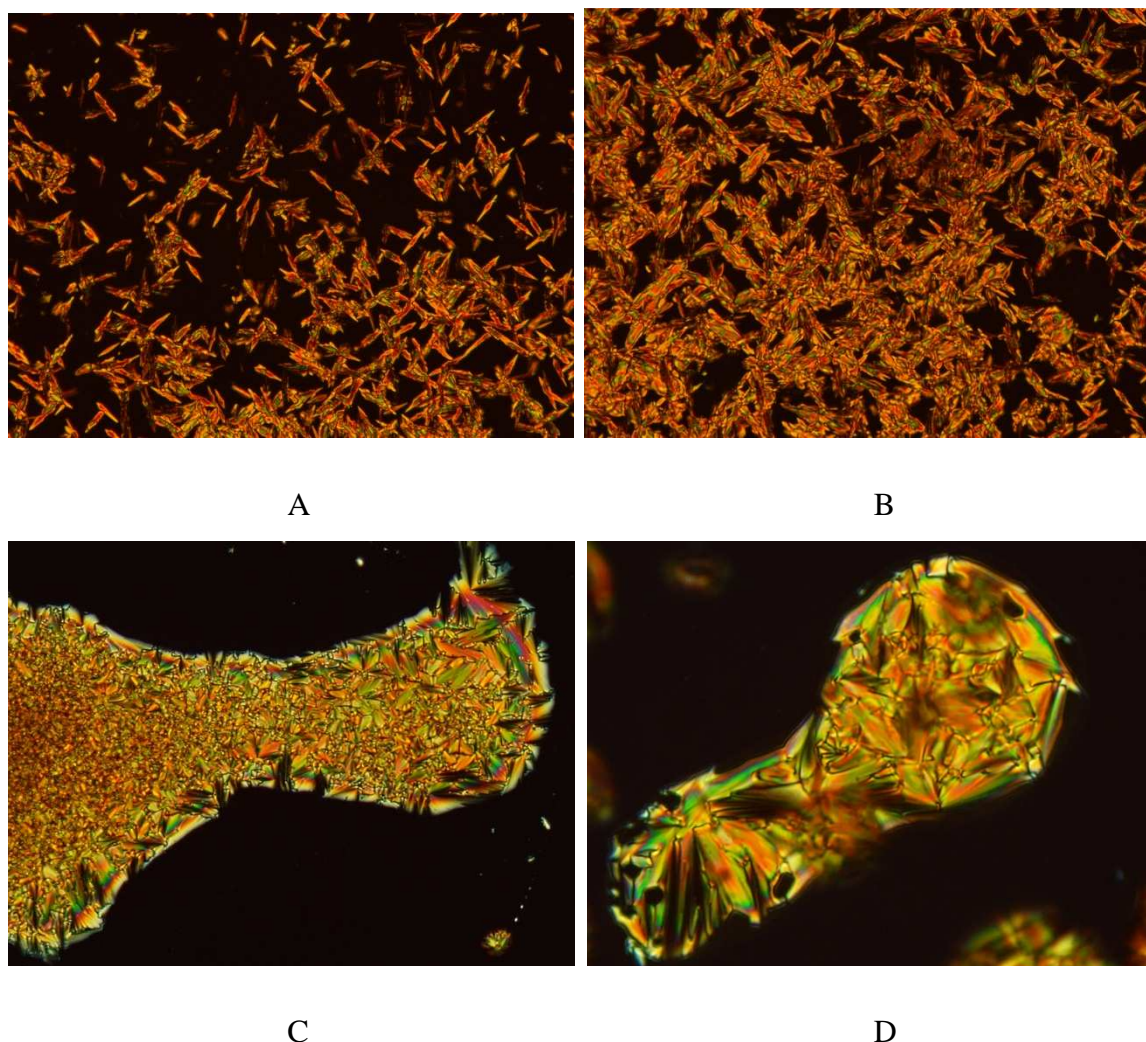


Figure 21: POM microphotograph (sample prepared between two glasses, 100x) of Poly[(*S*)-**ML6A-C**] (A and C) and Star[(*S*)-**ML6A-C**] (B and D) upon cooling from the isotropic liquid (A and B) and after annealing at 90°C for four hours (C and D).

It was not possible to determine the nature of the mesophase of the other polymers: the existence of a mesophase is proved by thermal analysis but these systems seemed to be amorphous both at POM and for XRD analysis. Thus the only systems studied in depth up to now are the polymers of **ML6A-C**.

Moreover it is possible to find some trends in the stability of the different mesophases in relation with the number of chiral center present in the chain and the length of the alkyl spacer.

Short alkyl spacer and high number of chiral centers leads to less stable mesophases (lower T_i and ΔH^i), while longer spacer and less chiral centers lead to more stable liquid crystalline phases^[65].

In literature are reported the transition temperature of similar achiral polymers with high T_i : Poly[**M2A-C**] (nematic), and Poly[**M6A-C**] (smectic A)^[23]. Poly[*(S)*-**ML2A-C**], even if has a longer alkylic spacer and thus should have a T_i between the two former achiral derivatives has a lower isotropization temperature and a very low ΔH^i . Furthermore Poly[*(S,S)*-**MLL2A-C**] with two L-lactic acid residues in the lateral chain is amorphous: the T_i is lowered under the T_g .

The same trend can be observed for the polymers with six-carbon alkyl spacer: increasing the number of L-lactic residues passing from Poly[**M6A-C**] to Poly [*(S,S,S)*-**MLL6A-C**] the stability of the LC phases and the isotropization temperature is dramatically lowered of about 100°C.

The loss of stability with an increase of the number of chiral center can be explained in terms of elastic energy associates to the changes of the alignment director among the single liquid crystalline grain as reported in literature by Colling^[65]. The equilibrium state in the non-chiral systems is a uniform director in the whole domain: every deviation from this condition lead to the deviaton from the equilibrium state of a spring.

Because of the anisotropy of the systems the free energy of the free crystal can be expressed as the sum of several terms, with each of these associated with a different deformation of the lattice. The most important terms are three: splay, twist and bending (Figure 22).

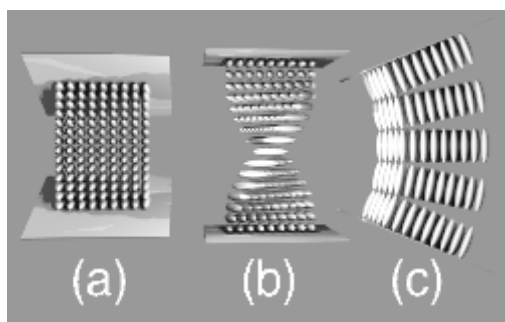


Figure 22: elastic deformation of a LC lattice a) splay, b) twist, c) bending)

If there is a rotation of the director in the LC domain, the free energy for volume unit will be higher respect to the case of non distorted one, due to the twisting term, implying that a LC spontaneously relax to a non-twisted state if possible.

If the chiral centers are present a spyralization of the lattice is introduced and thus the twisting deformation cannot be avoided and the free energy of the lattice is higher respect to the analogue anchiral phase, while the isotropic phase result unaffected. In this contest the introduction of several chiral center leads to a loss of stability both in terms of temperature and enthalpies of isotropization.

Finally it can be observed how the macromolecular geometry plays an important role on the thermal characteristic of the polymers: branched polymer displays always higher transition temperatures but lower enthalpies, this is due to a higher stiffness and a lower order respect to the linear derivatives.

Chiroptical properties in solution

The chiroptical properties have been studied for the polymers of (*S*)-**ML6A-C**, in order to make a comparison between these and the similar polymer of (*S*)-**ML6A**.

Anyway the CD spectra of both the monomer and the polymeric derivatives (Figure 23) in chloroformic solution are mostly silent, whit a small positive dichoric band centred on the absorption maxima of the $\pi \rightarrow \pi^*$ electronic transition of the azoaromatic chromophore, suggesting that the conformational chirality observed by polarimetric measurement (Table 3) of the macromolecular derivatives is not related to a chiral mutual organisation of the chromophoric units.

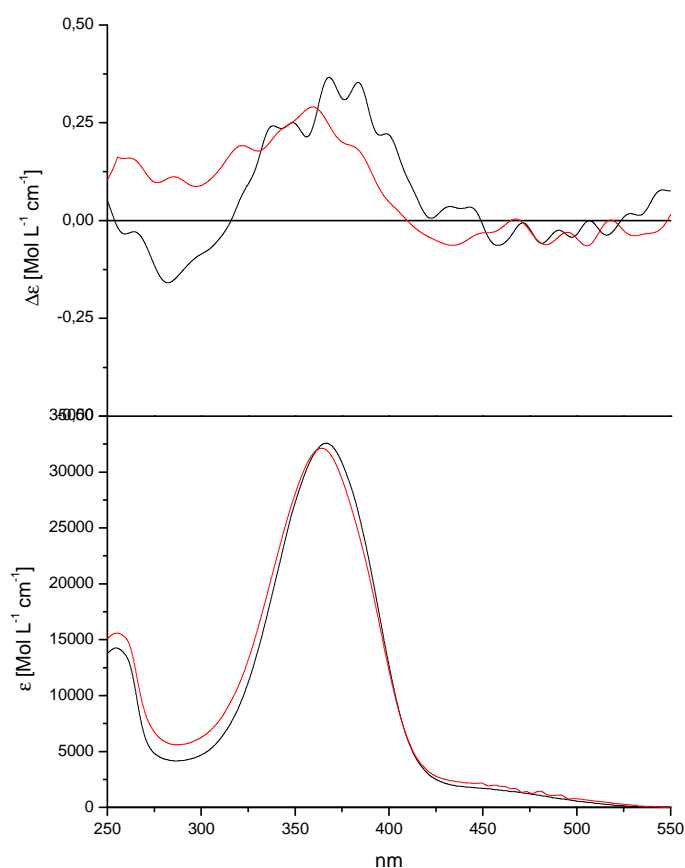


Figure 23. CD (up) and UV-Vis (bottom) spectra of (*S*)-ML6A-C (—) and of Poly[(*S*)-ML6A-C] (—) in chloroformic solution

Photomodulation of chiroptical properties in thin films

Thin films of Poly[(*S*)-**ML6A-C**] have been spin coated from chloroformic solution of the polymer onto clean slides of fused silica in order to study their chiroptical properties in the solid state. By inspection with POM, the virgin films at room temperature appear optically isotropic: no birefringence neither scattering are observed.

The main UV-Vis data of the polymeric materials are collected in Table 8 and the absorption spectra of Poly[(*S*)-**ML6A-C**] in the solid state are reported as an example in Figure 24 in addition to the typical $\pi \rightarrow \pi^*$ and $n \rightarrow \pi^*$ electronic transitions of the azoaromatic chromophore centered at around 357 and 440 nm, respectively, an additional band at around 248 nm, associated with the $\pi \rightarrow \pi^*$ transition of the single aromatic ring, is present.

The absorption band of the $\pi \rightarrow \pi^*$ transition of the azoaromatic chromophore in the virgin films appears broader with respect to the spectra in solution, with an additional shoulders at 380 nm, related to the formation of J-like (red shift) aggregates^[44] imposed by the structural constraints of the macromolecules in the solid state, while the presence of H-like aggregates in the virgin film should be quite irrelevant (no shoulder around 320-330 nm).

In order to develop the mesophase, a thermal treatment consisting of a heating above the clearing point temperature (T_i) for 5 minutes followed by annealing for 15 minutes at a temperature reduced by a factor of about 0.7 (T_{anneal}/T_i) has been carried out.

The annealed film of Poly[(*S*)-**ML6A-C**] displays broader, less intense absorption bands (Figure 24 and Table 8) and produces LC domains as observed by POM. The main absorption band is characterized by a bathochromic shift of the $\pi \rightarrow \pi^*$ azoaromatic absorption maximum to 372 nm. In addition, the shoulder related to the J-aggregates, around 390 nm, increases and another additional shoulder related to the presence of H-aggregate appears at 326 nm.

This can be related to development of aggregates and thus to more ordered chromophoric dipolar intra- and inter-chain interactions in the SmA phase compared to the solution and the amorphous solid state.

As observed previously for the similar derivatives of (*S*)-**ML6A**^[29] an homeotropic alignment of the azoaromatic moieties can be observed: in fact while the $\pi \rightarrow \pi^*$ transition of

the azoaromatic chromophores, which is highly anisotropic, decrease in intensities the transition of the single aromatic ring at 254 nm remains unvaried by the relative orientation.

Also the chiroptical proprieties change with thermal treatments. While the as-casted film display only a small positive CD band at 374 nm, the annealed film display an asymmetric CD couplet with a crossover point centered at 335 nm, related to the presence of chiral H-like aggregates. The asymmetry of the CD band could be explained as the superimposition of a positive CD band related to the presence of J-aggregates centred at 400 nm.

It is possible to photomodulate the chiroptical properties of this polymer by irradiation with circularly polarised light (CP) (Table 8, Figure 24 and Figure 25).

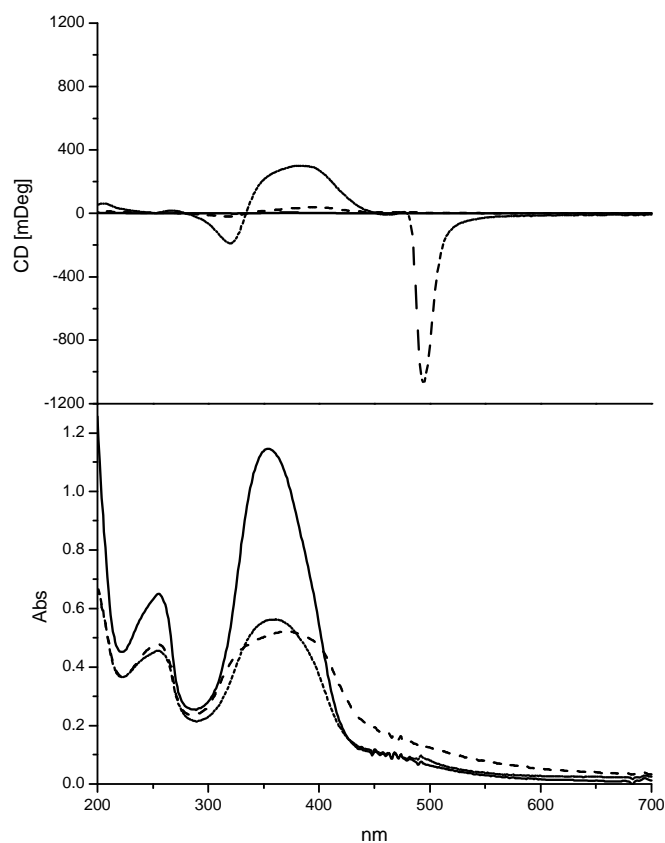


Figure 24 CD (up) and UV-Vis (bottom) spectra of thin film of Poly[(*S*)-ML6A-C] in the virgin state (—), after annealing (⋯) and after irradiation with *l*-CP (---)

In the UV-Vis spectra after irradiation with CP the amount of H-aggregates decrease in importance, while the shoulder of J-aggregates remains still visible.

The positive CD couplet associated to the $\pi \rightarrow \pi^*$ transition of the azoaromatic chromophores is enhanced in intensities: the maximum intensities of the CD band from the pristine 37 mDeg rise to 300 mDeg. Moreover a noticeable bluishift can be observed both in CD and UV spectra. After irradiation the shoulder at 390 nm is almost disappeared and the band is more symmetrical, also the maximum of the CD band is blueshifted of 10 nm from 393 to 383 nm.

Table 8. UV-Vis data of the investigated compounds in CHCl_3 solution and as thin films after different treatments.

Samples		$\lambda^{\phi \rightarrow \phi^* [a]}$	$\lambda^{\pi \rightarrow \pi^* [a]}$	$\lambda^{\text{H-agg. [a,b]}}$	$\lambda^{\text{J-agg. [a,b]}}$	$\lambda^{\text{n} \rightarrow \pi^* [a,b]}$
(S)-ML6A-C	solution	- ^[c]	366	-	-	440
Poly[(S)-ML6A]	solution	- ^[c]	364	-	-	440
Poly[(S)-ML6A-C]	virgin film	255	354	-	390	440
Poly[(S)-ML6A-C]	annealed film	255	372	326	490	440
Poly[(S)-ML6A-C]	irradiated film	254	359	-	390	440
	(<i>l</i> -CP)					
Poly[(S)-ML6A-C]	irradiated film	254	359	-	390	440
	(<i>r</i> -CP)					
Poly[(S)-ML6A-C]	irradiated film	254	359	-	390	440
	(<i>r+l</i> -CP)					

[a] Wavelength of maximum absorbance in nm. [b] Shoulder. [c] Not observed due to solvent cut-off.

With the increase of the CD band related to the $\pi \rightarrow \pi^*$ transition also a sharp band at 494 nm appears. This band is similar to the one observed in the irradiated polymers of M6A. Anyway this is the first time that this kind of band is observed in a smectic LC polymer.

As expected by changing the sign of the CP light also the sign of the band is switched (Figure 25).

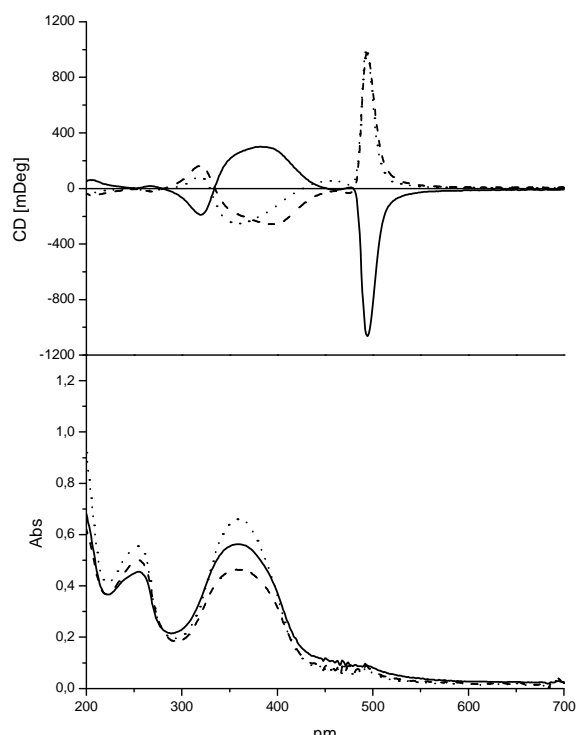


Figure 25. CD (up) and UV-Vis (bottom) spectra of thin film of Poly[(*S*)-ML6A-C] after irradiation with *l*-CP (—), *r*-CP (---) and *r*-CP after a previous irradiation with *l*-CP (⋯)

Conclusion

We synthesized several similar polymeric derivatives, all monodisperse, with similar average molecular weight and all bearing an azoaromatic chromophore of the azobenzene type in Rau's classification^[64] and the same two alkylic spacer. Despite the similar molecular structure these polymers exhibit different chiroptical properties both in terms of magnitude of the signal of the CD band and in terms of photoinduced chiroptical properties. As a matter of fact no simple correlation can be found between molecular structure, LC phase and photoinduced chiroptical properties. As an example, in some spectra a sharp CD artifact appears at 494 nm after irradiation with CPL. Among the studied polymers, it appeared two times in a nematic and in a smectic A polymers (Poly(**M6A**) and Poly[(*S*)-**ML6A-C**], while did not occur in another similar smectic A polymer (Poly[(*S*)-**ML6A**]).

But besides this not yet understood behavior other trends have been clearly identified by using monodisperse and well defined polymers: it was highlighted how that the macromolecular chain plays an important role on the chiroptical and photoinduced chiroptical properties.

This work thus has to be considered as a new starting point for the study of chirality in polymeric systems, as for the first time strong structure properties correlation has been showed and understood.

Experimental Section

Physico-chemical measurements:

^1H - and ^{13}C -NMR spectra were obtained at room temperature, on 5-10% CDCl_3 solutions, using a Varian NMR Gemini 300 spectrometer. Chemical shifts are given in ppm from tetramethylsilane (TMS) as the internal reference. ^1H -NMR spectra were run at 300 MHz by using the following experimental conditions: 24,000 data points, 4.5-kHz spectral width, 2.6-s acquisition time, 128 transients. ^{13}C -NMR spectra were recorded at 75.5 MHz, under full proton decoupling, by using the following experimental conditions: 24,000 data points, 20-kHz spectral width, 0.6-s acquisition time, 64,000 transients. FT-IR spectra were carried out on a Perkin-Elmer 1750 spectrophotometer, equipped with an Epson Endeavour II data station, on sample prepared as KBr pellets. UV-Vis absorption spectra were recorded at 25°C in the 700-250 nm spectral region with a Perkin-Elmer Lambda 19 spectrophotometer on CHCl_3 solutions by using cell path lengths of 0.1 cm. Concentrations in azobenzene chromophore of about $3 \cdot 10^{-4} \text{ mol} \cdot \text{L}^{-1}$ were used. Optical activity measurements were accomplished at 25°C on CHCl_3 solutions ($c \approx 0.250 \text{ g dL}^{-1}$) with a Perkin Elmer 341 digital polarimeter, equipped with a Toshiba sodium bulb, using a cell path length of 1 dm. Specific $\{[\alpha]_{\text{D}}^{25}\}$ and molar $\{[\Phi]_{\text{D}}^{25}\}$ rotation values at the sodium D line are expressed as $\text{deg} \cdot \text{dm}^{-1} \cdot \text{g}^{-1} \cdot \text{cm}^3$ and $\text{deg} \cdot \text{dm}^{-1} \cdot \text{mol}^{-1} \cdot \text{dL}$, respectively. Circular dichroism (CD) spectra were carried out at 25°C on CHCl_3 solutions on a Jasco 810 A dichrograph, using the same path lengths and solution concentrations as for the UV-Vis measurements. $\Delta\epsilon$ values, expressed as $\text{L} \cdot \text{mol}^{-1} \cdot \text{cm}^{-1}$ were calculated from the following expression: $\Delta\epsilon = [\Theta]/3300$, where the molar ellipticity $[\Theta]$ in $\text{deg} \cdot \text{cm}^2 \cdot \text{dmol}^{-1}$ refers to one azobenzene chromophore. Number average molecular weights of the polymers (\bar{M}_n) and their polydispersity indexes (\bar{M}_w/\bar{M}_n) were determined in THF solution by SEC using HPLC Lab Flow 2000 apparatus, equipped with an injector Rheodyne 7725i, a Phenomenex Phenogel 5-micron MXL column and a UV-VIS detector Linear Instrument model UVIS-200, working at 254 nm. Calibration curve for MXL column was obtained by using monodisperse polystyrene standards in the range 800-35000. Phase-transition temperatures values were determined by differential scanning calorimetry (DSC) on a TA Instrument DSC 2920 Modulated apparatus at a heating/cooling rate of 10°K/min under nitrogen atmosphere on samples weighing 5-9 mgr. T_g values were measured as the midpoint in the heat capacity increase and the other thermal transitions were taken as the maximum of

the transition peak. Texture observation of the liquid crystalline behaviour was carried out with an Zeiss Axioscope2 polarising microscope equipped with a Nikon Coolpix E995 digital camera through crossed polarisers fitted with a Linkam THMS 600 hot stage. X-ray diffraction (XRD) studies were carried out using a Pinhole camera (Anton-Paar) operating with a point focused Ni-filtered Cu K α beam. The samples were held in Lindemann glass capillaries (1 mm diameter) and heated, when necessary, with a variable-temperature attachment. The diffraction patterns were collected on a flat photographic film perpendicular to the x-ray beam.

Polymer film preparation, characterization and irradiation with circularly polarized light:

Thin films were prepared by casting solutions of the LC polymers in dichloromethane (0.4 mg into 200 μ l of solvent) onto clean fused silica slides and subsequently dried at 30 °C under vacuum during 24 h. The film thickness, measured by a Tencor P-10 profilometer, was in the range 150-300 nm, so as to give UV-Vis spectra with maximum absorbance values between 0.7 and 1.5, depending on the procedure conditions. The obtained films were then heated above the clearing temperature (T_i) for 5 min and annealed for 15 min at lower temperature ($T_{\text{annealing}}/T_i$ around 0.7). Then, the samples were placed on a metal block at 25°C for 30 min in order to get a glassy liquid crystalline phase. Annealed films were irradiated for 30 min with *l*-CPL or *r*-CPL, respectively, by 488 nm light-of an Ar⁺ laser (power 20 mW/cm²). The UV-vis and CD spectra of the native and of the illuminated films were carried out under the same instrumental conditions as the related solutions after having left the samples in the dark at room temperature for 30 min. In order to exclude any optical effect (linear dichroism and linear birefringence) due to anisotropy of orientation in the ordered systems, the polymeric films of both native and irradiated samples were placed in a rotating holder around the probe beam and UV-Vis and CD spectra recorded every 60 degrees without observing any difference in the spectra.

Materials:

(*S*)-(-)-Methacryloyl-L-lactic (**ML**) acid $\{[\alpha]_D^{25} = -28.0$ ($c = 1$, EtOH) $\}$ was synthesized as previously reported.^[66] Methacryloyl chloride (Aldrich) was distilled under inert atmosphere, in the presence of traces of 2,6-di-*tert*-butyl-*p*-cresol as polymerization inhibitor just before use. 4-Dimethylaminopyridinium 4-toluenesulphonate (**DPTS**) was

prepared from 4-dimethylaminopyridine and 4-toluensulphonic acid as described [32]. 4-Hydroxy-4'-(ethoxy)-azobenzene was synthesised as previously described [30, 31]. 2-2'-azobisisobutyronitrile (**AIBN**) was crystallised by methanol before use. THF and CH₂Cl₂ were purified and dried according to the reported procedures [67] and stored under nitrogen. The trifunctional initiator 1,3,5-(2'-bromo-2'-methylpropionato)benzene (**BMPB**) was prepared as previously described [68, 69]. (+)-L-Lactic acid (Aldrich), 1,3-diisopropylcarbodiimide (**DIPC**, Aldrich), 4-dimethylaminopyridine (Aldrich), the monofunctional initiator allyl 2-bromine 2-methylpropionate (**ABIB**) (Aldrich), 1,1,4,7,10,10-hexamethyltriethylenetetramine (**HMTETA**), copper bromide and all the other reagents and solvents (Aldrich) were used as received.

Synthesis of 4-(6-hydroxyhexyloxy)-4'-ethoxyazobenzene [H6A]:

This intermediate was prepared by following a different method than that reported [30, 31]. 6-Chlorine hexanol (6,9 ml, 0,0496 mol) was added dropwise under vigorous stirring to a solution of 4-hydroxy-4'-(ethoxy)-azobenzene (6 g, 0,0248 mol), KOH (0,6 g, 0,011 mol) and KI (1,64 g, 0,0099 mol) in 96% ethanol (80 ml) at reflux. The reaction was followed by TLC (eluent CH₂Cl₂:EtOAc= 4:1 v/v) until the total conversion of 4-hydroxy-4'-(ethoxy)-azobenzene (48h) was observed. The precipitated material was filtered off, the solvent volume reduced to 15 ml under vacuum, then aq 1% NaOH was added under vigorous stirring. The solid formed was filtered and crystallized twice with absolute ethanol to give a orange crystalline material (77% yield).

FT-IR: 3308 (ν_{OH}), 3069 (ν_{CH}, arom.), 2978 and 2864 (ν_{CH}, aliph.), 1600 and 1517 (ν_{C=C}, arom.), 1150 and 1111 (ν_{C-O} ether), 845 and 815 (δ_{CH} 1,4 disubst. arom. ring) cm⁻¹.

¹H-NMR (CDCl₃): 7.90 (d, 4H, arom. 2-H and 2'-H), 6.90 (d, 4H, arom. 3-H and 3'-H), 4.15 (m, 4H, CH₃-CH₂-O and CH₂-CH₂-O), 3.65 (t, 2H, CH₂-OH), 1.85-1.40 (m, 12H, CH₂-CH₂-CH₂-CH₂, CH₃-CH₂-O and OH) ppm.

Synthesis of (S)-4-[6-(2-methacryloyloxypropanoyloxy)hexyloxy]-4'-ethoxyazobenzene [(S)-ML6A]

The monomer (S)-**ML6A** was prepared by esterification of methacryloyl-L-lactic acid (**ML**) with **H6A** in the presence of N,N-diisopropylcarbodiimide (**DIPC**) and **DPTS**, as coupling agent and condensation activator, respectively^[32], the reaction being described in detail as follows: a solution of **ML** (2,0 g, 0,0126 mol), 2,6-di-*tert*-butyl-*p*-cresol (0.05 g) as polymerisation inhibitor and **H6A** (4,34 g, 0,0126 mol) in 50 ml of anhydrous CH₂Cl₂, was placed in a 100 mL three necked round-bottomed vessel, kept under dry nitrogen atmosphere, then **DPTS** (3,64 g, 0,0126 mol) and **DIPC** (2,60 ml, 0,0168 mol) were successively added under magnetic stirring.. The reaction mixture was left at room temperature for 72 h, the solid N,N-diisopropylurea, thus formed, filtered off and the liquid phase washed with several portions of aq 1M HCl, aq 5% Na₂CO₃ and water, in that order. After drying the organic layer on anhydrous Na₂SO₄ and evaporation of the solvent under vacuum, the crude product was purified by column chromatography on silica gel (70-230 mesh) by using CH₂Cl₂ as eluent and finally crystallized from methanol to give pure (S)-**ML6A** as a red-orange crystalline material in 41% yield.

FT-IR: 3067 (ν_{CH}, arom.), 2993 and 2864 (ν_{CH}, aliph.), 1738 (ν_{C=O} lactic ester), 1720 (ν_{C=O} methacrylic ester), 1638 (ν_{C=C} methacrylic), 1600 and 1517 (ν_{C=C}, arom.), 1150 and 1112 (ν_{C-O} ether), 845 and 815 (δ_{CH} 1,4 disubst. arom. ring) cm⁻¹.

¹H-NMR (CDCl₃): 7.90 (d, 4H, arom. 2-H and 2'-H), 6.90 (d, 4H, arom. 3-H and 3'-H), 6.20 and 5.60 (dd, 2H, CH₂=), 5.1 (m, 1H, CH-CH₃), 4.10 (m, 2H, CH₃-CH₂-O and 4H, CH₂-CH₂-O), 2.05 (s, 3H, CH₃-C=), 1.85-1.40 (m, 14H, CH₂-CH₂-CH₂-CH₂, CH₃-CH₂-O and CH-CH₃) ppm.

¹³C-NMR (CDCl₃): 176,9 (CO methacrylic), 171.1 (CO lactic ester), 161.7 and 161.6 (arom 4-C and 4'-C), 147.7 (arom 1-C and 1'-C), 136.1 (C=CH₂), 127.0 (CH₂=C), 125.0 (arom 2-C and 2'-C), 115.3 (arom 3-C and 3'-C), 69.6 (CH-CH₃), 68.7 (CH₂-CH₂-O-), 65.9 (CH₃-CH₂-O-), 64.4 (COO-CH₂-), 29.8, 29.1, 26.4 and 26.3 (aliph spacer CH₂), 18.9 (C-CH₃), 17.7 (CH₃-CH), 15.4 (CH₃-CH₂) ppm.

Polymerization of monomer (S)-ML6A:

Several homopolymeric samples with different average molecular weights, polydispersity values and molecular structure were obtained from (S)-ML6A through three different synthetic methods as described below. All the products were characterized by FT-IR, ^1H and ^{13}C NMR.

Synthesis of linear Poly[(S)-ML6A]-AIBN: The reaction mixture [0.2 g of (S)-ML6A, 2 % wt. of 2,2'-azoisobutyronitrile (AIBN) as free radical initiator in 3 mL of dry THF] was introduced into a glass vial under nitrogen atmosphere, submitted to several freeze-thaw cycles and heated at 60 °C for 72 h. The polymerization was then stopped by pouring the mixture into a large excess (100 mL) of methanol, and the coagulated polymer filtered off. The solid product was redissolved in CH_2Cl_2 , precipitated again into methanol and finally dried at 50 °C under vacuum for several days to constant weight.

Synthesis of linear Poly[(S)-ML6A]-14 by ATRP: The homopolymerization of (S)-ML6A was carried out in glass vials using ABIB as the linear monofunctional initiator, HMTETA as the ligand, Cu(I)Br as catalyst and dry THF as solvent [(S)-ML6A/THF 1/15 g/ml]. The reaction mixture [(S)-ML6A/ABIB/HMTETA/CuBr = 50:1:1:1 by mol] was introduced into a glass vial under nitrogen atmosphere, submitted to several freeze-thaw cycles and heated at 60°C. To stop the polymerization reaction, the vial was frozen after 14 hours reaction times with liquid nitrogen and the obtained linear polymer purified by precipitation in a large excess of methanol (100 mL). The final purification of the product was made in the same way as above.

Synthesis of Star[(S)-ML6A]s by ATRP: All homopolymerizations of (S)-ML6A were carried out in several glass vials using BMPB as the three arm star-shaped trifunctional initiator, HMTETA as the ligand, and Cu(I)Br as catalyst in dry THF [(S)-ML6A/THF 1/15 g/mL]. The mixture [(S)-ML6A/BMPB/HMTETA/CuBr = 150:1:3:3 by mol] was introduced into each vial under nitrogen atmosphere, submitted to several freeze-thaw cycles and heated at 60 °C. To stop the polymerization reaction, each vial was frozen in liquid nitrogen after known reaction times, ranging from 2 to 24 h, and the obtained polymeric products (Star[(S)-ML6A]-2 through Star[(S)-ML6A]-24) were purified in the same way as above.

As an example, the spectroscopic data for Star[(*S*)-**ML6A**]-8, obtained after 8 h of reaction, are here reported:

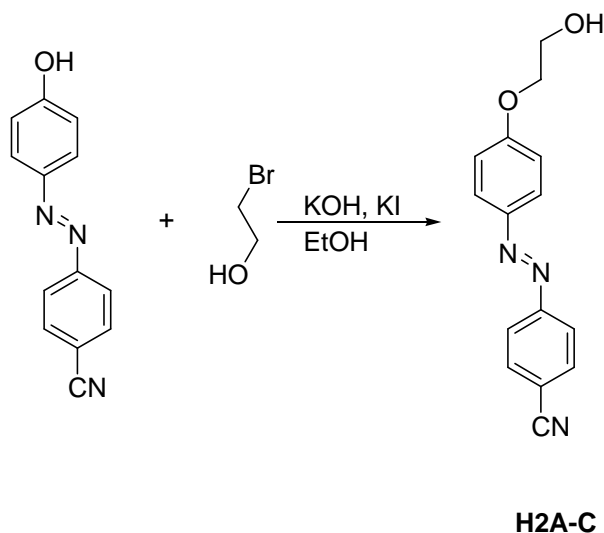
FT-IR: 3069 (ν_{CH} , arom.), 2980 and 2865 (ν_{CH} , aliph.), 1733 ($\nu_{\text{C=O}}$ lactic ester and $\nu_{\text{C=O}}$ main chain methacrylic ester), 1598 and 1517 ($\nu_{\text{C=C}}$, arom.), 1150 and 1111 ($\nu_{\text{C-O}}$ ether), 844 and 815 (δ_{CH} 1,4 disubst. arom. ring) cm^{-1} .

$^1\text{H-NMR}$ (CDCl_3): 7.90 (d, 4H, arom. 2-H and 2'-H), 6.90 (m, 3H, arom core and 4H, 3- and 3'-H), 5.10-4.90 (m, 1H, $\underline{\text{CH}}\text{-CH}_3$), 4.10-3.80 (m, 2H, $\text{CH}_3\text{-}\underline{\text{CH}}_2\text{-O}$ and 4H, $\text{CH}_2\text{-}\underline{\text{CH}}_2\text{-O}$), 2.20 ($\text{CH}_2\text{-C-Br}$), 1.95 (m, 3H, $\text{CH}_3\text{-C-Br}$), 1.85-0.90 (m, 19H, aliph spacer CH_2 , $\underline{\text{CH}}_3\text{-CH}_2\text{-O}$, $\text{CH-}\underline{\text{CH}}_3$, backbone CH_3 and CH_2 and 18H, $\text{C}(\text{CH}_3)_2\text{-COO}$) ppm.

$^{13}\text{C-NMR}$ (CDCl_3): 176.9 (CO methacrylic repeating unit), 171.1 (CO lactic ester), 167.8 (CO core), 161.7 and 161.6 (arom 4-C and 4'-C), 153.1 (C-O arom core), 147.6 (arom 1-C and 1'-C), 125.0 (arom 2-C and 2'-C), 115.3 (arom 3-C and 3'-C), 113.1 (arom $\underline{\text{C}}\text{-H}$ core), 70.0 ($\underline{\text{CH}}\text{-CH}_3$), 68.7 ($\text{CH}_2\text{-}\underline{\text{CH}}_2\text{-O-}$), 65.7 ($\text{CH}_3\text{-}\underline{\text{CH}}_2\text{-O-}$), 64.4 ($\text{COO-}\underline{\text{CH}}_2\text{-}$), 58.0 ($\underline{\text{C}}(\text{CH}_3)\text{-Br}$), 54.2 (main chain $\underline{\text{C}}\text{-CH}_2$), 46.2 and 45.9 (main chain $\underline{\text{CH}}_2\text{-C}$), 42.2 ($\underline{\text{C}}(\text{CH}_3)_2\text{-CH}_2$), 38.9 ($\underline{\text{CH}}_2\text{-C}(\text{CH}_3)\text{-Br}$), 27.5 ($\text{C}(\underline{\text{CH}}_3)\text{-Br}$), 29.8, 29.1, 26.5 and 26.4 (aliph spacer CH_2), 23.2 ($\text{C}(\underline{\text{CH}}_3)_2\text{-CH}_2$), 19.9 and 17.7 (main chain CH_3), 17.7 ($\underline{\text{CH}}_3\text{-CH}$), 15.4 ($\underline{\text{CH}}_3\text{-CH}_2$) ppm.

Synthesis of monomers and polymeric derivatives bearing the chromophore 4'-cyano-4-oxy-azobenzene

Synthesis of 4-(2-hydroxyethyl)-4'-cyanoazobenzene [H2A-C]:

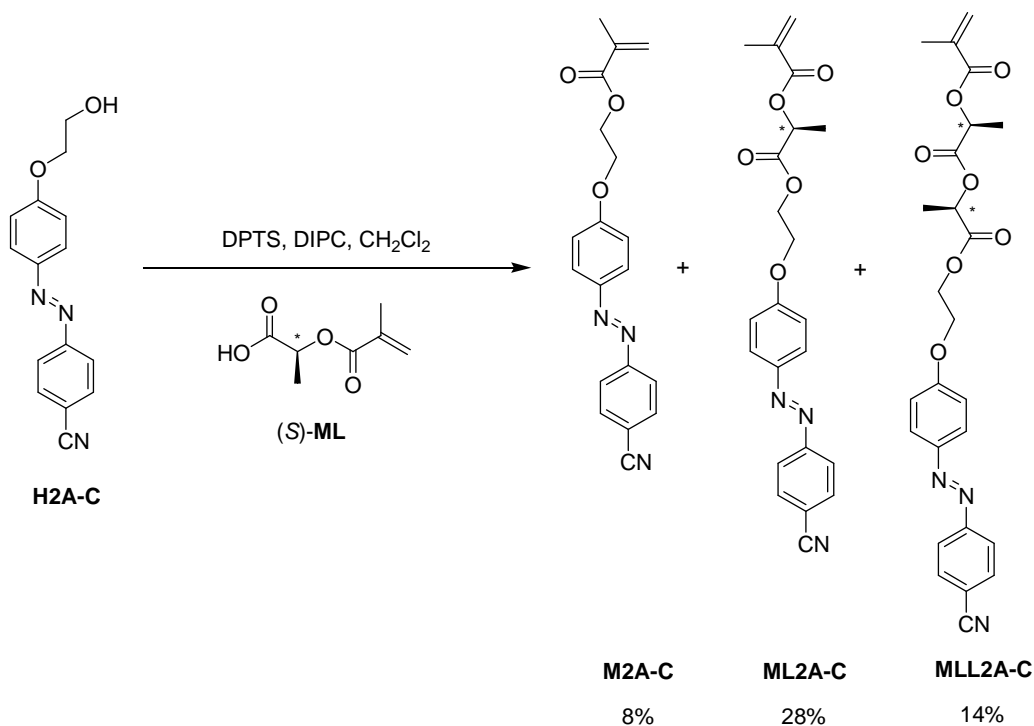


This intermediate was prepared by following the same method used for similar **H6A**. 2-Bromo ethanol (3,6 ml, 0,0496 mol) was added dropwise under vigorous stirring to a solution of 4-hydroxy-4'-(ciano)-azobenzene (4 g, 0,01792 mol), KOH (0,6 g, 0,011 mol) and KI (1,64 g, 0,0099 mol) in 96% ethanol (80 ml) at reflux. The reaction was followed by TLC (eluent $\text{CH}_2\text{Cl}_2:\text{EtOAc} = 4:1$ v/v) until the total conversion of 4-hydroxy-4'-(ciano)-azobenzene (48h) was observed. The precipitated material was filtered off, the solvent volume reduced to 15 ml under vacuum, then aq 1% NaOH was added under vigorous stirring. The solid formed was filtered and crystallized twice with absolute ethanol to give a orange crystalline material (65% yield).

FT-IR: 3300 (ν_{OH}), 3093 (ν_{CH} , arom.), 2959 and 2881 (ν_{CH} , aliph.), 2226 (ν_{CN} nitrile) 1600 and 1500 ($\nu_{\text{C=C}}$, arom.), 1150 and 1111 ($\nu_{\text{C-O}}$ ether), 842 and 811 (δ_{CH} 1,4 disubst. arom. ring) cm^{-1} .

$^1\text{H-NMR}$ (CDCl_3): 7,9 (d, 4H, 2-H e 2'-H), 7,8 (d, 2H, 3'-H), 7,1 (d, 2H, 3-H), 4,6 (m, 1H, OH), 4,1 (t, 2H, $\text{CH}_2\text{CH}_2\text{-O}$), 3,9 (m, 2H, $\text{CH}_2\text{-OH}$) ppm.

Synthesis of 4- {2-[(S)-2-methacryloyloxypropanoyloxy]ethoxy }-4'-cyanoazobenzene [(S)-ML2A-C] and 4-(2-{(S)-2-[(S)-2-methacryloyloxypropanoyloxy]propanoiloxy }ethoxy)-4'-cyanoazobenzene [(S,S)-MLL2A-C]



In a 150 ml three neck flask with magnetic stirrer, under nitrogen flow, 0,96 g of **H2A-C** (0,00362 mol), 0,57 g. of L-methacryloyl lactic acid [(S)-**ML**] (0,00362 mol), 1,05 g of DPTS (0,00362 mol) e 0.2 g di 2,6-di-ter-buthyl-paracresole (polimerization inhibitor) and 11 ml of anhydrous CH_2Cl_2 are introduced. To this solution under vigorous stirring 0,73 ml of N,N-di-isopropyl carbodimide (DIPC) (0,00471 mol) are added.

The clear solution is left at room temperature under stirring and nitrogen atmosphere for 72 hours, then the formed urea is filtered off. The liquid phase is washed with HCl 0,1 M, Na_2CO_3 5% and distilled water, then anidrifed with Na_2SO_4 and the solvent evaporated under vacuum.

(S)-**ML2A-C** is therefore purified by chromatography on silica gel (20-230 mesh) using CH_2Cl_2 as eluent and finally crystallized from methanol (yeald 28%). From these reaction also **M2A-C** (yeald 8%) and (S,S)-**MLL2A-C** (yeald 14%) are obtained.

(S)-ML2A-C

FT-IR (ATR): 3093 (ν_{CH} arom.), 2959 and 2881 (ν_{CH} aliph.), 2226 (ν_{CN}), 1745 ($\nu_{\text{C=O}}$ hester of lactic acid residue), 1724 ($\nu_{\text{C=O}}$ hester of methacrylic residue), 1635 ($\nu_{\text{C=C}}$ vinylic), 1600 and 1500 ($\nu_{\text{C=C}}$ arom.), 1404 (ν_{CH} CH_3), 1151 and 1110 ($\nu_{\text{C-O}}$ ether), 850, 842 and 811 (δ_{CH} 1,4 disubst. Arom. ring) cm^{-1} .

$^1\text{H-NMR}$ (CDCl_3): 7,9 (d, 4H, 2-H and 2'-H), 7,8 (d, 2H, 3'-H), 7,0 (d, 2H, 3-H), 6,2 and 5,6 (dd, 2H, $\text{CH}_2=\text{C}$), 5,1 (q, 1H, CH), 4,5 (m, 2H, $\text{CH}_2\text{-O-Azo}$), 4,3 (t, 2H, $\text{CH}_2\text{-O-CO-}$), 2,0 (s, 3H, CH_3 methacrylic), 1,6 (m, 6H, CH_3) ppm.

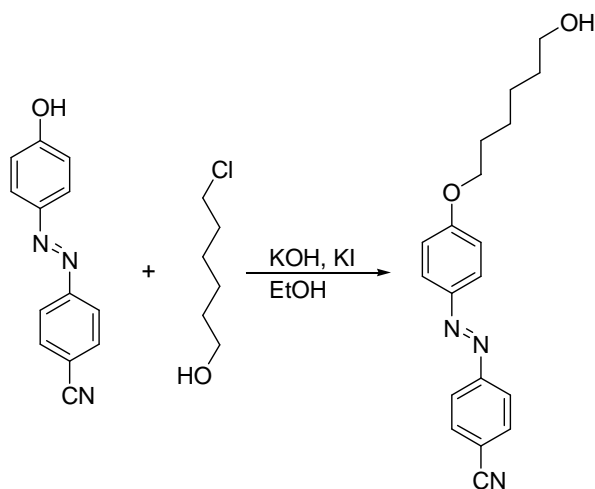
$^{13}\text{C-NMR}$ (CDCl_3) (ppm): 171,0 (CH-CO-O), 162,1 (C-CO-O), 155,0, 147,4, 133,5, 125,8, 123,4, 118,8, 115,2 113,5 (arom. and $-\text{CN}$), 136,1 ($\text{CH}_2=\text{C}$), 126,9 ($\text{CH}_2=\text{C}$), 69,2 (CH-CH_3), 68,6 ($\text{CH}_2\text{-CH}_2\text{-O-}$), 63,4 ($\text{COO-CH}_2\text{-}$), 18,4 (C-CH_3), 17,2 ($\text{CH}_3\text{-CH}$) ppm.

(S,S)-MLL2A-C

FT-IR (ATR): 3093 (ν_{CH} arom.), 2959 and 2881 (ν_{CH} aliph.), 2226 (ν_{CN}), 1745 ($\nu_{\text{C=O}}$ hester of lactic acid residue), 1726 ($\nu_{\text{C=O}}$ hester of methacrylic residue), 1635 ($\nu_{\text{C=C}}$ vinylic), 1600 and 1500 ($\nu_{\text{C=C}}$ arom.), 1404 (ν_{CH} CH_3), 1151 and 1110 ($\nu_{\text{C-O}}$ ether), 851, 844 and 810 (δ_{CH} 1,4 disubst. Arom. ring) cm^{-1} .

$^1\text{H-NMR}$ (CDCl_3): 7,9 (d, 4H, 2-H and 2'-H), 7,8 (d, 2H, 3'-H), 7,0 (d, 2H, 3-H), 6,2 and 5,6 (dd, 2H, $\text{CH}_2=\text{C}$), 5,1 (m, 2H, CH), 4,5 (m, 2H, $\text{CH}_2\text{-O-Azo}$), 4,3 (t, 2H, $\text{CH}_2\text{-O-CO-}$), 2,0 (s, 3H, CH_3 methacrylic), 1,6 (m, 6H, CH_3) ppm

$^{13}\text{C-NMR}$ (CDCl_3): 170,6 and 170,5 (CH-CO-O), 162,0 (C-CO-O), 155,0, 147,4, 133,5, 125,8, 123,4, 118,8, 115,2 113,5 (arom. and $-\text{CN}$), 135,7 ($\text{CH}_2=\text{C}$), 126,9 ($\text{CH}_2=\text{C}$), 69,3 and 68,8 (CH-CH_3), 68,6 ($\text{CH}_2\text{-CH}_2\text{-O-}$), 63,4 ($\text{COO-CH}_2\text{-}$), 18,4 (C-CH_3), 17,1 and 17,0 ($\text{CH}_3\text{-CH}$) ppm.

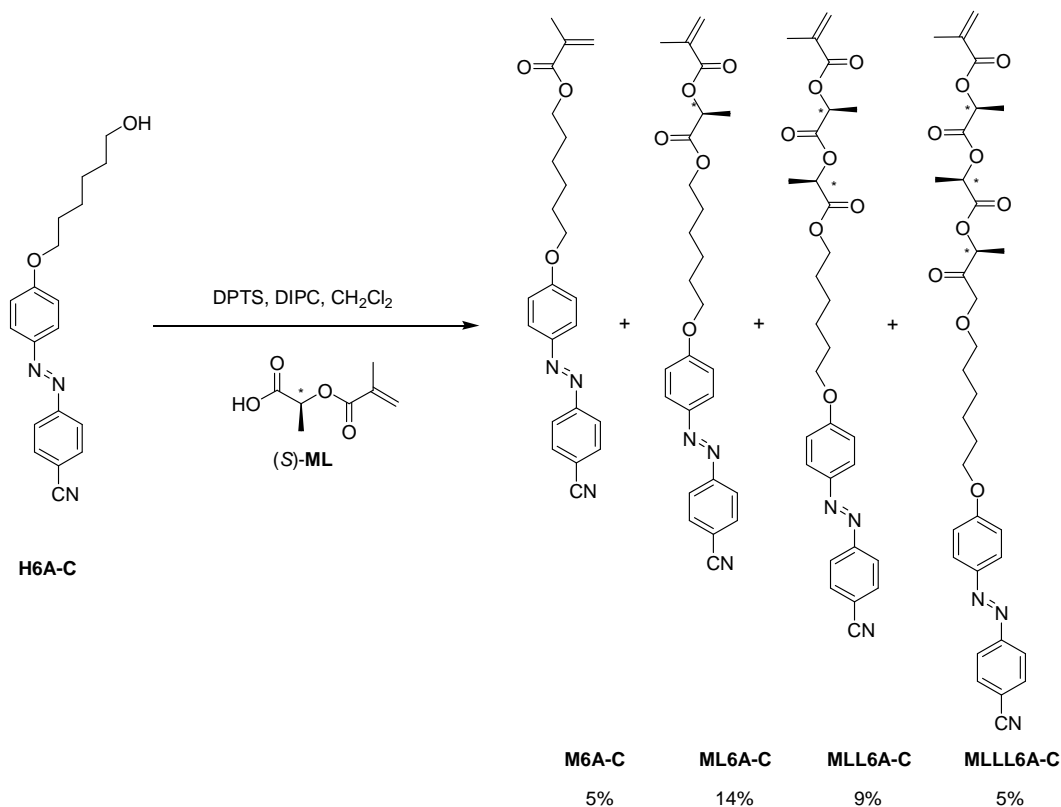
Synthesis of 4-(6-hydroxyhexyloxy)-4'-(cyano)azobenzene [H6A-C]:**H6A-C**

This intermediate was prepared by following the same method used for similar **H6A**. 6-Chlorine hexanol (6,9 ml, 0,0496 mol) was added dropwise under vigorous stirring to a solution of 4-hydroxy-4'-(cyano)-azobenzene (5,5 g, 0,0248 mol), KOH (0,6 g, 0,011 mol) and KI (1,64 g, 0,0099 mol) in 96% ethanol (80 ml) at reflux. The reaction was followed by TLC (eluent $\text{CH}_2\text{Cl}_2:\text{EtOAc} = 4:1$ v/v) until the total conversion of 4-hydroxy-4'-(cyano)-azobenzene (48h) was observed. The precipitated material was filtered off, the solvent volume reduced to 15 ml under vacuum, then aq 1% NaOH was added under vigorous stirring. The solid formed was filtered and crystallized twice with absolute ethanol to give a orange crystalline material (87% yield).

FT-IR: 3300 (ν_{OH}), 3093 (ν_{CH} , arom.), 2959 and 2881 (ν_{CH} , aliph.), 2226 (ν_{CN}) 1600 and 1500 ($\nu_{\text{C=C}}$, arom.), 1150 and 1111 ($\nu_{\text{C-O}}$ ether), 842 and 811 (δ_{CH} 1,4 disubst. arom. ring) cm^{-1} .

$^1\text{H-NMR}$ (CDCl_3): 7.90 (d, 4H, arom. 2-H and 2'-H), 7.80 (d, 2H, arom. 3'-H), 7.10 (d, 2H, 3-H) 4.15 (t, 2H, $\text{CH}_2\text{-O-C}$), 3.65 (t, 2H, $\text{CH}_2\text{-OH}$), 1.85-1.40 (m, 8H, $\text{CH}_2\text{-CH}_2\text{-CH}_2\text{-CH}_2$) ppm.

Synthesis of 4-{6-[(*S*)-methacryloyloxypropanoyloxy]hexyloxy}-4'-cyanoazobenzene [(*S*)-ML6A-C], 4-(6-{(*S*)-2-[(*S*)-methacryloyloxy propanoyloxy]propanoyloxy}hexyloxy)-4'-cyanoazobenzene [(*S,S*)-MLL6A-C] 4-(6-[(*S*)-2-[(*S*)-2-[(*S*)-2-methacryloyloxy propanoyloxy]propanoyloxy]-propanoyloxy}hexyloxy)-4'-cyanoazobenzene [(*S,S,S*)-MLLL6A-C]



The new monomer (*S*)-ML6A-C has been synthesized as (*S*)-ML2A-C using the intermediate H6A-C instead of H2A-C.

3,40 g of H6A-C (0,0107 mol), 1,69 g of ML (0,0107 mol), 3,12 g of DPTS (0,0107 mol), 0,2 g of 2,6-di-ter-butyl-paracresol (polymerization inhibitor), 95 ml of dry CH₂Cl₂ and 2,15 ml of DIPC (0,014 mol) were used.

After chromatographic separation and crystallization from methanol 0,7 g of (*S*)-ML6A-C (yeald 14%) 0,2 g of M6A-C (5%), 0,5 g of MLL6A-C (9%), 0,3 g of MLLL6A-C (5%) have been obtained.

(S)-ML6A-C

FT-IR (ATR): 3090 (ν_{CH} arom.), 2960 and 2880 (ν_{CH} aliph.), 2226 (ν_{CN}), 1743 ($\nu_{\text{C=O}}$ lactic ester), 1722 ($\nu_{\text{C=O}}$ methacrylic ester), 1635 ($\nu_{\text{C=C}}$ vinylic), 1600 and 1500 ($\nu_{\text{C=C}}$ arom.), 1404 (ν_{CH} CH_3), 1151 e 1110 ($\nu_{\text{C-O}}$ ether), 850, 842 and 811 (δ_{CH} 1,4 disubst. arom. ring) cm^{-1} .

$^1\text{H-NMR}$ (CDCl_3): 7,9 (d, 4H, 2-H and 2'-H), 7,8 (d, 2H, 3'-H), 7,0 (d, 2H, 3-H), 6,2 and 5,6 (dd, 2H, CH_2 vinylic), 5,1 (q, 1H, CH), 4,3 (t, 2H, $\text{CH}_2\text{-O-AZO}$), 4,1 (t, 2H, $\text{CH}_2\text{-O-CO}$) 2,0 (s, 3H, CH_3 metacrilico), 1,4-1,8 (m, 8H, CH_2 aliph. and 3H, CH_3) ppm

$^{13}\text{C-NMR}$ (CDCl_3): 171,3 (CH-CO-O), 163,0 (C-CO-O), 155,1, 147,1, 133,5, 125,8, 123,4, 119,0, 115,2 113,5 (arom. and $-\text{CN}$), 135,7 ($\text{CH}_2=\text{C}$), 126,8 ($\text{CH}_2=\text{C}$), 69,2 (CH-CH_3), 68,6 ($\text{CH}_2\text{-CH}_2\text{-O-}$), 65,5 ($\text{COO-CH}_2\text{-}$), 29,3, 28,8, 25,9 e 25,8 (CH_2 aliph. spacer), 18,9 (C-CH_3), 17,7 ($\text{CH}_3\text{-CH}$) ppm

(S,S)-MLL6A-C

FT-IR (ATR): 3090 (ν_{CH} arom.), 2960 and 2880 (ν_{CH} aliph.), 2226 (ν_{CN}), 1743 ($\nu_{\text{C=O}}$ lactic ester), 1722 ($\nu_{\text{C=O}}$ methacrylic ester), 1635 ($\nu_{\text{C=C}}$ vinylic), 1600 and 1500 ($\nu_{\text{C=C}}$ arom.), 1404 (ν_{CH} CH_3), 1151 e 1110 ($\nu_{\text{C-O}}$ ether), 850, 842 and 811 (δ_{CH} 1,4 disubst. arom. ring) cm^{-1} .

$^1\text{H-NMR}$ (CDCl_3): 7,9 (d, 4H, 2-H and 2'-H), 7,8 (d, 2H, 3'-H), 7,0 (d, 2H, 3-H), 6,2 and 5,6 (dd, 2H, CH_2 vinylic), 5,1 (m, 2H, CH), 4,3 (t, 2H, $\text{CH}_2\text{-O-AZO}$), 4,1 (t, 2H, $\text{CH}_2\text{-O-CO}$), 2,0 (s, 3H, CH_3 methacrylic), 1,4-1,8 (m, 8H, CH_2 aliph. and 6H, CH_3) ppm.

$^{13}\text{C-NMR}$ (CDCl_3): 170,7 and 170,6 (CH-CO-O), 163,0 (C-CO-O), 155,1, 147,1, 133,5, 125,8, 123,4, 119,0, 115,2 113,5 (arom. and $-\text{CN}$), 135,8 ($\text{CH}_2=\text{C}$), 127,0 ($\text{CH}_2=\text{C}$), 69,6 and 69,4 (CH-CH_3), 68,6 ($\text{CH}_2\text{-CH}_2\text{-O-}$), 65,5 ($\text{COO-CH}_2\text{-}$), 29,3, 28,8, 25,9 and 25,8 (CH_2 alkylic spacer), 18,9 (C-CH_3), 17,2 and 17,1 ($\text{CH}_3\text{-CH}$) ppm.

(S,S,S)-MLLL6A-C

FT-IR (ATR): 3090 (ν_{CH} arom.), 2960 and 2880 (ν_{CH} aliph.), 2226 (ν_{CN}), 1743 ($\nu_{\text{C=O}}$ lactic ester), 1722 ($\nu_{\text{C=O}}$ methacrylic ester), 1635 ($\nu_{\text{C=C}}$ vinylic), 1600 and 1500 ($\nu_{\text{C=C}}$ arom.), 1404 (ν_{CH} CH_3), 1151 and 1110 ($\nu_{\text{C-O}}$ etereo), 850, 842 and 811 (δ_{CH} 1,4 disubst. arom. ring) cm^{-1} .

$^1\text{H-NMR}$ (CDCl_3): 7,9 (d, 4H, 2-H and 2'-H), 7,8 (d, 2H, 3'-H), 7,0 (d, 2H, 3-H), 6,2 and 5,6 (dd, 2H, CH_2 vinylic), 5,1 (m, 3H, CH), 4,3 (t, 2H, $\text{CH}_2\text{-O-AZO}$), 4,1 (t, 2H, $\text{CH}_2\text{-O-CO}$), 2,0 (s, 3H, CH_3 methacrylic), 1,4-1,8 (m, 8H, CH_2 aliph. and 9H, CH_3) ppm.

$^{13}\text{C-NMR}$ (CDCl_3): 170,6, 170,3 and 170,0 (CH-CO-O), 163,0 (C-CO-O), 155,1, 147,1, 133,5, 125,8, 123,4, 119,0, 115,2 113,5 (arom. and $-\text{CN}$), 135,7 ($\text{CH}_2=\text{C}$), 127,0 ($\text{CH}_2=\text{C}$), 69,5, 69,1 and 68,8 (CH-CH_3), 68,4 ($\text{CH}_2\text{-CH}_2\text{-O-}$), 65,6 ($\text{COO-CH}_2\text{-}$), 29,3, 28,8, 25,9 and 25,8 (CH_2 aliph. spacer), 18,4 (C-CH_3), 17,1, 17,0 and 16,9 ($\text{CH}_3\text{-CH}$) ppm

Synthesys of polymeric derivatives of (S)-ML2A-C, (S,S)-MLL2A-C, (S)-ML6A-C, (S,S)-MLL6A-C and (S,S,S)-MLLL6A-C

Linear and star shaped polymers have been synthesized as previously described for the polymeric derivatives of (S)-ML6A.

The catalytic system used was CuBr/HMTETA and the initiator used were ABiB for linear derivatives and BMPB for star shaped polymers, using a molar ratio Monomer/ABiB/CuBr/HMTETA = 50/1/1/1 or Monomer/BMPB/CuBr/HMTETA = 150/1/1/1, dry THF as solvent and a monomer concentration of 0.2 M.

The quantities used are reported in Table 9.

Table 9. synthesis of the polymeric derivatives

Sample	Monomer [g (mol)]	Initiator [mg, (mol)]	CuBr [mg (mol)]	HMTETA [μl (mol)]	THF (ml)
Poly[(S)-ML2A-C]	0,150 (3,68 10 ⁻⁴)	ABiB 1,5 (7,36 10 ⁻⁶)	0,91 (7,36 10 ⁻⁶)	2,0 (7,36 10 ⁻⁶)	1,84
Poly[(S,S)-MLL2A-C]	0,200 (4,17 10 ⁻⁴)	ABiB 1,7 (8,34 10 ⁻⁶)	1,2 (8,34 10 ⁻⁶)	2,27 (8,34 10 ⁻⁶)	2,0
Poly[(S)-ML6A-C]	0,300 (6,47 10 ⁻⁴)	ABiB 2,7 (1,29 10 ⁻⁵)	1,85 (1,29 10 ⁻⁵)	3,52 (1,29 10 ⁻⁵)	3,23
Poly[(S,S)-MLL6A-C]	0,250 (4,67 10 ⁻⁴)	ABiB 1,9 (9,34 10 ⁻⁶)	1,15 (9,34 10 ⁻⁶)	2,54 (9,34 10 ⁻⁶)	2,33
Poly[(S,S,S)-MLLL6A-C]	0,150 (2,47 10 ⁻⁴)	ABiB 1,0 (4,94 10 ⁻⁶)	0,61 (4,94 10 ⁻⁶)	1,34 (4,94 10 ⁻⁶)	1,24
Star[(S)-ML6A-C]	0,200 (4,91 10 ⁻⁴)	BMPB 2,2 (3,27 10 ⁻⁶)	1,21 (9,82 10 ⁻⁶)	2,67 (9,82 10 ⁻⁶)	2,45
Star[(S,S)-MLL6A-C]	0,250 (4,67 10 ⁻⁴)	BMPB 1,8 (3,11 10 ⁻⁶)	1,15 (9,34 10 ⁻⁶)	2,54 (9,34 10 ⁻⁶)	2,33

The polymeric derivatives were characterized by FT-IR, ¹H- and ¹³C-NMR, UV-Vis spectroscopy, GPC and DSC.

Poly[(*S*)-**ML2A-C**]

FT-IR (ATR): 3093 (ν_{CH} arom.), 2959 and 2881 (ν_{CH} aliph.), 2226 (ν_{CN}), 1745 ($\nu_{\text{C=O}}$ lactic ester), 1732 ($\nu_{\text{C=O}}$ methacrylic ester), 1598 and 1499 ($\nu_{\text{C=C}}$ arom.), 1403 (ν_{CH} CH_3), 1151 and 1110 ($\nu_{\text{C-O}}$ ether), 845 and 811 (δ_{CH} 1,4 disubst. arom. ring) cm^{-1} .

$^1\text{H-NMR}$ (CDCl_3): 7,9 (m, 4H, 2-H and 2'-H), 7,8 (m, 2H, 3'-H), 6,9 (m, 2H, 3-H), 5,9 (m, 1H, $\text{CH}_2=\underline{\text{CH}}-\text{CH}_2\text{-O}$), 5,3 (m, 2H, $\underline{\text{CH}}_2=\text{CH}-\text{CH}_2$), 5,1-4,9 (m, 1H, CH), 4,6-4,4 (m, 2H, $\text{CH}_2\text{-O-AZO}$ and m, 2H, $\text{CH}_2=\text{CH}-\underline{\text{CH}}_2$), 4,4-4,2 (m, 2H, $\text{CH}_2\text{-O-CO}$), 2,2-1,8 (m, 2H, CH_2 main chain), 1,6-0,9 (m, 6H, $\text{CH}-\underline{\text{CH}}_3$ and CH_3) ppm.,

$^{13}\text{C-NMR}$ (CDCl_3): 170,5 ($\text{CH}-\underline{\text{C}}\text{O-O}$), 161,9 ($\text{C}-\underline{\text{C}}\text{O-O}$), 154,7, 147,43, 133,5, 125,7, 123,4, 118,8, 115,2 and 113,9 (arom. and $-\text{CN}$), 69,6 ($\underline{\text{C}}\text{H}-\text{CH}_3$), 66,2 ($\text{CH}_2-\underline{\text{C}}\text{H}_2\text{-O-}$), 63,2 ($\text{COO}-\underline{\text{C}}\text{H}_2\text{-}$), 54,5 ($\underline{\text{C}}-\text{CH}_2$ main chain), 45,9 and 45,5 ($\underline{\text{C}}\text{H}_2\text{-C}$ main chain), 42,2 ($\underline{\text{C}}(\text{CH}_3)_2\text{-CH}_2$), 34,5 ($\underline{\text{C}}\text{H}_2\text{C}(\text{CH}_3)\text{Br}$), 28,3 ($\underline{\text{C}}(\text{CH}_3)\text{Br}$), 20,0 ($\text{C}-\underline{\text{C}}\text{H}_3$), 17,2 ($\underline{\text{C}}\text{H}_3\text{-CH}$) ppm.

Poly[(*S,S*)-**MLL2A-C**]

FT-IR (ATR): 3093 (ν_{CH} arom.), 2959 and 2881 (ν_{CH} aliph.), 2226 (ν_{CN}), 1745 ($\nu_{\text{C=O}}$ lactic ester), 1732 ($\nu_{\text{C=O}}$ methacrylic ester), 1598 and 1499 ($\nu_{\text{C=C}}$ arom.), 1403 (ν_{CH} CH_3), 1151 and 1110 ($\nu_{\text{C-O}}$ ether), 845 and 811 (δ_{CH} 1,4 disubst. arom. ring) cm^{-1} .

$^1\text{H-NMR}$ (CDCl_3): 8,0-7,8 (m, 4H, 2-H and 2'-H), 7,8-7,6 (m, 2H, 3'-H), 7,0-6,9 (m, 2H, 3-H), 5,9 (m, 1H, $\text{CH}_2=\underline{\text{C}}\text{H}-\text{CH}_2\text{-O}$), 5,2-5,0 (m, 2H, CH), 5,0-4,8 (m, 1H, CH and m, 2H, $\text{CH}_2=\text{CH}-\text{CH}_2$), 4,6-4,3 (m, 2H, $\text{CH}_2\text{-O-AZO}$ and m, 2H, $\text{CH}_2=\text{CH}-\underline{\text{C}}\text{H}_2$), 4,2-4,1 (m, 2H, $\text{CH}_2\text{-O-CO}$), 2,2-1,8 (m, 2H CH_2 main chain), 1,6-0,9 (m, 9H, $\text{CH}-\underline{\text{C}}\text{H}_3$, CH_3 main chain) ppm.

$^{13}\text{C-NMR}$ (CDCl_3): 170,5 and 170,3 ($\text{CH}-\underline{\text{C}}\text{O-O}$), 161,9 ($\text{C}-\underline{\text{C}}\text{O-O}$), 154,7, 147,43, 133,5, 125,7, 123,4, 118,8, 115,2 113,9 (arom. and $-\text{CN}$), 69,6 and 69,5 ($\underline{\text{C}}\text{H}-\text{CH}_3$), 66,2 ($\text{CH}_2-\underline{\text{C}}\text{H}_2\text{-O-}$), 63,2 ($\text{COO}-\underline{\text{C}}\text{H}_2\text{-}$), 54,5 ($\underline{\text{C}}-\text{CH}_2$ main chain), 45,9 and 45,5 ($\underline{\text{C}}\text{H}_2\text{-C}$ main chain), 42,2 ($\underline{\text{C}}(\text{CH}_3)_2\text{-CH}_2$), 34,5 ($\underline{\text{C}}\text{H}_2\text{C}(\text{CH}_3)\text{Br}$), 28,3 ($\underline{\text{C}}(\text{CH}_3)\text{Br}$), 20,0 ($\text{C}-\underline{\text{C}}\text{H}_3$), 17,3 e 17,2 ($\underline{\text{C}}\text{H}_3\text{-CH}$) ppm.

Poly[(*S*)-**ML6A-C**]

FT-IR (ATR): 3093 (ν_{CH} arom.), 2959 and 2881 (ν_{CH} aliph.), 2226 (ν_{CN}), 1745 ($\nu_{\text{C=O}}$ lactic ester), 1732 ($\nu_{\text{C=O}}$ methacrylic ester), 1598 and 1499 ($\nu_{\text{C=C}}$ arom.), 1403 (ν_{CH} CH₃), 1151 and 1110 ($\nu_{\text{C-O}}$ ether), 845 and 811 (δ_{CH} 1,4 disubst. arom. ring) cm⁻¹.

¹H-NMR (CDCl₃): 8,0-7,8 (m, 4H, 2-H and 2'-H), 7,8-7,7 (m, 2H, 3'-H), 7,0-6,9 (m, 2H, 3-H), 5,9 (m, 1H, CH₂=CH-CH₂-O), 5,3 (m, 2H, CH₂=CH-CH₂), 5,0-4,8 (m, 1H, CH), 4,5 (m, 2H, CH₂=CH-CH₂), 4,2-4,0 (m, 2H, CH₂-O-AZO), 4,0-3,8 (m, 2H, CH₂-O-CO), 2,2-0,9 (m, 16H, CH₂ aliph. spacer, CH-CH₃, CH₃ and CH₂ main chain) ppm.

¹³C-NMR (CDCl₃): 170,1 (CH-CO-O), 162,8 (C-CO-O), 154,9, 146,9, 133,4, 125,7, 123,2, 118,8, 115,1 and 113,9 (arom. and -CN), 69,3 (CH-CH₃), 68,4 (CH₂-CH₂-O-), 65,6 (COO-CH₂-), 54,5 (C-CH₂ main chain), 45,9 and 45,5 (CH₂-C main chain), 42,2 (C(CH₃)₂-CH₂), 34,5 (CH₂C(CH₃)Br), 30,5, 28,2, 28,6 and 25,9 (CH₂ aliph. spacer), 28,3 (C(CH₃)Br), 20,0 (C-CH₃), 17,1 (CH₃-CH) ppm.

Star[(*S*)-**ML6A-C**]

FT-IR (ATR): 3093 (ν_{CH} arom.), 2959 and 2881 (ν_{CH} aliph.), 2226 (ν_{CN}), 1745 ($\nu_{\text{C=O}}$ lactic ester), 1732 ($\nu_{\text{C=O}}$ methacrylic ester), 1598 and 1499 ($\nu_{\text{C=C}}$ arom.), 1403 (ν_{CH} CH₃), 1151 and 1110 ($\nu_{\text{C-O}}$ ether), 845 and 811 (δ_{CH} 1,4 disubst. arom. ring) cm⁻¹.

¹H-NMR (CDCl₃): 7,9 (m, 4H, 2-H and 2'-H), 7,7 (m, 2H, 3'-H), 6,9 (m, 2H, 3-H and arom. initiator ring), 5,0 (m, 1H, CH), 4,1 (m, 2H, CH₂-O-AZO), 3,9 (m, 2H, CH₂-O-CO), 2,2-0,9 (m, 16H, CH₂ aliph. spacer, CH-CH₃, CH₃ and CH₂ main chain, and 18H, C(CH₃)₂-COO from initiator residue) ppm.

¹³C-NMR (CDCl₃): 171,3 (CH-CO-O), 162,8 (C-CO-O), 154,9, 147,0, 133,5, 125,8, 123,4, 119,0, 115,2 113,5 (arom. and -CN), 69,2 (CH-CH₃), 68,6 (CH₂-CH₂-O-), 65,5 (COO-CH₂-), 57,5 (C(CH₃)-Br), 54,2 (C-CH₂ main chain), 46,2 and 45,9 (CH₂-C main chain), 42,6 (C(CH₃)₂-CH₂), 34,5 (CH₂C(CH₃)Br), 29,3, 28,8, 25,9 e 25,8 (CH₂ aliph. spacer), 28,4 (C(CH₃)Br), 19,7 (C-CH₃), 18,9 (C-CH₃), 17,7 (CH₃-CH) ppm.

Poly[(*S,S*)-**MLL6A-C**]

FT-IR (ATR): 3093 (ν_{CH} arom.), 2959 and 2881 (ν_{CH} aliph.), 2226 (ν_{CN}), 1745 ($\nu_{\text{C=O}}$ lactic ester), 1732 ($\nu_{\text{C=O}}$ methacrylic ester), 1598 and 1499 ($\nu_{\text{C=C}}$ arom.), 1403 (ν_{CH} CH_3), 1151 and 1110 ($\nu_{\text{C-O}}$ ether), 845 and 811 (δ_{CH} 1,4 disubst. arom. ring) cm^{-1} .

$^1\text{H-NMR}$ (CDCl_3): 8,0-7,8 (m, 4H, 2-H and 2'-H), 7,8-7,7 (m, 2H, 3'-H), 7,0-6,9 (m, 2H, 3-H), 5,9 (m, 1H, $\text{CH}_2=\text{CH}-\text{CH}_2-\text{O}$), 5,2-5,0 (m, 1H, CH and m, 2H, $\text{CH}_2=\text{CH}-\text{CH}_2$), 5,0-4,9 (m, 1H, CH), 4,5 (m, 2H, $\text{CH}_2=\text{CH}-\text{CH}_2$), 4,2-3,9 (m, 2H, $\text{CH}_2-\text{O}-\text{AZO}$ and m, 2H, $\text{CH}_2-\text{O}-\text{CO}$), 2,2-0,9 (m, 19H, CH_2 aliph. spacer, $\text{CH}-\underline{\text{CH}_3}$, CH_3 and CH_2 main chain) ppm.

$^{13}\text{C-NMR}$ (CDCl_3): 170,2 and 170,1 ($\text{CH}-\underline{\text{CO}}-\text{O}$), 162,8 ($\text{C}-\underline{\text{CO}}-\text{O}$), 154,9, 146,9, 133,4, 125,7, 123,2, 118,8, 115,1, 113,9 (arom. and $-\text{CN}$), 69,5 and 69,1 ($\underline{\text{C}}\text{H}-\text{CH}_3$), 68,4 ($\text{CH}_2-\underline{\text{CH}_2}-\text{O}-$), 65,6 ($\text{COO}-\underline{\text{CH}_2}-$), 54,5 ($\underline{\text{C}}-\text{CH}_2$ main chain), 45,9 and 45,5 ($\underline{\text{C}}\text{H}_2-\text{C}$ main chain), 42,2 ($\underline{\text{C}}(\text{CH}_3)_2-\text{CH}_2$), 34,5 ($\underline{\text{C}}\text{H}_2\text{C}(\text{CH}_3)\text{Br}$), 30,5, 28,2, 28,6 e 25,9 (CH_2 aliph. spacer), 28,3 ($\underline{\text{C}}(\text{CH}_3)\text{Br}$), 20,0 ($\text{C}-\underline{\text{C}}\text{H}_3$), 17,1 and 16,9 ($\underline{\text{C}}\text{H}_3-\text{CH}$) ppm.

Star[(*S,S*)-**MLL6A-C**]

FT-IR (ATR): 3093 (ν_{CH} arom.), 2959 and 2881 (ν_{CH} aliph.), 2226 (ν_{CN}), 1745 ($\nu_{\text{C=O}}$ lactic ester), 1732 ($\nu_{\text{C=O}}$ methacrylic ester), 1598 and 1499 ($\nu_{\text{C=C}}$ arom.), 1403 (ν_{CH} CH_3), 1151 and 1110 ($\nu_{\text{C-O}}$ ether), 845 and 811 (δ_{CH} 1,4 disubst. arom. ring) cm^{-1} .

$^1\text{H-NMR}$ (CDCl_3): 8,0-7,8 (m, 4H, 2-H and 2'-H), 7,8-7,7 (m, 2H, 3'-H), 7,0-6,9 (m, 2H, 3-H), 5,2-5,1 (m, 1H, CH), 5,1-4,9 (m, 1H, CH), 4,2-3,9 (m, 2H, $\text{CH}_2-\text{O}-\text{AZO}$ and m, 2H, $\text{CH}_2-\text{O}-\text{CO}$), 2,2-0,9 (m, 19H, CH_2 aliph. spacer, $\text{CH}-\underline{\text{CH}_3}$, CH_3 e CH_2 main chain).

$^{13}\text{C-NMR}$ (CDCl_3): 171,4 and 171,3 ($\text{CH}-\underline{\text{CO}}-\text{O}$), 162,8 ($\text{C}-\underline{\text{CO}}-\text{O}$), 154,9, 147,0, 133,5, , 125,8, 123,4, 119,0, 115,2 and 113,5 (arom. and $-\text{CN}$), 69,5 and 69,3 ($\underline{\text{C}}\text{H}-\text{CH}_3$), 68,6 ($\text{CH}_2-\underline{\text{CH}_2}-\text{O}-$), 65,5 ($\text{COO}-\underline{\text{CH}_2}-$), 57,5 ($\underline{\text{C}}(\text{CH}_3)-\text{Br}$), 54,2 ($\underline{\text{C}}-\text{CH}_2$ main chain), 46,2 and 45,9 ($\underline{\text{C}}\text{H}_2-\text{C}$ main chain), 42,6 ($\underline{\text{C}}(\text{CH}_3)_2-\text{CH}_2$), 34,5 ($\underline{\text{C}}\text{H}_2\text{C}(\text{CH}_3)\text{Br}$), 29,3, 28,8, 25,9 and 25,8 (CH_2 aliph. spacer), 28,4 ($\underline{\text{C}}(\text{CH}_3)\text{Br}$), 19,7 ($\text{C}-\underline{\text{C}}\text{H}_3$), 18,9 ($\text{C}-\underline{\text{C}}\text{H}_3$), 17,8 and 17,7 ($\underline{\text{C}}\text{H}_3-\text{CH}$) ppm.

Poly[(*S,S,S*)-**MLLL6A-C**]

FT-IR (ATR): 3093 (ν_{CH} arom.), 2959 and 2881 (ν_{CH} aliph.), 2226 (ν_{CN}), 1745 ($\nu_{\text{C=O}}$ lactic ester), 1732 ($\nu_{\text{C=O}}$ methacrylic ester), 1598 and 1499 ($\nu_{\text{C=C}}$ arom.), 1403 (ν_{CH} CH_3), 1151 and 1110 ($\nu_{\text{C-O}}$ ether), 845 and 811 (δ_{CH} 1,4 disubst. arom. ring) cm^{-1} .

$^1\text{H-NMR}$ (CDCl_3): 8,0-7,8 (m, 4H, 2-H and 2'-H), 7,8-7,7 (m, 2H, 3'-H), 7,0-6,9 (m, 2H, 3-H), 5,9 (m, 1H, $\text{CH}_2=\text{CH}-\text{CH}_2-\text{O}$), 5,3-5,1 (m, 1H, CH, m 1H, CH and m, 2H, $\text{CH}_2=\text{CH}-\text{CH}_2$), 5,1-4,9 (m, 1H, CH), 4,5 (m, 2H, $\text{CH}_2=\text{CH}-\text{CH}_2$), 4,2-4,1 (m, 2H, $\text{CH}_2-\text{O}-\text{AZO}$), 4,1-3,9 (m, 2H, $\text{CH}_2-\text{O}-\text{CO}$), 2,2-0,9 (m, 22H, CH_2 aliph. spacer, $\text{CH}-\text{CH}_3$, CH_3 and CH_2 main chain) ppm.

$^{13}\text{C-NMR}$ (CDCl_3): 170,5, 170,2 and 170,1 ($\text{CH}-\text{CO}-\text{O}$), 162,8 ($\text{C}-\text{CO}-\text{O}$), 154,9, 146,9, 133,4, 125,7, 123,2, 118,8, 115,1, 113,9 (arom. and $-\text{CN}$), 69,6, 69,5 and 69,1 ($\text{CH}-\text{CH}_3$), 68,4 ($\text{CH}_2-\text{CH}_2-\text{O}$), 65,6 ($\text{COO}-\text{CH}_2$), 54,5 ($\text{C}-\text{CH}_2$ main chain), 45,9 and 45,5 (CH_2-C main chain), 42,2 ($\text{C}(\text{CH}_3)_2-\text{CH}_2$), 34,5 ($\text{CH}_2\text{C}(\text{CH}_3)\text{Br}$), 30,5, 28,2, 28,6 and 25,9 (CH_2 aliph. spacer), 28,3 ($\text{C}(\text{CH}_3)\text{Br}$), 20,0 ($\text{C}-\text{CH}_3$), 17,2, 17,1 and 16,9 (CH_3-CH) ppm.

References

- [1] M. Irie, *Chem. Rev. (Washington, D. C.)* **2000**, 100, 1683.
- [2] L. Angiolini, T. Benelli, L. Giorgini, E. Salatelli, *Polymer* **2005**, 46, 2424.
- [3] E. Gomar-Nadal, J. Veciana, C. Rovira, D. B. Amabilino, *Advanced Materials* **2005**, 17, 2095.
- [4] Y. Agata, M. Kobayashi, H. Kimura, M. Takeishi, *Polym. Int.* **2005**, 54, 260.
- [5] B. L. Feringa, R. A. van Delden, N. Koumura, E. M. Geertsema, *Chem. Rev. (Washington, D. C.)* **2000**, 100, 1789.
- [6] T. Kaneko, Y. Umeda, T. Yamamoto, M. Teraguchi, T. Aoki, *Macromolecules* **2005**, 38, 9420.
- [7] Y. Oaki, H. Imai, *J. Am. Chem. Soc.* **2004**, 126, 9271.
- [8] T. J. Wigglesworth, D. Sud, T. B. Norsten, V. S. Lekhi, N. R. Branda, *J. Am. Chem. Soc.* **2005**, 127, 7272.
- [9] T. Kajitani, H. Masu, S. Kohmoto, M. Yamamoto, K. Yamaguchi, K. Kishikawa, *J. Am. Chem. Soc.* **2005**, 127, 1124.
- [10] L. Angiolini, T. Benelli, L. Giorgini, E. Salatelli, R. Bozio, A. Dauru, D. Pedron, *Eur. Polym. J.* **2005**, 41, 2045.
- [11] L. Angiolini, D. Caretti, L. Giorgini, E. Salatelli, *Macromol. Chem. Phys.* **2000**, 201, 533.
- [12] G. D. Jaycox, *J. Polym. Sci., Part A: Polym. Chem.* **2004**, 42, 566.
- [13] L. Nikolova, T. Todorov, M. Ivanov, F. Andruzzi, S. Hvilsted, P. S. Ramanujam, *Opt. Mater. (Amsterdam)* **1997**, 8, 255.
- [14] I. Nayadenova, L. Nikolova, P. S. Ramanujam, S. Hvilsted, *J. Opt. A: Pure Appl. Opt.* **1999**, 1, 438.
- [15] M. Ivanov, I. Naydenova, T. Todorov, L. Nikolova, T. Petrova, N. Tomova, V. Dragostinova, *J. Mod. Opt.* **2000**, 47, 861.
- [16] L. Nikolova, L. Nedelchev, T. Todorov, T. Petrova, N. Tomova, V. Dragostinova, P. S. Ramanujam, S. Hvilsted, *Appl. Phys. Lett.* **2000**, 77, 657.
- [17] G. Iftime, F. L. Labarthe, A. Natansohn, P. Rochon, *J. Am. Chem. Soc.* **2000**, 122, 12646.
- [18] M.-J. Kim, B.-G. Shin, J.-J. Kim, D.-Y. Kim, *J. Am. Chem. Soc.* **2002**, 124, 3504.
- [19] L. Angiolini, R. Bozio, L. Giorgini, D. Pedron, G. Turco, A. Dauru, *Chem.--Eur. J.* **2002**, 8, 4241.
- [20] L. Angiolini, T. Benelli, R. Bozio, A. Dauru, L. Giorgini, D. Pedron, *Synth. Met.* **2003**, 139, 743.
- [21] L. Angiolini, L. Giorgini, R. Bozio, D. Pedron, *Synth. Met.* **2003**, 138, 375.
- [22] D. Hore, Y. Wu, A. Natansohn, P. Rochon, *J. Appl. Phys.* **2003**, 94, 2162.
- [23] R. M. Tejedor, M. Millaruelo, L. Oriol, J. L. Serrano, R. Alcalá, F. J. Rodriguez, B. Villacampa, *J. Mater. Chem.* **2006**, 16, 1674.
- [24] R. M. Tejedor, L. Oriol, J. L. Serrano, F. P. Urena, J. J. L. Gonzalez, *Adv. Funct. Mater.* **2007**, 17, 3486.
- [25] E. L. Eliel, S. H. Wilen, L. N. Mander, *Stereochemistry of Organic Compounds*, Wiley-VCH, New York, **1994**.
- [26] K. Matyjaszewski, J. Xia, *Chemical Reviews* **2001**, 101, 2921.
- [27] L. Angiolini, T. Benelli, L. Giorgini, F. Paris, E. Salatelli, M. P. Fontana, P. Camorani, *Eur. Polym. J.* **2008**, 44, 3231.

- [28] L. Angiolini, T. Benelli, L. Giorgini, F. Paris, E. Salatelli, T. Zuccheri, *Int. J. Polym. Mater.* **2007**, 56, 789.
- [29] J. Barberá, L. Giorgini, F. Paris, E. Salatelli, Rosa M. Tejedor, L. Angiolini, *Chemistry - A European Journal* **2008**, 14, 11209.
- [30] D. Wolff, H. Cackovic, H. Krueger, J. Ruebner, J. Springer, *Liq. Cryst.* **1993**, 14, 917.
- [31] A. S. Angeloni, D. Caretti, C. Carlini, E. Chiellini, G. Galli, A. Altomare, R. Solaro, M. Laus, *Liq. Cryst.* **1989**, 4, 513.
- [32] J. S. Moore, S. I. Stupp, *Macromolecules* **1990**, 23, 65.
- [33] X.-Z. Wang, H.-L. Zhang, D.-C. Shi, J.-F. Chen, X.-Y. Wang, Q.-F. Zhou, *Eur. Polym. J.* **2005**, 41, 933.
- [34] L. Angiolini, T. Benelli, L. Giorgini, E. Salatelli, *Macromolecules* **2006**, 39, 3731.
- [35] K. Matyjaszewski, P. J. Miller, J. Pyun, G. Kickelbick, S. Diamanti, *Macromolecules* **1999**, 32, 6526.
- [36] S. Angot, K. S. Murthy, D. Taton, Y. Gnanou, *Macromolecules* **1998**, 31, 7218.
- [37] L. Angiolini, C. Carlini, D. Caretti, E. Salatelli, *Macromol. Chem. Phys* **1995**, 196, 2737
- [38] L. Angiolini, D. Caretti, L. Giorgini, E. Salatelli, A. Altomare, C. Carlini, R. Solaro, *Polymer* **1998**, 39, 6621
- [39] L. Angiolini, D. Caretti, L. Giorgini, E. Salatelli, A. Altomare, C. Carlini, R. Solaro, *Polymer* **2000**, 41, 4767
- [40] P. Davidson, A. M. Levelut, M. F. Achard, F. Hardouin, *Liq. Cryst.* **1989**, 4, 561.
- [41] M. Kozlovsky, B.-J. Jungnickel, H. Ehrenberg, *Macromolecules* **2005**, 38, 2729.
- [42] H. H. Jaffé, M. Orchin, *Theory and application of ultraviolet spectroscopy*, Wiley, New York, **1962**.
- [43] L. Angiolini, T. Benelli, L. Giorgini, E. Salatelli, *Polymer* **2006**, 47, 1875.
- [44] M. Shimomura, T. Kunitake, *J. Am. Chem. Soc.* **1987**, 109, 5175.
- [45] J. G. Meier, R. Ruhmann, J. Stumpe, *Macromolecules* **2000**, 33, 843.
- [46] I. Zebger, M. Rutloh, U. Hoffmann, J. Stumpe, H. W. Siesler, S. Hvilsted, *Macromolecules* **2003**, 36, 9373.
- [47] F. Ciardelli, C. Carlini, R. Solaro, A. Altomare, O. Pieroni, J. L. Houben, A. Fissi, *Pure Appl. Chem.* **1984**, 56, 329.
- [48] A. Painelli, F. Terenziani, L. Angiolini, T. Benelli, L. Giorgini, *Chem.--Eur. J.* **2005**, 11, 6053.
- [49] L. M. Blinov, M. V. Kozlovsky, G. Cipparrone, *Chem. Phys.* **1999**, 245, 473.
- [50] G. Srajer, R. Pindak, M. A. Waugh, J. W. Goodby, J. S. Patel, *Phys. Rev. Lett.* **1990**, 64, 1545.
- [51] J. W. Goodby, *Struct. Bonding (Berlin)* **1999**, 95, 83.
- [52] A. C. Ribeiro, H. T. Nguyen, Y. Galerne, D. Guillon, *Liq. Cryst.* **2000**, 27, 27.
- [53] M. S. Spector, S. K. Prasad, B. T. Weslowski, R. D. Kamien, J. V. Selinger, B. R. Ratna, R. Shashidhar, *Phys. Rev. E: Stat. Phys., Plasmas, Fluids, Relat. Interdiscip. Top.* **2000**, 61, 3977.
- [54] J. Xue, N. A. Clark, *Phys. Rev. E* **1990**, 64, 307.
- [55] N. Berova, K. Nakanishi, R. W. Woody, *Circular Dichroism Principles and Applications*, Wiley-VCH Inc, New York, **2000**.
- [56] S. Pages, F. Lagugne-Labarthe, T. Buffeteau, C. Sourisseau, *Appl. Phys. B: Lasers Opt.* **2002**, 75, 541.
- [57] T. Fujiwara, N. Nanba, K. Hamada, F. Toda, K. Tanaka, *J. Org. Chem.* **1990**, 55, 4532.
- [58] A. Moradpour, J. F. Nicoud, G. Balavoine, H. Kagan, G. Tsoucaris, *J. Am. Chem. Soc.* **1971**, 93, 2353.
- [59] K. S. Burnham, G. B. Schuster, *J. Am. Chem. Soc.* **1999**, 121, 10245.

-
- [60] N. P. M. Huck, W. F. Jager, B. de Lang, B. L. Feringa, *Science* (Washington, D. C.) **1996**, 273, 1686.
- [61] S.-W. Choi, S. Kawauchi, N. Y. Ha, H. Takezoe, *Phys. Chem. Chem. Phys.* **2007**, 9, 3671.
- [62] S. Sajti, A. Kerekes, M. Barabas, E. Lorincz, S. Hvilsted, P. S. Ramanujam, *Opt. Commun.* **2001**, 194, 435.
- [63] S.-W. Choi, T. Izumi, Y. Hoshino, Y. Takanishi, K. Ishikawa, J. Watanabe, H. Takezoe, *Angew. Chem., Int. Ed.* **2006**, 45, 1382.
- [64] H. Rau, *Photochemistry and photophysics*, CRC, USA, **1990**.
- [65] P. J. Collings, M. Hird, *Introductions to liquid crystal*, Taylor & Francis, London **1997**.
- [66] V. A. Miller, R. R. Brown, E. B. Gienger, Jr., (International Latex Corp.). *Application: US*, **1962**, p. 7 pp.
- [67] D. D. Perrin, W. L. F. Amarego, D. R. Perrin, *Purification of Laboratory Chemicals*, Pergamon Press, Oxford, **1996**.
- [68] D. M. Haddleton, C. Waterson, *Macromolecules* **1999**, 32, 8732.
- [69] A. Carlmark, R. Vestberg, E. M. Jonsson, *Polymer* **2002**, 43, 4237.

Chapter 4

Cholesteric polymers***Introduction***

The Bragg reflection of cholesteric liquid crystals has been object of an enormous number of studies and thus this kind of systems found applications in several devices: from photonic systems to laser to thermometers. The cholesteric or chiral nematic (N^*) phase can be induced in nematic liquid crystal by doping with a small amount of chiral molecules that can force a twisting of the nematic director and thus induce the phase transition. The efficiency of the chiral doping is express by the rotation power (β), a parameter typical of each substance that is influenced by several factor like the matrix interaction, temperature, and the structure of the chiral residue.

In literature is reported a plethora of these compounds, the more efficient are based on chiral spiro compound and asymmetrical bisnaphthalene but their use, despite their efficiency, is limited by their complex synthesis and purification. Natural chiral compounds, due to their relative low cost and optical purity are therefore more applicable if real applications are seek.

When the axes of the induced helix are normal to the surface (planar alignment) these systems are able to reflect a specific wavelength (Bragg reflection):

$$\lambda = \bar{n} P \sin \theta$$

where \bar{n} is the average refractive index, P the helix pass and θ the light tilt angle. If the helix pass is of the magnitude of visible light these phases will result highly colored (Figure 1).

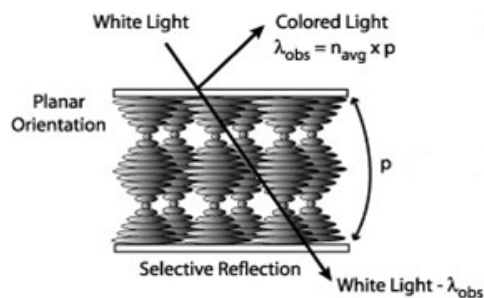


Figure 1: planar alignment and selective reflection

The helix pass is inverse proportion to the concentration (c), twisting power (β) and the enantiomeric excess (ee) of the chiral moiety:

$$P = \frac{1}{\beta \cdot ee \cdot c}$$

Is therefore possible to modulate the helix pass by acting on these parameters ^[1].

In the case of liquid crystals polymers a chiral nematic phase can be obtained in two ways ^[2]:

- 1) By adding to a nematic polymer a small amount of low molecular weight chiral doping
- 2) By copolymerization of mesogenic and chiral monomers (Figure 2)

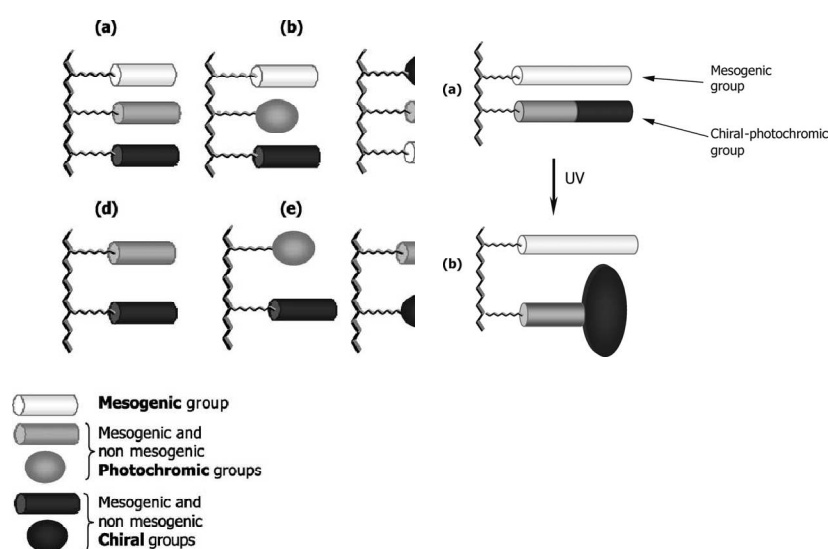


Figure 2 Structures of chiral nematic copolymers

The presence in the same structure of photochromic groups, as the azaromatic mesogen, and chiral centers allows the photomodulation of the Bragg reflection ^[3].

In literature are reported also photochromic cholesteric copolymers containing nematogenic monomers and comonomer that bring on the same lateral chain chiral and photochromic groups. The mesogen monomer induce the nematic phase that is doped by the chiral co-unit and the photochromic group (e.g. azaromatic group) if opportunely irradiated can modify its geometry and thus can modify the twisting power of the chiral center.

With irradiation with UV light *trans-cis* isomerization in azaromatic units can be induced with the consequent change of shape from a mesogenic rod-shaped *trans* isomer to bended non planar *cis* form and thus destabilization of the supramolecular order. (Figure 3).

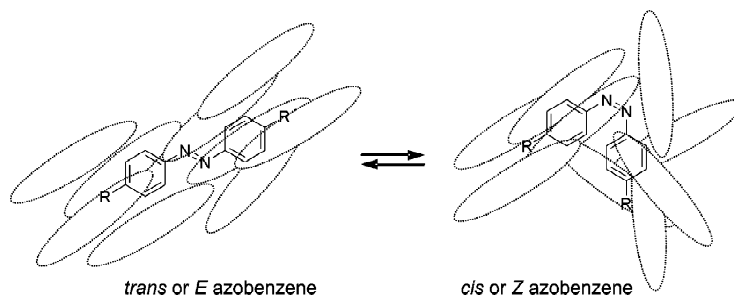


Figure 3: isomerization of an azoaromatic moiety into a LC matrix

Thus a progressive untwisting of the helix can be performed with consequent shift of the Bragg reflection.

This phenomenon is totally reversible and in the dark the back isomerization will bring the system to the initial thermodynamic stable conformation. Photoinduced untwisting of the helix and thermally induced twisting to the pristine condition is thus possible ^[4]

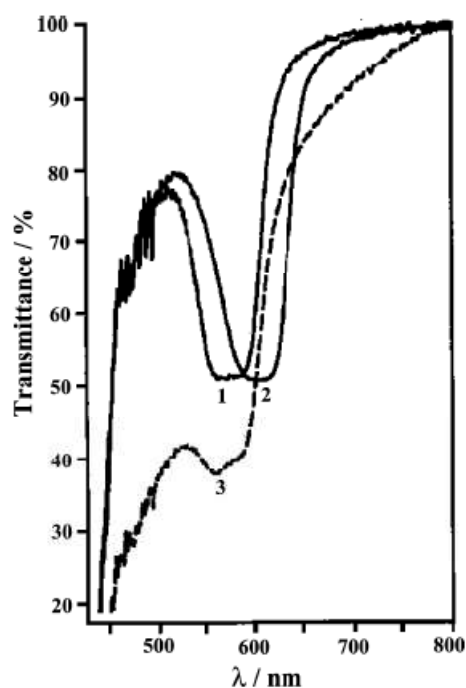


Figure 4. Shift of the Bragg reflection in the thermodynamically stable state (1), after 10 minutes of irradiation with UV light (2) and after 30 minutes (3).

Anyway, even if the photochromic groups can undergo backisomerization for allowing the system to relax to the twisted conformation is necessary that the temperature is above the glass transition, otherwise the system is frozen into a metastable state.

The aim of this work is to synthesize a material able to change reversibly its color by irradiation and to store the information until the temperature reaches a threshold value, then the information is erased and the pristine configuration restored.

The use of photochromic cholesteric polymer is therefore favorable: by irradiation a photoinduced phase transition between the highly colored LC phase (N*) and amorphous phase can be achieved with a huge change in the UV-Vis spectra of the material that is conserved until the temperature is below the glass transition of the polymer. By tailoring the glass transition we can tune the trigger temperature at which the system will relax to the thermodynamically stable LC state (N*) with re-establishment of the previous UV-Vis characteristic.

This kind of materials could be used for the fabrication of “smart” label for the certification of the thermal history of a product: in fact the possibility of such a certification is highly desirable as a quality warren for several products in which this certification can be an additional value: from drugs to high quality food.

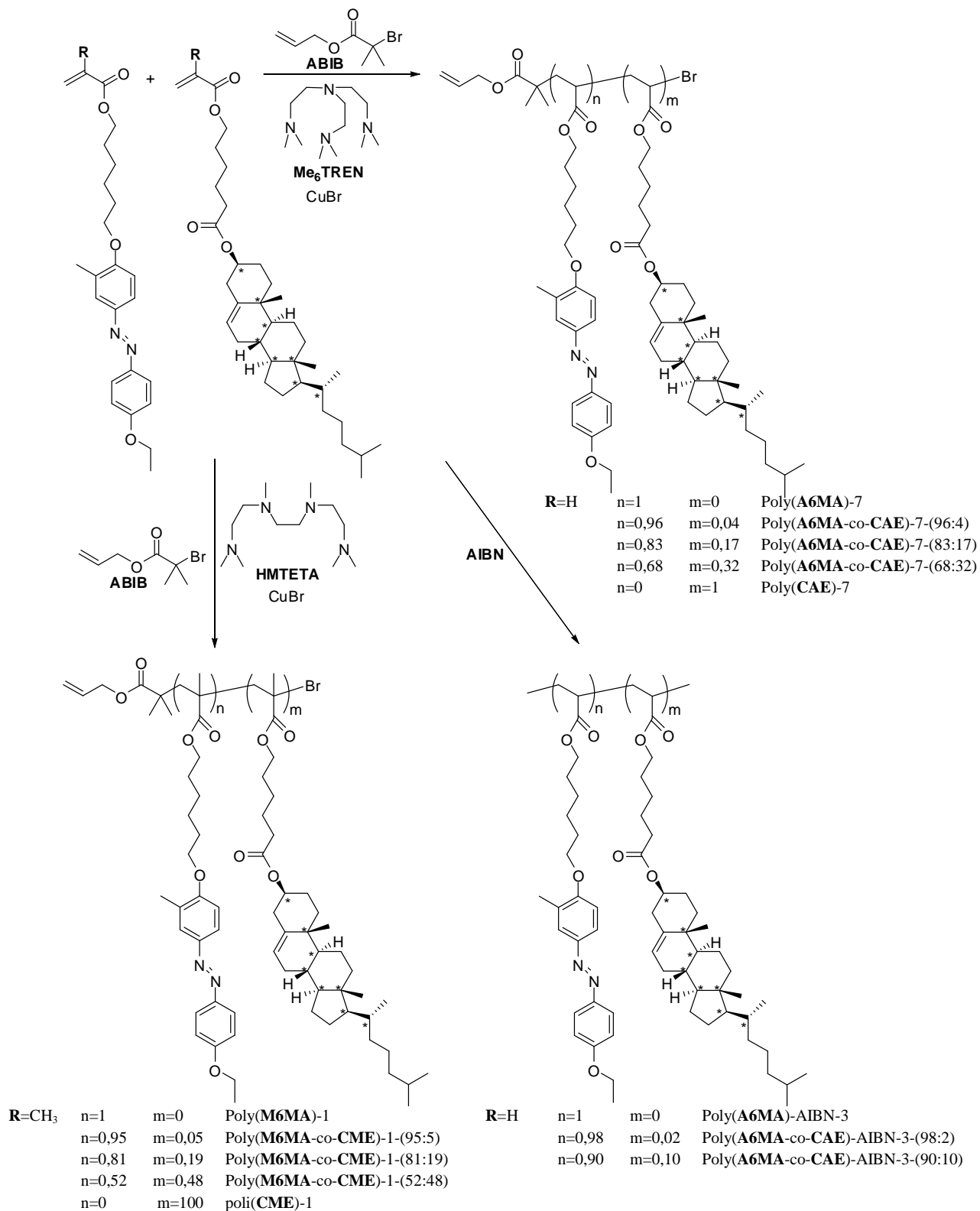
Nowadays some products of this kind are already used, but they are based on thermal sensitive dyes that undergo chemical transformations above a certain temperature. These materials are themselves sensitive to the temperature and the trigger temperature cannot be tailored easily. Thus their applicability is widely limited in a small range of temperature.

For the synthesis of this new material we choose the azoaromatic moiety as the photochromic unit, as is enough robust against photodegradation and its photochemistry can be exploited for passing from the mesogenic *trans* isomer to the non mesogenic *cis* isomer with a huge impact on the stability of the LC phase.

We used a cholesterol residue as chiral unit as is itself mesogenic, readily available and quite cheap, thus could be potentially used also in commercial application.

Finally we choose to synthesize these polymers by ATRP, as this technique allows us to tailor easily the molecular weight, the polydispersity and the geometry of the macromolecules and thus allow us to tune precisely the glass transition temperature, overcoming the limitation of a non tunable trigger temperature as in the case of dyes.

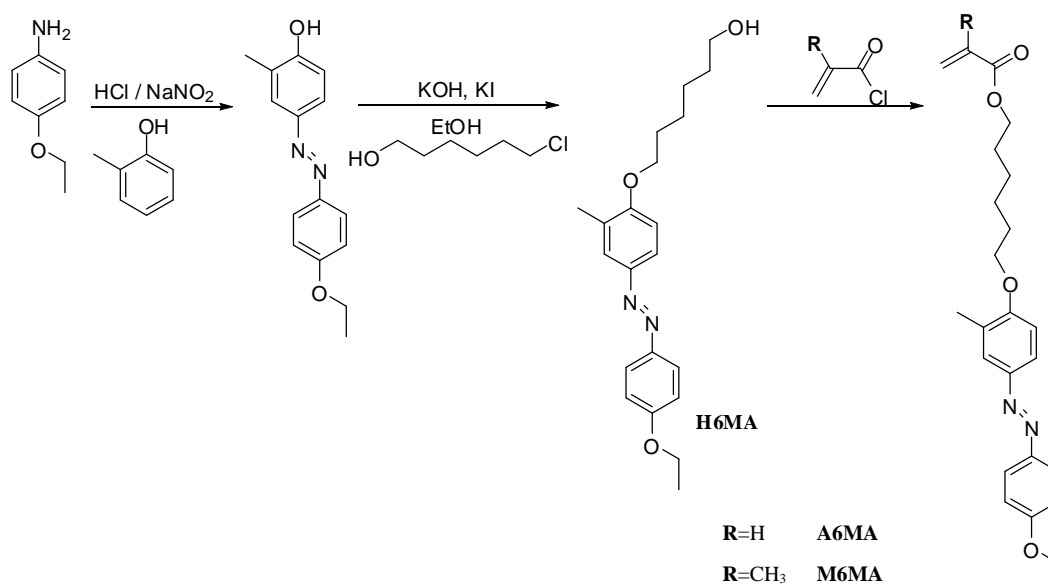
The structure of the synthesized monomers and polymers are reported below in Scheme 3.



Scheme 1: synthesis of the polymeric derivatives

Monomers synthesis

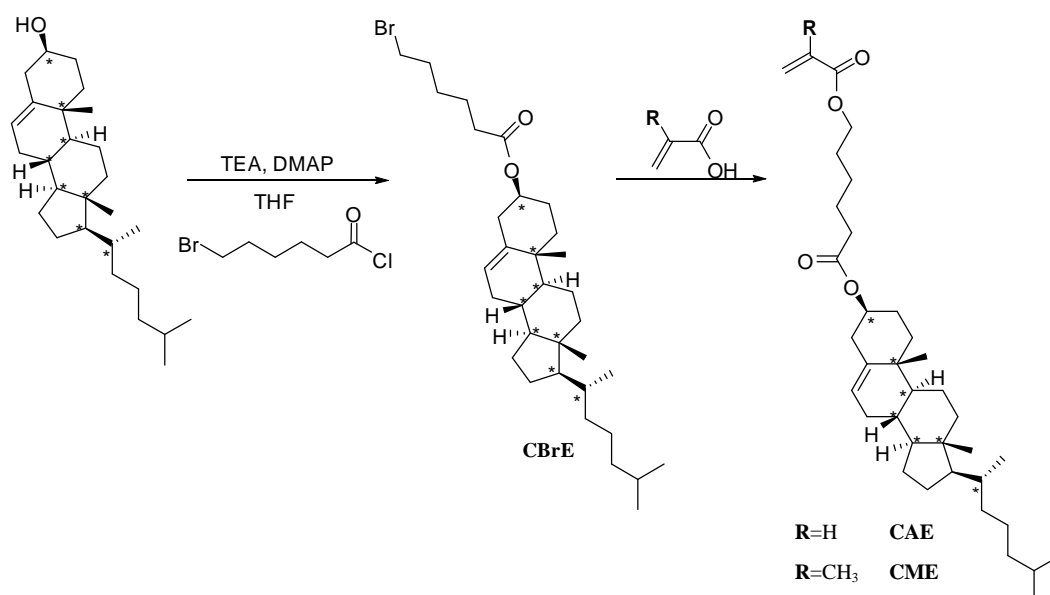
The photochromic azoaromatic monomers 3-methyl-4-(6-acryloyloxyhexyloxy)-4'-(ethoxy)-azobenzene (**A6MA**) and 3-methyl-4-(6-methacryloyloxyhexyloxy)-4'-(ethoxy)-azobenzene (**M6MA**) were synthesized following the three steps procedure reported in literature ^[5] (Scheme 1).



Scheme 1: synthesis of the photochromic monomers

The first step is the azocoupling reaction of the diazonium salt of 4-ethoxy aniline with *o*-cresol obtaining the azoic alcohol 3-methyl-4-hydroxy-4'-(ethoxy)-azobenzene (**MA**) that is etherificated with 6-chlorohexanol to give the key intermediate 3-methyl-4-(6-hydroxyhexyloxy)-4'-(ethoxy)-azobenzene with a total yield of 40%. This compound is esterificated with acryloyl or methacryloyl chloride to give the desired monomers **A6MA** or **M6MA** respectively with a yield of 85-90% in both cases.

The monomers 6-acryloyl-oxyhexanoyl-1-cholesterol (**CAE**) and 6-methacryloyl-hexanoyl-1-cholesterol (**CME**) were synthesized following the two steps procedure reported in literature ^[6] Scheme 2.



Scheme 2: Synthesis of the cholesterol containing monomers **CAE** and **CME**.

The first step is the esterification of commercially available cholesterol with 6-bromohexanoyl chloride in presence of TEA and DMAP to give the intermediate 6-bromohexanoyl-1-cholesterol (**CBrE**) that is esterificated with acryl or methacrylic acid in basic condition in presence of tetrabutylammoniumsulfate as phase transfer catalyst to give respectively CAE or CME with a yield of 68% and 88%.

$^1\text{H-NMR}$ and FT-IR characterizations of the monomers and intermediates are in agreement with the expected structures and literature data ^[6].

Synthesis of the polymeric derivatives

In order to have a good correlation structure-properties and a fine tuning of the glass transition several homopolymers and copolymers of the four prepared monomers (**CAE**, **CME**, **A6MA** and **M6MA**) were synthesized by ATRP with different molecular weight and composition (Scheme 1).

Due to the different reactivity of the acrylic and methacrylic monomers in an ATRP polymerization different catalysts are needed. In the case of methacrylic monomers, due to the high reactivity of the methacrylic residue, a medium active catalyst can be used, as CuBr/PMDETA to achieve both a good control over the polymerization and short times. The polymerization of the acrylic monomers instead in diluted condition is more complicated: the low activity^[7, 8] and low concentration make the choice of a highly active ligand necessary to have reasonable polymerization times with a small loss over the polymerization control.

In this contest the polymerizations of the acrylic monomers were carried out using two different molar ratio monomer: initiator: CuBr: ligand = 50: 1: 1: 1 and 100: 1: 1: 1 varying the concentration of monomer in solution and the activity of the catalyst and the polymerization time (Table 1). This enabled to define the right conditions for the polymerization of all the macromoleculars derivatives of interest using **ABiB** as initiator, Me₆TREN as ligand and a monomer: **ABiB**: CuBr: Me₆TREN= 50: 1: 1: 1 molar ratio at 80°C in dry anisole for seven days.

In order to have a full view over some acrylic polymeric derivatives were synthesized by free radical polymerization with AIBN as initiator carrying on the polymerization for 72 hours at 60°C in dry THF as solvent (Table 1 and Scheme 1).

In order to investigate the correlation between the transition temperatures and the structure and composition of the macromolecules a series of analogous methacrylic homo and copolymers was synthesized using the more active methacrylic monomers **M6AM** and **CME**. Due to their higher activity the ATRP polymerizations were carried in shorter times (24 hours), lower temperature using **ABiB** as initiator, CuBr as catalyst and HMTETA as ligand with a ratio 50: 1: 1: 1^[9].

The relevant synthetic data for the polymeric derivatives are gathered in Table 1.

Table 1: synthesis of the polymeric derivatives

Sample	%A6MA (feed)	%CAE (feed)	b)	c)	b)
	¹ H-NMR ^{a)}	¹ H-NMR ^{a)}	$\bar{M}_{n,GPC}$	$\bar{X}_{n,GPC}$	\bar{M}_w/\bar{M}_n
Poly(A6MA)-AIBN-3 ^{e)}	(100) 100	(0) 0	2900	7,1	1,46
Poly(A6MA-co-CAE)-AIBN-3-(98:2) ^{e)}	(95) 98	(5) 2	2900	7,0	1,44
Poly(A6MA-co-CAE)-AIBN-3-(90:10) ^{e)}	(80) 90	(20) 10	4400	10,4	1,36
	%A6MA (feed)	%CAE (feed)	d)	c)	b)
	¹ H-NMR ^{a)}	¹ H-NMR ^{a)}	$\bar{M}_{n,^1H-NMR}$	$\bar{X}_{n,^1H-NMR}$	\bar{M}_w/\bar{M}_n
Poly(A6MA)-3-(50:1:1:1) ^{f)}	(100) 100	(0) 0	5700	13,3	1,25
Poly(A6MA)-3-(100:1:1:1) ^{g)}	(100) 100	(0) 0	9300	22,2	1,20
Poly(A6MA)-7 ^{h)}	(100) 100	(0) 0	23600	57,1	1,53
Poly(A6MA-co-CAE)-7-(96:4) ^{h)}	(95) 96	(5) 4	34800	83,2	1,41
Poly(A6MA-co-CAE)-7-(83:17) ^{h)}	(80) 83	(20) 17	11800	26,7	1,48
Poly(A6MA-co-CAE)-7-(68:32) ^{h)}	(50) 68	(50) 32	18200	39,5	1,24
Poly(CAE)-7 ^{h)}	(0) 0	(100) 100	17300	30,8	1,21
	%M6MA (feed)	%CME (feed)	d)	c)	b)
	¹ H-NMR ^{a)}	¹ H-NMR ^{a)}	$\bar{M}_{n,^1H-NMR}$	$\bar{X}_{n,^1H-NMR}$	\bar{M}_w/\bar{M}_n
Poly(M6MA)-1 ⁱ⁾	(100) 100	(0) 0	14300	33,3	1,25
Poly(M6MA-co-CME)-1-(95:5) ⁱ⁾	(95) 95	(5) 5	45300	105	1,26
Poly(M6MA-co-CME)-1-(81:19) ⁱ⁾	(80) 81	(20) 19	32000	70,3	1,18
Poly(M6MA-co-CME)-1-(58:42) ⁱ⁾	(50) 58	(50) 42	37300	76,9	1,14
Poly(CME)-1 ⁱ⁾	(0) 0	(100) 100	13600	24,0	1,20

a) Determinated by ¹H-NMR spectroscopy by integration of the signal at 5.30 ppm of the vinylic proton of the cholesterol derivatives and the aromatic proton 3' at 6.90 ppm of the azoaromatic residue.

b) Determinated by GPC in THF at 25°C on a MXL column

c) Average polymerization degree calculated as $(\bar{M}_{n(^1H-NMR \text{ or } GPC)} - PM_I)/PM_M$

d) Determinated by ¹H-NMR spectroscopy by integration of the terminal units

e) 2% w/w of AIBN respect to the monomer, [A6MA]=0,24 M, 72 h, 60°C

f) [A6MA]:[ABIB]:[CuBr]:[Me₆TREN]=50:1:1:1, [A6MA]=0,24M, 72 h, 70°C

g) [A6MA]:[ABIB]:[CuBr]:[Me₆TREN]=100:1:1:1, [A6MA]=0,48M, 72 h, 70°C

h) [mon]:[ABIB]:[CuBr]:[Me₆TREN]=50:1:1:1, [mon]=0,24M, 7 days, 80°C

i) [mon]:[ABIB]:[CuBr]:[HMTETA]=50:1:1:1, [mon]=0,18M, 24 h, 60°C

The polymerization is confirmed by $^1\text{H-NMR}$ spectroscopy by the broadening of the signals and the disappearance of the signals relative to the double bond of the monomers and by FT-IR spectroscopy by the disappearance of the vibration of the vinyl bond and by the shift of the carbonyl signal around 1740 cm^{-1} . The living character of the polymerization is confirmed by the presence in the $^1\text{H-NMR}$ spectra of the signals of the terminal units (initiator and methylenic protons bound to the terminal bromine atom at 2.3ppm).

Also $^{13}\text{C-NMR}$ spectra shows in the methacrylic polymers the signal of the quaternary carbon bond to the terminal bromine atom at 54.5 ppm and in the acrylic derivatives at 42.0 ppm the signal of the analogue tertiary carbon. Moreover by $^1\text{H-NMR}$ spectroscopy it is possible to calculate the molar composition of counits in the macromolecular chain by relative integration of the 3'-proton of the azoaromatic residue at 6.90 ppm and the vinylic proton at 5.30 ppm of the cholesterol residue. The data collected in Table 1 show how the composition is in good agreement with the feed composition for the methacrylic copolymers while in the acrylic copolymers there is an enrichment of the azoaromatic comonomer (**A6MA**).

$^1\text{H-NMR}$ spectroscopy, by integration of the signals of the terminal units (allylic protons of the initiator) compared to the one of the repeating units ($\bar{M}_{n,^1\text{H-NMR}}$), can also give information on the average molecular weight of the macromolecules. The average macromolecular weight values obtained by GPC chromatography using polystyrene standard resulted to be lower than the ones obtained by $^1\text{H-NMR}$. This apparent discrepancy can be explained with the lower hydrodynamic volume of polymers with big side chains moieties as already observed for similar derivatives ^[9].

The average molecular weights of the polymers obtained by classical FRP cannot be calculated by H-NMR spectroscopy and in Table 1 are reported only the values determinate by GPC.

However, the thermal characteristics of these polymers (Table 2) suggest that their molecular weights are similar or even higher than those of the polymers obtained by ATRP.

The analysis of the polydispersities (Table 1) reveal that the methacrylic polymers are monodisperse ($\bar{M}_w/\bar{M}_n < 1,26$) while the acrylic polymers have a boarder distribution with a \bar{M}_w/\bar{M}_n in the range 1,21 - 1,53, similar to the ones obtained by FRP. This behavior could be related to the loss of control during the polymerization because of the use of active ligand and too long polymerization times ^[8].

Thermal analysis and optical characterization

In order to investigate the thermal characteristics of the synthesized polymers and to establish direct correlation between structure, composition and the thermal properties, the polymeric derivatives have been studied by differential scanning calorimetry (DSC) and polarized optical microscopy (POM). The principal results are gathered in Table 2.

Table 2: thermal characteristic of the polymeric derivatives

Sample	LC transition					
Poly(A6MA) ^{a)}	G	25		N		102 I
Poly(A6MA)-AIBN-3	G	11	S	64	N	81 I
Poly(A6MA-co-CAE)-AIBN-3-(98:2)	G	17	S	59	N*	81 I
Poly(A6MA-co-CAE)-AIBN-3-(90:10)	G	2	S	56	N*	73 I
Poly(A6MA)-3-(50:1:1:1)	G	3	S	66	N	81 I
Poly(A6MA)-3-(100:1:1:1)	G	9	S	69	N	81 I
Poly(A6MA)-7	G	3	S	66	N	85 I
Poly(A6MA-co-CAE)-7-(96:4)	G	3	S	62	N*	83 I
Poly(A6MA-co-CAE)-7-(83:17)	G	6	S	59	N*	82 I
Poly(A6MA-co-CAE)-7-(68:32)	G	4		N*		71 I
Poly(CAE) ^{b)}	G	28		N*		180 I
Poly(CAE)-7	G	27		N*		157 I
Poly(M6MA)-1	G	44		N		88 I
Poly(M6MA-co-CME)-1-(95:5)	G	50		N*		90 I
Poly(M6MA-co-CME)-1-(81:19)	G	41		N*		89 I
Poly(M6MA-co-CME)-1-(58:42)	G	48		N*		121 I
Poly(CME) ^{b)}	G	39		N*		168 I
Poly(CME)-1	G	48		N*		144 I

a) Rif. ^[10] $\bar{M}_n = 48000$, $\bar{M}_w/\bar{M}_n = 2,7$

b) Rif. ^[11] $\bar{M}_w = 150000$

An analysis of the data collected in Table 2 shows a similar behavior between the acrylic polymers synthesized by FRP and ATRP.

In literature ^[12] is reported that the azoic homopolymer Poly(**A6MA**) ($\bar{M}_n = 48000$ g/mol) synthesized by FRP exhibit only a nematic (N) phase. Considering that our polymers

have lower molecular weights and they have two different LC phase is reasonable to think that these polymers are able to self organize in more ordered phases such as smectic ones (S) at lower temperature than the nematic phase.

These behavior is confirmed by POM analysis on cells of Poly(**A6MA**)-7 after annealing for 2 hours at 40 and 75°C in order to develop the LC phase (Figure 5).

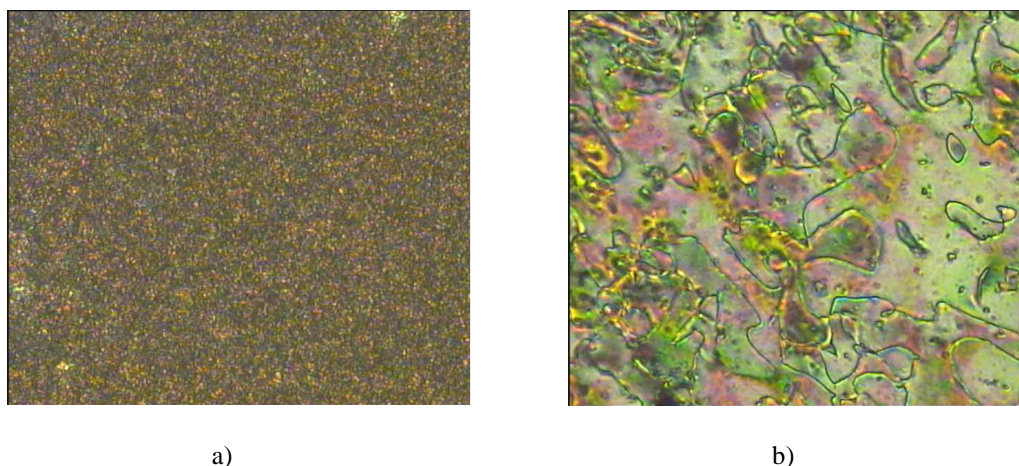


Figure 5. POM microphotograph, 32x magnification, of Poly(**A6MA**)-7 at 40°C (a) and at 75°C (b) after isotropization

The acrylic copolymers at different molar content of chiral comonomers (**CAE**) show similar thermal properties, one T_g and two different phase transitions: a chiral nematic phase (N^*) can be easily identified by the iridescent green reflection. The nature of the phase at lower temperature require a more detailed XRD analysis but POM observations suggest the presence of a smectic A phase. The thermal stability of the N^* phase is increased with the increase of the chiral comonomer until up to 70°C in Poly(**A6MA-co-CAE**)-7-(68:32) where it is the only stable phase as in the homopolymer Poly(**CAE**)-7 (Table 2).

It should be underlined that only a 2% amount of chiral count is enough to induce the N^* phase.

As expected the glass transition temperature (T_g) in the methacrylic polymers are higher than those of the acrylic derivatives. As an example we can compare Poly(**A6MA-co-CAE**)-7-(83:17) and Poly(**M6MA-co-CME**)-1-(81:19), and notice that the latter has an higher T_g of 35°C at similar molecular weights.

The homopolymer Poly(**CAE**)-7 has only a N^* phase as well as Poly(**CME**)-1 (Figure 6).

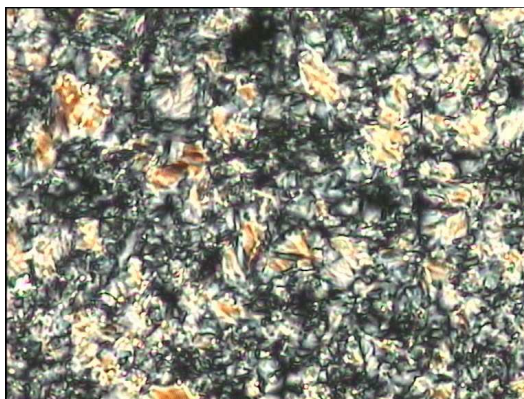


Figure 6: POM microphotograph, 32x magnification, of Poly(**CME**)-1 at 90°C after isotropization

Also the methacrylic comonomer **CME** can induce chiral nematic phases (N^*) in its copolymers, without affecting the glass transition. In order to have a big difference in the transition temperatures the molar fraction of chiral counts should be as high as 50%. In fact Poly(**M6MA-co-CME**)-1-(58:42) has a T_i 40°C higher than the other polymeric derivatives of the same series. However, Poly(**CME**)-1 has a T_i only 20°C lower than that reported in literature for the same derivatives with 10 times higher molecular weight ^[11].

The observed N^* phase (Figure 7) is characterized by a typical Bragg reflection at the same wavelength (477nm) of similar acrylic and methacrylic derivatives reported in literature ^[11] that have a λ_{max} at 475 and 482 nm respectively.

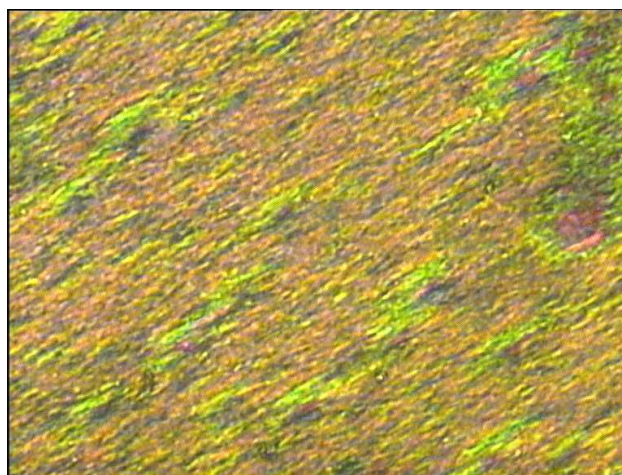


Figure 7. POM microphotograph, 32x magnification, of Poly(**M6MA-co-CME**)-1 at 80°C after isotropization

As an example in Figure 8 is reported the UV-Vis spectra in transmission of a 8,8 μm thick film of Poly(**M6MA-co-CME**)-1-(58:42) after an annealing of one hour at 100°C to develop the N^* phase. The spectra of the homopolymer Poly(**M6MA**)-1 has been subctrated

to highlight the position of the Bragg reflection. In this way a reflection band at 477, partially overlapping the $\pi \rightarrow \pi^*$ transition of the azoaromatic units can be clearly seen.

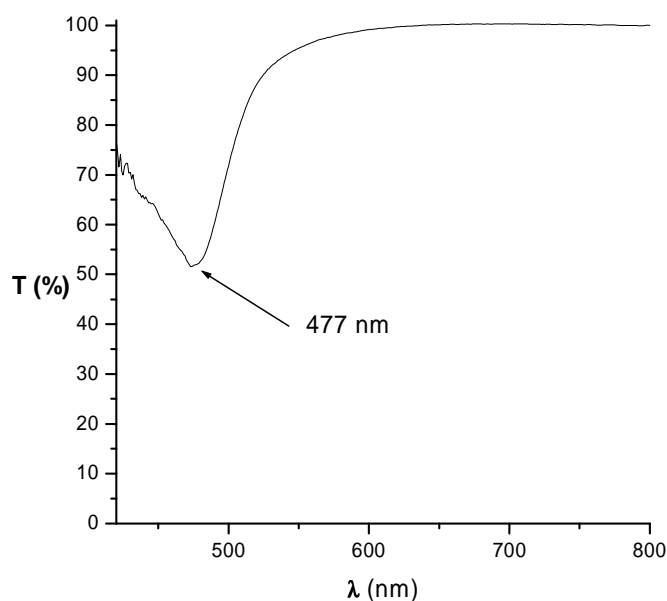


Figure 8. UV-Vis spectra of a 8,8 μm thick film of Poly(M6MA-co-CME)-1-(58:42) in N^* phase without the contribution of the azoaromatic counts

As explained above the wavelength of the Bragg reflection depends on the composition of the polymers and if is of the same wavelength of the visible light highly colored materials are produced.

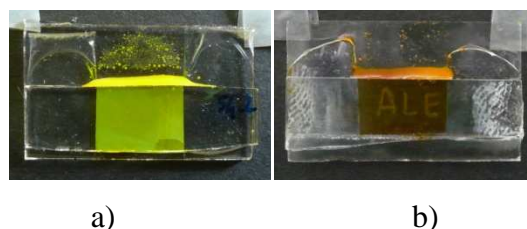


Figure 9. 8,8 μm film of Poli(M6MA-co-CME)-1-(58:42) in N^* mesophase (a) isotropic phase (b)

It is useful to show the visual difference of the aspect (from bright green to dull yellow) of the material due to isotropization (Figure 9 a and b). The isotropic state can be frozen by a rapid cooling of the system below the T_g .

The presence of the Bragg reflection gives a bright appearance to the material (Figure 9a) useful for the fabrication of a device able to evidence macroscopically the thermal history of the material itself.

An example of a smart label is depicted below: a 8,8 μm cell filled with Poly(M6MA-co-CME)-1-(58:42) is annealed to develop the N^* green phase (Figure 10a). The cell is then

heated above the clearing point and the Bragg reflection is lost (Figure 10b). The cell is then quenched below the T_g and the amorphous state is frozen (Figure 10c) and cannot relax in the thermodynamic favorite LC state until the temperature arise over the glass transition. (Figure 10d)

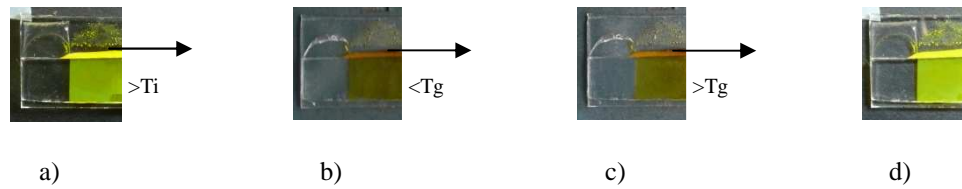


Figure 10. Smart label

UV-Vis analysis and photochromic properties

The UV-Vis spectra in chloroform solution of the monomers **A6MA** and **M6MA** and of their polymeric derivatives (Figure 11 and Table 3) exhibit in the region 250-600 nm two absorption bands. The first one, centered at 363 nm is related to the $\pi \rightarrow \pi^*$ transition of the azoaromatic chromophore, the second one, centered around 450 nm and partially overlapped to the former one, is related to the $n \rightarrow \pi^*$ transition of the azoaromatic chromophore ^[13].

As an example in Figure 11 is reported the UV-Vis spectra of Poly(**A6MA**)-7.

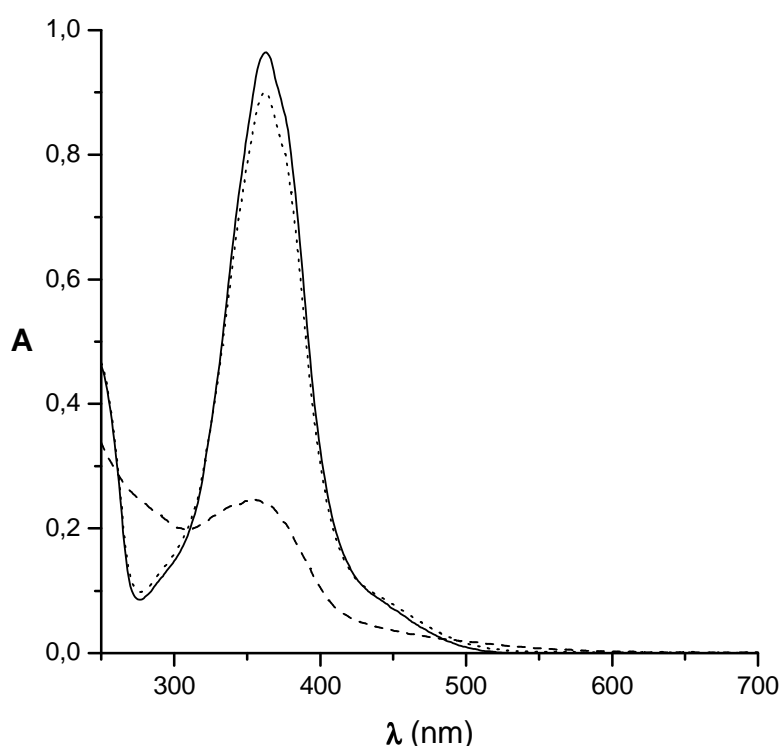


Figure 11. UV-Vis spectra of Poly(**A6MA**)-7 in CHCl_3 : (—) all *trans* isomers of the azoaromatic units, (---) after irradiation at 366 nm in order to reach a promote the *trans-cis* isomerization of azoaromatic chromophores, (⋯) after seven days in the dark at room temperature..

The values of the molar absorbance, collected in Table 1, does not evidence any hypochromic effect by passing from the monomers to the polymeric derivatives and suggesting that the chromophoric units in solution are essentially isolated and no dipolar interactions are present. No differences are observed either in the copolymers varying the molar fraction of **CME**.

Table 3. UV-Vis spectra in CHCl₃ solution

Sample	λ_{\max} ^{a)}	ϵ ^{b)}
A6MA	363	31700
Poly(A6MA)-7	362	31200
M6MA	362	29400
Poly(M6MA)-1	362	31200
Poly(M6MA-co-CME)-1-(95:5)	362	31000
Poly(M6MA-co-CME)-1-(81:19)	362	28600
Poly(M6MA-co-CME)-1-(58:42)	363	29300

a) wavelength of the maximum absorbance.

b) Molar absorptivity express in L·mol⁻¹·cm⁻¹ and calculated for azoaromatic repeating units.

The photochromic behavior of the synthesized compounds have been studied by irradiation in solution of Poly(**A6MA**)-7 and Poly(**M6MA**)-1 with UV light (366 nm) at 25°C for six hours to promote the *trans-cis* photoisomerization (Figure 11).

In particular a strong decrease and blueshift of the $\pi \rightarrow \pi^*$ band and an increase of the $n \rightarrow \pi^*$ band are observed (typical of the *cis* isomer). The backisomerization is achieved by leaving the samples for seven days in the dark, the *cis-trans* isomerization takes place and UV-Vis spectra of the *trans* isomer is restored (Figure 11).

The photochromic behavior has been tested also in the solid state, by irradiation of several 8,8 μm cells filled with the polymeric derivatives.

In these cases the macroscopic differences are not due to the different absorption spectra of the *trans* and *cis* azoaromatic isomers but are due to the photoinduced phase transition between LC and isotropic phases.

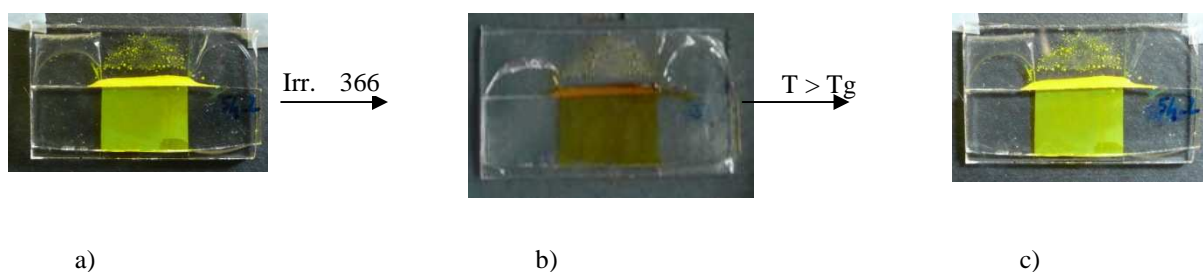


Figure 12. Smart label for the certification of thermal history

In Figure 12 is shown a LC cell in the N* green phase (a), the LC order and thus also the relative Bragg reflection can be suppressed by irradiation with UV light (366nm) below the T_g : as the population of *cis* isomers increase the LC phase is destroyed. When the UV irradiation is stopped the chromophores thermally back isomerize to the more stable *trans* isomer but the system is frozen in an amorphous methastable state and cannot relax to the chiral nematic phase until the temperature arise over the T_g .

When the temperature arises above the T_g the system is able to restore the pristine configuration and the information photoinscribed is lost.

In particular the same behavior observed thermally (Figure 10) can be easily induced only by irradiation with UV light at room temperature.

These materials therefore act as the desired smart label: they could be printed and photomodulated over the packaging of the product certifying that until this labels are yellow the temperature has always been below the threshold. Only when the temperature rises above the glass transition (that can be tuned precisely by design of the macromolecular structure) the system relax to the stable LC state with a big change in the visual aspect.

Chiroptical properties

Also a CD characterization of these materials has been done. In chloroform solution all the polymeric derivatives are CD silent and thus no chiral conformations are present.

The solid state is more interesting for a CD characterization. Thin films of 150-200 nm spin coated on quartz slide shows a particular CD behavior dependent on the thermal history of the samples.

In Figure 13 are reported the CD and UV-Vis spectra of a thin film of Poly(**M6MA-co-CME**). The CD spectra of the native film is CD silent but after a thermal annealing above the T_g strong CD bands arise. The former ones can be erased by irradiation with UV light (366 nm) in a fully reversible way by a subsequent heating above the T_g .

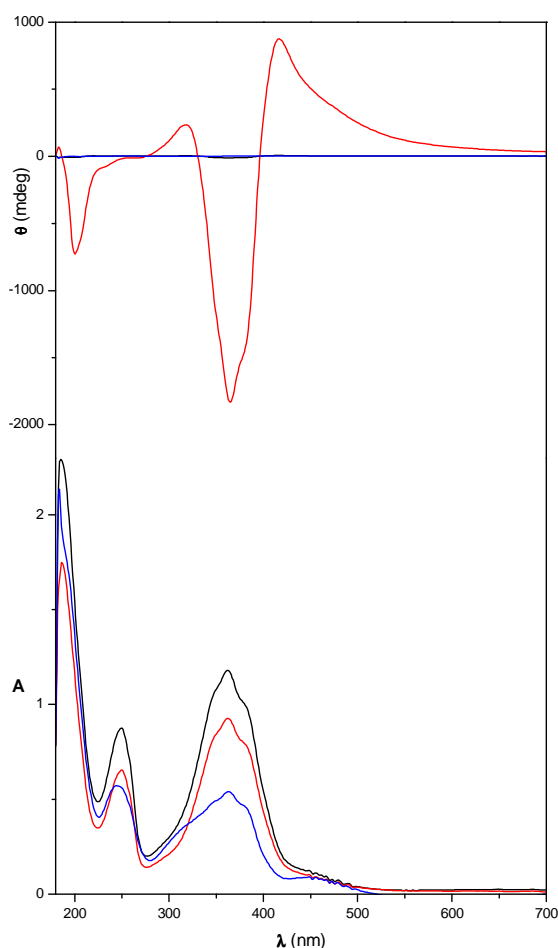


Figure 13. CD (up) and UV-Vis (down) spectra of a 200 nm thick film of Poly(**M6A-co-CME**)-1-(58:42) as casted film(—), after annealing at 100°C for 2 hours (—) and after irradiation at 366 nm for 4 hours (—)

In particular, in correspondence of the $\pi \rightarrow \pi^*$ electronic transition of the azoaromatic chromophore the presence of a positive CD band centered at 414 nm, a negative one at 364 nm (with a shoulder at 383 nm), a positive band at 319 nm and a negative band at 200 nm are observed.

It is well known that chromophoric aggregation influence the absorption of azoaromatic chromophores^[14], in this case (Figure 13) the chromophores can aggregate in the following modes:

- H aggregate with λ_{\max} around 300 nm
- Face-face dimers with $\lambda_{\max} = 340-350$ nm
- Isolated chromophores with $\lambda_{\max} = 363$ nm
- J aggregates with $\lambda_{\max} = 370-390$ nm

It is clear that a substantial variation in the aggregation in the LC and native and isotropic state occurs and are observed both in the CD and UV-Vis spectra.

This suggest that the chiral *co*-units can induce the aggregation of the azoaromatic units in ordinate chiral superstructure even in thin film, but this chiral induction observed in the annealed films is not due to a circular Bragg reflection, typical of chiral nematic phases, because of the small thickness of the film that is even thinner than the helix itself (around 480-500 nm).

In fact a strong circular reflection is observed only in the CD spectra of a thick films (Figure 14).

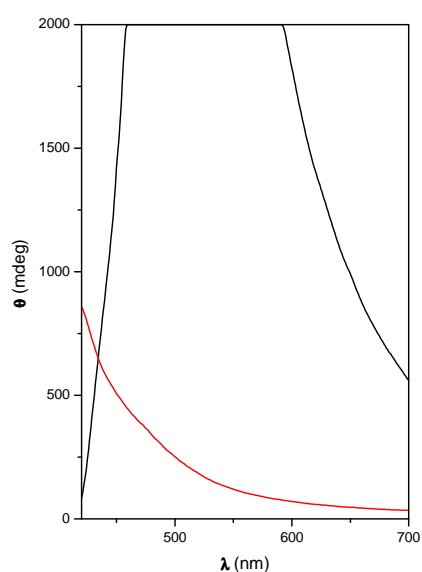


Figure 14. CD spectra of Poly(M6MA-co-CME)-1-(58:42) after annealing at 100°C of a film of 200 nm (—) and 8,8 micron (—).

In particular, a huge reflection band is present in the CD spectra of a thick film (8,8 μm) in correspondence of the selective reflection observed in the UV-Vis spectra due to the circular Bragg reflection of a chiral nematic phase, not present in the CD spectra of the 200 nm thin film (Figure 14).

These phenomena has been observed in literature ^[15-19] and described theoretically in cholesteric systems doped with different chiral units but in this case the optical activity is at least one order of magnitude higher. This suggests the presence of dichroic effects due to the formation of partial helix highly ordered even in thin film, with the axes perpendicular to the support. Anyway the presence of other chiral LC phases stabilized by the surface effect as a blue phases or similar cannot be excluded ^[20-24]

Anyway, for our knowledge, this is the first observation of strong CD effects in a chiral nematic polymeric system with a thickness lower than the helix pitch.

Finally, by irradiation at 366 nm the *trans-cis* isomerization is induced and the CD spectra become silent due to the destruction of the chiral aggregation as observed above.

Conclusion

A series of new polymers has been synthesized copolymerizing by ATRP mesogenic counts bringing an azoaromatic residue and a cholesteric chiral one.

These materials exhibit a chiral nematic phase and thus an intense Bragg reflection gives an iridescent and bright appearance to thick films of these derivatives. The photochromic properties of the azoaromatic residue can then be exploited to photoinduce below the glass transition an adiabatic isotropization of the material. The Bragg reflection is therefore erased and the new metastable isotropic state cannot relax to the chiral nematic phase until the temperature reaches a trigger value. Then the chiral nematic phase and thus the Bragg reflection are restored.

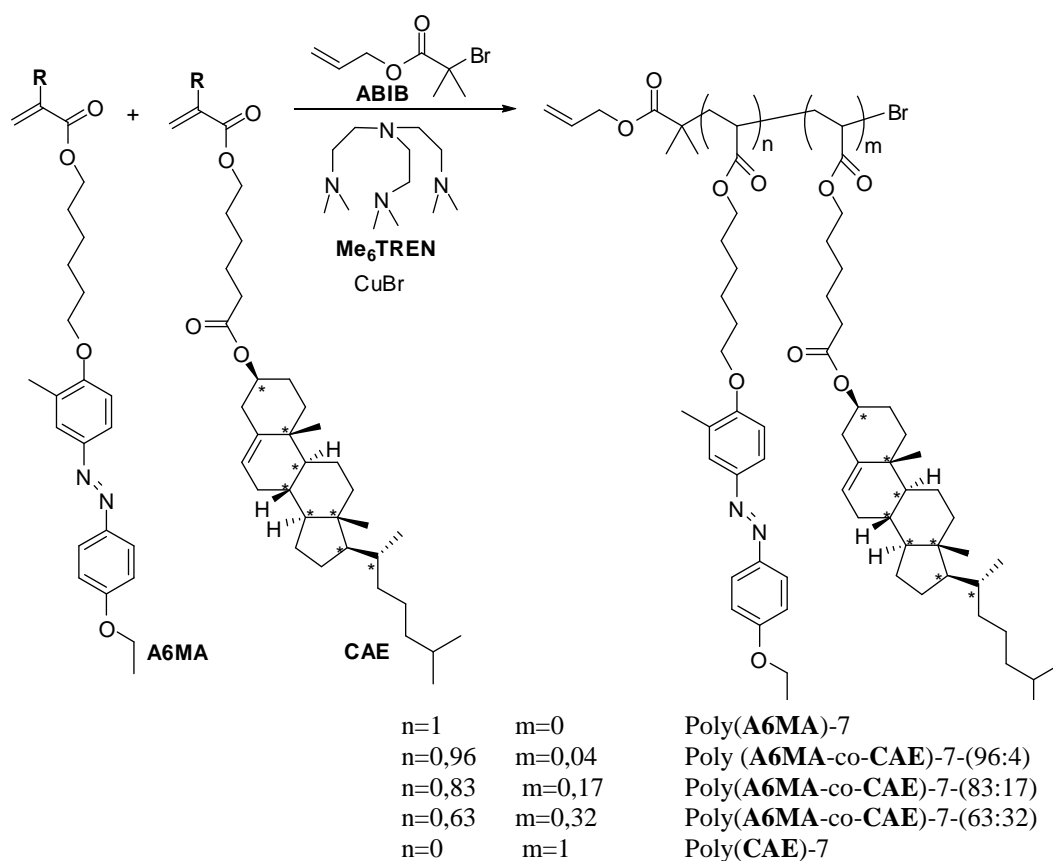
These material therefore act as smart label, that can certify that the temperature did not reach the trigger value after the irradiation with UV light.

Moreover due to the high control allowed by ATRP polymerization, these polymeric derivatives have tunable thermal characteristic that allows the fabrication of tailor made label for a huge variety of products.

Experimental part:

Synthesis of acrylic polymers

Homopolymeric and copolymeric derivatives of **A6MA** and **CAE** were synthesized by ATRP using as initiator allyl 2-bromo-2-methylpropionate (**ABiB**), CuBr as catalyst and tris[2-(dimethylamino)-ethyl]amine (**Me₆TREN**) as ligand. In all the polymerization molar ratio [monomer]: [initiator]: [CuBr]: [ligand] = 50: 1: 1: 1, dry anisole as solvent and a total monomer concentration of 0,24M have been used.



The polymerization procedure is as follow: the amount of reagent and solvent have been introduced under nitrogen flow in a vial and sealed. The oxygen have been removed with three freeze pump cycle and then CuBr have been introduced under vigorous nitrogen flow in the vial. Another freeze pump cycle had been then performed and the polymerization had been carried out at 80°C for 186 hours (7 days).

The obtained derivatives were purified from the residual monomer, CuBr and ligand by filtration on SiO₂ using CH₂Cl₂ as eluent in order to remove the residual monomer, then the product were eluted with a mixture CH₂Cl₂:CH₃OH 9:1 (v:v) to separate the polymeric derivatives. Finally the polymers were precipitated in cold hexane, except for Poly(CAE)-7 precipitated in methanol.

The final products after being dried under vacuum are characterized by FT-IR, ¹H-¹³C-NMR spectroscopy.

The more relevant data for the synthesis of these systems are collected in Table 4

Table 4. Relevant synthetic data of the acrylic polymers

Sample	A6MA mg (mmol)	CAE mg (mmol)	ABIB μl (mmol)	CuBr mg (mmol)	Me₆TREN μl (mmol)	anisole ml	Yield^{a)} [g (%)]
Poly(A6MA)-7	500 (1,22)	-	3,9 (2,44 10 ⁻²)	3,5 (2,44 10 ⁻²)	6,6 (2,44 10 ⁻²)	5	20
Poly(A6MA -co- CAE)-7- (96:4)	500 (1,22)	36 (6,40 10 ⁻²)	4,1 (2,57 10 ⁻²)	3,7 (2,57 10 ⁻²)	6,9 (2,57 10 ⁻²)	5,3	25
Poly(A6MA -co- CAE)-7- (83:17)	400 (9,75 10 ⁻¹)	135 (2,44 10 ⁻¹)	3,9 (2,44 10 ⁻²)	3,5 (2,44 10 ⁻²)	6,6, (2,44 10 ⁻²)	5	19
Poly(A6MA -co- CAE)-7- (63:32)	225 (5,48 10 ⁻¹)	304 (5,48 10 ⁻¹)	3,5 (2,19 10 ⁻²)	3,1 (2,19 10 ⁻²)	5,4 (2,19 10 ⁻²)	4,5	8
Poly(CAE)-7	-	500 (9,01 10 ⁻¹)	2,9 (1,80 10 ⁻²)	2,6 (1,80 10 ⁻²)	4,9 (1,80 10 ⁻²)	3,7	11
Poly(A6MA)-3-50:1:1:1	500 1,22	-	3,9 2,44 10 ⁻²	3,5 2,44 10 ⁻²	6,6 2,44 10 ⁻²	5	22
Poly(A6MA)-3-100:1:1:1	1000 2,44	-	3,9 2,44 10 ⁻²	3,5 2,44 10 ⁻²	6,6 2,44 10 ⁻²	5	20

a) Calculated as (g of polymer/g of monomer) * 100.

b) The two homopolymeric derivatives Poly(**A6MA**)-3-(50:1:1:1) and Poly(**A6MA**)-3-(100:1:1:1) were synthesized in order to define the better polymerization condition

Poly(**A6MA**)-3-(50:1:1:1): [**A6MA**]=0,24, [**A6MA**]:[**ABIB**]:[**CuBr**]:[**Me₆TREN**]=50:1:1:1, 72 ore a 70°C.

Poly(**A6MA**)-3-(100:1:1:1): [**A6MA**]=0,48, [**A6MA**]:[**ABIB**]:[**CuBr**]:[**Me₆TREN**]=100:1:1:1, 72 ore a 70°C.

As an example are reported the characterization of Poly(**A6MA**)-7, Poly(**CAE**)-7 and Poly(**A6MA-co-CAE**)-7-(83:17).

Poly(**A6MA**)-7

FT-IR (ATR) (cm^{-1}): 3069 (ν_{CH} arom.), 2935 e 2860 (ν_{CH} aliph.), 1727 ($\nu_{\text{C=O}}$ ester), 1598 and 1580 ($\nu_{\text{C=C}}$ arom.), 1392 (δ_{CH} CH_3), 1142 and 1106 (ν_{CO} ether), 840 and 829 (δ_{CH} aroma. 1,4 disubst.), 730 (δ_{CH} arom. 1, 3, 4 trisubst.).

$^1\text{H-NMR}$ (CDCl_3): 7.95-7.75 (2H, arom. 2'-H), 7.75-7.56 (2H, arom. 2-H), 7.06-6.85 (2H, arom. 3'-H), 6.85-6.68 (1H, arom. 3-H), 5.39-5.12 (2H, $\underline{\text{CH}_2}=\text{CH}$ ABiB), 4.52 (2H, $\text{CH}_2\text{-O}$ ABiB), 4.22-3.76 (6H, $\text{CH}_2\text{-O}$), 2.34-2.13 (3H, CH_3 arom.), 1.93-1.01 (8H, CH_2 alkyl spacer, 3H, $\underline{\text{CH}_3}\text{-CH}_2\text{-O}$, CH_2 and CH main chain).

$^{13}\text{C-NMR}$ (CDCl_3) (ppm): 175.2 (C=O), 161.2 and 159.7 (arom. 4-C e 4'-C), 147.4 and 146.8 (arom. 1-C and 1'-C), 127.8 (arom. 3-C(CH_3)), 124.6 and 123.8 (arom. 2-C, 2'-C), 115.0 (arom. 3'-C), 110.9 (arom. 3-C), 68.4 ($-\text{CH}_2\text{-}\underline{\text{CH}_2}\text{-O}$), 64.1 ($\text{CH}_3\text{-}\underline{\text{CH}_2}\text{-O}$), 63.2 ($\text{COO-}\underline{\text{CH}_2}$ -), 42.0 ($\text{CH}_2\text{-}\underline{\text{CH}}\text{-Br}$), 29.6, 26.3, 26.1, 25.9 (CH_2 aliph.), 16.7 (CH_3 arom.), 15.1 ($\underline{\text{CH}_3}\text{-CH}_2\text{-O}$).

Poly(**CAE**)-7

FT-IR (KBr) (cm^{-1}): 2938 e 2867 (ν_{CH} aliph.), 1733 ($\nu_{\text{C=O}}$ hester), 1384 (δ_{CH} CH_3), 1167 (ν_{CO} hester).

$^1\text{H-NMR}$ (CDCl_3) (δ in ppm dal TMS): 5.36 (1H, CH=), 4.68-4.49 (1H, CH-O and 2H, $\text{CH}_2\text{-O}$ ABiB), 4.16-3.88 (2H, $\text{CH}_2\text{-O}$), 2.38-2.20 (4H, $\text{CH}_2\text{-COO}$ and $\text{CH}_2\text{-CH=}$), 2.14-1.05 (32H, CH and CH_2 of cholesterol and alkyl spacer), 1.02 (3H, 19- CH_3), 0.91 (3H, 21- CH_3), 0.87 (6H, 26 and 27- CH_3), 0.68 (s, 3H, 18- CH_3).

$^{13}\text{C-NMR}$ (CDCl_3) (ppm): 173.0 (C=O), 140.0 (5-C), 123.0 (6-C), 74.1 (3-C), 64.5 ($\text{COO-}\underline{\text{CH}_2}$), 57.1 and 56.5 (12-C and 9-C), 50.4 (16-C), 42.0 ($\text{CH}_2\text{-}\underline{\text{CH}}\text{-Br}$), 42.7 (13-C), 40.1-12.2 (CH_2 and CH alkylic spacer and cholesterol, $-\text{CH}_3$ cholesterol).

Poly(**A6MA-co-CAE**)-7-(83:17)

FT-IR (ATR) (cm^{-1}): 3062 (ν_{CH} arom.), 2931 and 2863 (ν_{CH} aliph.), 1728 ($\nu_{\text{C=O}}$ hester), 1596 and 1578 ($\nu_{\text{C=C}}$ arom.), 1383 (δ_{CH} CH_3), 1150 and 1107 (ν_{CO} ether) 840 and 829 (δ_{CH} aroma. 1,4 disubst.), 728 (δ_{CH} arom. 1, 3, 4 trisubst.).

$^1\text{H-NMR}$ (CDCl_3): 7.90-7.76 (2H, arom. 2'-H), 7.76-7.58 (2H, arom. 2-H), 7.83-6.69 (2H, arom. 3'-H, 1H, arom. 3-H), 5.31 (1H, CH= cholesterol), 5.19 (2H, $\underline{\text{CH}_2}=\text{CH}$ ABiB), 4.66-4.47 (1H, CH-O , 2H, $\text{CH}_2\text{-O}$ ABiB), 4.25-3.82 (6H, $\text{CH}_2\text{-O}$), 2.52-2.15 (3H, CH_3 arom.), 2.07-0.49 (32H, CH and CH_2 of cholesterol and alkylic spacer **CAE**; 15H, $-\text{CH}_3$ of cholesterol; 11H, CH_2 , $\underline{\text{CH}_3}\text{-CH}_2\text{-O}$ of **A6MA**).

$^{13}\text{C-NMR}$ (CDCl_3) (ppm): 175.0 and 173.1 (C=O), 161.2 and 159.8 (arom. 4-C and 4'-C), 147.4 and 146.8 (arom. 1-C and 1'-C), 139.2 (5-C **CAE**), 127.8 (arom. 3-C **A6MA**), 124.6 and 123.8 (arom. 2-C, 2'-C), 115.0 (arom. 3'-C), 110.9 (arom 3-C(CH_3)), 74.1 (3-C **CAE**), 68.4 ($-\text{CH}_2\text{-}\underline{\text{CH}_2}\text{-O}$ **A6MA**), 64.1 ($\text{CH}_3\text{-}\underline{\text{CH}_2}\text{-O}$ **A6MA**), 63.3 ($\text{COO-}\underline{\text{CH}_2}\text{-}$ **A6MA**), 57.1 and 56.5 (12-C and 9-C **CAE**), 50.3 (16-C **CAE**), 42.0 ($\text{CH}_2\text{-}\underline{\text{CH}}\text{-Br}$), 42.6 (13-C **CAE**), 42.0 ($\text{CH}_2\text{-}\underline{\text{CH}}\text{-Br}$), 29.6, 26.3, 26.1, 25.9 (CH_2 aliph. **A6MA**), 16.7 (CH_3 arom. **A6MA**), 15.1 ($\underline{\text{CH}_3}\text{-CH}_2\text{-O}$ **A6MA**), 40.1-12.2 (CH_2 and CH cholesterol and alkylic spacer, CH_3 cholesterol).

In order to have more information also linear polymeric derivatives were synthesized by free radical polymerization using 2% w/w of AIBN as thermal initiator and dry THF as solvent in quantity for obtaining a 0,24 M concentration of monomer. The polymerization were carried for 72 hours at 60°C.

The procedure for the purification is the same as the derivatives synthesized by ATRP.

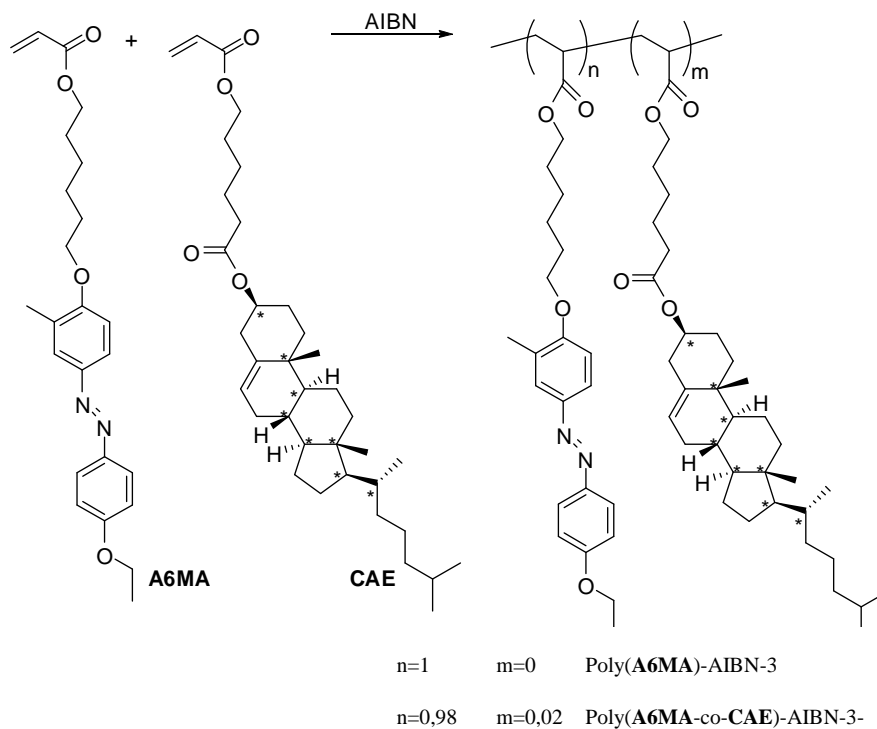


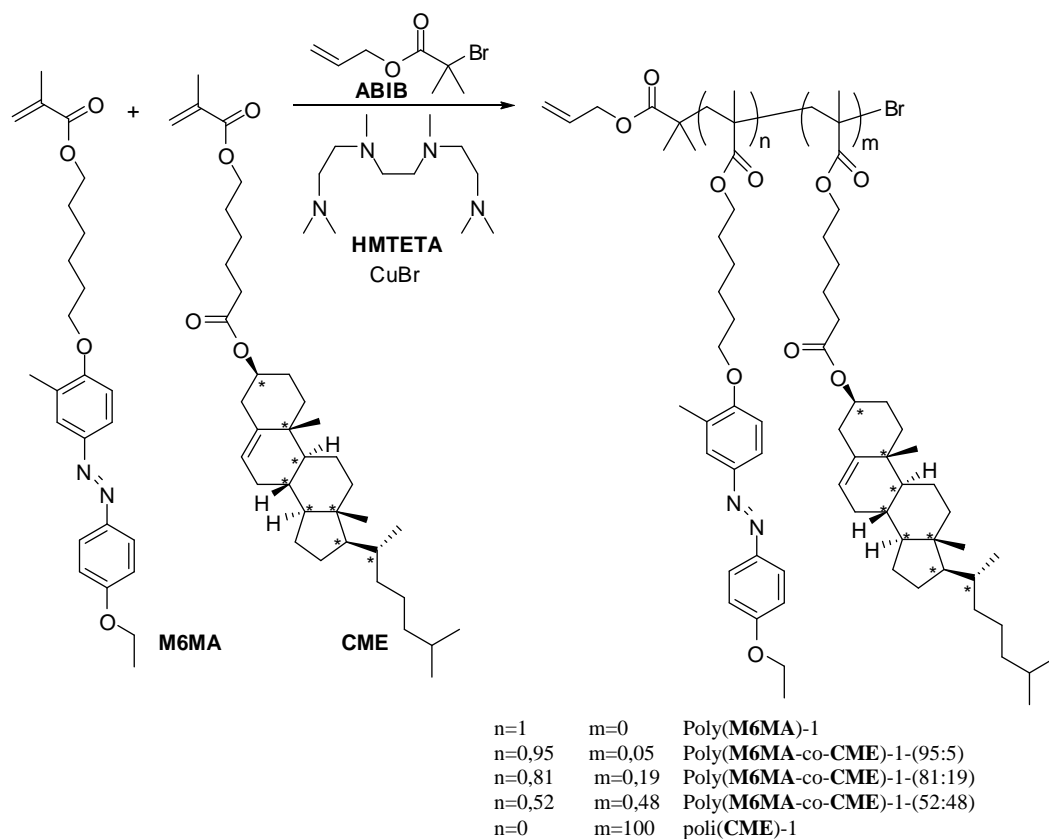
Table 5. Relevant synthetic data of the polymeric derivatives by FRP

Sample	A6MA	CAE	AIBN	THF	Yield ^{a)}
	mg	mg	mg	ml	[g (%)]
	(mmol)	(mmol)	(mmol)		
Poly(A6MA)-AIBN-3	500	-	10	5	24
	(1,22)	-			
Poly(A6MA-co-CAE)-AIBN-3-(98:2)	300	20	6,4	3,2	43
	(7,31 10^{-1})	(3,66 10^{-2})			
Poly(A6MA-co-CAE)-AIBN-3-(83:17)	300	81	7,6	3,8	24
	(7,31 10^{-1})	(1,46 10^{-2})			

a) Calculated as (g of polymer/g of monomer) * 100.

Synthesis of the methacrylic polymeric derivatives

Homopolymeric and copolymeric derivatives of **M6MA** and **CME** were synthesized by ATRP using as initiator allyl 2-bromo 2 methylpropionate (**ABiB**), CuBr as catalyst and 1,1,4,7,10,10-hexamethylen, triethylen, tetramine (**HMTETA**) as ligand. In all the polymerization the molar ratio [monomer]: [initiator]: [CuBr]: [ligand] = 50: 1: 1: 1, dry THF as solvent and a total monomer concentration of 0,18M were used.



The procedure of the synthesis and purification of these derivatives is the same as the acrylic derivatives except that the polymerization were carried for 24 hours at 60°C and the polymers were precipitated in cold methanol.

The final products after being dried under vacuum are characterized by FT-IR, ^1H - ^{13}C -NMR spectroscopy.

Table 6. Relevant synthetic data of methacrylic polymers

Sample	M6MA mg (mmol)	CME mg (mmol)	ABiB μ l (mmol)	CuBr mg (mmol)	HMTETA μ l (mmol)	THF ml	Yield ^{a)} [g (%)]
Poly(M6MA)-1	500 (1,18)	-	3,8 (2,36 10 ⁻²)	3,4 (2,36 10 ⁻²)	6,4 (2,36 10 ⁻²)	6,6	51
Poly(M6MA-co-CME)-1-(95:5)	500 (1,18)	34 (6,00 10 ⁻²)	4,0 (2,48 10 ⁻²)	3,6 (2,48 10 ⁻²)	6,8 (2,48 10 ⁻²)	6,9	49
Poly(M6MA-co-CME)-1-(81:19)	400 (9,42 10 ⁻¹)	134 (2,36 10 ⁻¹)	3,8 (2,36 10 ⁻²)	3,4 (2,36 10 ⁻²)	5,4 (2,36 10 ⁻²)	6,4	49
Poly(M6MA-co-CME)-1-(58:42)	250 (5,90 10 ⁻¹)	336 (5,90 10 ⁻¹)	3,8 (2,36 10 ⁻²)	3,4 (2,36 10 ⁻²)	6,4 (2,36 10 ⁻²)	6,6	36
Poly(CME)-1	-	500 (1,76 10 ⁻²)	2,8 (1,76 10 ⁻²)	2,5 (1,76 10 ⁻²)	4,8 (1,76 10 ⁻²)	4,9	25

a) Calculated as (g of polymer/g of monomer) * 100.

As an example are reported the characterization of Poly(**M6MA**)-1 and Poly(**M6MA-co-CME**)-1-(58:42)

Poly(**M6MA**)-1

FT-IR (ATR) (cm⁻¹): 3071 (ν_{CH} arom.), 2933 and 2858 (ν_{CH} aliph.), 1727 ($\nu_{\text{C=O}}$ hester), 1598 and 1580 ($\nu_{\text{C=C}}$ arom.), 1392 (δ_{CH} CH₃), 1142 and 1106 (ν_{CO} ether) 840 and 829 (δ_{CH} aroma. 1,4 disubst.), 728 (δ_{CH} arom. 1, 3, 4 trisubst.).

¹H-NMR (CDCl₃): 7.87-7.75 (2H, arom. 2'-H), 7.71-7.59 (2H, arom. 2-H), 7.03-6.84 (2H, arom. 3'-H), 6.84-6.66 (1H, arom 3-H), 5.34-5.11 (2H, CH₂=CH ABiB), 4.56-4.43 (CH₂-O ABiB), 4.26-3.70 (6H, CH₂-O), 2.38-2.15 (3H, CH₃ arom.), 2.13-0.70 (8H, CH₂ spacer, 3H, CH₃-CH₂, CH₂ main chain, 3H, CH₃ methacrylic).

¹³C-NMR (CDCl₃) (ppm): 177.8 (C=O), 161.1 and 159.6 (arom 4-C and 4'-C), 147.3 e 146.7 (arom 1-C and 1'-C), 127.6 (arom 3-C), 124.6 and 123.8 (arom 2-C, 2'-C), 114.9 (arom 3'-C), 110.8 (arom 3-C(CH₃)), 68.3 (-CH₂-CH₂-O), 65.2 (CH₃-CH₂-O), 64.0 (COO-CH₂-), 54.5 (54.5 (C(CH₃)Br), 45.2 (CH₂ main chain), 29.5, 28.4, 26.2, 26.1 (CH₂ aliph.), 19.1 (CH₃ main chain), 16.8 (CH₃ arom.), 15.1 (CH₃-CH₂-O).

Poly(**M6MA**-co-**CME**)-1-(58:42)

FT-IR (ATR) (cm^{-1}): 3060 (ν_{CH} arom.), 2928 and 2863 (ν_{CH} aliph.), 1728 ($\nu_{\text{C=O}}$ hester), 1596 and 1578 ($\nu_{\text{C=C}}$ arom.), 1380 (δ_{CH} CH_3), 1150 and 1107 (ν_{CO} ether) 840 and 829 (δ_{CH} aroma. 1,4 disubst.), 728 (δ_{CH} arom. 1, 3, 4 trisubst.).

$^1\text{H-NMR}$ (CDCl_3): 7.82 (2H, arom. 2'-H), 7.69 (2H, arom. 2-H), 6.94 (2H, arom. 3'-H), 6.70 (1H, arom. 5-H), 4.55 (1H, CH-O, 2H, $\text{CH}_2\text{-O}$ ABiB), 4.25-3.80 (6H, $\text{CH}_2\text{-O}$), 2.26 (3H, CH_3 arom.), 2.07-0.49 (32H, CH and CH_2 of cholesterol and alkylic spacer of **CME**; 6H, CH_3 methacrylic; 15H, $-\text{CH}_3$ of cholesterol; 11H, CH_2 , $\underline{\text{CH}_3}\text{-CH}_2\text{-O}$ of **M6MA**).

$^{13}\text{C-NMR}$ (CDCl_3) (ppm): 177.8 and 173.0 (C=O), 161.1 and 159.7 (arom. 4-C and 4'-C), 147.3 and 146.7 (arom. 1-C and 1'-C), 139.9 (5-C **CME**), 127.6 (arom. 3-C **M6MA**), 124.6 and 123.8 (arom. 2-C and 2'-C), 114.9 (arom. 3'-C), 110.8 (arom. 3-C(CH_3)), 74.1 (3-C **CME**), 68.4 ($-\text{CH}_2\text{-CH}_2\text{-O}$ **M6MA**), 64.1 ($\text{CH}_3\text{-CH}_2\text{-O}$ **M6MA**), 54.5 ($\underline{\text{C}}(\text{CH}_3)\text{Br}$), 56.9 and 56.5 (12-C and 9-C **CME**), 50.3 (16-C **CME**), 42.6 (13-C **CME**), 29.6, 26.3, 26.1, 25.9 (CH_2 aliph. **M6MA**), 19.1 (CH_3 main chain), 16.8 (CH_3 arom. **M6MA**), 15.1 ($\underline{\text{C}}\text{H}_3\text{-CH}_2\text{-O}$ **M6MA**), 40.1-12.2 (CH_2 alkylic spacer, CH_2 and CH aliph and CH_3 **CME**).

References

- [1] R. Eelkema, B. L. Feringa, *Org. Biomol. Chem* **2006**, 4.
- [2] V. Shibaev, A. Bobrovsky, N. Boiko, *Prog. Polym. Sci.* **2003**, 28, 729.
- [3] M. Brehmer, J. Lub, P. V. d. Vitte, *Adv. Mater.* **1998**, 10, 1874.
- [4] N. I. Boiko, V. P. Shibaev, M. Kozlovsky, *J. Polym. Sci., Part B: Polym. Phys.* **2005**, 43, 2352.
- [5] A. S. Angeloni, D. Caretti, M. Laus, E. Chiellini, G. Galli, *Journal of Polymer Science Part A: Polymer Chemistry* **2003**, 29 1865
- [6] P. J. Shannon, *Macromolecules* **1983**, 16, 1677.
- [7] J. Xia, K. Matyjaszewski, *Macromolecules* **1997**, 30, 7692.
- [8] K. Matyjaszewski, J. Xia, *Chem. Rev.* **2001**, 101, 2921.
- [9] L. Angiolini, T. Benelli, L. Giorgini, E. Salatelli, *Polymer* **2005**, 46, 2424.
- [10] S. Angeloni, D. Caretti, M. Laus, E. Chiellini, G. Galli, *Journal of Polymer Science Part A: Polymer Chemistry* **1991**, 29.
- [11] P. J. Shannon, *Macromolecules (Washington, DC, U. S.)* **1984**, 17, 1873.
- [12] F. Ciardelli, C. Carlini, R. Solaro, A. Altomare, O. Pieroni, J. L. Houben, A. Fissi, *Pure Appl. Chem.* **1984**, 56, 329.
- [13] H. H. Jaffé, M. Orchin, *Theory and application of ultraviolet spectroscopy*, Wiley, New York, **1962**.
- [14] I. Zebger, M. Rutloh, U. Hoffmann, J. Stumpe, H. W. Siesler, S. Hvilsted, *Macromolecules* **2003**, 36, 9373.
- [15] F. D. Saeva, J. J. Wysocki, *J. Am. Chem. Soc.* **1971**, 93, 5928.
- [16] I. Chabay, *Chem. Phys. Lett.* **1972**, 17, 283.
- [17] F. D. Saeva, *J. Am. Chem. Soc.* **1972**, 94, 5135.
- [18] E. Sackmann, J. Voss, *Chem. Phys. Lett.* **1972**, 14, 528.
- [19] S. Kurihara, S. Nomiyama, T. Nonaka, *Chem. Mater.* **2001**, 13, 1992.
- [20] H. Stegemeyer, H. Onusseit, *Makromol. Chem. Rapid Commun.* **1989**, 10, 571.
- [21] J. M. Gilli, M. Kamaye, P. Sixou, *J. Phys.* **1989**, 50, 2911.
- [22] J. M. Gilli, M. Kamaye, P. Sixou, *Mol. Cryst. Liq. Cryst.* **1991**, 199, 79.
- [23] H. Stegemeyer, T. Blumel, K. Hiltrop, H. Onusseit, F. Porsch, *Liq. Cryst.* **1986**, 1, 3.
- [24] E. Demikhov, H. Stegemeyer, *Liq. Cryst.* **1993**, 14, 1801.
- [25] P. J. Shannon, *Macromolecules* **1938** 16, 1667.

Chapter 4

Functionalization of surfaces with polymeric chains

Introduction

Beside the bulk properties of materials (e.g. mechanical and electrical properties) the properties of the surfaces are of big interest. In fact the possibility of tailoring the surface properties of a material leaving untouched the properties of the bulk can give the possibility for the development of a new generation of hybrid materials that can push the level a step further of the common technology.

As an example the choice of the material for fabrication of medical prosthesis is limited by the biocompatibility of the material itself. In this field a huge effort has been made in the past years (and still continues) for the development of biocompatible or biomimetic ceramic materials that can combine good mechanical properties, low specific weight and avoid rejection when implanted. The biocompatibility of a material is a issue of surface properties, as the contact between the body and the prosthesis pass through a surface.

With a suitable modification it is possible in principle to tailor the surface nature to have a biocompatible surface on the topmost of a non biocompatible material that possess the desired mechanical properties. No compromise anymore.

In literature are reported several examples of surface modification for tailoring the surface properties, in term of wettability or chemical nature with a huge impact on the properties of the material.

As example Meng Chen and coworkers ^[1] functionalized a mica surface with poly[2-(methacryloyloxy) ethyl phosphorylcholine]. When this material is immersed in an aqueous ambient, even under high pressure, the strong hydration of the zwitterionic polymeric layer can assure an ultra low friction of the surface, with μ values as low as 0.0004 at a pressure high as 7.5 Gpa, which is even higher of the pressure of the hips joint. This extreme

lubrication is by far the lowest ever reached in a human made object and even lower the friction coefficient of synovial joints of the human body at physiological pressure.

Another interesting example is the protein resistance (nonfouling) properties of a PEG coated surface. The use of protein resistant or “non-fouling” surfaces is of great interest for a variety of biomedical devices where the prevention of unwanted adsorption of proteins is critical to the performance of the device ^[2].

Examples of applications in which reducing protein adsorption can be beneficial range from in vitro diagnostics, where adventitious adsorption can compromise the sensitivity of the diagnostic, to in vivo applications, such as biomedical implants where protein adsorption can lead to an undesirable sequel of events that can include thrombus formation or fibrosis and scar tissue formation. Indeed, the importance of protein resistance in medicine and biotechnology spans length scales from the macroscopic to the molecular: modification of the macroscale surfaces of clinical diagnostics with protein-resistant polymers can significantly increase their analytical sensitivity, while modification of nanoscale drug-delivery vehicles, such as polymer micelles and liposomes, and the molecular surfaces of protein pharmaceuticals with this class of polymers can confer long in vivo circulation times and thereby improve their efficacy ^[3].

In this contest Chilkoti and coworkers ^[4] functionalized silicon oxide or gold surfaces with a dense layer poly[oligo(ethylene glycol)methacrylate] (POEGMA), a PEG-like monomer that can be polymerized by radical polymerization, in particular by ATRP. It is well known that PEG coated surface exhibit a good protein resistance, in particular using self assembled monolayers (SAMs). But comparing the performance of non coated, coated with a PEG SAM or a brush of POEGMA it can be seen that the protein absorption on the latter is by far the lowest. Chilkoti and coworker then made an analytical device using this technology pushing the detection limit two order of magnitude lower compared to the ones made with PEG coated materials.

A surface can be functionalized in several ways, by physical or chemical absorption of small molecules or polymeric chains.

There is a plethora of methods suitable for the functionalization of flat surfaces or nanoparticles. Among them the functionalization that involve the formation of covalent bonds between the surface and the functionalizing moiety are the most important.

These methods rely on the chemistry of the surface group of the material to be modified. As an example the functionalization of oxides, in particular of silicon oxide, is based mainly on the formation of a Si-O bond by the condensation of the surface silanolic group (Si-OH) and an alkoxy or chloro silane. In this way, with mild conditions, the formation of a well defined SAM can be achieved and new functionality can be addressed on the topmost of the surface by using tailor made silanes. For example fluorescent silica nanoparticles can be synthesized by condensation of a fluorescent chlorosilane and silica nanoparticles^[5].

The functionalization of gold surface instead proceeds via chemisorption of thiols onto the gold surface and the formation of a relatively stable Au-S bond^[6].

Also polymeric materials can be modified using the chemistry of the surface group, as an example PVC sheet can be modified^[7] by reaction of a chlorine atom with aminothiophenol resulting in an amino functionalized surface. Other reactions on the amino group can be used to tailor the surface composition. Zou and coworkers for example functionalized an amino surface with glycidol to have a surface rich in hydroxyl groups for a final esterification with an acyclic bromide.

In many cases the effect of modification with a small molecule is not effective due to the very small amount of functionality addressed on the surface. In many cases functionalization with polymeric chains is therefore preferred.

The functionalization of surface with polymeric chains can be obtained in two ways by condensation of the macromolecules onto the surface (grafting onto) or by the growth from suitable groups bounded onto the surface (grafting from). Both ways are suitable for the functionalization of a surface and high grafting densities (chains/nm²) can be achieved with both approaches, even if high densities can be achieved more easily with the “grafting” from method.

The huge development of controlled radical polymerization (CRP) and atom transfer radical polymerization (ATRP) has made possible to synthesize new types of materials, with well controlled molecular weight, morphology leading to materials exhibiting new interesting properties. In fact ATRP has been used for the synthesis of several types of materials once of difficult and expensive synthesis as block copolymers, star polymers and macromolecular brushes, a new class of materials with polymeric chains threaded by one end to the surface, that adopt a stretched conformation instead because of steric overcrowding.

The first step for the functionalization with macromolecules is the formation of a suitable SAM onto the surface. The nature of the SAM depends on the method to be employed.

Grafting onto

In this method the surface is modified with a SAM bearing a group that can be condensed easily with the terminal group of a telechelic polymer. Well defined end group are therefore required and the development of controlled radical polymerization (CRP) in particular ATRP and RAFT gave an enormous contribute for the simplicity of synthesis of well defined macromolecules ^[8]. A common example is the functionalization of a silicon surface with an azide and then the condensation via Huisgen reaction with an alkyne terminated polymeric chain.

With this approach anyway dense polymeric layers cannot be achieved as increasing the coverage of the surface the steric hindrance of the macromolecules tethered to the surface inhibits the ones in solution to approach the surface. Thus a big kinetic barrier can be found in this step. A detailed analysis shows how this barrier is related to the solvation energy of the macromolecules: a solvated polymeric chain in fact can approach easily the surface if this is clean. But when certain coverage is reached and the polymeric chains collapse into a “mushroom” structure covering the whole surface a macromolecules in solution should be desolvated, adsorbed on the surface and should diffuse into the polymeric layer until the terminal group can reach the surface, and finally react. This process requires a huge activation energy and therefore after a certain coverage the functionalization is inhibited. This limitation can be overcome by functionalization from a melt. In this case in fact no solvation energy is involved and the reaction can proceed until very high grafting densities are reached ^[9]. In this case the preferred reaction is a condensation between an hydroxide group and an epoxy ring.

Grafting from

Surface initiated ATRP in particular is a very promising technique for surface modification as provides a good control over the grafting densities, the thickness of the polymeric brush and the possibility of functionalization with all polymerizable monomers. Thus, synthesizing a tailored monomer bearing the target moieties a robust functional layer

can be easily synthesized. Anyway the classical SI ATRP has a drawback for the synthesis of brushes of functional and precious monomer in the needs of free initiator, with consequent loss of polymerizable monomer and the needs of further purification of the residual monomer for further synthesis. As a matter of fact in literature there are only few reports about the synthesis and the characterization of functional brushes. In particular almost no study on azobenzene containing brushes has been made.

It can be seen how the functionalization of surfaces with polymeric chains can lead to new applications. In this contest our attention was focused on systems suitable for the manipulation of liquids by external stimuli; in particular the photomanipulation of liquid crystals using azoaromatic brushes and the synthesis and characterization of adaptative surfaces, in which the wettability can be automatically changed by the different environmental conditions.

Functionalization with azoaromatic polymers: photocontrol and chirality

Introduction

Since the first report in the far 1988 by Ichimura ^[10] the photoalignment of liquid crystal displays by using a photochromic thin layer has been object of extensive studies.

This method for the photomanipulation of LC is know as surface-assisted LC photoalignment and is performed by fabricating LC cells using substrate plates, the surface of which is modified with photochromic molecules. Changes in chemical structures as well as orientational directions of photochromic molecules at a surface layer trigger the transformation of LC alignment. This sort of photoactive surface has been called *command surface*,^[11, 12] emphasizing the fact that the alignment of a large number of LC molecules is determined by a photochromic monolayer attached to a substrate surface.

In this kind of devices the orientation direction of the molecular axis (director) of LCs relative to a surface plane of a substrate is critically determined by the nature of the surface^[13]. There are two extremes of LC orientation: homeotropic alignment, where the LC director is perpendicular to a substrate surface, and planar one, which displays the LC director parallel to a substrate whereas the molecular direction is randomly distributed.

Homeotropic alignment is readily available by modifying the surface with amphiphilic molecules or long-chain alkyl silylating reagents ^[14]. On the other hand, a typical method to yield a homogeneous (unidirectionally parallel) alignment is based on the rubbing treatment of a polymer thin film covering a substrate.

When a substrate surface is modified with photochromic molecules to alter the chemical structures and molecular orientation of the uppermost surface (command surface) in molecular levels, the alignment of nematic LC is controlled reversibly by alternate irradiation^[11, 12].

There are four modes of the LC alignment controlled by command surfaces, as illustrated in Figure 1. The first one called 'out-of-plane alignment' photocontrol involves the reversible alignment change between homeotropic and planar modes. When UV actinic light is linearly polarized to lead to the polarization photochromism of azobenzenes on surfaces, a planar alignment becomes uniaxial to give a homogeneous alignment which reverses to the

homeotropic alignment due to the backward isomerization. Slantwise exposure with nonpolarized UV light also gives rise to a homogeneous alignment^[15]. This is the second type. The third one is referred to as the ‘in-plane alignment’ photocontrol which has been achieved by irradiation with linearly polarized light for photochromic reactions of surface molecules. The fourth consists of the control of tilt angles of an LC director by an appropriate choice of photoactive molecules at the uppermost surfaces, which is subjected to slantwise photoirradiation.

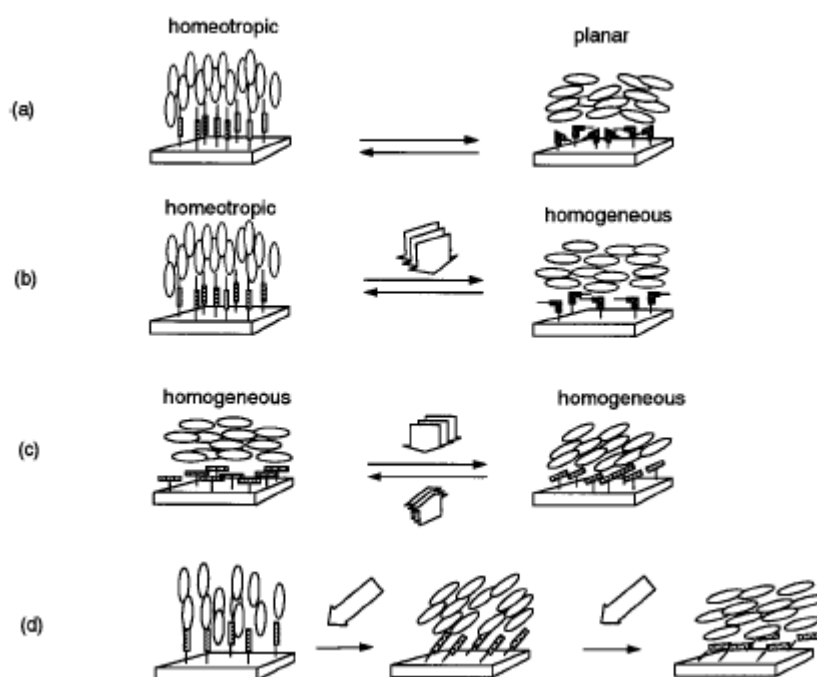


Figure 1: Illustrative representation of surface-assisted photoalignment control of LC molecules triggered by photochromic molecules tethered to a substrate surface. (a) Out-of-plane LC photoalignment between homeotropic and planar modes triggered by *trans-cis* photoisomerization of photochromic surface molecules upon alternate irradiation with nonpolarized light UV and visible light. (b) Out-of-plane LC photoalignment between homeotropic and homogeneous modes triggered by alternate irradiation with linearly polarized UV light and nonpolarized light. (c) In-plane photoalignment by irradiation with linearly polarized light. (d) Tilt-angle generation with slantwise photoirradiation.

In this work we are focused our attention on the mechanism c), namely in-plane homogeneous to homogeneous photoreorientation.

The photochromic layer can be of various nature but the most used photochromic groups are azobenzenes^[11, 12], benzospiropyranes^[16], stilbenes^[17] and cinnamates^[18]. For example, the switch between the neutral spiroopyrane and the charged merocyanine group induce an homeotropic alignment of the nematic director and the possibility of the switch between homeotropic and planar alignment of the nematic phase in the illuminated zones of the display.

Among all of these photochromic units the azobenzene are the most promising ones for the realization of such a device because of their good thermal and photochemical stability and thus the possibility to perform several cycles of irradiation without too high fatigue.

Even if the azobenzene moiety is quite stable this technology did not develop due to the low stability of the photochromic layer. In fact in literature two major deposition techniques are used. The first is the chemisorptions of reactive photochromic molecule for the synthesis of a monolayer of azoaromatic molecules. This technique lead to a well defined layer but has several drawbacks as the extreme fragility of the monolayer and the high control over the reaction condition for obtaining monolayer of the same density. Moreover also the photostability of a monolayer is not good enough: in fact after several cycles some azobenzene molecules can be degraded leading to a “dead” area. Is possible to fabricate a command surface also by spin coating of a thin (few tens of nanometers) film of an azobenzene containing polymer ^[19], in this case the fabrication is extremely simple and cheap, the film is less fragile respect to the chemisorbed monolayer and no photo degradation is observed even after many cycles of irradiation due to the high content of azobenzene. Anyway other problems arise: the presence of topological defect (e.g disclination) in the liquid crystal and the dewetting of the casted polymer for partial dissolution of the polymer in the nematic media ^[19].

As a matter of fact it was observed that the uniaxial orientation of the mesophase fades away gradually even in the dark, however. This probably arises from the permeation of low molecular weight LC molecules into the polymer film to relax the photoriented state of the azobenzene moiety. This suggests that the combination of LCs with azobenzene polymers plays an essential role in the persistence of the photoinduced in-plane alignment of LCs.

In connection with the elucidation of the working mechanism of the in-plane photoalignment controlled by linearly polarized light irradiation, the experimental results are summarized as follows:

(1) the in-plane LC photoalignment emerges upon irradiation of photochromic residues localized at the uppermost surfaces with linearly polarized light as a result of the photoreorientation of the photochromic moieties to give optical anisotropy, which is transferred to nematic LC layers.

(2) photochromic moieties capable of performing the in-plane photoalignment include azobenzene, stilbene, cinnamate, and spiropyran.

(3) larger exposure doses of linearly polarized light are required for the photoreorientation of LC molecules after cell assembly, when compared with those needed for the generation of optical anisotropy of films of photochromic polymers in absence of an LC.

(4) the rate of photoreorientation of an LC assisted by photochromic monolayers attached to a silica plate through silylation is markedly enhanced by heating the LC cell at temperatures above T_{NI} of the LC.

(5) photoalignment behavior of an LC brought about by azobenzene polymer films is crucially influenced by the chemical structures of azobenzenes.

It is clear that for making this technology useful a robust photochromic layer should be made.

In a recent work Seki and coworker reported the first synthesis by ATRP of an mesogenic azopolymeric brush ^[20], showing a big difference in the molecular orientation between a spin coated film, with homeotropic orientation after annealing, and a polymeric brush in which the azobenzene moieties adopt an homogeneous alignment. In a further work Seki ^[21] shows how is possible to induce a high in-plane orientation of the azo groups after irradiation with linearly polarized light.

Here we are describing in detail a synthetic approach of polymeric brush of the monomer 4- ω -methacryloyloxy-hexyloxy-4'-ethoxyazobenzene ^[22] that avoid the use of free initiator, making possible an easy recycle of the non reacted monomer for further synthesis, and the high advantage of the use of these brushes for the fabrication of command surfaces. Anyway we believe that this approach to this new class of polymeric derivatives open a new way towards the realization of improved and more stable functional materials for all those areas where surface effects and thin layer of active materials are involved. In particular using tailored methacrylic or acrylic azoaromatic monomers brushes can be used for the development of improved optical memories or for the fabrication of plasmonic switches devices, just for mentioning a couple of areas, with a procedure that minimize the loss of monomer and decrease the number of the needed purifications.

Surface Initiated ATRP polymerizations (SI ATRP):

The SI polymerizations were carried out in absence of sacrificial initiator and adding a deactivator [Cu(II)] from the beginning. In this way is possible to perform a SI ATRP without using free initiator. This procedure, even if is more complicated, is preferable for avoiding loss of monomer. As a matter of fact in a common SI ATRP free initiator is required to reach the Cu(I)-Cu(II) equilibrium state, with the Cu(II) coming from some chain termination in the early stage of polymerization due to the persistent radical effect^[23]. If no free initiator is added all the growing chains from the surface will be killed before reaching the equilibrium. Therefore some free initiator is always added, with the consequent consumption of monomer due to the solution polymerization. If some Cu(II) is added in the proper ratio from the beginning this problem is avoided, and a well controlled SI ATRP can be performed with no free initiator^[24].

We have checked different conditions before finding the optimal experimental conditions. A first problem is the low solubility of our monomer in common organic solvent, and therefore concentration higher than 0.5 M cannot be achieved, this slows the reaction rate in comparison to the bulk polymerizations using low molecular weight monomers reported in literature^[24].

The conditions used for the polymerizations of M6A are reported in Table 1, the polymerizations have been carried on for different times in order to produce thicker layer of polymeric derivatives.

While the polymerizations in THF and THF/DMF seemed to be not well controlled (slow at the earlier stage and then terminated at longer polymerization times) a better control can be achieved using DMF as solvent (entry 5), even if the solubility of the monomer is lower. The low control over the layer thickness, controlled by ellipsometry and UV-Vis spectroscopy respectively on the Si wafer and the glass slide can be attributed to chain transfer due to the THF molecules. As a matter of fact the GPC analysis of the reaction mixture shows the presence of a highly dispersed polymer in solution ($\bar{M}_n=13000$, $\bar{M}_n/\bar{M}_w=1.6$, Figure 2). As no free initiator is added and the surfaces are well cleaned from the physically adsorbed initiator the presence of such polymeric derivatives is a clear indication of a chain transfer to the monomer or solvent.

Table 1. Conditions for the graft polymerizations

Entry	Solvent	Monomer concentration [mol/l]	M: CuBr: CuBr ₂ :L
1	THF	0.25	50: 1: 0.1: 2.2
2	THF	0.25	50: 1: 0.04: 2.2
3	THF: DMF = 1: 1	0.25	50: 1: 0.1: 2.2
4	THF: DMF = 1: 1	0.5	50: 1: 0.04: 2.2
5	DMF	0.5	50: 1: 0.1: 2.2

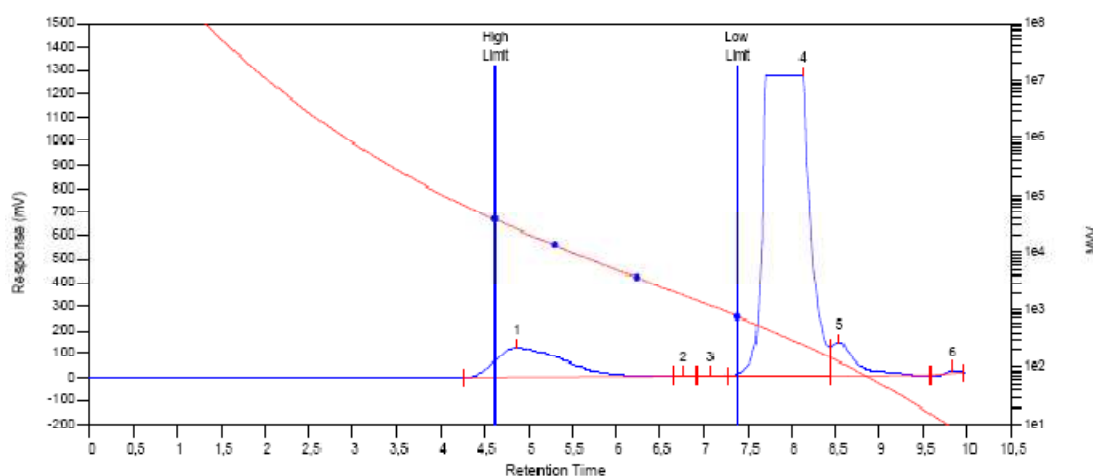


Figure 2: GPC chromatograph of the polydisperse polymer in solution

As can be seen in Figure 4, a good control over the thickness of the polymeric film can be achieved (first order kinetic) and a thicker layer can be obtained even with faster rate (is well known that polar systems as DMF can accelerate the rate of an ATRP due to partial dissociation of Cu-Br bond). In this way a well controlled polymerization can be obtained. The GPC analysis of the liquid phase after polymerization (entry 5) in this condition shows the total absence of polymeric derivatives and thus the absence of chain transfers reaction.

With the aim to study the effect of the grafting density and so the chain conformation we have synthesized several brushes with different grafting densities, using surfaces modified with mixtures of SBiB and TMCS as dummy initiator. Is well known that not all the active sites can start a polymerization because of the overcrowding of the surface, especially when bulky monomers are used. Thus we used molar ratio of SBiB and TMCS of 1:0 (full coverage with SBiB.), 1:1, 1:50, 1:200 and 1:1000. (Figure 3)

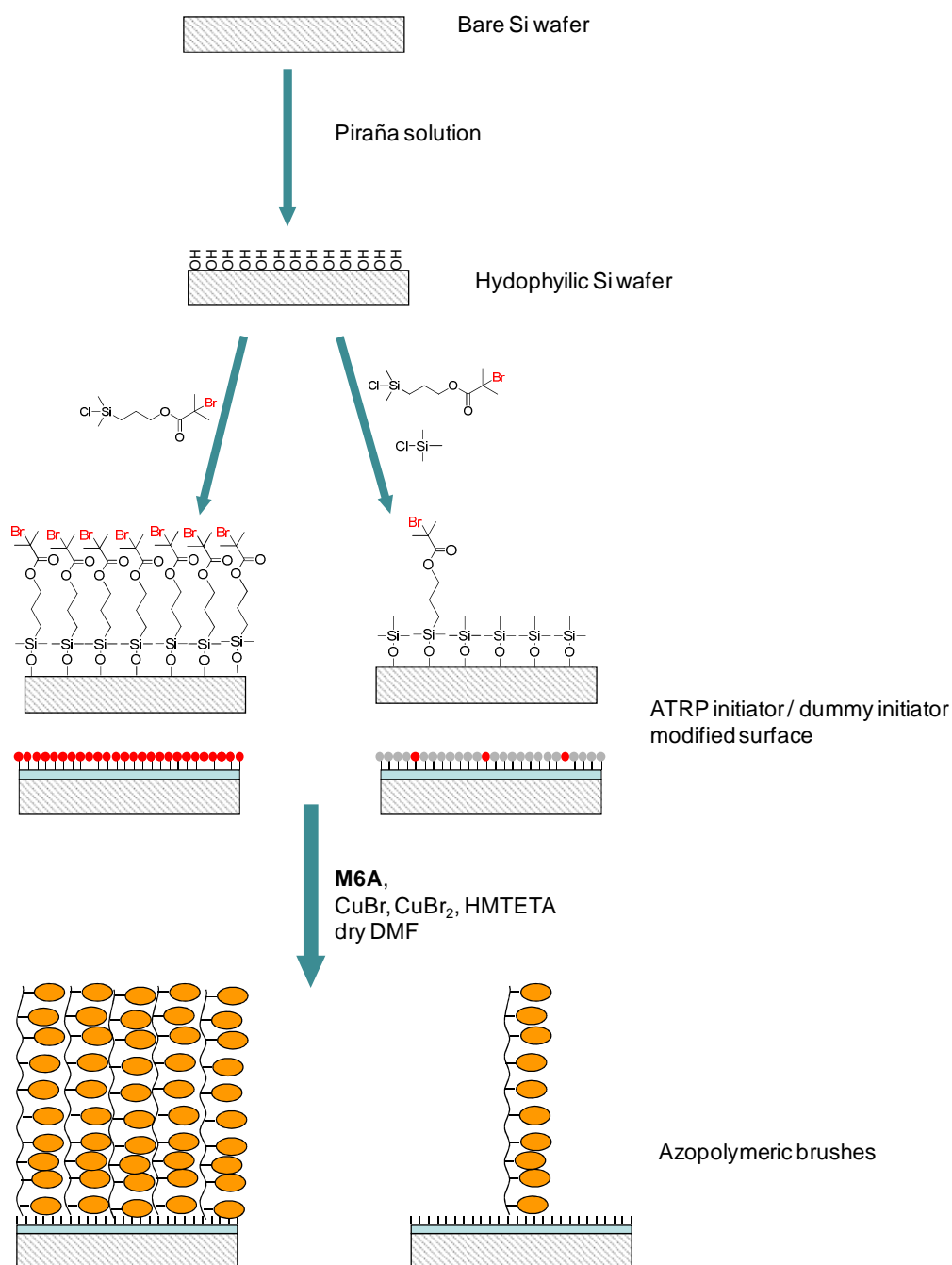


Figure 3: SI-ATRP of **M6A** from functionalized Si surfaces

All the tested conditions are reported in the following tables (Table 2, Table 3).

The evolution of the layer thickness observed by ellipsometry on the Si wafer and by UV-Vis on the glass slide are in perfect agreement as can be seen by the two plots of Figure 4 and Figure 5.

Table 2. Data relative to the synthesis of M6A brushes on Si substrates

SBIB : TMCS functionalization	Solvent	Monomer Concentration [M]	Molar ratios [M]:[CuBr]:[CuBr ₂]:[L]	Time (h)
1 : 0	DMF	0,5 M	50 : 1 : 0,1 : 2,2	4
1 : 0	DMF	0,5 M	50 : 1 : 0,1 : 2,2	17,5
1 : 0	DMF	0,5 M	50 : 1 : 0,1 : 2,2	24
1 : 0	THF	0,25M	50 : 1 : 0,1 : 2,2	23,5
1 : 0	THF	0,25M	50 : 1 : 0,1 : 2,2	48
1 : 0	THF	0,25M	50 : 1 : 0,1 : 2,2	89
1 : 0	THF	0,25M	50 : 1 : 0,1 : 2,2	118
1 : 50	THF	0,25M	50 : 1 : 0,1 : 2,2	23,5
1 : 50	THF	0,25M	50 : 1 : 0,1 : 2,2	48
1 : 50	THF	0,25M	50 : 1 : 0,1 : 2,2	89
1 : 50	THF	0,25M	50 : 1 : 0,1 : 2,2	118
1 : 200	THF	0,25M	50 : 1 : 0,1 : 2,2	23,5
1 : 200	THF	0,25M	50 : 1 : 0,1 : 2,2	48
1 : 200	THF	0,25M	50 : 1 : 0,1 : 2,2	89
1 : 200	THF	0,25M	50 : 1 : 0,1 : 2,2	118
1 : 500	THF	0,25M	50 : 1 : 0,1 : 2,2	23,5
1 : 500	THF	0,25M	50 : 1 : 0,1 : 2,2	48
1 : 500	THF	0,25M	50 : 1 : 0,1 : 2,2	89
1 : 500	THF	0,25M	50 : 1 : 0,1 : 2,2	118
1 : 1000	THF	0,25M	50 : 1 : 0,1 : 2,2	23,5
1 : 1000	THF	0,25M	50 : 1 : 0,1 : 2,2	48
1 : 1000	THF	0,25M	50 : 1 : 0,1 : 2,2	89
1 : 1000	THF	0,25M	50 : 1 : 0,1 : 2,2	118
1 : 0	DMF:THF=1:1	0,25M	50 : 1 : 0,1 : 2,2	24
1 : 0	DMF:THF=1:1	0,25M	50 : 1 : 0,1 : 2,2	48
1 : 0	DMF:THF=1:1	0,25M	50 : 1 : 0,1 : 2,2	160
1 : 1	DMF:THF=1:1	0,25M	50 : 1 : 0,1 : 2,2	24
1 : 1	DMF:THF=1:1	0,25M	50 : 1 : 0,1 : 2,2	48
1 : 1	DMF:THF=1:1	0,25M	50 : 1 : 0,1 : 2,2	160
1 : 1000	DMF:THF=1:1	0,25M	50 : 1 : 0,1 : 2,2	24
1 : 1000	DMF:THF=1:1	0,25M	50 : 1 : 0,1 : 2,2	48
1 : 1000	DMF:THF=1:1	0,25M	50 : 1 : 0,1 : 2,2	160
1 : 0	DMF:THF=1:1	0,25M	50 : 1 : 0,04 : 2,2	24
1 : 0	DMF:THF=1:1	0,25M	50 : 1 : 0,04 : 2,2	48
1 : 0	DMF:THF=1:1	0,25M	50 : 1 : 0,04 : 2,2	160
1 : 1	DMF:THF=1:1	0,25M	50 : 1 : 0,04 : 2,2	24
1 : 1	DMF:THF=1:1	0,25M	50 : 1 : 0,04 : 2,2	48
1 : 1	DMF:THF=1:1	0,25M	50 : 1 : 0,04 : 2,2	160
1 : 1000	DMF:THF=1:1	0,25M	50 : 1 : 0,04 : 2,2	24
1 : 1000	DMF:THF=1:1	0,25M	50 : 1 : 0,04 : 2,2	48
1 : 1000	DMF:THF=1:1	0,25M	50 : 1 : 0,04 : 2,2	160

Table 3. Data relative to the synthesis of M6A brushes on glass slides

SBIB : TMCS functionalization	Solvent	Monomer Concentration [M]	Molar ratios [M]:[CuBr]:[CuBr₂]:[L]	Time (h)
1 : 0	DMF	0,5M	50 : 1 : 0,1 : 2,2	4
1 : 0	DMF	0,5 M	50 : 1 : 0,1 : 2,2	17,5
1 : 0	DMF	0,5 M	50 : 1 : 0,1 : 2,2	24
1 : 0	THF	0,25M	50 : 1 : 0,1 : 2,2	23,5
1 : 0	THF	0,25M	50 : 1 : 0,1 : 2,2	48
1 : 0	THF	0,25M	50 : 1 : 0,1 : 2,2	89
1 : 0	THF	0,25M	50 : 1 : 0,1 : 2,2	118
1 : 50	THF	0,25M	50 : 1 : 0,1 : 2,2	23,5
1 : 50	THF	0,25M	50 : 1 : 0,1 : 2,2	48
1 : 50	THF	0,25M	50 : 1 : 0,1 : 2,2	89
1 : 50	THF	0,25M	50 : 1 : 0,1 : 2,2	118
1 : 0	DMF:THF=1:1	0,25M	50 : 1 : 0,1 : 2,2	24
1 : 0	DMF:THF=1:1	0,25M	50 : 1 : 0,1 : 2,2	48
1 : 0	DMF:THF=1:1	0,25M	50 : 1 : 0,1 : 2,2	160
1 : 1	DMF:THF=1:1	0,25M	50 : 1 : 0,1 : 2,2	24
1 : 1	DMF:THF=1:1	0,25M	50 : 1 : 0,1 : 2,2	48
1 : 1	DMF:THF=1:1	0,25M	50 : 1 : 0,1 : 2,2	160
1 : 0	DMF:THF=1:1	0,25M	50 : 1 : 0,04 : 2,2	24
1 : 0	DMF:THF=1:1	0,25M	50 : 1 : 0,04 : 2,2	48
1 : 0	DMF:THF=1:1	0,25M	50 : 1 : 0,04 : 2,2	160
1 : 1	DMF:THF=1:1	0,25M	50 : 1 : 0,04 : 2,2	24
1 : 1	DMF:THF=1:1	0,25M	50 : 1 : 0,04 : 2,2	48
1 : 1	DMF:THF=1:1	0,25M	50 : 1 : 0,04 : 2,2	160

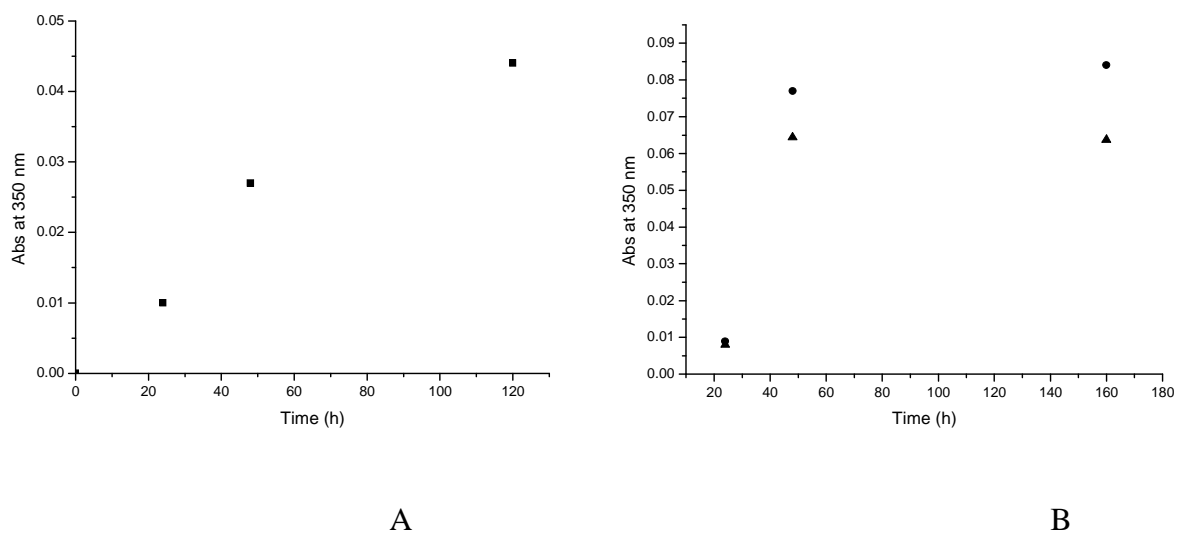


Figure 4: kinetic plot obtained by UV-Vis spectroscopy of the SI ATRP of the polymerization in THF (A), molar ratio M6A: CuBr: CuBr₂: HMTETA = 50:1:0.1:2.2 and in THF/DMF (B), M6A: CuBr: CuBr₂: HMTETA = 50:1:0.1:2.2 (▲), =50:1:0.04:2.2 (●).

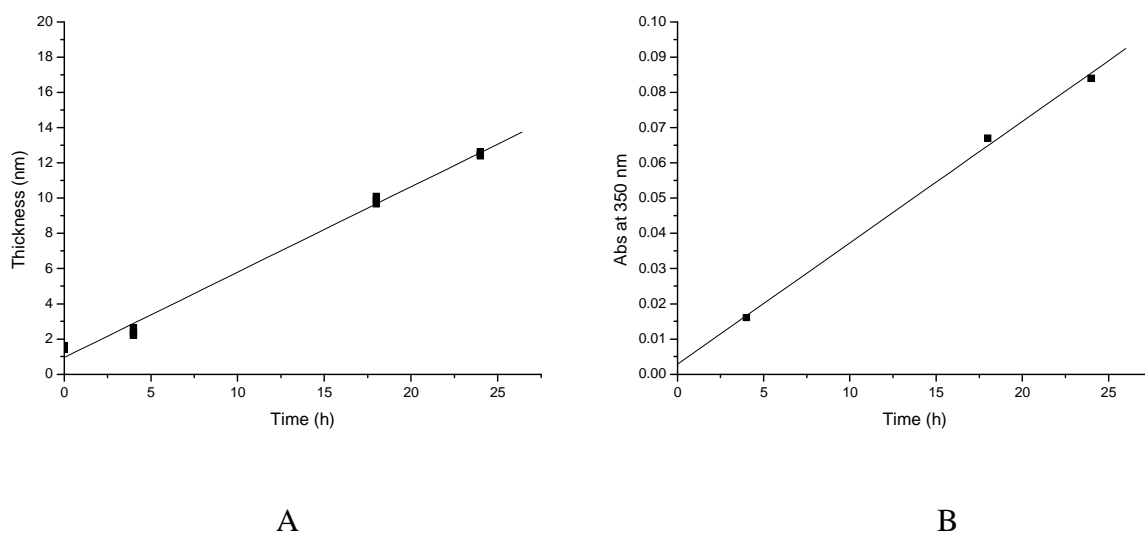


Figure 5. Kinetic plots of the SI ATRP of M6A in DMF (entry 5 in table 1) studied by ellipsometry on Si surfaces (A) and by UV-Vis spectroscopy on glass slide (B)

Also water contact angle has been checked after every surface reaction. Data are gathered in Table 4.

Table 4. Significant contact angles

Surface modification	Contact angle
Bare Si	1
SBiB	84
SBiB:TMCS 1:1000	84
PM6A full	76
PM6A lower grafting density	81

Even if it is known that mixed SAMs tend to segregate leading to the formation of islands our idea was to find a good composition to balance the surface overcrowding that lead to the formation of surface defects as bump and high roughness and the formation of segregated islands of polymers chains.

The growing of these less dense layers cannot be followed by ellipsometry as the produced layer is not flat, neither by UV-Vis spectroscopy, as the absorbance of the polymeric layer is getting lower and lower decreasing the concentration of active initiator.

So the growth of the polymeric layer and its morphology has been checked by AFM and SEM.

The surface with full coverage of SBiB is uniform and smooth as can be seen in Figure AFM A, moreover it was possible to find a defect in the functionalization, a small hole with no coverage. In this way it was possible to have a measure of the thickness by two independent methods and a perfect agreement was found between them, with a thickness by ellipsometry of 11.5 nm and by AFM of 11.0 nm.

The surfaces modified with a 1:1 mixture ratio after the polymerization gave uniform and smooth polymeric brushes over several microns, making it suitable for the fabrication of command surfaces.

Increasing the amount of TMCS to a ratio of 1:200 the topography of the surface changes (Figure 6) with the transition from a smooth and flat surface to a non uniform covered surface with the presence of spherical island of similar size (diameter of ~ 80 nm) regularly distributed onto the surface. The size of these islands is too big for an isolated chain,

so likely neighboring chains preferably self assemble into bigger domains rather than staying isolated on the surface .

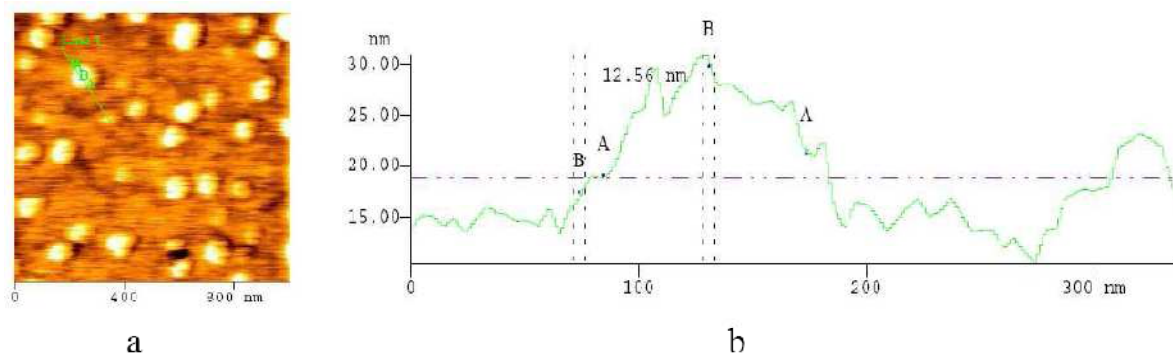


Figure 6: AFM analysis of a polymeric brush from a 1:200 SBiB: TMCS surface

Beside the AFM characterization also a SEM investigation was done, in fact due to the scale of the observed phenomenon (micrometers scale) only an AFM characterization is not totally significative.

As can be seen from the SEM images reported in Figure 7 the topography of the surface changes by changing the concentration of ATRP initiator (**SBiB**) on the surface. It can be seen how with little amount of ATRP initiator the coverage of the surface is not uniform, with islands of polymer of dimension of about 80-100 nm of diameter. Increasing the ratio SBiB/TMCS to 1:50 result in a smooth surface, with some little hole-like defects. If only ATRP initiator is used a total coverage of the surface is obtained, but due to the overcrowding of the surface some small bump-like defects are also present (Figure 7).

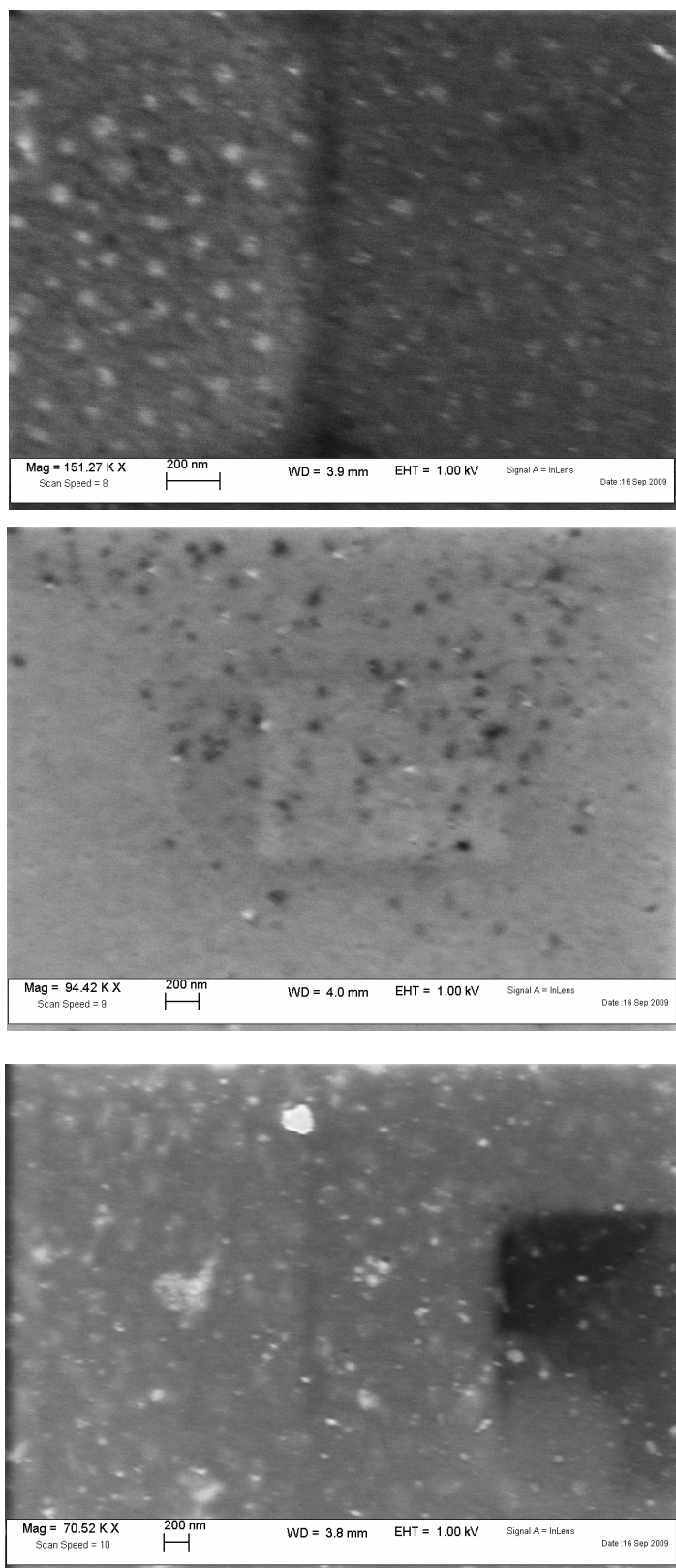


Figure 7: SEM images of M6A brushes on silica surface with different coverage of ATRP initiator after polymerization. SBiB: TMCS ratio (from top to down) = 1:1000; 1:50, 1:0

This behavior suggest that during the formation of the SAM the ATRP and dummy initiator tend to segregate forming islands over the surface due to their chemical incompatibility. This led to the formation, after polymerization, of isolated hill in the surfaces with lower coverage. On the other side if no dummy initiator is added a rough surfaces is obtained due to the overcrowding of the surface due to the high sterical hindrance of M6A brushes. So a smooth film can be obtained using a suitable ratio of SBiB and TMCS during the formation of the initiator SAM that lead to the formation of a monolayer of randomly distributed molecules or at least to enough small island to give a smooth surface after polymerization.

Photochromic and photomechanic properties: comparison between spin coated film and brush.

In order to verify the different photochromic behavior between a polymeric brush and a spin coated film of Poly(M6A) of the same absorbance a comparison of their photoisomerization kinetics has been done. Both the brushes and the spin coated film have an absorbance of 0.080 at their absorption maximum (350 nm). In Figure 8 are reported the kinetics of the isomerization under UV irradiation at 366 nm.

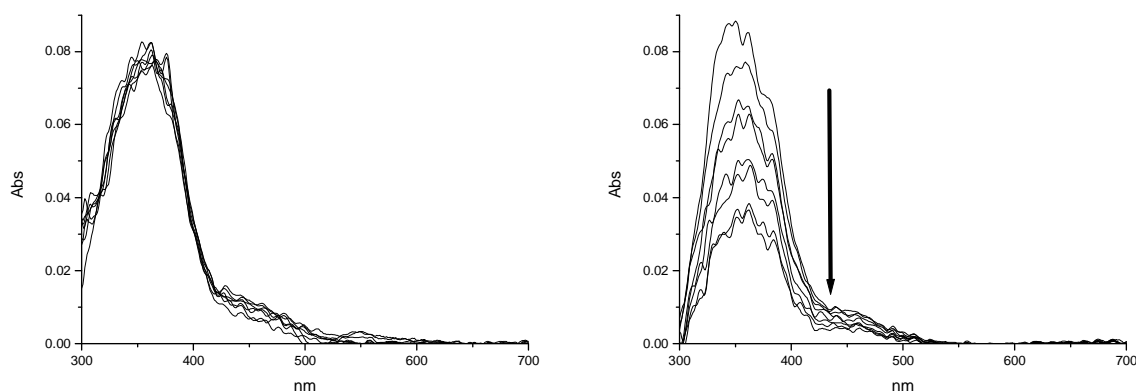


Figure 8: UV-Vis Isomerization kinetics of (a) Poly(M6A) brush and (b) spin coated film of Poly(M6A)

As can be seen by the UV-Vis spectra the spin coated film display a normal isomerization kinetic with the reaching of the photostationary state after 240 minutes, while the polymeric brush of the same thickness cannot isomerizes. This behavior can be explained by the high steric hindrance in the molecular brush that prevent the *trans-cis* isomerization while in the spin coated film there is enough free volume to allow the photoisomerization process.

Using more intense light source is possible to induce a *trans-cis* isomerization. In this case we have followed the kinetic of the photoexpansion of a M6A brush on a Si wafer compared with a spin coated film of the same thickness by ellipsometry. As previously described in chapter 2 ^[25] the photo expansion of a thin film of monodisperse azoaromatic polymer under UV irradiation proceeds relatively fast (few minutes to reach saturation) with a compression ratio of 20%.

Under the same illumination condition the contraction of the brush is one order of magnitude slower, taking up to 50 minutes to reach a steady state and show a little hysteresis

with no reaching of the pristine volume (Figure 9). Even if a model for this kind of phenomena is not yet developed is clear that the photoinduced properties involving the free volume and thus affected by the overcrowding of the brush regime are dramatically changed.

Anyway is worthy to notice that the amount of compression is quite large for such a small layer, reaching up to 12%, more that observed for spin coated thin films of polydisperse polymers, highlighting again the importance of the molecular distribution and mobility on this kind of phenomena. In conclusion the photoexpansion of the polymeric brushes seems to be inhibited and retarded by the low aviability of free volume in the polymeric layer and by the low mobility of the threaded chains.

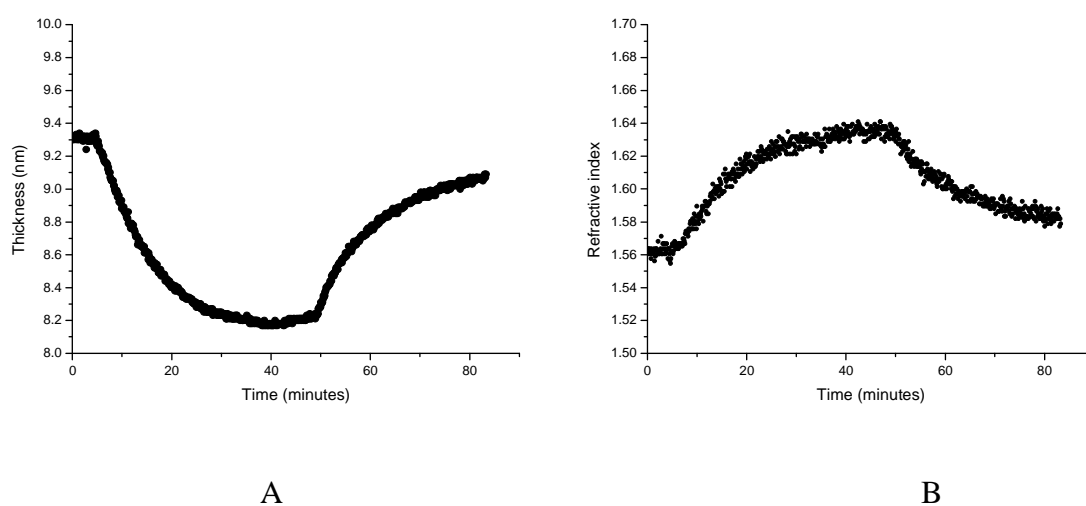


Figure 9: changing of thickness (A) and refractive index (B) of a Poly(M6A) brush under UV illumination (from 0 to 50 mins) and Vis (after 50 mins).

Chiroptical properties of brushes of chiral monomers

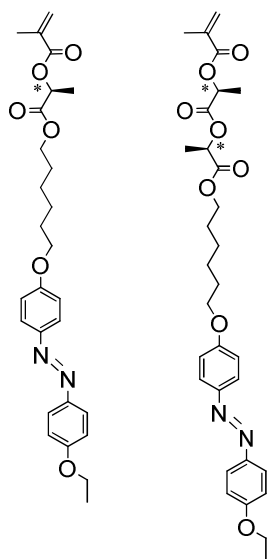
In order to investigate the different behavior between thin films obtained by spin coating (Chapter 3) and analogue polymeric brushes we synthesized brushes of (*S*)-**ML6A** and (*S*)-**MLL6A** (Figure 10) on glass slide and Si substrate, with the same synthetic procedure described above for the brushes of M6A, and their UV-Vis and CD properties were studied.

The experimental data are reported in Table 5 Data relative to the synthesis of (*S*)-ML6A and (*S*)-MLL6A brushes on Si substrates and glass slides

Table 5 Data relative to the synthesis of (*S*)-ML6A and (*S*)-MLL6A brushes on Si substrates and glass slides

SBIB : TMCS functionalization	Solvent	Monomer [M]	Molar ratios [M]:[CuBr]:[CuBr ₂]:[L]	Time (h)
1 : 0	DMF:THF=1:1	(<i>S</i>)-ML6A - 0,25M	50 : 1 : 0,1 : 2,2	24
1 : 0	DMF:THF=1:1	(<i>S</i>)-ML6A - 0,25M	50 : 1 : 0,1 : 2,2	48
1 : 1	DMF:THF=1:1	(<i>S</i>)-ML6A - 0,25M	50 : 1 : 0,1 : 2,2	24
1 : 1	DMF:THF=1:1	(<i>S</i>)-ML6A - 0,25M	50 : 1 : 0,1 : 2,2	48
1 : 0	DMF:THF=1:1	(<i>S</i>)-MLL6A - 0,25M	50 : 1 : 0,1 : 2,2	24
1 : 0	DMF:THF=1:1	(<i>S</i>)-MLL6A - 0,25M	50 : 1 : 0,1 : 2,2	48
1 : 1	DMF:THF=1:1	(<i>S</i>)-MLL6A - 0,25M	50 : 1 : 0,1 : 2,2	24
1 : 1	DMF:THF=1:1	(<i>S</i>)-MLL6A - 0,25M	50 : 1 : 0,1 : 2,2	48

The brushes were grown for 24 (Brush[(*S*)-**ML6A**-24 and Brush[(*S,S*)-**MLL6A**-24]) and 48 hours (Brush[(*S*)-**ML6A**-48 and Brush[(*S,S*)-**MLL6A**-48]) resulting in different thickness of the polymeric layer as can be seen by the UV-Vis spectra in Figure 11 and Figure 12.



(S)-ML6A (S,S)-MLL6A

Figure 10: Structures of the monomers (S)-ML6A and (S,S)-ML6A

UV-Vis and CD spectra have been recorded on the virgin samples, after a washing in dry and hot THF and after a thermal annealing. The washing in THF is used to erase the thermal history of the sample, in this way a solvation of the bounded chain should occur.

In order to allow a supramolecular organization of the polymeric chains and the chromophore moieties the brushes were heated under vacuum for two hours at 150°C, then the temperature was decreased to room temperature at a rate of 5°C/minute. By inspection with POM no birefringence was detected and all the samples seemed to be amorphous.

The brushes of (S)-**ML6A** are silent at CD both in the virgin state and after the thermal annealing. In Chapter 3 it was shown that thin spin coated film of the Poly[(S)-**ML6A**] possess a huge chirality. This different behavior between thin films and polymeric brushes emphasizes the influence of bounding one end of the polymeric chain to a substrate.

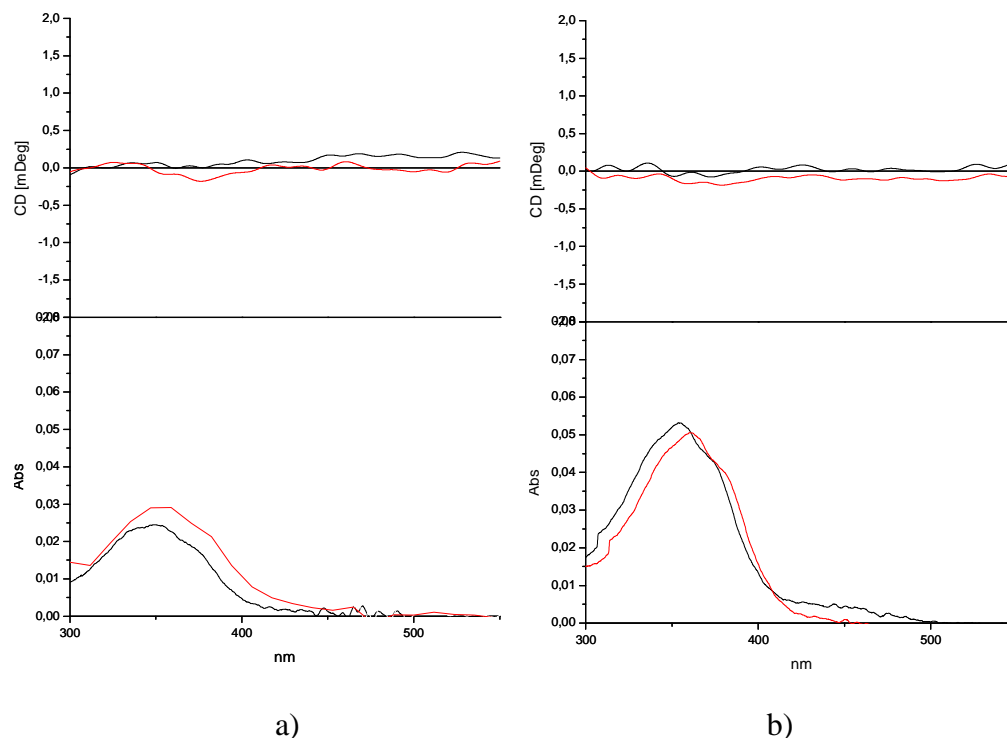


Figure 11. CD (up) and UV-Vis (down) spectra of brushes on glass slide of: a) (*S,S*)-**MLL6A-24** and b) (*S,S*)-**MLL6A-48** in the virgin state (—) and after a thermal annealing (—)

Instead the brushes of (*S,S*)-**MLL6A** have interesting CD properties, depending on the thickness of the layer and on their thermal history (Figure 12).

The CD spectrum of Brush[(*S,S*)-**MLL6A-24**] in the virgin state, shows a positive dichroic band corresponding to the $\pi \rightarrow \pi^*$ transition of the azoaromatic chromophore, centered at 360 nm whose intensities increase after thermal annealing.

Brush[(*S,S*)-**MLL6A-48**] instead shows intense CD bands in the virgin state whose intensities increase after thermal annealing, in particular positive CD couplets with crossover point at 345 nm, can be observed.

According to what reported in literature for similar linear derivatives^[26] and with the exciton rules^[27], a positive excitonic couplet is due to a right handed disposition of the chromophores. The observed high asymmetry is due to the overlapping of several dichroic bands: a positive CD couplet related to H-like aggregates overlapped to one or more positive signal associated to the electronic transitions of J aggregates, around 380 nm, and of the non aggregates chromophore at 360 nm^[28].

The shape of this excitonic CD couplet suggests the formation of ordered supramolecular aggregates in a mutual chiral geometry of one prevailing screw sense^[29].

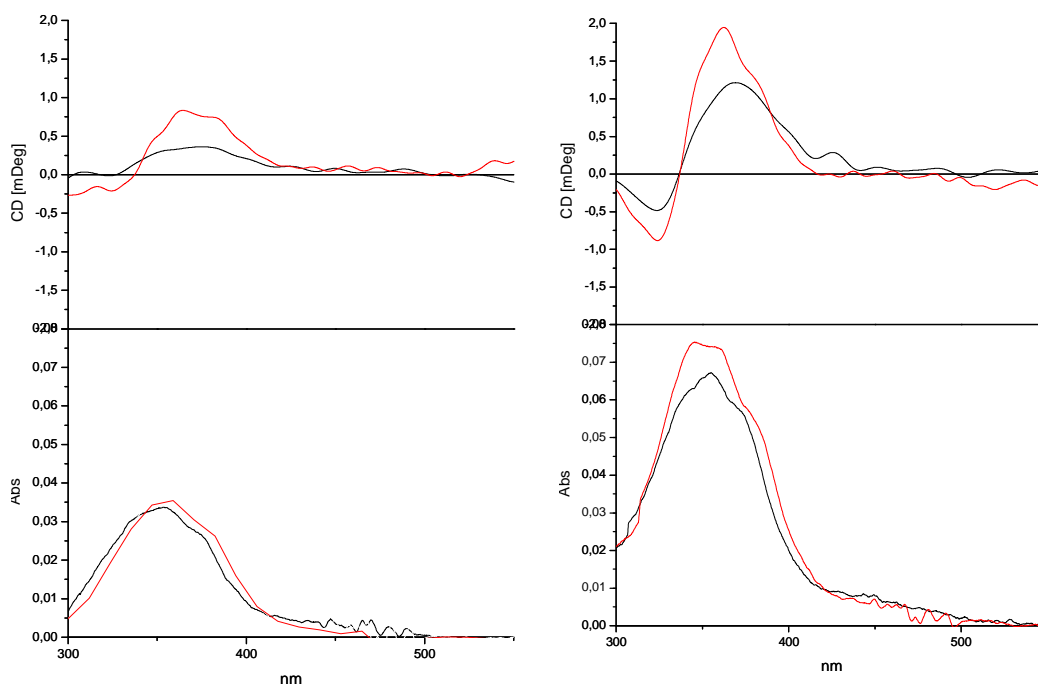


Figure 12. CD (up) and UV-Vis (down) of brushes of: a) (S) -MLL6A-24 and b) (S,S) -MLL6A-48 in the virgin state (—) and after a thermal annealing (—)

It is clear that (S,S) -MLL6A brushes can self assemble into chiral supramolecular structure leading to a high population of H aggregates. (Figure 13)

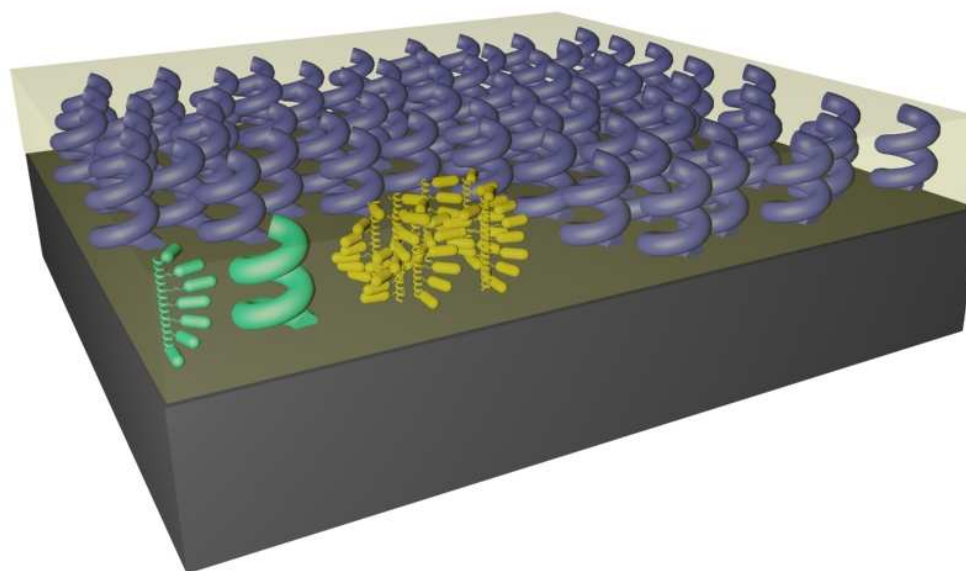


Figure 13. Idealization of chiral brushes

Command surfaces

The prepared polymeric brushes substrates of M6A have been employed for the fabrication of photo-switchable twisted/planar LC cells filled with the low molecular weight nematic pentyl-cyanobiphenyl (5CB). The cells have been produced using two different boundary glass walls, namely a reference and a command surface. The reference substrate has been coated with a polyimide layer, which has been mechanically rubbed in order to induce a strong homogeneous planar orientation, while the azo-polymer brush provides the photo-controllable command surface. The substrates have been assembled with a 10 μm spacer and filled with 5CB in its isotropic phase at 45°C. After slow cooling (0.5°C/min) to room temperature, the cells display a planar alignment along the direction imposed by the reference surface. Twisted or planar structures have been then achieved by aligning the azobenzene mesogens on the command surface, respectively perpendicularly or parallel to the rubbing direction of the reference substrate, by mean of polarized illumination with the 488nm Ar/Kr⁺ laser line. The images in Figure 14 report an example of micropatterning in a cell prepared in the twisted configuration by macroscopic polarized irradiation and then locally (20 μm) reverted to planar by focused illumination with perpendicular polarization.

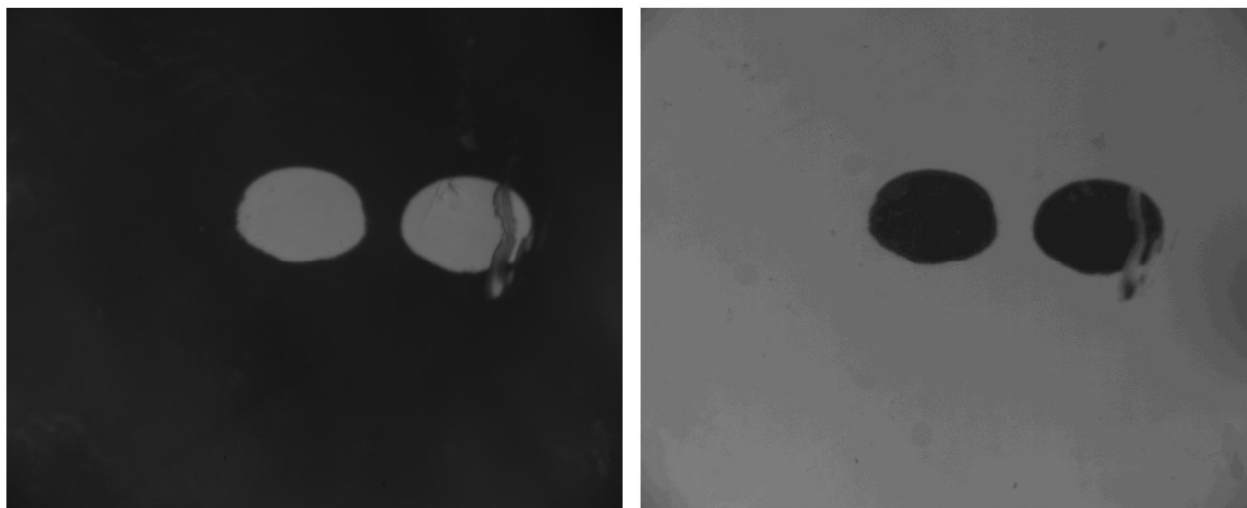


Figure 14: Polarizing microscopy images of 20 μm diameter planar structures in a twisted cell. Left and right images have been acquired respectively with parallel and crossed polarisers.

These brushes therefore act as command surfaces, the homogeneous layer of azoaromatic polymer can be easily manipulated by illumination with linearly polarized light and can induce a reorientation from a homogeneous (Figure 15a) to a twisted nematic alignment of a LC cell (Figure 15b).

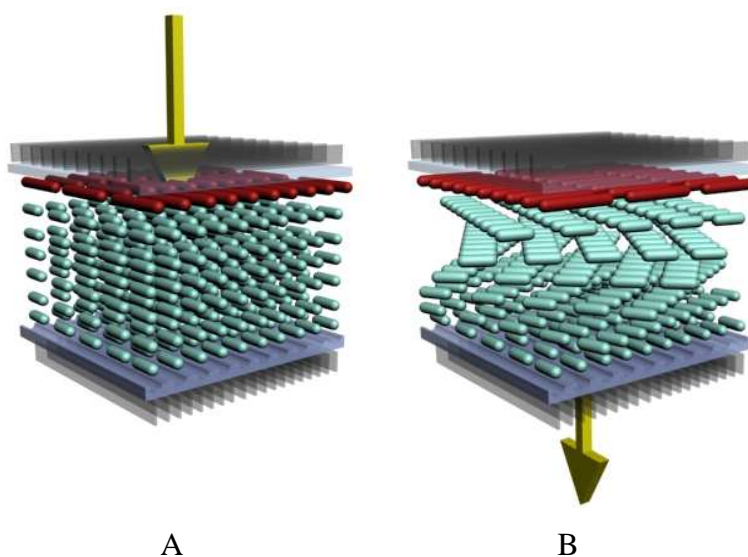


Figure 15: idealization of a LC cell driven by a photochromic command surface. A) linear alignment B) twisted nematic alignment.

We compared, through polarizing optical microscopy, the photoinduced structures thus obtained with those produced in the same experimental condition in cells where the command surface was provided by a spin coated layer of polymers synthesized from the same monomer. We assembled the cells employing azo-polymers of different molecular weight and geometry (linear and star) ^[26, 30] and the photo-induced patterning resulted not clearly visible under microscope. On the contrary the structures produced on azo polymeric brush cells display a high contrast (in the order of 1:100) and appear uniform either on macroscopic or microscopic scale, without LC defects like disclination lines.

We then proceeded with the Raman characterization of the LC order at the polymeric brush interface using the same confocal microscope employed for the patterning. The laser emission has been set to the 647nm line, outside the azobenzene absorption band, in order to avoid further photoinduced effects. The spectra have been collected in the back scattering geometry with a Jobin Yvon-Horiba T64000 spectrometer equipped with a liquid N₂ cooled CCD detector. The polarized micro-Raman study has been carried out measuring the 5CB peaks intensities as a function of the incident polarization and the analyzer directions along the two orthogonal axis V and H, respectively parallel and perpendicular to the nematic director. More specifically, the measurement consists of the acquisition in the peak intensity for the four possible geometries I_{VV} , I_{VH} , I_{HH} , and I_{HV} , where the first index refers to the incident polarization and the second to the analyzer direction.

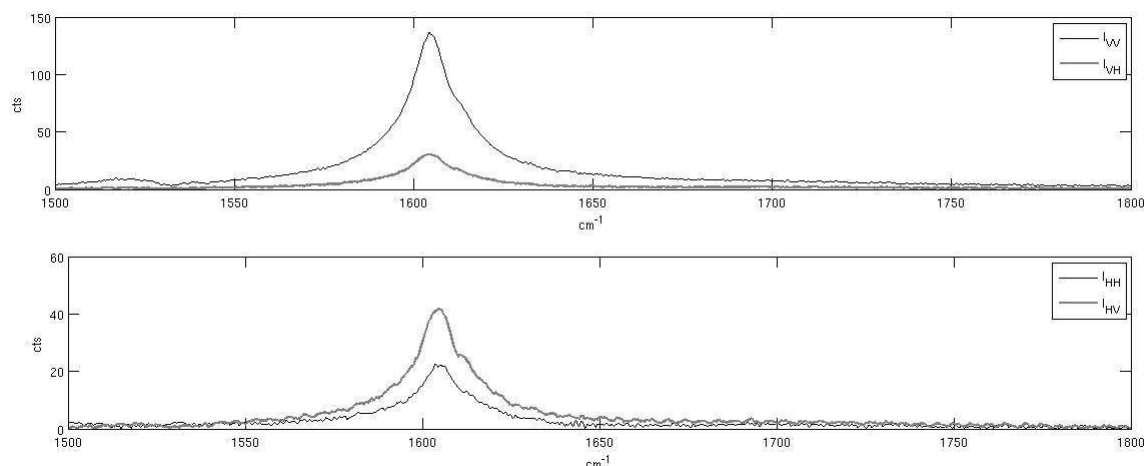


Figure 16: Raman peak of 5CB corresponding to the symmetric stretching of the benzene rings (1605cm^{-1}) measured in the four geometries I_{VV} , I_{VH} , I_{HH} , and I_{HV} .

In Figure 16 is reported the characteristic Raman peak of 5CB corresponding to the symmetric stretching of the benzene rings (1605 cm^{-1}) measured in the four geometries on the pristine cell. The selected 1605 cm^{-1} vibrational mode provides a suitable Raman probe for the orientation measurement since the main axis of the vibration is parallel to the central rigid part of the molecule, namely along the main axis of the mesogenic group. Such vibration is also particularly suitable for the order parameters calculation since it is uniaxial and strongly polarized with a ratio of the diagonal terms of the molecular polarizability tensor close to zero ($\alpha_H/\alpha_V = 0.045$ ^[31]). The high anisotropy of the selected vibration allows to obtain the order parameters P_2 on the basis of scattering anisotropies R_1 and R_2 defined as $R_1 = I_{HV}/I_{VV}$ and $R_2 = I_{HV}/I_{HH}$, by the calculation of the second average cosine powers of the molecular orientation θ through the approximated formula ^[32]:

$$\langle (\cos \theta)^2 \rangle = \frac{3R_2(2R_1 + 1)}{8R_1 + 3R_2 + 12R_1R_2}$$

The scattering anisotropies R_1 and R_2 have been measured on the pristine surfaces and on the illuminated areas as a function of the energy dose of the pump beam. Twisted microstructures ($20\text{ }\mu\text{m}$ diameter) have been photo-induced on the original planar cell varying both pump power ($200\text{ }\mu\text{W}$ – 20 mW) and exposure time (1–10 sec). The scattering anisotropies as a function of power multiplied by exposure are reported in Figure 17. The data show a threshold energy about 0.5 mJ where R_2 becomes greater than R_1 and saturation about 100 mJ where the parameters remain roughly constant. The average order parameter P_2 calculated at the saturation energy dose results 0.53 which is increased respect to the original

value $P_2 = 0.48$ and of the same order of that measured on the reference rubbed substrate of 0.52.

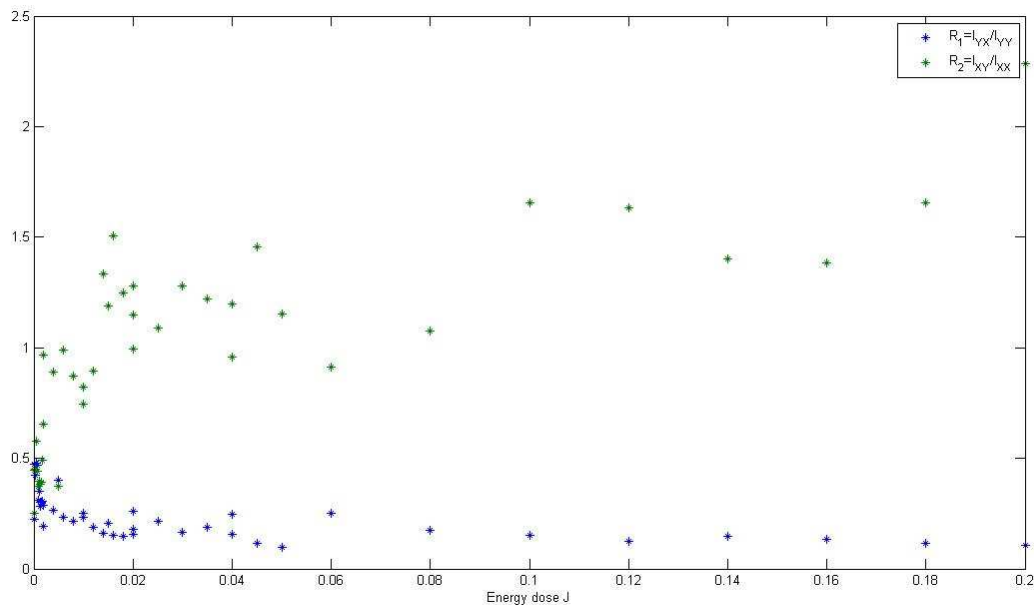


Figure 17: Scattering anisotropies R_1 and R_2 measured on the illuminated areas as a function of the energy dose in Joule of the pump beam.

We can conclude that these systems can be utilized as command surfaces with excellent performances if compared to other similar systems. Moreover their stability increase the usability for this kind of application: after several cycles and more than one year these devices are still working, while the ones build up with spin coated films suffered from dewetting, being unusable after this period of time.

Adaptative surfaces

As mentioned above, in many studies, special attention is devoted to tuning the interface for specific applications, and careful design of the topmost surface layer incorporating all of the necessary elements controlling a predictable surface response, or a variable surface response under different conditions^[33-36]. For this reason, the structure and characteristics of the phase boundaries are of the utmost importance for an understanding of the materials properties in processing and use. Moreover, further advances in materials science imposes requirements for dual surface properties that frequently are in conflict: a given material, depending on the conditions under which it is utilized, has to be hydrophobic and hydrophilic, acidic and basic, conductive or non-conductive, adhesive or repellent, and be able to release or adsorb some species. With the increasing demand for more sophisticated surfaces, one current approach is to fabricate and understand materials with interfacial properties capable of undergoing reversible changes according to outside conditions or stimuli.

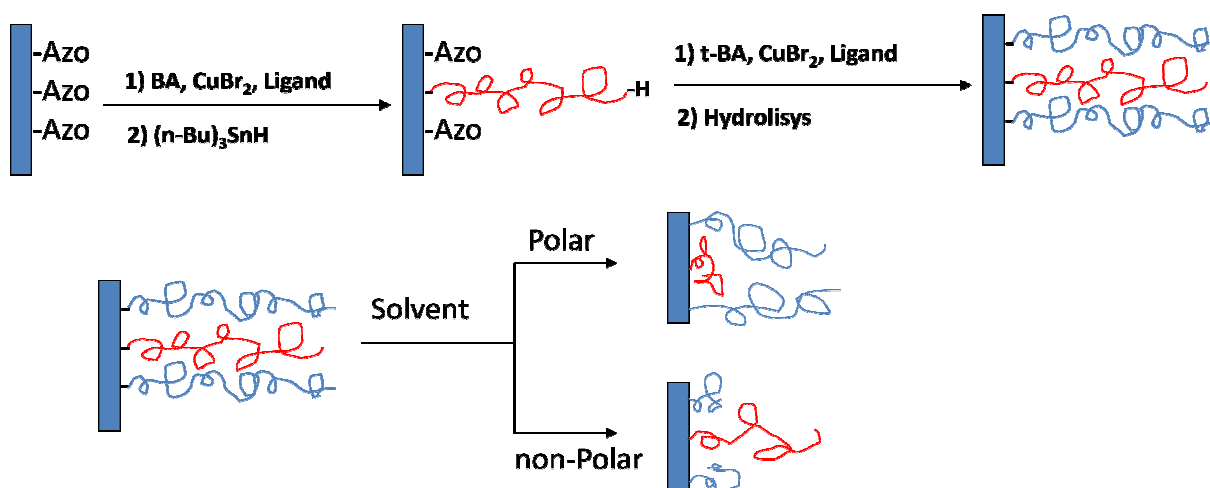
Intensive study in the field of the adaptive/responsive surfaces began several decades ago in an attempt to understand the relationships between bulk properties/composition of pristine polymeric materials and their surface characteristics. With time, the focus of research has moved to the design of materials with 'smart' or 'intelligent' surface behavior. A number of approaches have been employed to reach this goal, including, but not limited to (a) synthesis of functional polymers with specific composition and architecture; (b) blending of a virgin polymer material with small amounts of (macro)molecular additive; (c) surface modification by various chemical/physical treatments.

Significant efforts have also been made to prepare, characterize, and understand the structure/properties relationships of adaptive/responsive surface layers attached to or deposited on the materials surface.

The functionalization of the surface with incompatible polymeric functional polymeric chains is a promising route for the fabrication of such surfaces: if a flat surface is functionalized with incompatible chains bearing different functionality and the polymeric brush is not too dense to prevent self assembly the topmost surface composition will be determined by the environment. These surfaces, called adaptative surfaces, are therefore able to change their functionality to adapt to the changed conditions and offering to the new environment engineered properties.

Minko and coworkers^[37] fabricated these kind of surfaces by surface initiated free radical polymerization, using a surface bounded thermal azoinitiator. The synthesis of this surface followed two step: a pristine decomposition of half of the azo-initiator and subsequent polymerization process from half of the polymerizable sites, rising of the surface and a second polymerization with an incompatible monomer from the other half of initiator. By tuning accurately the time and the temperature of polymerization the composition of the surface can be tuned, decomposing a certain percentage of the initiating site during the first step, but no control over the polymeric chain can be achieved with this approach.

In order to develop a general method for the fabrication of these surface that allows control on the surface composition and on the polymer characteristic, having well defined polymers on the surface, in this work we tried to use surface initiated reverse ATRP (SI-RATRP) to grow a well defined mixed polymeric brush. The outline of the work is depicted in Scheme 1.



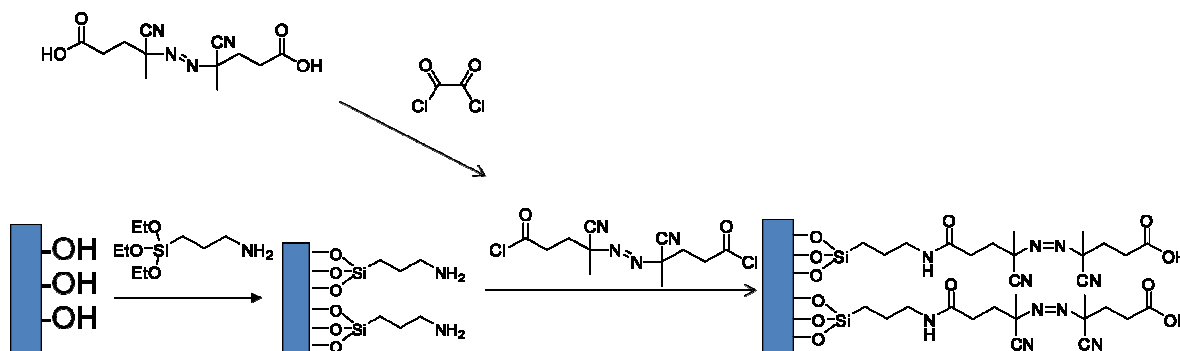
Scheme 1: Synthesis and reorganization of the mixed polymeric brush

The idea is to grow by SI-ATRP from a modified Si surface a first population of hydrophobic and soft Poly(*n*-Butylacrylate) (PBA) chains and in a second step another population of Poly(*tert*-Butylacrylate) (PtBA). Then the PtBA is hydrolyzed to Poly(acrylic acid) (PAA) and the topmost surface is in contact with different solvents (polar or non polar) the topmost composition change.

Initiator synthesis and SAM formation

In order to have a well defined surface is very important to synthesize a smooth and homogeneous layer of free radical initiator.

We made a first attempt to functionalize Si surface using 3-aminopropyl triethoxysilane to obtain an amino rich surface that can react with the acyclic chloride of an acid symmetric azo initiator. (Scheme 2).



Scheme 2 functionalization of the surface with triethoxy silane and acyclic chloride initiator

With this procedure it was not possible to deposit a single monolayer but rather a multilayer of the amino silane was attached onto the surface so the thickness of this SAM was not reproducible and different from one substrate to the other. In fact, this reaction is very sensitive to moisture and a slight difference can lead to the formation of an uncontrolled multilayer (Figure 18). Therefore, the functionalization with the azo diacid chloride will result in an inhomogeneous multilayer of initiator with some species linked to one or two amino group.

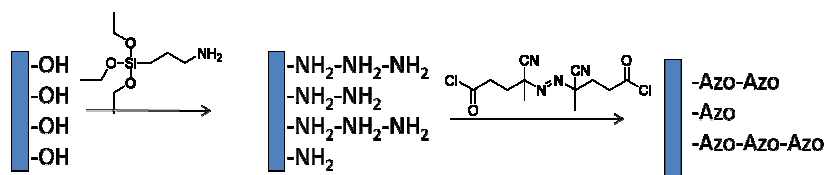
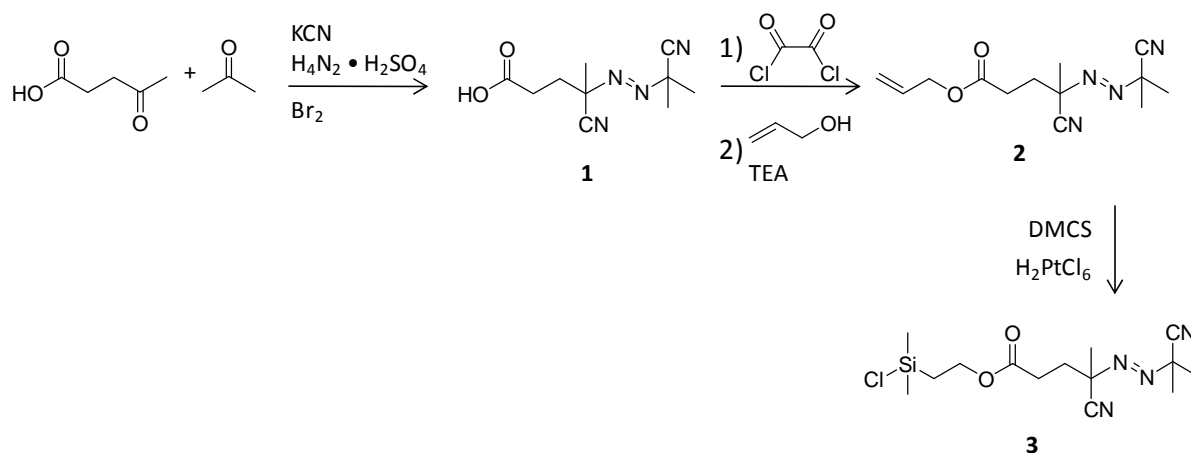


Figure 18: formation of a multilayer on the Si surface

So an asymmetric initiator has been synthesized following a procedure already reported in literature^[38] and depicted in Scheme 3



Scheme 3: synthesis of the asymmetric initiator

We used leuonic acid and acetone as oxo compound for the synthesis of asymmetric azo acid 1 using a typical Haines and Waters method. Then the acid has been chlorinated with oxalyl chloride and immediately reacted with allyl alcohol in presence of a TEA to give the compound 2. The target molecule 3 has been obtained by hydrosilylation using Pt catalyst and dimethyl chlorosilane (DMCS) in large excess. The excess of DMCS was removed by distillation and the product 3 (CSAN) was used with no further purification for substrates modification.

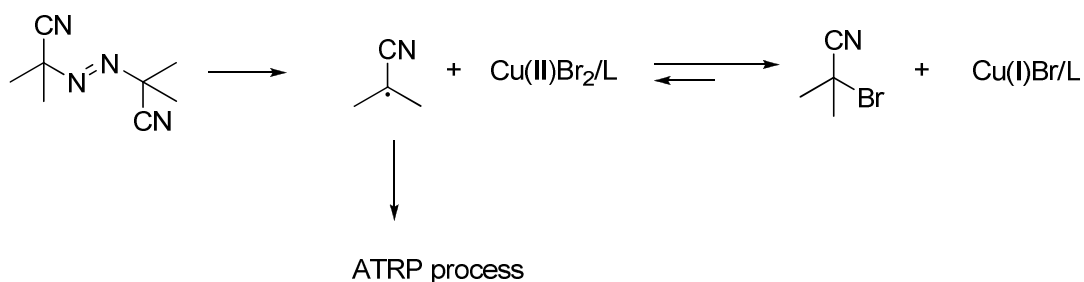
The intermediates and the final compound were characterized by ¹H-NMR and FT-IR spectroscopy and the spectra are in accordance with the chemical structure and literature datas.

The azo-initiator was immobilized at room temperature on clean Si surface using a solution of 1.5g of 3 and 2 ml of dry triethyl amine in 80 ml of dry toluene.

The use of a monofunctional asymmetric initiator gives a good control over the surface modification, as seen by ellipsometric measurement with a reproducible increase of the thickness of only 1.5 nm, in good agreement with the calculated length of the initiator molecule.

RATRP of nBA

The RATRP polymerization involves the use of Cu(II) catalyst that is reduced in situ to Cu(I) by reaction with the radical generated by decomposition of AIBN. In this way the active catalyst and initiator are generated in situ and the atom transfer polymerization can start (Scheme 4).



Scheme 4: RATRP process

The SI-RATRP of nBA were carried on the Si modified surfaces. The goal was to carry out the RATRP polymerization from a certain percentage of the initiating site and to being able to tune the molecular weight of the grafted polymer.

All the polymerization have been carried out in dry anisole using AIBN as free initiator to avoid the termination of surface chain due to the persistent radical effect^[39].

In Figure 19 are shown the kinetics of decomposition of AIBN at different temperatures. It can be clearly seen that, while a decomposition at 65 or 70°C is relatively fast, at 40°C the decomposition is negligible and thus polymerization can be carried out with no more initiation.

Several condition were tested. In fact in order to polymerize the nBA from only a small percentage of the azo-initiator tethered to the surface two opposite condition should be met: a short time for a precise decomposition of the desired percentage of azo initiator and longer time of polymerization for having a well controlled radical polymerization.

A compromise was found with a two step polymerization. A first, short, step at higher temperature in order to decompose the desired amount of azo-initiator and to form the active Cu(I) catalyst, followed by a longer step at 40°C, temperature at which the decomposition of initiator is negligible and, using an active catalyst, the RATRP polymerization can be carried out if an active ligand is used.

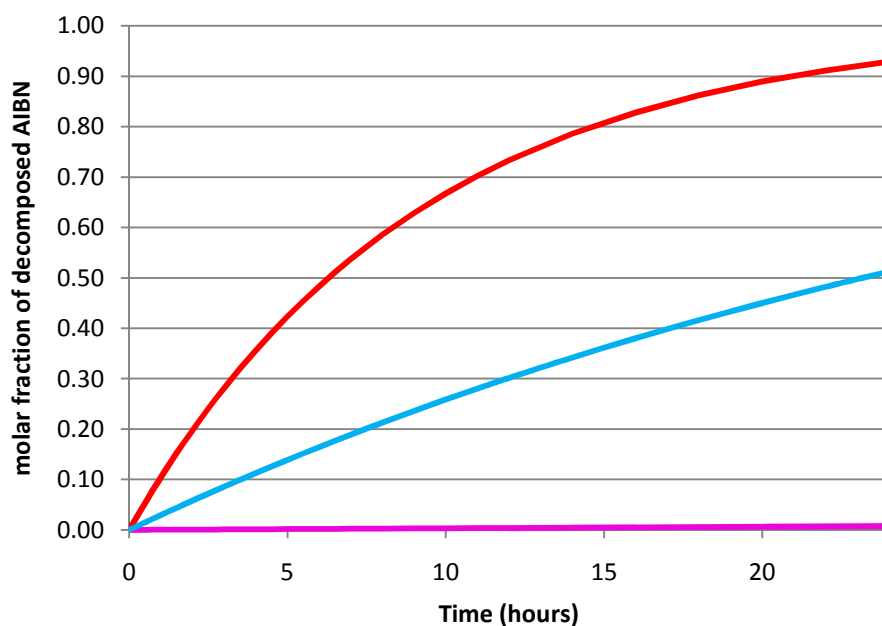


Figure 19: decomposition of AIBN at different temperatures (—) 70°C, (—) 65°C, (—) 40°C.

The polymerization were carried using a ratio of monomer: free initiator: CuBr_2 : TPMA = 1000: 1: 2,2x: 2,2x were x is the target of AIBN decomposition.

In fact, due to the ATRP equilibrium, if not all the CuBr_2 is reduced to Cu(I) the polymerization can not continue because of the presence of too much deactivator. On the other hand if all the Cu(II) is reduced to Cu(I) no control on the polymerization can be achieved because of the persistent radical effect^[23]. Thus the ratio 2,1 x: 1 = Cu(II): AIBN it is effective to obtain a good control over the polymerization.

The presence of free AIBN is useful, besides the needs due to the persistent radical effect, for controlling the polymerization: it is assumed that the polymer grown on the surface is similar to the polymer grown in the bulky phase. In fact, kinetic studies of the bulky phase (Figure 20) show that this approach is successful for a RATRP from the desired percentage of initiating sites. The good agreement of GPC and theoretical molecular weight and the low polydispersities means that the initiator efficiency is close to 1 and, when the polymerization starts, no further initiation is present.

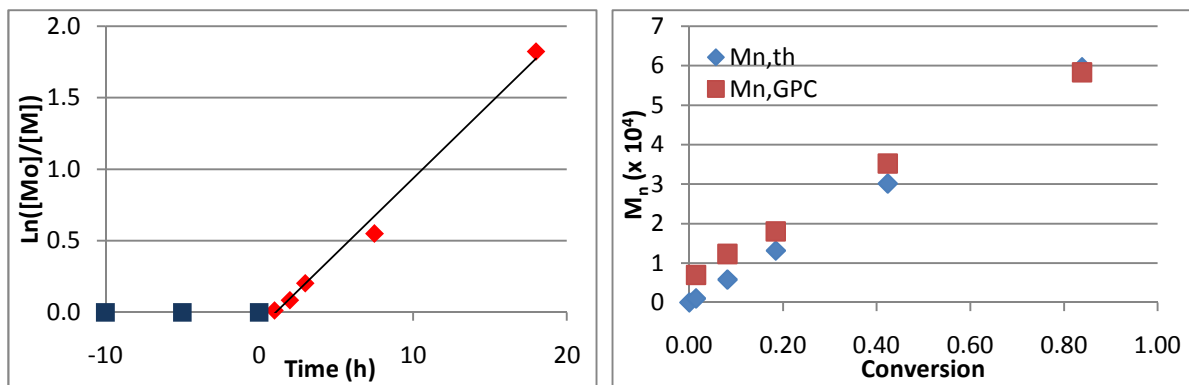


Figure 20: Kinetics of two step temperature polymerization with 30% of AIBN decomposition, red point on the plot are after decrease of temperature at 40°C

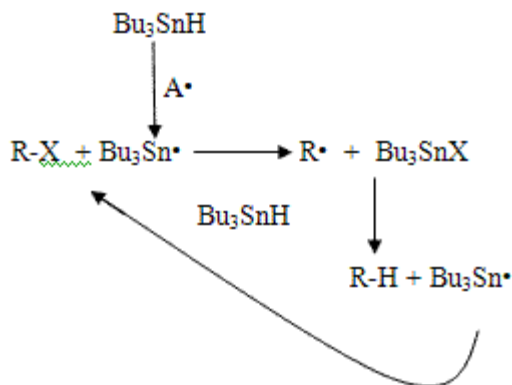
Several surfaces have been modified by grafting PBA chains in different percentage and different molar fraction on the surfaces (Table 6).

Table 6: PBA brushes characterization

Entry	AIBN conversion	Thickness (nm)	M_n	PDI	Grafting density (σ , chains nm^{-2})
1	0.15	7.1	63000	1.10	0.04
2	0.15	2.0	20000	1.20	0.05
3	0.30	4.6	30000	1.08	0.08
4	0.30	8.8	58000	1.17	0.08
5	0.5	20.0	64000	1.54	0.18

Due to the living RATRP mechanism the chains are terminated with an active Br atom that can be useful for the synthesis of block copolymers. For our specific scope the Br atom must be deactivated.

The cleavage of Br atom can be easily achieved by reaction with tributyl tin hydride under radical conditions^[40] with the mechanism shown in Scheme 5.



Scheme 5 Dehalogenation of living chains

Growth of the mixed brush.

The growth of the second population of PtBA by SI-RATRP needed less attention than the previous one as all the remaining reactive site has to be decomposed.

Thus the polymerization of tBA were carried on at 60°C in anisole with CuBr₂/PMDETA until the desired conversion is reached.

While the polymerization in solution continued in a controlled fashion on the surface no control is achieved. The second polymerization can be carried out on the surface and mixed brushes are obtained but no reproducibility on the polymeric layer thickness is achieved (Table 7).

This can be attributed to the crowding of the surface and then to the difficulty for the second population of the brushes to grow from the surface. Moreover some clustering on the surface can occur as likely the decomposition rate of initiator close to a growing chain should be faster than the one of initiator far away from a chain and thus with less steric repulsion.

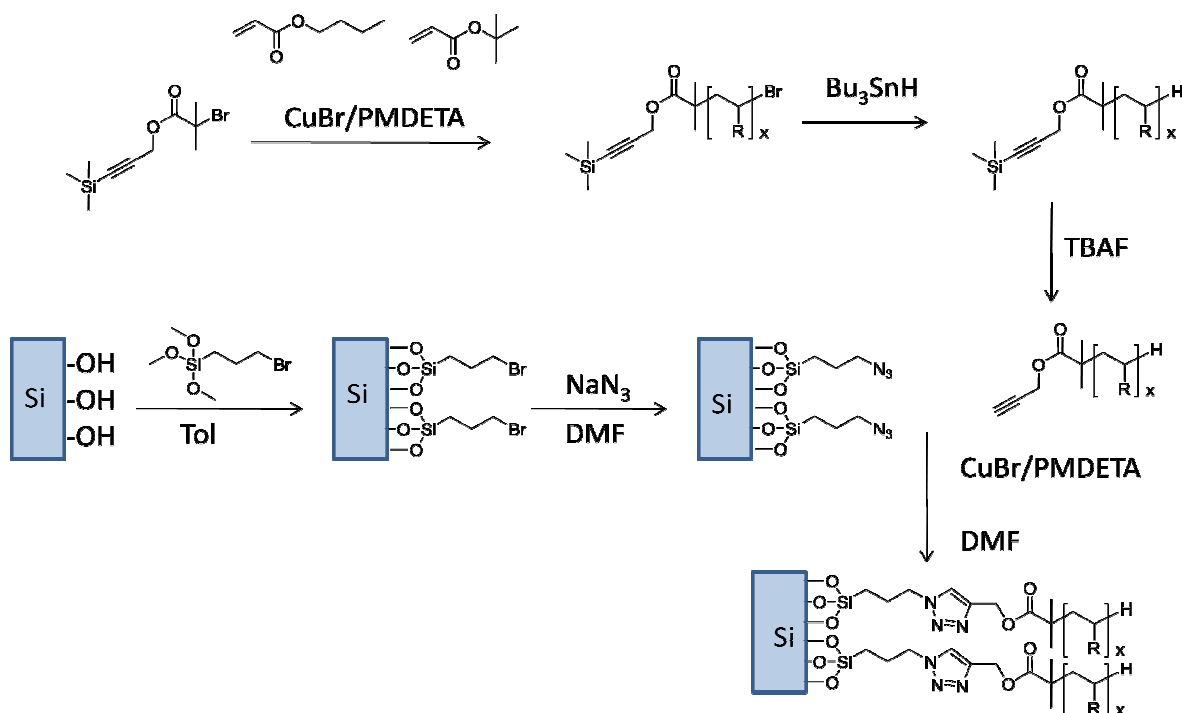
Table 7 thickness of the mixed brushes

Entry	Thickness (nm)		Mn (PtBA)	PDI (PtBA)	σ (chains nm ⁻²) (overall)
	PBA brush	Mixed brush			
1	7.1	7.6	43000	1.16	0.06
2	2.0	6.3	25000	1.10	0.08
3	4.6	4.7	37000	1.14	0.08
4	8.8	18.0	50000	1.16	0.18
5	20.0	20.8	48000	1.24	0.19

This approach is, at least in principle, extremely versatile but did not gave the expected results, and thus in order to obtain the desired mixed brushes also a “grafting onto” method have been successfully tried.

Adaptative surfaces by “grafting onto”

The outline of this synthetic pathway is depicted in Scheme 6.



Scheme 6: mixed brushes by “grafting onto” method

The general synthesis of PBA and PtBA consist in the polymerization of BA and tBA using a propargyl initiator, protected with a trimethylsilyl group. The obtained living chains are then dehalogenated and the propargyl group has been deprotected with tetrabutyl ammonium fluoride (TBAF).

A SAM was deposited onto clean Si wafer using 3-bromopropyl trimethoxy silane, the bromine atom was then substituted with an azide group by reaction of the surface with sodium azide in hot DMF using 15-crown-5 as catalyst.

Finally the mixed brushes have been grafted onto the surfaces by the 2+3 Cu(I) catalyzed Huisgen cycloaddition between the alkyne terminated macromolecules and the azido groups of the surface.

Surface modification

The Si wafers are cleaned with piranha solution (20 ml H₂O₂ 30% and 60 ml H₂SO₄) at 80°C for two hours. Then the surfaces are rinsed several time with deionized water and dried under air stream. The surfaces after piranha cleaning are highly hydrophilic. The SiO₂ layer is checked by ellipsometry after cleaning and results of 2 nm.

Immediately after cleaning and drying the surfaces are modified using a solution of 3-bromopropyl trimethoxy silane (0.30 ml in 10 ml of dry toluene). The surfaces are putted in a large vial taking care that they don't overlap. The functionalization has been carried out for 30 minutes at 80°C.

After this time the surfaces are rinsed with clean toluene, sonicated with pure acetone for 30 seconds and rinsed with water. The water is then blown away. The surfaces after this step are highly hydrophobic.

The exchange bromo-azido is performed putting the surfaces in a saturated DMF solution of NaN₃ (0.15 g in 10 ml of DMF) using 0.1 ml of 5-crown-15 as catalyst at 70°C for three days in the dark. The surfaces are then rinsed with DMF, sonicated in acetone for 30 seconds and rinsed with deionized water. The surfaces then are kept in the dark.

After azido exchange the surface are less hydrophobic and the thickness of the organic layer measured by ellipsometry is about 3.5 nm.

Synthesis of alkyne terminated polymers

PBA and PtBA of different molecular weight and narrow PDI have been synthesized by normal ATRP using 3-(trimethylsilyl)propargyl 2-bromo-2-methylpropanoate as ATRP initiator, CuBr as catalyst and pentamethyldiethyltriamine (PMDETA) as ligand in anisole at 60°C. In Table 8 are reported the principal characterization data of the four synthesized samples.

Table 8: characterization of the polymers used for the grafting onto reaction

Sample	Mn	PDI
PBA _{30k} ^{a)}	30600	1.10
PtBA _{30k} ^{a)}	29700	1.08
PBA _{48k} ^{b)}	48000	1.09
PtBA _{50k} ^{b)}	50000	1.10

When the desired molecular weights were obtained (the reaction have been monitored by GPC) the monomers were removed under vacuum, avoiding oxygen coming into the flask and deoxygenated anisole (10 ml) with a 10 fold excess of tributyl tin hydride has been added. The dehalogenation reaction was carried out overnight at 60°C. No increase of molecular weight is observed by GPC.

The samples have been purified by filtration on neutral alumina and the solvent and the residual monomer have been removed under vacuum.

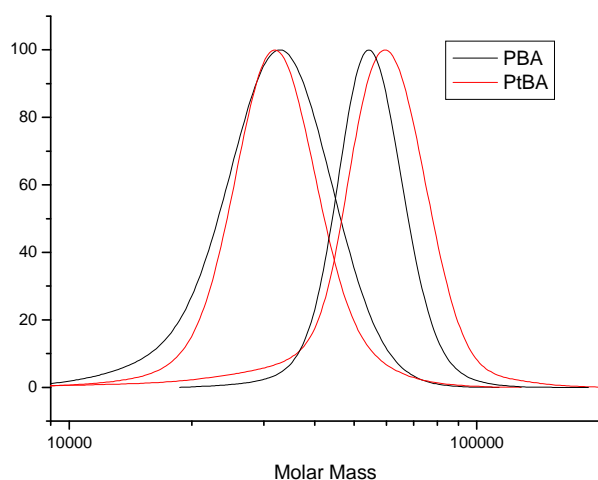


Figure 21: GPC chromatograms of the deprotected PBA and PtBA synthesized

The deprotection of the silyl protected alkyne moiety has been done with tetrabutyl ammonium fluoride 1.0 M in THF. The reaction is carried out using a 100 fold excess and stirring overnight at room temperature. Water was then added and the organic layer separated and washed one more time with water and dried. The solvent was finally evaporated under vacuum.

The ^1H - NMR spectra confirms that the deprotection of the terminal group is quantitative.

In Figure 21 are reported the GPC traces of the four polymeric derivatives after deprotection and purification.

“Grafting onto” and hydrolysis of PtBA chains

The “grafting onto” has been achieved using a 2+3 Cu(I) catalyzed Huisgen cycloaddition.

The experimental condition used are the following: deoxygenated DMF as solvent, 0.6% w/w polymers concentration, 0.01 M CuBr/PMDETA as catalyst, ascorbic acid as reducing agent (0.002 M), temperature 60°C.

In order to have different surface modification different relative molar ratio of PBA and PtBA as well as different molecular weights have been used. The reactions have been carried out into purged flask under nitrogen flow for 0,5, 6 and 48 hours (Table 9).

Table 9. Characterization data of the double component surfaces.

Entry	Composition [BA:tBA]	\bar{M}_n	Time (h)	Thickness (nm)	Grafting densities
1	50:50	30K	0.5	4.6	0.09
2	50:50	30K	6	6.8	0.14
3	50:50	30K	48	8.0	0.16
4	25:75	30K	0.5	3.6	0.07
5	25:75	30K	6	5.4	0.11
6	25:75	30K	48	6.5	0.13
7	75:25	30K	0.5	3.6	0.07
8	75:25	30K	6	4.2	0.08
9	75:25	30K	48	7.0	0.14
10	50:50	50K	0.5	5.4	0.07
11	50:50	50K	6	6.5	0.08
12	50:50	50K	48	8.0	0.10
14	100:0	30K	48	6.4	0.08
15	0:100	30K	0.5	3.6	0.07
16	0:100	30K	48	6.1	0.08

After the desidered time the flasks has been opened and the functionalized surfaces cleaned with DMF, CH₂Cl₂, sonicated in acetone for 30 seconds and finally dried under nitrogen flow.

The thickness has been measured by ellipsometry (Table 9).

The PtBA has been hydrolyzed putting the surfaces in a 1% solution of methansulfonic acid in dichlorometane for 60 seconds ^[41].

From the data gathered in Table 9 it can be seen how is possible to tune easily the grafting densities by changing the reaction time (or the catalyst amount) and the surface composition by changing the reaction mixture composition.

Surface reorganization

In order to verify the reorganization of the topmost surface after contact with different environment, the mixed PBA: PAA brushes were immersed in different liquids and then investigated by AFM microscopy.

Each surface was thus immersed in water and hexane for two hours in order to let the self-assembly of the polymeric layer and then checked. By comparing the phase image of the surfaces after immersion in different solvents we can see a reorganization of the surface, with soft (dark) PBA rich surfaces after immersion in hexane and hard (bright) PAA rich surface after immersion in water (Figure 22). In the following figures are reported the height and phase AFM images of the adaptative surfaces after reorganization in polar (water) and non polar (hexane) liquids (Figure 23, Figure 24 and Figure 25).

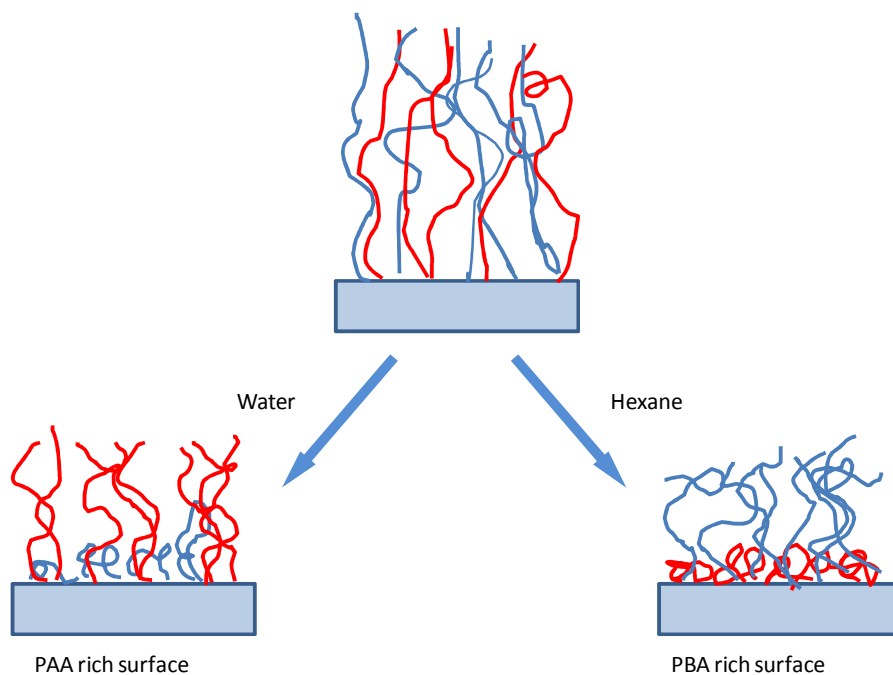
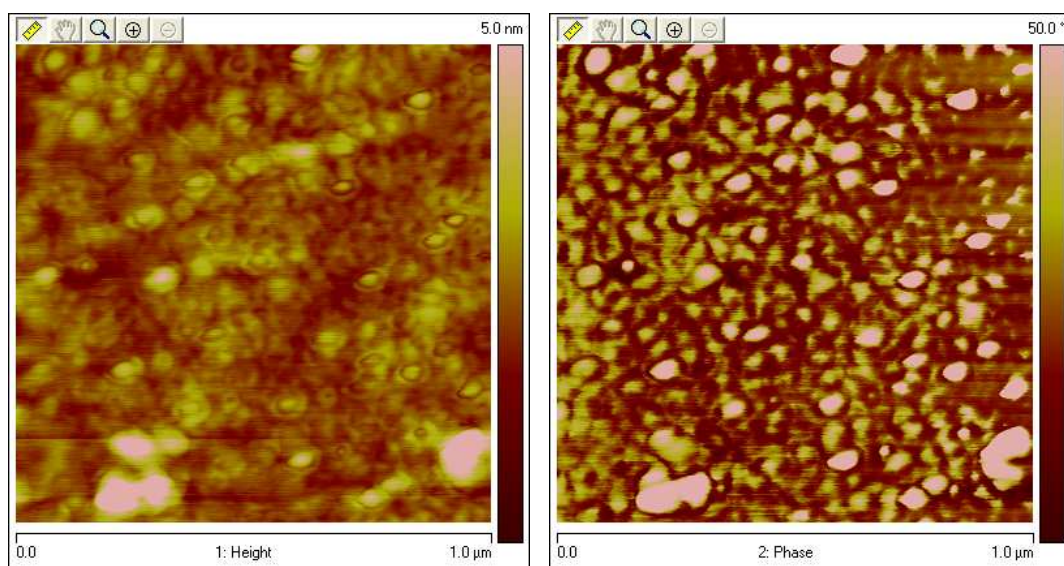


Figure 22: Surface reorganization of the mixed brushes

PBA: PAA = 50: 50

Water



Hexane

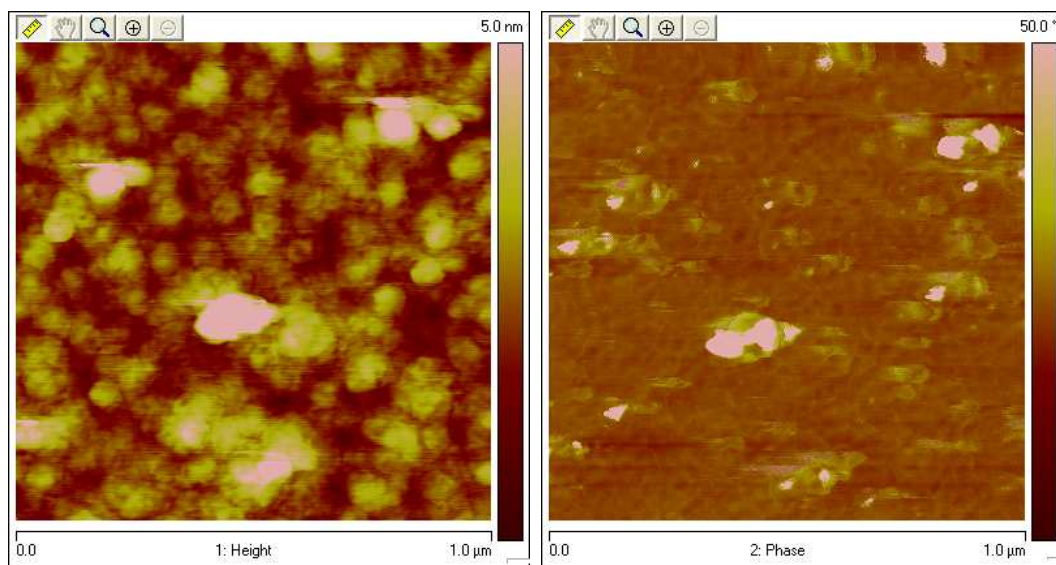
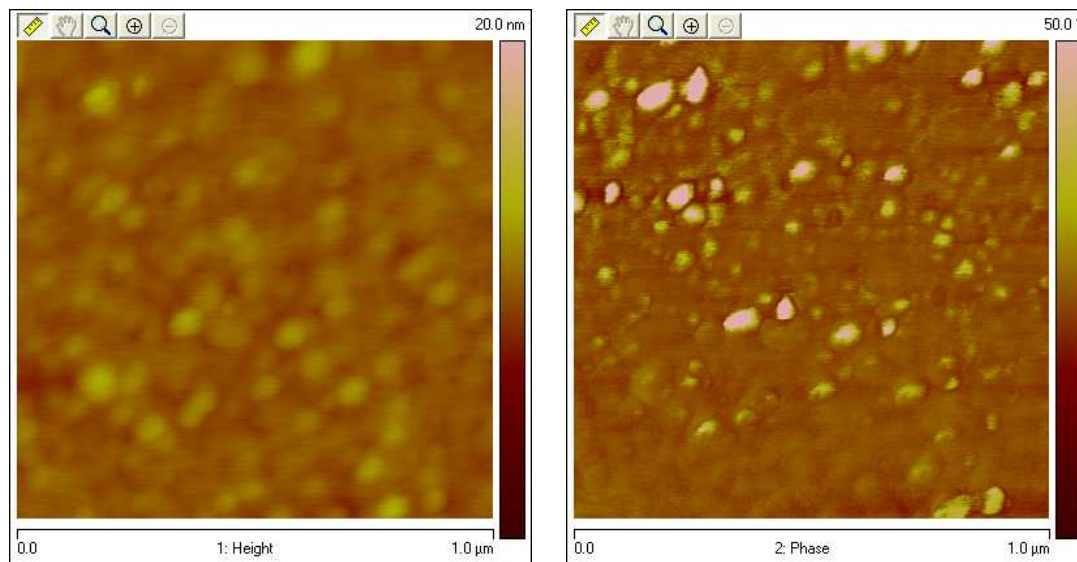


Figure 23: AFM images (topography and phase image) of PBA: PAA = 50: 50 after immersion in water and hexane.

PBA: PAA = 75:25

Water



Hexane

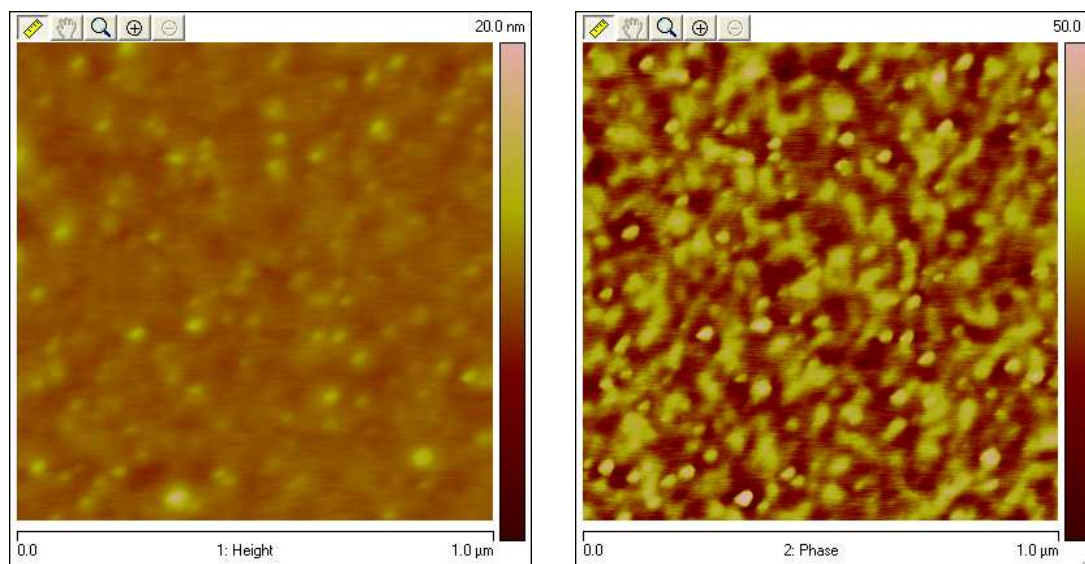
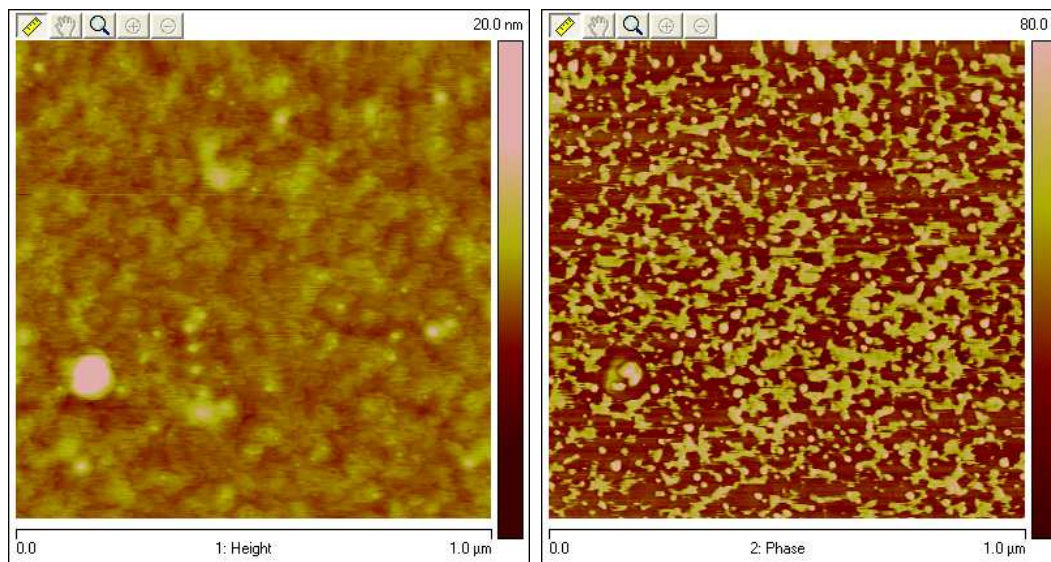


Figure 24 AFM images (topography and phase image) of PBA: PAA = 75: 25 after immersion in water and hexane.

PBA: PAA = 25: 75

Water



Hexane

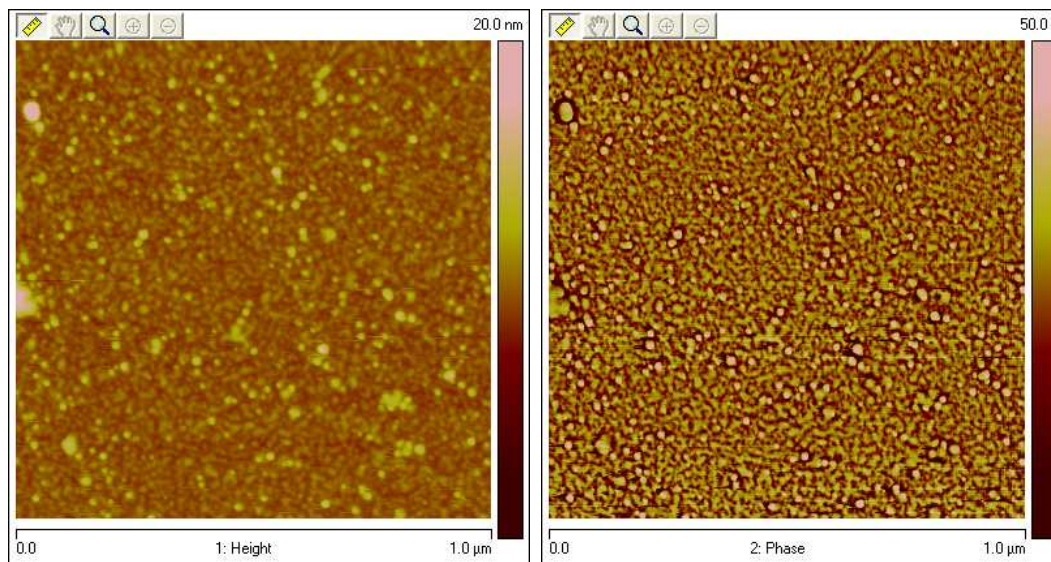


Figure 25 AFM images (topography and phase image) of PBA: PAA = 25: 75 after immersion in water and hexane.

The reorganization has also an effect on the roughness of the surfaces: in fact a surface richer in PBA is smoother than a surface rich in PAA due the different softness of the two polymers (soft PBA, stiff PAA). In fact the analysis of the roughness measured by AFM confirms this trend: while the PBA molar fraction increase (because of the different composition of the polymeric layer or after hexane contact) the surface is smoother (Table 10).

Table 10: Surface roughness of the adaptative surfaces

Roughness	Acetone	Water
PBA:PtBA 25:75	0.64	0.66
PBA:PtBA 50:50	0.60	0.79
PBA:PtBA 75:25	0.46	0.46

We can thus conclude that this approach can be successfully used for the fabrication of adaptative surfaces by simple grafting of immiscible polymers onto a surface. These surfaces are then able to reorganize in answer to changed environmental conditions. In this case the surfaces are able to show selectively hydrophilic or hydrophobic chains after specific reorganization.

This kind of study has to be considered preliminary, and this kind of surfaces opens a huge number of possibilities for the synthesis of smart materials able to self assemble in specific ways reacting to precise environmental conditions exposing different functionality tuned for specific conditions.

Conclusions

Various surfaces were successfully modified using different methods. These surfaces were characterized by ellipsometry, AFM and SEM. In the case of azoaromatic brushes also optical (UV-Vis and CD) characterization was performed.

The growing kinetics were studied for all the method used.

The optical properties of the azoaromatic brushes were studied and compared to the ones of similar thin films deposited by spin coating. Different behaviors in terms of photochromic and chirooptical properties were found.

The optical properties of the azoaromatic brushes have been used for the fabrication of LC cell driven by optical command surfaces. Due to the high robustness of the macromolecular brush these devices overcame the problems related to the dewetting of the sensitive layers that limited their application in the past.

Also adaptive surfaces were successfully synthesized via a grafting to method. These well defined surfaces are able to reorganize the topmost layer reacting to changed environmental condition, by incorporation of functionality in these brushes it is possible, at least in principle, to prepare surfaces able to reorganize and to act in different ways to target environmental condition.

Experimental part

THF, DMF, toluene and CH_2Cl_2 has been purified and dried according to reported procedures^[42] and stored under nitrogen. Acetone used for washing the Si wafer was Acetone HPLC grade purchased from Aldrich. Ultra pure water used for washing is made with Milli-Q plus instrument by Millipore.

Trimethylchlorosilane (TMCS) is freshly distilled prior to use and stored under nitrogen.

The monomer 4- ω -methacryloyloxy-hexyloxy-4'-ethoxyazobenzene (**M6A**) has been synthesized as previously described^[43].

The synthesis of the monomers (*S*)-**ML6A**^[26] and (*S,S*)-**MLL6A** is described in Chapter 3.

Polymeric films were spin coated film onto a clean glass slide using a 0.1% solution of Poly(**M6A**) in CH_2Cl_2 , the thickness of the film, measured by UV-Vis spectroscopy, was adjusted changing the spin rate to obtain the desired absorption ($A^{350} = 0.080$).

Polymerization initiator:

The ATRP initiator 3-(chlorodimethylsilyl)propyl 2 bromo isobutyrate (**SBiB**) was synthesized as previously described^[44] by Pt catalyzed hydrosylation of the commercially available allyl 2-bromo isobutyrate with dimethyl chloro silane.

The ATRP initiator 3-(trimethylsilyl)propargyl 2-bromo-2-methylpropanoate has been synthesized as previously described^[45]

The azo initiator 2',4-azo-(2'-cyanopropyl)(4-cyanopentanoxy-(3''-chlorodimethylsilyl)propylate) (**CSAN**) has been synthesized as previously described^[38].

Si wafer and glass slide cleaning

Si wafers cutted in pieces of 1x2 cm and glass slide of 2x3 cm has been cleaned with piranha solution ($\text{H}_2\text{SO}_4: \text{H}_2\text{O}_2$ (30%) = 7: 3) at 80°C for two hours. The surfaces have been then rinsed with abundant Millipore water and dried under nitrogen flow.

Si wafer modification with SBiB and TMCS

Clean Si wafer have been functionalized with the ATRP initiator by immersion of the surfaces (paying much attention to avoid contact between the surfaces themselves) in 0.01 M solution of **SBiB** in dry toluene and keeping under dry nitrogen flow overnight at room temperature.

In order to achieve lower grafting densities also surface with a different amount of non active dummy initiator have been prepared using the previously described procedure. For the synthesis of these surfaces mixtures of **SBiB** and **TMCS** have been used in the molar ratio of **SBiB: TMCS** = 1:1, 1:50, 1:200, 1:1000.

The same procedure, molar quantities, times and temperature were used for the modification of Si wafer with the azo initiator **CSAN**.

After modification the surfaces have been cleaned with distilled solvents of increasing polarity (toluene, dichloromethane, THF, acetone and Millipore water) by sonication for 5 minutes

Surface modification for the “grafting onto” reaction

clean Si surfaces have been modified in a large vial using a solution of 3-bromopropyl trimethoxy silane (0.30 ml in 10 ml of dry toluene). The modifications are carried on for 30 minutes at 80°C, then the surfaces have been rinsed with clean toluene, sonicated with pure acetone for 30 seconds and finally with water. The surfaces after this functionalization appear highly hydrophobic.

The exchange bromo-azido has been performed putting the surfaces in a saturated solution of NaN_3 (0.15 g in 10 ml DMF) using 0.1 ml of 5-crown-15 as catalyst. The exchange has been carried out at 70°C for three days in the dark. The surfaces have been rinsed with DMF, sonicated in acetone for 30 seconds and finally rinsed with deionized water. The surfaces were kept in the dark to avoid the decomposition of the azido groups.

Polymerization reaction:

The linear polymer Poly(**M6A**) has been synthesized by ATRP as previously described in chapter 2 [25].

Polymerization of BA and tBA

The linear homopolymers PBA and PtBA have been synthesized by ATRP following the procedure reported here for example for PBA_{30k}.

Distilled butyl acrylate (10 ml), anisole (2 ml), PMDETA (41.4 μ l) and the propargyl initiator (45.6 μ l) have been put in a shlenk flask and the oxygen has been evacuated with three freeze pump cycles. Then, under vigorous nitrogen flow, CuBr (28.5 mg) has been introduced into the vial. The vial was then sealed and other two freeze pump cycles have been done. The polymerization has been started by putting the vial in an oil bath for 24h at 60°C.

The polymerization has been stopped after reaching the desired conversion by introduction of a deoxygenated solution of Bu₃SnH in anisole (0,560 ml in 4 ml of anisole).

The solvent and the unreacted monomers have been removed under vacuum until constant weight was reached. The polymeric derivatives were dissolved in THF and tin and copper have been removed by filtration on neutral alumina.

The THF have been removed under vacuum and the polymer was deprotected with 1,0 M TBAF in THF (100 fold excess). The reaction mixture has been filtered on acid alumina and the THF was removed under vacuum.

¹H-NMR spectra are in agreement with the expected structure.

The quantities used for the other polymerization are gathered in Table 11

Table 11: quantities used for the symthesis of PBA and PtBA.

Sample	Ratio	Monomer (ml)	Initiator (μ l)	CuBr (mg)	PMDETA (μ l)	Anisole (ml)
PBA _{30k}	350:1:1:1	10	45.6	28.5	41.4	2
PtBA _{30k}	350:1:1:1	10	45.1	28.0	40.7	2
PBA _{48k}	600:1:1:1	10	26.7	16.6	24.2	2
PtBA _{50k}	600:1:1:1	10	26.3	16.3	23.7	2

SI ATRP

A typical ATRP polymerization on SI substrates was carried out in dry solvent (THF or THF/DMF 1:1 v/v or DMF) using the following procedure: 2.2 g of **M6A** (5.36 mmol), 15.35 mg of CuBr (0.107 mmol) and 2.39 mg of CuBr₂ (0.0107 mmol) were put in a flask and deoxygenated with five freeze-pump cycles. Then 20 ml of deoxygenated dry solvent and 64 µl of 1, 1, 4, 7, 10, 10-hexamethyltriethyltetraamine (**HMTETA**) have been transferred via syringe in the vial and the solution was stirred until all the compounds were dissolved. Then four samples of 5 ml were withdrawn and transferred to other deoxygenated flask containing the ATRP initiator modified surfaces. The flasks were then sealed and the polymerizations were carried on at 80°C for different times. After polymerization, polymer grafted substrates were washed with THF for several times to remove unreacted monomer and free linear soluble polymer, and dried at room temperature.

SI-RATRP of BA

A typical SI-RATRP polymerization has been carried out in the following procedure: modified surfaces in a protection ring were put in a vial with CuBr₂ (15.4 mg), BA (15 ml), TPMA (21 mg), AIBN (23 mg) and anisole (7,5 ml). The vial has been deoxygenated with three freeze pump cycle and put in an oil bath at 65°C for the desired time in order to decompose the target amount of azo-initiator. After the desired time (the color of the solution turned from dark green to a pale green due to the reduction of the colored Cu(II) species) the flask was moved to an oil bath at 40°C and the growth of the molecular weight checked by GPC. The polymerization was stopped after reaching the desired molecular weight by introduction of a deoxygenated solution of Bu₃SnH in anisole (0,560 ml in 4 ml of anisole) and let stir overnight.

The functionalized Si wafer has been recuperated and washed with abundant acetone and water.

SI-RATRP of tBA

The second SI-RATRP was carried in the same way, except that only the step at 65°C was done and PMDETA was used instead of TPMA: a Si wafer with a PBA brush is put in a vial in a protection ring with CuBr₂ (15.4 mg), BA (15 ml), TPMA (21 mg), AIBN (23 mg) and anisole (7,5 ml). The vial was deoxygenated with three freeze pump cycle and put in an

oil bath at 65°C and the evolution of molecular weight is checked by GPC. When the desired molecular weight is reached the vial is open, the wafer recuperated and washed with abundant acetone and water.

Grafting onto reaction

here is reported as an example the grafting of PBA_{30k} and PtBA_{30k} in a 1:1 molar ratio. Azido modified Si wafer were put in a vial with the desired molar mixture of PBA_{30k} (150mg), PtBA_{30k} (150mg), anisole (10 ml), PMDETA (14 µl) and ascorbic acid (50 mg). Oxygen was eliminated by three freeze pump cycles and CuBr was introduced in the vial under nitrogen flow. The reaction was carried on for 24 hours and the vial was open, the wafer recuperated and rinsed with abundant acetone and water.

The other surfaces were modified following the same procedure, changing the mixture of PBA and PtBA and the reaction times.

Hydrolysis of PtBA brushes

Mixed brushes of PBA and PtBA were immersed at room temperature in a 1% solution of methansulfonic acid in CH₂Cl₂. The surfaces were then washed with fresh CH₂Cl₂, acetone and water.

Topmost reorganization of mixed brushes

Mixed PBA-PAA brushes were immersed in 0,1M K₂CO₃ aqueous solution, for giving a hydrophilic surface or in hexane, for giving a hydrophobic surface, for 4 hours at room temperature. The Si wafer was then removed from the vial and the liquid was blown away with nitrogen flow.

References

- [1] M. Chen, W. H. Briscoe, S. P. Armes, J. Klein, *Science* **2009**, 323, 1698.
- [2] S. Krishnan, C. J. Weinman, C. K. Ober, *J. Mater. Chem.* **2008**, 18, 3405.
- [3] R. Gref, A. Domb, P. Quellec, T. Blunk, R. H. Muller, J. M. Verbavatz, R. Langer, *Adv. Drug Delivery Rev* **1995**, 16, 215.
- [4] A. Hucknall, S. Rangarajan, A. Chilkoti, *Adv. Mater.* **2009**, 21, 2441.
- [5] W. Yang, C. G. Zhang, H. Y. Qua, H. H. Yang, J. G. Xu, *Analytica Chimica Acta* **2004**, 503, 163.
- [6] V. S. Khire, T. Y. Lee, C. N. Bowman, *Macromolecules (Washington, DC, U. S.)* **2007** 40 5669.
- [7] Y. Zou, J. N. Kizhakkedathu, D. E. Brook, *Macromolecules* **2009**, 42 3258.
- [8] V. Coessens, T. Pintauer, K. Matyjaszewski, *Prog. Polym. Sci.* **2001**, 26, 337.
- [9] S. Minko, S. Patil, V. Datsyuk, F. Simon, K.-J. Eichhorn, M. Motornov, D. Usov, I. Tokarev, M. Stamm, *Langmuir* **2002**, 18, 289.
- [10] K. Ichimura, Y. Suzuki, T. Seki, A. Hosoki, K. Aoki, *Langmuir* **1988**, 4, 1214.
- [11] K. Ichimura, T. Seki, Y. Kawanishi, Y. Suzuki, M. Sakuragi, T. Tamaki, M. Irie, *Photoreactive Materials for Ultrahigh-Density Optical Memory*, Elsevier Science, Amsterdam, **1994**.
- [12] K. Ichimura, V. Shibaev, *Polymers as Electrooptical and Photooptical Active Media*, Springer, Berlin, **1996**.
- [13] B. Jerome, *Rep. Prog. Phys.* **1991**, 54, 391.
- [14] J. Cognard, *Mol. Cryst. Liq. Cryst., Suppl. Ser.* **1982**, 1, 1.
- [15] Y. Kawanishi, T. Tamaki, K. Ichimura, *Polym. Mater. Sci. Eng.* **1992**, 66, 263.
- [16] S. Furumi, H. Akiyama, S. Morino, K. Ichimura, *J. Mater. Chem.* **1998**, 8, 65.
- [17] K. Ichimura, H. Tomita, K. Kudo, *Liq. Cryst.* **1996**, 20, 161.
- [18] H. Tomita, K. Kudo, K. Ichimura, *Liq. Cryst.* **1996**, 20, 171.
- [19] K. Ichimura, H. Akiyama, N. Ishizuki, Y. Kawanishi, *Makromol. Chem., Rapid Commun.* **1993**, 14, 813.
- [20] T. Uekusa, S. Nagano, T. Seki, *Langmuir* **2007**, 23, 4642.
- [21] T. Uekusa, S. Nagano, T. Seki, *Macromolecules* **2009**, 42, 312.
- [22] P. Camorani, L. Cristofolini, M. P. Fontana, L. Angiolini, L. Giorgini, F. Paris, *Mol. Cryst. Liq. Cryst* **2009**, 502, 56
- [23] H. Fischer, *Chem. Rev* **2001**, 101, 3581.
- [24] K. Matyjaszewski, H. Dong, W. Jakubowski, J. Pietrasik, A. Kusumo, *Langmuir* **2007**, 23, 4528.
- [25] L. Angiolini, T. Benelli, L. Giorgini, F. Paris, E. Salatelli, M. P. Fontana, P. Camorani, *Eur. Polym. J.* **2008**, 44, 3231.
- [26] J. Barberá, L. Giorgini, F. Paris, E. Salatelli, Rosa M. Tejedor, L. Angiolini, *Chemistry - A European Journal* **2008**, 14, 11209.
- [27] N. Berova, K. Nakanishi, R. W. Woody, *Circular Dichroism Principles and Applications*, Wiley-VCH Inc, New York, **2000**.
- [28] R. M. Tejedor, L. Oriol, J. L. Serrano, F. P. Urena, J. J. L. Gonzalez, *Adv. Funct. Mater.* **2007**, 17, 3486.
- [29] L. Angiolini, D. Caretti, L. Giorgini, E. Salatelli, *Macromol. Chem. Phys.* **2000**, 201, 533.
- [30] L. Angiolini, T. Benelli, L. Giorgini, F. Paris, E. Salatelli, T. Zuccheri, *Int. J. Polym. Mater.* **2007**, 56, 789.
- [31] D. Bauman, *J. Mol. Struct.* **2005**, 307, 744.

- [32] S. Jen, N. A. Clark, P. S. Pershan, E. B. Priestley, *J. Chem. Phys.* **1977**, *66*, 4635.
- [33] T. P. Russel, *Science* **2002**, *297*, 964.
- [34] V. V. Tsukruk, V. N. Bliznyuk, *Langmuir* **1998**, *14*, 446.
- [35] D. N. Theodorou, *Macromolecules* **1988**, *21*, 1411.
- [36] D. N. Theodorou, *Macromolecules (Washington, DC, U. S.)* **1988**, *21*, 1422.
- [37] A. Sidorenko, S. Minko, K. Schenk-Meuser, H. Duschner, M. Stamm, *Langmuir* **1999**, *15* 8349.
- [38] O. Prucker, J. Rhe, *Langmuir* **1998**, *14* 6893.
- [39] H. Fischer, *J. Polym. Sci., Part A: Polym. Chem.* **1999**, *37*, 1885.
- [40] V. Coessens, K. Matyjaszewski, *Macromol. Rapid Commun.* **1999**, *20*, 66.
- [41] M. Retsch, A. Walther, K. Loos, A. H. E. Muller, *Langmuir* **2008**, *24* 9421.
- [42] D. D. Perrin, W. L. F. Amarego, D. R. Perrin, *Purification of Laboratory Chemicals*, Pergamon Press, Oxford, **1996**.
- [43] D. Wolff, H. Cackovic, H. Krueger, J. Ruebner, J. Springer, *Liq. Cryst.* **1993**, *14*, 917.
- [44] Y. Nikagawa, *Polymer* **1998**, *39*, 5139
- [45] B. Lego, W. G. Skene, S. Giasson, *Langmuir* **2008**, *24*, 379.

Ringraziamenti

Innanzitutto voglio ringraziare il gruppo Polimeri, siamo stati assieme per quattro anni, e a ciascuno devo qualcosa: Prof. Angiolini e Daniele.

Ma soprattutto Loris e Titti. Abbiamo lavorato bene noi tre. Tanto e bene!

Un ringraziamento doveroso va anche ai vari tesisti che mi hanno più che aiutato nella realizzazione di questo lavoro: Maurizio, Giorgia, Bobi e Ale. Senza di voi questa tesi non avrebbe visto la luce.

Un ringraziamento speciale va ai professori Krzysztof Matyjaszewski e Joaquín Barberá che mi hanno accolto nei loro laboratori e pazientemente insegnato tanto.

Un grazie anche ai miei collaboratori di Parma, Gigi Cristofolini e Paolo Camorani.

Sara, Alice e Fabbri: anche voi siete stati fondamentali!

Infine voglio ringraziare tutti (e sono tantissimi) coloro che, fuori dal laboratorio, mi hanno aiutato a proseguire in questa strada, spesso in salita. Ma la salita, si sa, è la parte gustosa della montagna!